Berichte
zur Polar-
und Meeresforschung

643
2012

Reports
on Polar and Marine Research

The Expedition of the Research Vessel "Sonne" to the subpolar North Pacific and the Bering Sea in 2009 (SO202-INOPEX)

Edited by
Rainer Gersonde
with contributions of the participants

HELMHOLTZ GEMEINSCHAFT

ALFRED-WEGENER-INSTITUT FÜR
POLAR- UND MEERESFORSCHUNG
in der Helmholtz-Gemeinschaft
D-27570 BREMERHAVEN
Bundesrepublik Deutschland

ISSN 1866-3192

Hinweis

Die Berichte zur Polar- und Meeresforschung werden vom Alfred-Wegener-Institut für Polar- und Meeresforschung in Bremerhaven* in unregelmäßiger Abfolge herausgegeben.

Sie enthalten Beschreibungen und Ergebnisse der vom Institut (AWI) oder mit seiner Unterstützung durchgeführten Forschungsarbeiten in den Polargebieten und in den Meeren.

Es werden veröffentlicht:

- Expeditionsberichte (inkl. Stationslisten und Routenkarten)
- Expeditionsergebnisse (inkl. Dissertationen)
- wissenschaftliche Ergebnisse der Antarktis-Stationen und anderer Forschungs-Stationen des AWI
- Berichte wissenschaftlicher Tagungen

Die Beiträge geben nicht notwendigerweise die Auffassung des Instituts wieder.

Notice

The Reports on Polar and Marine Research are issued by the Alfred Wegener Institute for Polar and Marine Research in Bremerhaven*, Federal Republic of Germany. They are published in irregular intervals.

They contain descriptions and results of scientific activities in polar regions and in the seas either conducted by the Institute (AWI) or with its support.

The following items are published:

- expedition reports (incl. station lists and route maps)
- expedition results (incl. Ph.D. theses)
- scientific results of the Antarctic stations and of other AWI research stations
- reports on scientific meetings

The papers contained in the Reports do not necessarily reflect the opinion of the Institute.

The „Berichte zur Polar- und Meeresforschung” continue the former „Berichte zur Polarforschung”

* Anschrift / Address
Alfred-Wegener-Institut
für Polar- und Meeresforschung
D-27570 Bremerhaven
Germany
www.awi.de

Editor:
Dr. Horst Bornemann

Assistant editor:
Birgit Chiaventone

Die "Berichte zur Polar- und Meeresforschung" (ISSN 1866-3192) werden ab 2008 als Open-Access-Publikation herausgegeben (URL: http://epic-reports.awi.de).

Since 2008 the "Reports on Polar and Marine Research" (ISSN 1866-3192) are available as open-access publications (URL: http://epic-reports.awi.de)

The Expedition of the Research Vessel "Sonne" to the subpolar North Pacific and the Bering Sea in 2009 (SO202-INOPEX)

Edited by
Rainer Gersonde
with contributions of the participants

Please cite or link this publication using the identifier
hdl: 10013/epic.38996 or http://hdl.handle.net/10013/epic. 38996

ISSN 1866-3192

SO202- INOPEX

Innovative North Pacific Experiment

Tomakomai, July 7 – Busan, August 29, 2009

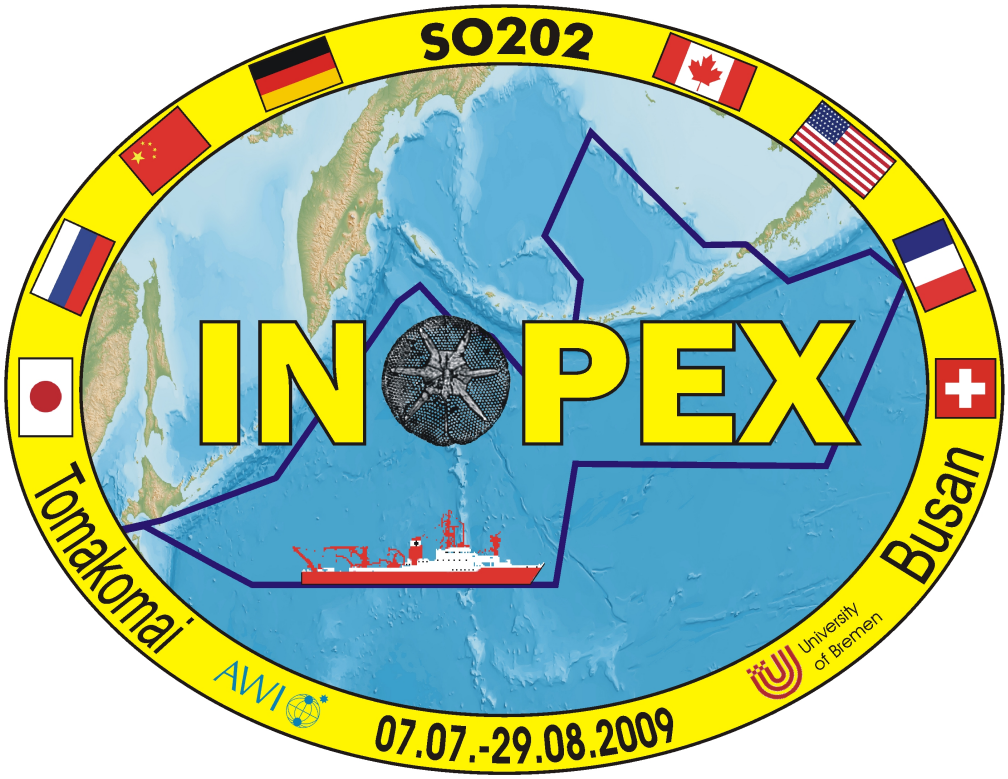

SPONSORED BY THE

Federal Ministry
of Education
and Research

TABLE OF CONTENTS

SUMMARY

The cruise SO202-INOPEX with the German R/V *Sonne* started in Tomakomai (Japan) on July 8, 2009 and ended in Busan (Korea) on August 28, 2009. The cruise is central to the interdisciplinary "Innovative North Pacific Experiment" (INOPEX), generously funded by the German Ministry of Education and Science (Bundesministerium für Bildung und Forschung, BMBF, project 03G0202A) and led and coordinated by scientists from the Alfred Wegener Institute for Polar and Marine Research (AWI) located in Bremerhaven, Germany. INOPEX amalgamates national and international expertise in the application of modern biogeochemical and paleoceanographic, as well as dating methods to produce a major step towards a more substantial understanding of past climate processes involving the ocean and atmosphere as well as continental ice (during glacial periods) in the polar North Pacific realm. The project seeks to fill a knowledge gap in a yet not sufficiently studied area of the globe critical to past and present global climate development. Besides scientists from the AWI and the German project partner at the University of Bremen (FB Geoscience, MARUM), scientists from institutions in Canada, PR China, Japan, Russia, Switzerland and the U.S. participated in the cruise and are involved in shore-based studies of the collected samples and data.

During SO202-INOPEX sampling of water, plankton and sediment was accomplished at 45 sites, complemented by bathymetric (SIMRAD EM120) and sediment-echosounding (PARASOUND P70) survey along 6677 nm. The sampling and acoustic surveys were conducted a) in Russian waters east of the Kuril-Kamchatka Trench and off Kamchatka (Obruchev Rise) between July 10-16, 2009, b) in U.S. waters south of the Aleutian Trench (Detroit Seamount, Aleutian Rise, Sirius Seamount, Patton Seamounts) and in the Bering Sea (Bowers Ridge, eastern Bering Slope, Umnak Plateau) between July 17 and August 3, 2009, and c) in international waters of the Subarctic North Pacific between 54°N – 37°N (e.g. area of Gibson Seamount, Chinook Trough, Emperor Trough, Hess Rise, Shatsky Rise, Northwest Pacific Basin) until August 23, 2009. For six prominent undersea topographic features documented by acoustic survey names have been proposed, five have been accepted by the GEBCO Sub-Committee on Undersea Feature Names (SCUFN), for one topographic structure additional bathymetric data have been requested.

Hydrographic casts with the CTD and rosette water sampler were done at 8 sites to bottom and at 20 sites to 1000 m water depth. The latter are related to the sampling of microplankton with a multinet at 5 depth intervals in the upper 1000 m of water. Additionally, plankton was collected with a Nansen net in the upper 100 m at 20 sites and during transit from the ships seawater pump (67 samples). Surface sediment has been recovered with a multicorer at 39 sites (444 tubes). Sediment coring was accomplished at 44 sites. Most of the coring was done using a piston corer with 25 m tube length (43 deployments). At 5 sites a kasten corer, and at 3 sites a gravity corer was deployed. The coring resulted in a total recovery of 862 m (including piston core trigger cores) of sediment. On-board stratigraphic dating indicates that the oldest sediment, with an age around 4 Million years (Pliocene) was recovered in the center of the Subarctic Pacific.

The very successful sampling and survey will allow the completion of the primary scientific goals of INOPEX. This includes the estimate of surface water conditions (e.g. temperature, salinity, stratification, sea ice), the reconstruction of water mass

development, the influence of physical and biological parameters (such as primary productivity and export) on ocean ventilation, ocean-atmosphere exchange, biogeochemical cycles and related implications on the regional and global climate during Pleistocene glacial and interglacial conditions at high and ultra-high time resolution (1 – 10^3 y). Resulting paleoceanographic and paleoclimatic time series will be compared with climate records from ice cores, Siberian lake sediments and marine records from other ocean basins to understand the role and response of the polar North Pacific realm on/to climate amplification and propagation processes. Such information will contribute to a better understanding of climate driving processes and will help in the generation of realistic numerical simulations of future, possibly warmer, climate conditions. Low-resolution records obtained from the central Subarctic Pacific document the onset of Northern Hemisphere glaciation around 3 Million y. before present and allow for further study of related paleoceanographic changes in the North Pacific high-latitudes. The surface sediment samples, data and samples from the water column will further improve geoscientific proxies for the reconstruction of past climate conditions.

The studies will be accomplished in national and international cooperation within INOPEX and in conjunction with the AWI program PACES, the program of the DFG Research Center „The Ocean in the Earth System“, the EU-Program „Past4Future“ and other national (DFG) and international projects (e.g. BMBF-Project KALMAR).

ZUSAMMENFASSUNG

Die Expedition SO202-INOPEX mit dem deutschen FS *Sonne* begann am 8. Juli 2009 in Tomakomai (Japan) und endete am 28. August, 2009 in Busan (Korea). Die Expedition ist zentraler Bestandteil des durch das Bundesministerium für Bildung und Forschung (BMBF) geförderte interdisziplinäre Projekt “Innovatives Nordpazifik Experiment” (INOPEX, Projektnummer 03G0202A), das von Wissenschaftlern des Alfred-Wegener-Institutes für Polar- und Meeresforschung (AWI) in Bremerhaven geleitet und koordiniert wird. Das Projekt verbindet nationale und internationale Expertise in der Anwendung moderner biogeochemischer und paläozeanographischer Methoden sowie Sedimentdatierungen. Damit soll ein fundamentaler Beitrag zum besseren Verständnis vergangener Klimaentwicklung und damit verbundener Prozesse und Wechselwirkungen zwischen Eis, Ozean und Atmosphäre im polaren Nordpazifikraum geleistet werden. Diese Anstrengungen werden einen deutlichen Wissenszuwachs für ein bislang nicht ausreichend untersuchtes, aber für die globale Klimaentwicklung bedeutendes Gebiet ergeben und damit helfen, eine bestehende Wissenslücke zu schließen. Neben Wissenschaftlern vom AWI und vom deutschen Projektpartner Universität Bremen (FB Geowissenschaften, MARUM) sind Wissenschaftler aus VR China, Japan, Kanada, Russland, Schweiz und den USA an der Expedition und der Auswertung der Daten und des Probenmaterials beteiligt.

Während SO202-INOPEX wurde die Wassersäule und das Sediment an 45 Stationen beprobt und darüber hinaus auf 6677 sm bathymetrische (SIMRAD EM120) und sediment-echographische (PARASOUND P70) Vermessungen durchgeführt. Die Vermessungen und Stationsarbeiten fanden statt a) in Gewässern der Russischen Föderation östlich des Kurilen-Kamtschatka Grabens und auf dem Obruchev Rücken im Zeitraum 10. - 16. Juli 2009, b) in U.S. Gewässern südlich des Aleuten Grabens

(Detroit Seamount, Aleuten Rücken, Sirius Seamount, Patton Seamounts) und im Beringmeer (Bowers Rücken, östlicher Beringhang, Umnak Plateau) vom 17. Juli bis 3. August 2009, und c) bis 23. August 2009 in internationalen Gewässern des subarktischen Pazifiks zwischen 54°N und 37°N (u.a. Gebiet Gibson Seamount, Chinook Graben, Emperor Graben, Hess Rücken, Shatsky Rücken und Nordwestpazifik Becken). Gestützt auf die hydroakustischen Vermessungen wurden Namen für sechs topographische Strukturen vorgeschlagen. Davon wurden 5 Namen durch das GEBCO “Sub-Committee on Undersea Feature Names” (SCUFN) angenommen, für eine Struktur werden zusätzliche bathymetrische Daten gefordert.

Hydrographische Untersuchungen mit der CTD und Rosette wurden an 8 Stationen bis zum Boden und an 20 Stationen bis 1000 m Wassertiefe durchgeführt. Parallel dazu wurde das Mikroplankton in 5 Tiefenintervallen über die oberen 1000 m mit einem Multinetz gefangen. Zusätzlich wurde das Mikroplankton an 20 Stationen in den oberen 100 m der Wassersäule mit einem Nansennetz und auf der Fahrstrecke mit der Schiffspumpe (67 Proben) gesammelt. Oberflächensedimentproben konnten mit einem Multicorer an 39 Stationen (444 Multicorerkerne) gewonnen werden. Sedimentkerne wurden an 44 Stationen gezogen. Dabei kam 43 Mal ein zumeist 25 m langes Kolbenlot zum Einsatz. An fünf Stationen wurden Sedimentkerne mit einem Kastenlot und an 3 Stationen mit dem Schwerelot gewonnen. Insgesamt konnten während SO202-INOPEX 862 m Sedimentkern (einschließlich Pilotkerne des Kolbenlotes) gezogen werden. Vorläufige stratigraphische Untersuchungen zeigen, dass die ältesten dabei gewonnenen Sedimente mit einem Alter um 4 Millionen Jahre (Pliozän) aus dem zentralen Bereich des subarktischen Pazifiks stammen.

Die erfolgreiche Probennahme in Wassersäule und Sediment und die umfangreichen Vermessungsarbeiten versprechen, dass die im Rahmen von INOPEX geplanten wissenschaftlichen Auswertungen in vollem Umfang durchgeführt werden können. Dazu gehören die Rekonstruktion von Deckschichtparametern wie Temperatur, Salzgehalt, Stratifikation und Meereisverbreitung sowie die Rekonstruktion der Wassermassenentwicklung und des Einflusses von physikalischen und biologischen Parametern (wie Primärproduktion und Export) auf die Durchmischung des Ozeans, den Ozean-Atmosphärenaustausch, biogeochemische Kreisläufe und damit verbundene Auswirkungen auf das regionale und globale Klimasystem im Wechsel pleistozäner Warm- und Kaltzeiten. Die gewonnenen Sedimente erlauben diese Rekonstruktionen in hoher bis sehr hoher zeitlicher Auflösung (1 – 10^3 Jahre). Die entwickelten paläozeanographischen und –klimatischen Zeitreihen werden mit Klimadaten aus Eiskernen, sibirischen Seesedimenten und marinen Sedimenten aus anderen Ozeanbecken verglichen. Damit sollen interne und externe Anfachungsmechanismen, aber auch die Rolle des polaren Nordpazifikgebietes bei der Verstärkung und Verbreitung von Klimasignalen besser verstanden werden. Solche Kenntnis wird dazu beitragen, die Entwicklung von Klimamodellen zu verbessern, um damit auch zukünftige, möglicherweise wärmere, Klimazustände realistischer simulieren zu können. Zeitlich gering auflösende Sedimentkerne aus dem zentralen subarktischen Pazifik dokumentieren die Vereisung der Nordhemisphäre vor ca. 3 Millionen Jahren und erlauben es, die damit verbundenen paläozeanographischen Änderungen im Nordpazifikraum zu untersuchen. Die Oberflächensedimentproben und Daten/Proben aus der Wassersäule sind wesentliche Grundlage für die Weiterentwicklung von Methoden zur paläozeanographischen Rekonstruktion.

Die Auswertung des SO202-INOPEX-Daten- und Probenmaterials erfolgt in nationaler und internationaler Zusammenarbeit im Rahmen des INOPEX Programmes sowie in Verbindung mit dem AWI-Forschungsprogramm PACES, dem DFG-Forschungszentrum „The Ocean in the Earth System“, dem EU-Programm „Past4Future“ und anderer nationaler (DFG) und internationaler Projekte (u.a. BMBF-Verbundprojekt KALMAR).

1. INTRODUCTION

Rainer Gersonde
Alfred Wegener Institute, Bremerhaven, Germany

1.1 INOPEX, the Scientific Goals and Methods

The “Innovative North Pacific Experiment” (INOPEX) is an interdisciplinary scientific project focusing on the biogeochemistry and paleoceanography of the subarctic Pacific and Bering Sea. The project is generously funded by the German Ministry of Education and Science (Bundesministerium für Bildung und Forschung, BMBF) and is led by scientists from the Alfred Wegener Institute for Polar and Marine Research (AWI) located at Bremerhaven, Germany. INOPEX amalgamates national and international expertise in the application of modern biogeochemical and paleoceanographic, as well as dating methods to produce a major step towards a more substantial understanding of past climate processes involving the ocean and atmosphere as well as continental ice in the polar North Pacific realm. The project seeks to fill a knowledge gap in a yet not sufficiently studied area of the globe critical to past and present global climate development.

Primary scientific goals of INOPEX include the reconstruction of surface water conditions (temperature, salinity, stratification, sea ice), water mass development and the influence of physical and biological parameters (such as primary productivity and export) on ocean ventilation, ocean-atmosphere exchange and related implications on global climate at glacial and interglacial conditions. Resulting paleoceanographic and paleoclimatic time series will be compared with climate records from ice cores, Siberian lake sediments and marine records from other ocean basins to understand the impact and external forcing and the role and response of the polar North Pacific realm on/to climate amplification and propagation processes. Such information will contribute to a better understanding of climate driving processes and will help in the generation of realistic numerical simulations of future, possibly warmer, climate conditions. In this context, one specific interest concerns the documentation of exchange processes between the Arctic Ocean, the Bering Sea and the Subarctic Pacific (SAP) and its implication on the distribution of water masses, nutrients and biota at past periods characterized by warmer climate and higher sea level conditions compared to the present.

Primary scientific goals of INOPEX include:

- Reconstruct surface ocean conditions (SST, salinity, stratification, sea-ice), water-mass development and the influence of physical parameters on water-mass distribution, ocean ventilation, development of an oxygen minimum zone (OMZ) ocean-atmosphere exchange of gases and nutrients, biological production and nutrient distribution.
- Document the history of deep and intermediate water masses, the occurrence and extent of low-oxygen conditions in the SAP and the Bering Sea and its implication for global circulation and biogeochemical cycles.
- Reconstruct changes in biological productivity regimes and export of biogenic components at intermediate to high time resolution, with a view toward understanding the influence of biological processes in the SAP and Bering

Sea on biogeochemical cycles, changes of atmospheric CO_2 and related implications on global climate.
- Quantify terrigenous sediment sources as indicators for atmospheric and oceanic circulation patterns, micro-nutrient (e.g. Fe) input and continental ice sheet/glacier dynamics and extent.
- Document exchange processes between the SAP and its marginal seas, as well as with the Arctic Ocean and its implications on distribution of water-masses, nutrients and biota.
- Generate high-resolution accurately-dated paleoceanographic and paleoclimatological time series from the SAP and Bering Sea for correlation with time series from ice cores (e.g. NGRIP, EPICA), terrestrial (e.g., Lake El'gygytgyn, East Siberia) and marine climate archives from other basins (e.g. Arctic, North Atlantic, Equatorial Pacific, Southern Ocean) to understand the impact of external forcing and the SAP role and response on/to climate amplification and propagation processes.
- Develop enhanced stratigraphies for the accurate dating of Holocene and Pleistocene records in sediments that lack biogenic carbonate based on a combination of geomagnetic paleointensity records, compound-specific radiocarbon dating of biomarkers, tephrochronology, opal-based oxygen isotope records as well as siliceous microfossil abundance patterns.
- Improve and develop paleobiological and geochemical proxies for paleoclimatic and paleoceanographic reconstructions.

Primary time windows of INOPEX are:

- time slices, such as the Holocene, Termination I and II, the last glacial and Marine Isotope Stage (MIS) 5.5;
- time series documenting climate conditions and variability during the past 40-60 kyrs at high to ultra-high (in laminated sections possibly annual) resolution;
- time series encompassing the past 200 – 300 kyrs, thus the past 2-3 climate cycles, at millenial-centennial resolution;
- time series documenting the long-term climate development since the onset of significant Northern hemisphere glaciation between 3 - 4 Ma.

The **major methods** proposed to be applied within INOPEX for multiproxy paleoceanographic reconstruction and dating of sediments include a large variety of partly novel approaches:

- Stable isotope measurements ($\delta^{15}N$, $\delta^{30}Si$, $\delta^{18}O$) of biogenic opal (diatoms, radiolarians and potentially sponge spicules) to generate estimates of nutrient utilization, surface water salinity, stratification, changes in biogeochemical cycles and to enhance the stratigraphy (e.g. De La Rocha et al. 1998, Shemesh et al. 2002, Brunelle et al. 2007, Robinson and Sigman 2008).
- Stable isotope measurements ($\delta^{18}O$, $\delta^{13}C$, $\delta^{15}N$) of benthic and planktic foraminifers to document water-mass generation and structure (ventilation), surface water salinity changes, nutrient utilization, changes in biogeochemical cycles (e.g. Keigwin 1987, Zahn et al. 1991, Ren et al. 2009) and to generate a baseline for the dating of records based on oxygen isotope stratigraphy (e.g. Lisiecki and Raymo 2005).
- Measurement of biomarkers (alkenones, n-alkanes, TEX_{86}-index, C_{25}-HBIs) for the reconstruction of sea surface temperature (SST), salinity, changes in

sea ice extent and terrestrial input (e.g. Martinez-Garcia et al. 2009, Weijers et al. 2006, Kim et al. 2008, Belt et al, 2007, Massé et al. 2008).

- Documentation of the distribution, abundance, and nitrogen isotopic composition of long-chain polyamines (LCPA) representing diatom species-specific silica-precipitating organic compounds (Kröger et al. 2000), to generate new biomarker proxies.
- Microfossil-based (diatoms, radiolarians, dinoflagellates) transfer functions (IKM, MAT, ANN) for the reconstruction of SST, sea ice extent and productivity regimes (e.g. Gersonde et al. 2005, Abelmann et al. 2006, De Vernal et al. 2006, 2006, Radi et al. 2007).
- Element analysis (XRF-scanner) at highest possible resolution (1 cm – 200µm) (e.g. Jansen et al. 1998, Röhl und Abrams 2000) paired with chemical analyses of biogenic (e.g. C_{org}, opal, $_{xs}Ba$) and terrestrial sediment composition (e.g. ICP-OES measurements for elemental composition), determination of ice rafted debris (IRD) components and provenance to document the variability of terrigenous and biogenic components and to generate time-series for high-resolution intercorrelation of sediment cores and documentation of laminations.
- Measurement of $xs^{230}Th$ to quantify vertical flux rates of biogenic phases (opal, C_{org}, biomarkers, $_{xs}Ba$) and terrestrial components as indicators of biogenic export and terrestrial input (e.g. Francois et al. 2004, Shigemitsu et al. 2007).
- Utilization of the terrestrial $^{4}He/^{232}Th$ ratio as an indicator of dust flux and dust provenance (e.g. discrimination of terrestrial and volcanogenic dust) (e.g. Anderson et al. 2006, McGee et al., 2007, Winckler et al., 2008).
- Determination of La/Yb and Th/Sc ratios to quantify the relative contributions of fine-grained eolian deposits and volcanic debris (e.g. Otosaka et al. 2004, Shigemitsu et al. 2007).
- Measurement of the mean and percentage of sortable silt to derive bottom water velocity (e.g. Bianchi and McCave 1999).
- Measurement of Nd isotope ratios for the reconstruction of water mass structure and circulation (Piotrowski et al. 2004).
- Measurement of the $^{231}Pa/^{230}Th$ ratio as a tracer of opal dissolution (Bradtmiller et al. 2007).
- Characterization of magnetic minerals for the tracing of terrigenous sediment provenance and transportation pathways.
- $AMS^{14}C$ dating of foraminifers and opal-bound organic compounds (Ingalls et al. 2004, Hatte et al. 2008) in combination with ^{210}Pb measurements.
- Measurement of geomagnetic intensity and polarity for the establishment of a chronostratigraphy (Bleil and von Dobeneck 1999, Franke et al. 2004, Valet et al. 2005).
- High-resolution correlation of sediment records based on physical parameters (e.g. magnetic volume susceptibility, electric resistivity, spectral light reflectance) and geomagnetic parameters (e.g. v. Dobeneck and Schmieder 1999, Hofmann and Fabian 2007, Bleil and Dillon 2008).
- Application of tephrostratigraphy for intercorrelation of sediment records and absolute dating of ash layers (e.g. Aoki et al. 2008).
- Determination of Plio-/Pleistocene cosmic particle flux (e.g. Taylor and Brownlee 1991).

1.2 SO202-INOPEX Itinerary and Work at Sites

The German R/V *Sonne* left Tomakomai on Hokkaido (Japan) on Wednesday, July 8, 2009, for the cruise SO202-INOPEX **(Fig. 1.2-1).** Onboard were 50 persons, of which 25 were crew and 25 were scientists (see sections A.1, A.2 and A.3 in appendix for names and affiliations).

One day after our start in Tomakomai we crossed the southern end of the Kuril-Kamchatka Trench with a maximum water depth of 10.542 m at the Witjas Deep. Acoustic survey with the SIMRAD EM120 multi-beam echosounder (see 2.1) and the PARASOUND P70 sediment echosounder (see 2.2) was started on Thursday, July 9, 23:02h UTC (considering the extension of the cruise track over different time zones and multiple crossings of the International Datum Line, IDL, all dates and times are given in Universal Time Coordinated, UTC) when the research area in deep-waters along the Kuril-Kamchatka Trench and in intermediate waters of Obruchev Rise was reached. This area is located in waters of the Russian Federation, which provided allowance to conduct marine geoscientific research in these waters **(Fig. 1.2-2)**. During the stay of R/V *Sonne* in Russian waters the ships position and the SO-202 sampling and survey program was reported to the Russian Pacific Fleet, each day at 12:00 Moscow time. Two Russian scientist, affiliated to the V.I. Il´ichev Pacific Oceanological Institute (POI) in Vladivostok were invited to join the cruise SO202-INOPEX (A.1, A.2).

The first sampling site in Russian waters was occupied on Friday, July 10, 05:00 UTC. Site SO202-1 at a water depth of 5280 m is located on the southern Zenkevich Rise (**Fig. 1.2-3**), close to the site of the 15.28 m long core RC14-103 with an average sedimentation rate of 17.5 cm/1000 y (Heusser and Morley, 1995). High sedimentation rates are also indicated by PARASOUND, showing a well-stratified sequence of sediment with an acoustic penetration of up to 70 m (**Fig. A.6-1**). While the CTD (see 3.1 for instrument details) measured a full profile of water temperature, salinity and oxygen across the water column, the rosette water sampler failed as a malfunction of the rosette steering unit. This was repaired one day later. The piston corer (see 3.4 for instrument details), deployed with a length of 20 m apparently sampled a long core after penetration into the sediments at the sea floor; however, when the corer was being recovered the crew made a handling mistake, which resulted in the total loss of the gear. Fortunately no one was injured, when the cable broke. The subsequently deployed multicorer (see 3.3 for instrument details) successfully recovered 11 tubes, each with ca. 30 cm surface sediment.

On July 11 a low-pressure system with gale winds (Bft 7-8) **(Fig. 1.2-4)** passed our position further en route to the northwestern North Pacific; however, rough seas remained only for a short period. The acoustic surveys could be continued and allowed for the mapping of two larger topographic structures newly named Svarichevskij Seamount and Billings Seamount (**Fig. 1.2-3, Table 1.2-1**). The sampling was continued at three deep-water stations on the Zenkevich Rise off the Kuril-Kamchatka Trench (SO202-2/-4) and two shallower water sites (SO202-5/-6) located on Obruchev Rise (**Fig. 1.2-3)**. Obruchev Rise represents the oldest volcanic structure (>85 Ma; Duncan and Keller, 2004) of the 6000 km long Hawaiian-Emperor Seamount Chain and is covered by thick sediments, extending in a south-eastern direction, the so-called Meiji Drift.

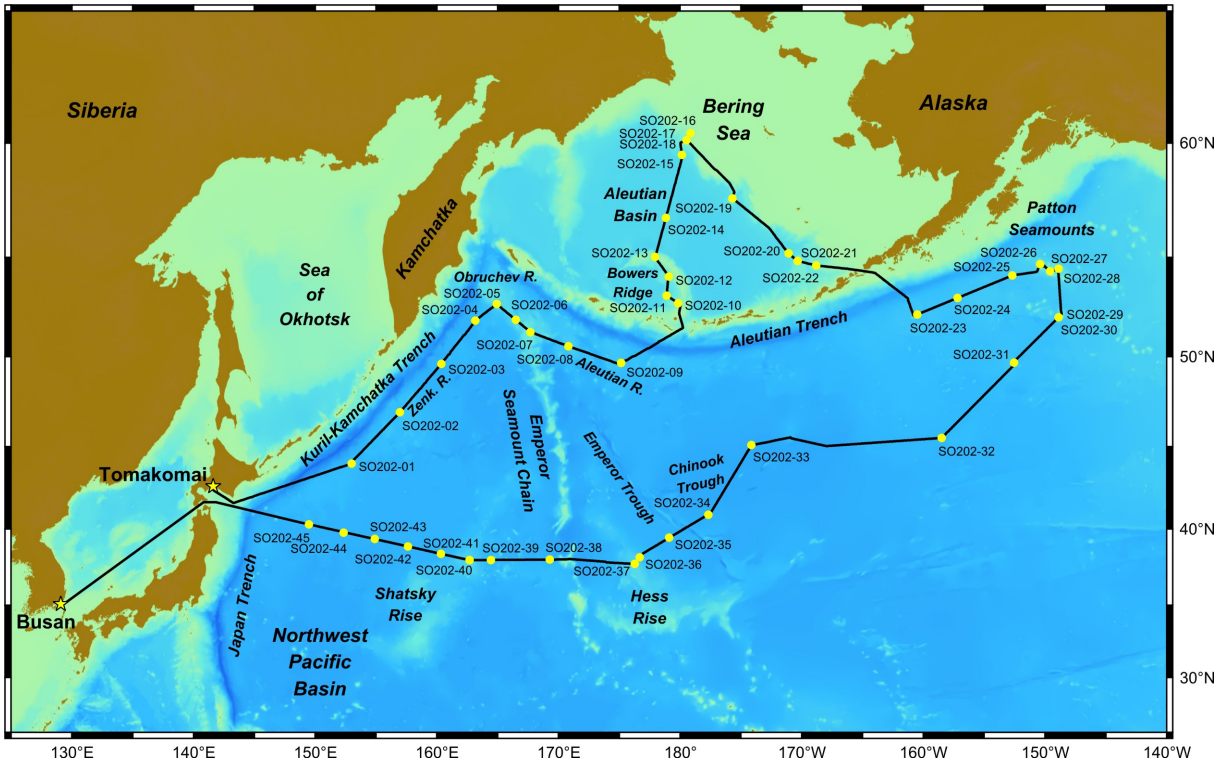

Fig. 1.2-1: *SO202-INOPEX cruise track and sample sites. Bathymetry according to GEBCO 1min.*

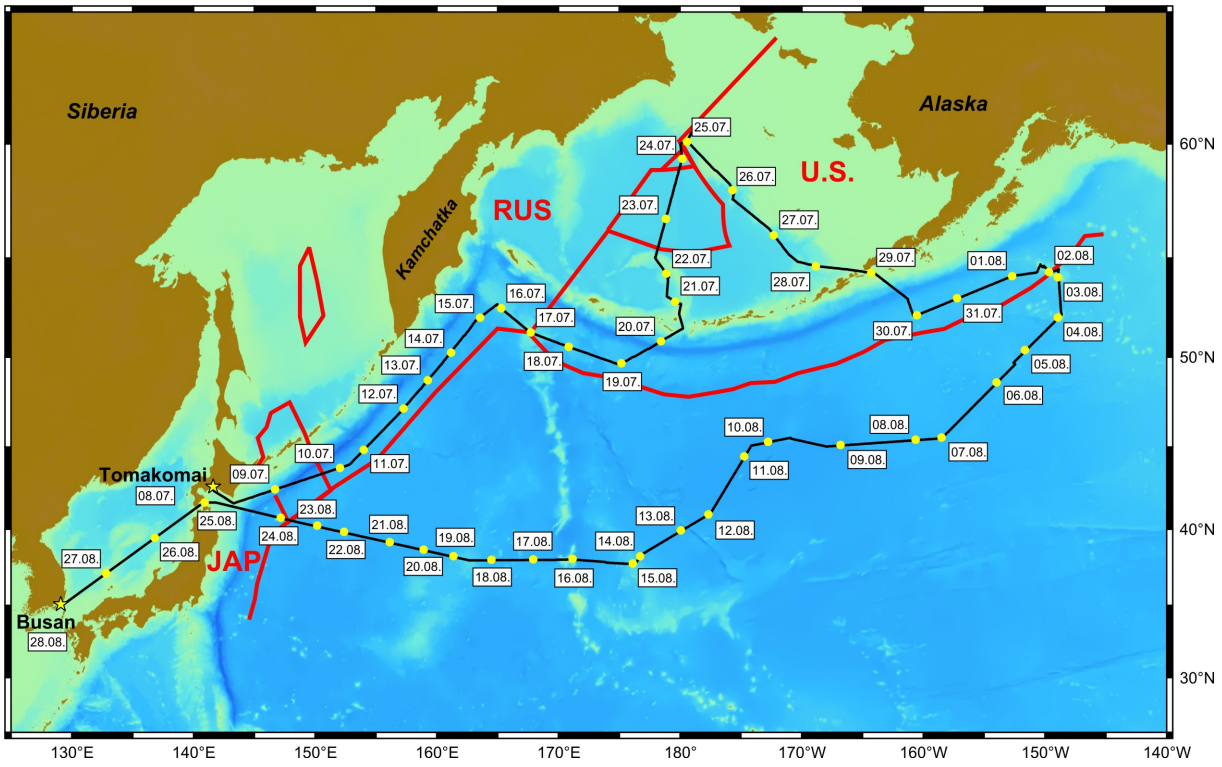

Fig. 1.2-2: *SO202-INOPEX cruise track with day-by-day marks and extension of Exclusive Economic Zone (EEZ) of Japan (JAP), the Russian Federation (RUS) and the U.S. Bathymetric map according to GEBCO 1min.*

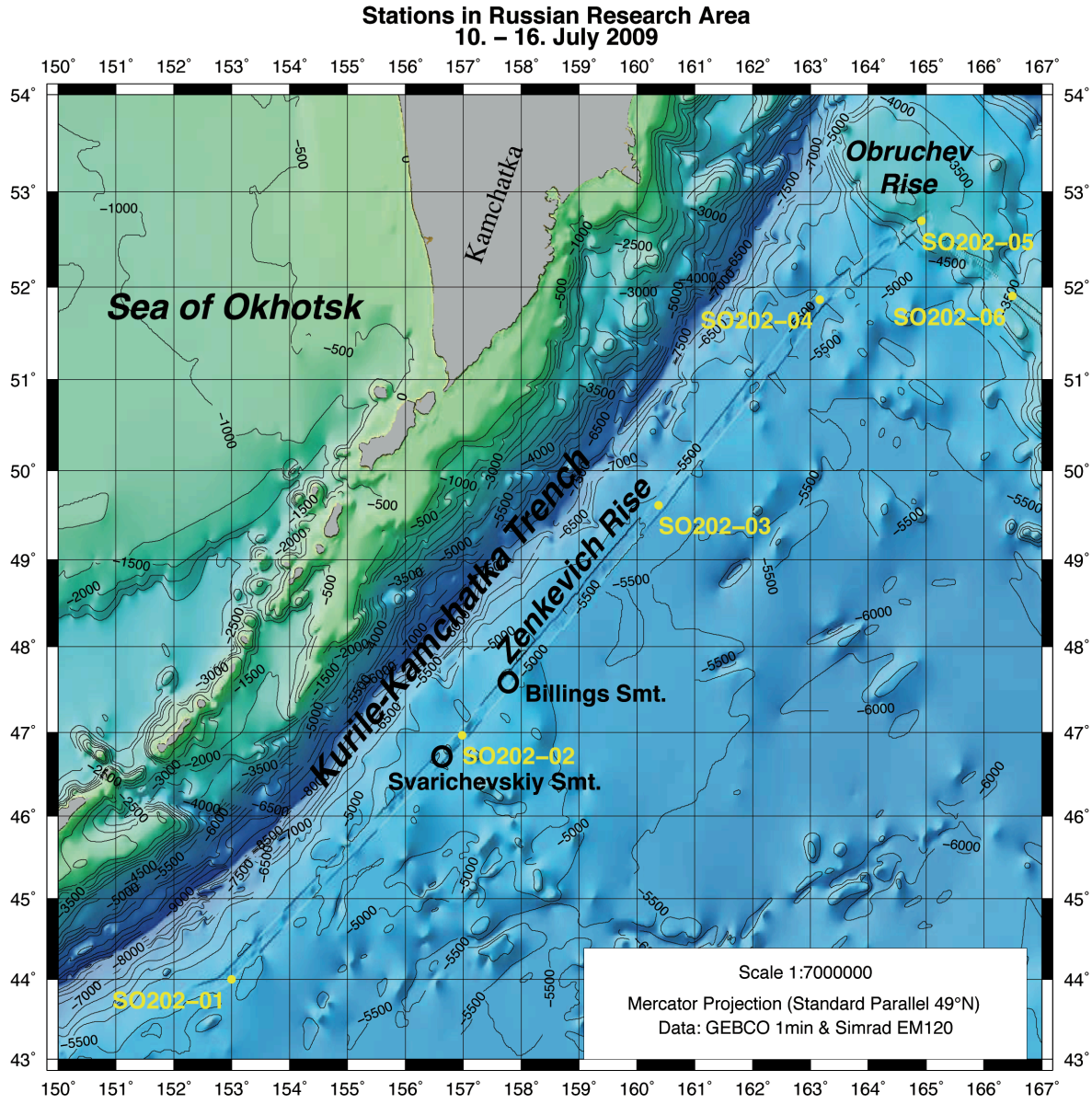

Fig. 1.2-3: *Bathymetric map of working area in waters of the Russian Federation) and location of SO202-INOPEX sites. Encircled are locations of two submarine volcanic structures newly named Svarichevskij Seamount and Billings Seamount (see **Table 1.2-1**). Bathymetric data include GEBCO 1min and SO202 survey with SIMRAD EM120.*

Applying a back-up piston corer, up to 15.56 m long cores were recovered at these sites. At three of them, the piston corer did not fully enter the sediment, which resulted in bending of the core tubes at the seafloor. On July 14, the first cores were opened and it became clear that the reduced penetration of the corer was due to the occurrence of multiple compact ash layers, reaching thicknesses up to 15 cm (see Chapter 7 and **Figs. A.5-1a-c** and **A.5-2a-c**). These ash layers represent prominent acoustic reflectors (**Figs. A.6-2, -3, -4, -5a,b, -6**). Preliminary dating of the two cores recovered from Obruchev Rise result in basal ages as old or older than 200 kyr. Previous cores from this area (e.g. RAMA44PC) are much shorter and constrain the paleoceanographic reconstruction from this area to the past ca. 20 kyr (Keigwin et al. 1992). CTD casts at SO202-01, -02, -03 and -05 reveal the peculiar upper water column hydrographic structure in the western Subarctic Pacific. This is characterized

by a shallow halocline (**Fig. 4.2-2**), which represents a barrier to convective overturn and allows for the development of a distinct shallow temperature minimum, which represents a remnant of winter cooling. This structure prevents deep-water mass formation (Warren, 1983). To gather more information on the effect of such water mass structure on the siliceous and calcareous microzooplankton the multinet was deployed to a water depth of 1000 m in conjunction with the CTD casts and additionally the phytoplankton were cached with a Nansen plankton net in the upper 100 meters (see 3.2 for instrument details). The Sites SO202-01/-05 are located in the cold Kamchatka Current, flowing south-westward from the Bering Strait, along the Siberian Pacific coast and the Kuril-Kamchatka Trench. Off Japan a portion of this current becomes the Oyashio Current while the remainder joins the warmer North Pacific Current (**Fig. 1.3-1**).

	Name	***Position (summit)***	***Minimum/ Maximum Depth (m)***	***Dimension/ Size***	***GEBCO-SCUFN Status***
1	Svarichevskiy Seamount	46°47.6´N 156°44.8´E (Fig. 1.2-3)	3361/5060	16 x 10 km, with a steep circular angle (Fig. 2.1.3-2)	accepted
2	Billings Seamount	47°36.7´N 157°50.5´E (Fig. 1.2-3)	3862/5201	13 x 9 km, with a steep circular angle (Fig. 2.1.3-3)	accepted
3	Krümmel Seamount	49°41.2´N 152°34.7´W (Fig. 1.2-9)	3655/5000	19 x 14 km, with a steep oval shape (Fig. 2.1.3-4)	accepted
4	Vancouver Knolls	eastern hill 49°22.2´N 152°44.3´W central hill 49°20.5´N 152°48.9´W western hill 49°22.5´N 152°54.6´W (Fig. 1.2-9)		20 x 11 km, with a rounded profile (Fig. 2.1.3-5)	accepted
5	Krauss Seamount	49°01.8´N 153°24.5´W (Fig. 1.2-9)	3513/4900	24 x 18 km, with a steep elongated shape (Fig. 2.1.3-6)	accepted
6	Beiersdorf Peak	52°09.0´N 148°44.4´W (Fig. 1.2-9)	1766/4531	13 x 8 km, isolated peak (Fig. 2.1.3-7)	pending

***Table 1.2-1**: Undersea features named based on SO202 acoustic surveys. Features 1-5 have been approved by the GEBCO Sub-Committee on Undersea Feature Names (SCUFN) on its 23rd meeting in September 2010. Position 6 is added to Reserve Section of the GEBCO Gazetteer until additional bathymetric information covering the highest point of the feature is provided (for SCUFN meeting reports see http://www.gebco.net/data_and_products/undersea_feature_names/#feature_links4).*

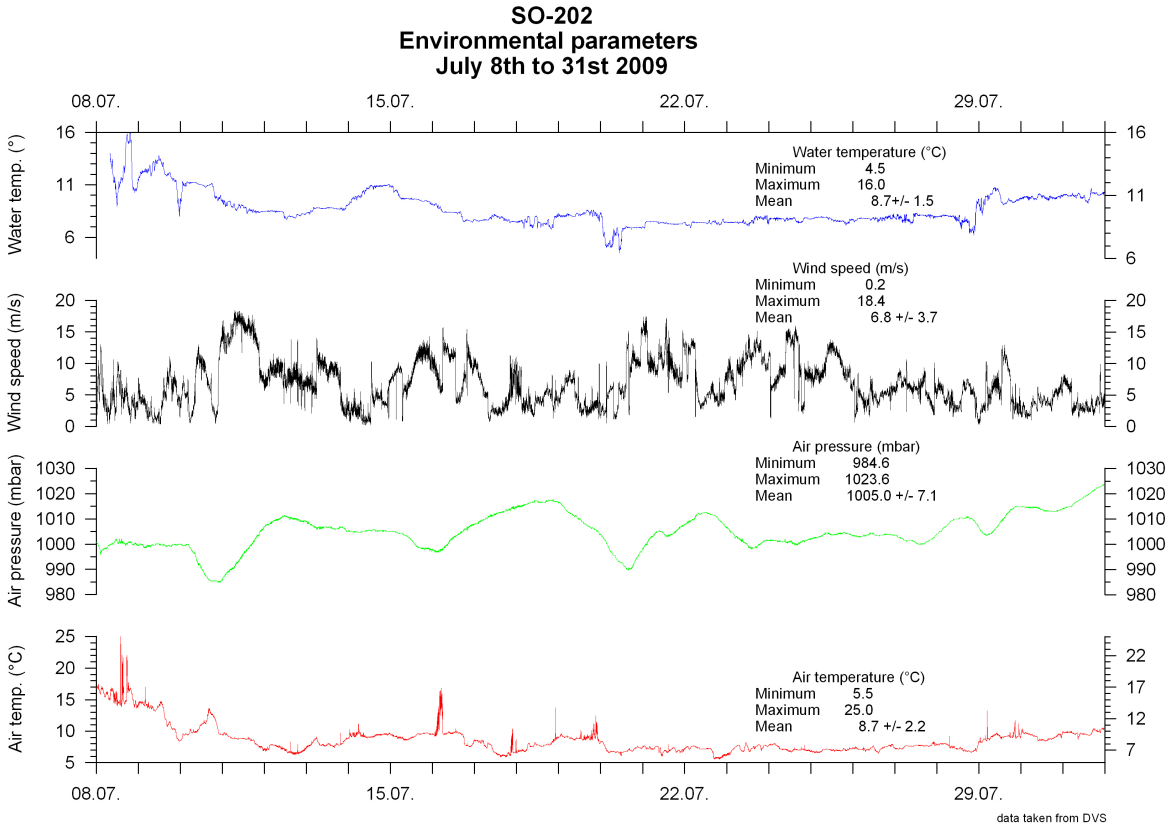

***Fig. 1.2-4**: Surface water temperature, wind speed, air pressure and air temperature as monitored by ships sensors between July 8 and July 31, 2009.*

On July 16, 15:48 UTC (51°35´N, 167°05´E) the waters of the Russian Federation were left after a survey of 868 nm and U.S. waters **(Fig. 1.2-2)** were entered to reach the top of the Detroit Seamount. Representing one of the few extended areas in the North Pacific with water depth shallow enough to allow for the deposition of calcareous microfossils, Detroit Seamount has been the target of different previous geoscientific cruises including deep sea drilling (ODP Sites 883, 884; Rea et al., 1993) and giant piston coring (MD01-2416; Gebhardt et al., 2008). However, the combination of different and novel paleoceanographic proxies within INOPEX requires the recovery of large volumes of sediment. For this reason besides a piston corer a kasten corer was deployed on Detroit Seamount at a water depth of 2350 m (SO202-07) (**Fig. 1.2-5**). The stiff sediments (**Fig. A.5-3**) prevented a deep penetration of the corer, but the 4.77 m long core will allow for a detailed of the past ca. 90 kyr at this site ideal for the combination of calcareous and siliceous proxies. Under favorable weather conditions with generally low wind speeds and a calm sea (**Fig. 1.2-4**) survey and sampling continued on the Aleutian Rise on July 18 and 19. Sediments were recovered at two locations at a water depth of 3630 and 5025 m. The suite of cores recovered south of the western Aleutian Trench between 2350 m and 5025 m (SO202-05 – SO202-09) represents a latitudinal transect across the Western Subarctic Gyre and a depth transect across the water column in the western Subarctic Pacific. At SO202-09 also the water column was sampled with a CTD+Rosette, the multinet and the plankton net, as a part of a N-S transect to monitor water mass characteristics and microplankton distribution in the central Subarctic Pacific and the Bering Sea between SO202-18 (60°N) and SO202-36 (38°N).

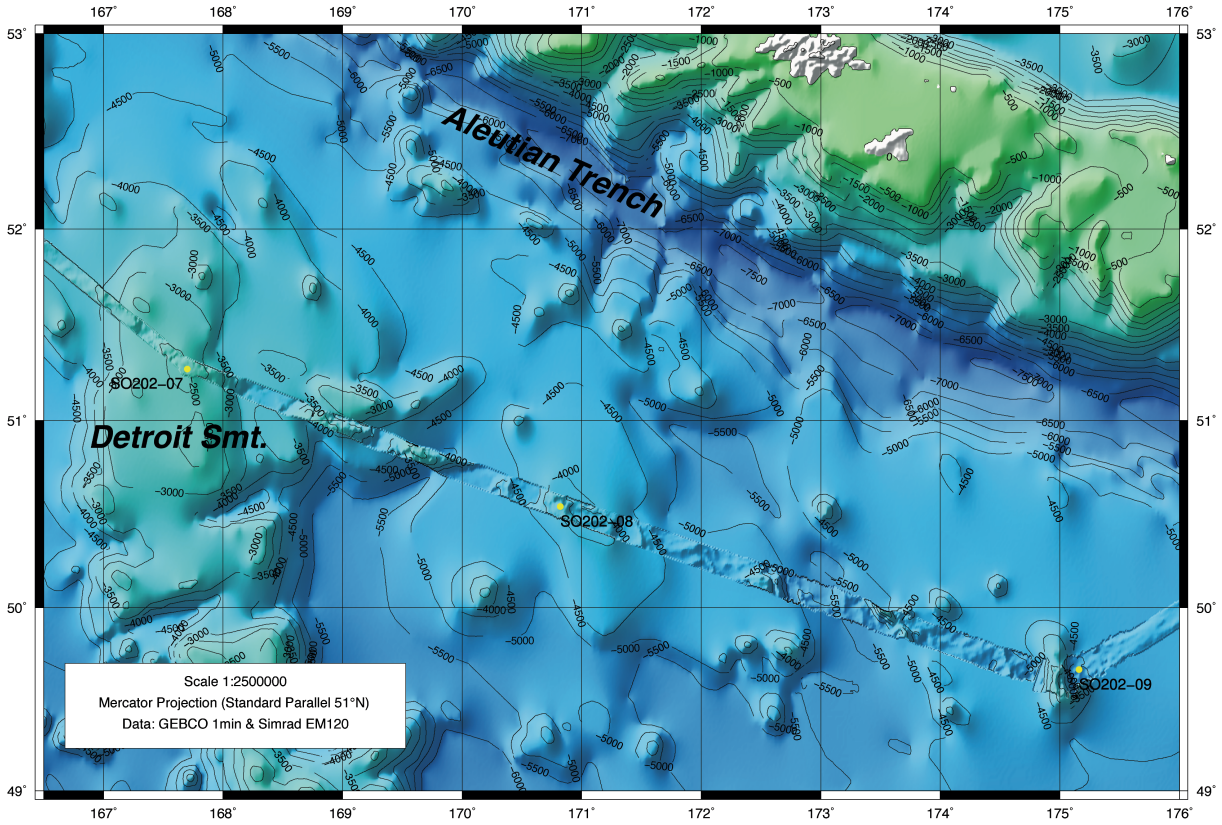

Fig. 1.2-5: *Bathymetric map of Detroit Seamount (SO202-07), Aleutian Rise (SO202-08), western Aleutian Trench and location of SO202-INOPEX sites. Bathymetric data include GEBCO 1min and SO202 survey with SIMRAD EM120.*

After completion of station work at Site SO202-09 in the morning of July 19, R/V *Sonne* headed towards the Amchitka Pass. The Amchitka Pass is in the center of the Aleutian Island Arc and separates the Rat Islands to the West and the Andreanov Islands to the East and represents one of the gateways between the Bering Sea and the North Pacific. After crossing the IDL, the Aleutian Trench was passed at a water depth of 7300 m on July 20. Surface water temperatures dropped to a minimum (**Fig. 1.2-4**).

In the Amchitka Pass and on the adjacent southern Bowers Ridge visibility was low due to dense fog. In the shallow waters of this area (<1200 m water depth) the sediment-echosounder showed hard grounds and no-penetration. After a change of heading, towards the western flank of Bowers Ridge, the PARASOUND penetration increased to >75 m (**Fig. A.6-10a,b**) and allowed for the recovery of a 22.63 m long piston core at Site SO202-10 (**Fig. 1.2-6**). The upper 6 m of the sediment core, however, were affected by deformation caused by implosion of the liner. Sediment and water column sampling of Bowers Ridge was continued until July 22 at two sites on the western flank of Bowers Ridge and one site on the northernmost plateau of the ridge. The four sites visited at Bowers Ridge cover a depth range between 1380 and 2700 m. At Site SO202-12 besides a 23.13 m long piston core, a 10.69 long kasten core was recovered to gather large sediment samples. The kasten core SO202-12-1 documents Holocene and last glacial sediments. The glacial/interglacial transition is marked by two sections with laminated sediments, the lower with a

thickness of 31 cm and the upper with 6 cm. Unfortunately, this core is disturbed by slumping below 6.78 m (**Fig. A.5-4a,b**). Although the core location is close to a tectonic structure, such disturbance could not be recognized in the sediment-echosounding (**Fig. A.6-12a,b**). The occurrence of laminated or dysaerobic intervals in deglacial sediments of the Bering Sea has been described by Cook et al. (2005) and the two laminated sections have been dated to be deposited between 14.450 and 10.320 cal y.

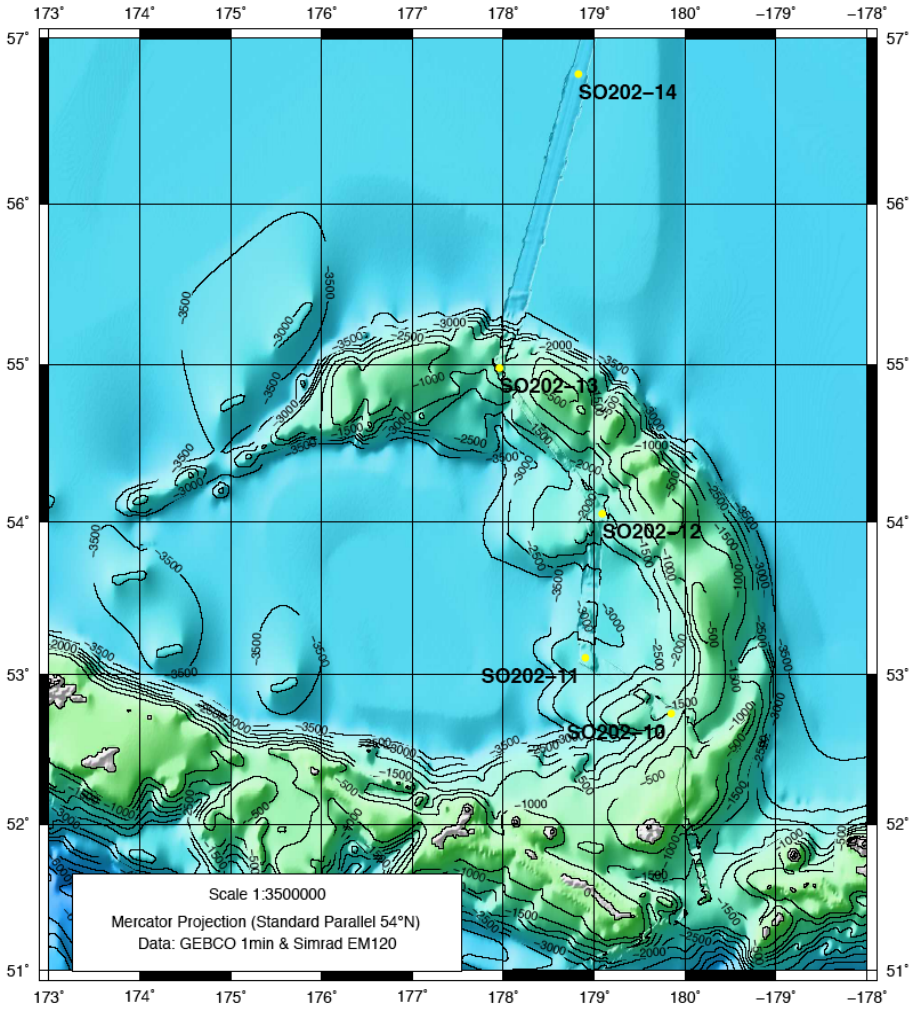

Fig. 1.2-6: *Amchitka Pass, Bowers Ridge (SO202-10, -11, -12, -13), Aleutian Basin (SO202-14) and location of SO202-INOPEX sites. Bathymetric data include GEBCO 1min and SO202 survey with SIMRAD EM120.*

After sampling the water column and the sediments in the central Aleutian Basin (SO202-14, water depth 3820 m) the northern Bering Slope was reached on July 24 in the area of the Navarin Canyon. This area is close to the boundary between the U.S. and the Russian Federation EEZ (**Fig. 1.2-2**) and crossed by the IDL. The plan to sample a sediment core transect from the uppermost slope to the deep basin was abandoned because PARASOUND indicated a strong surface reflector and sediments affected by erosional structures in the shallow waters (**Fig. A.6-16**). As such, only surface sediments were sampled at the most shallow site (SO202-16, water depth 550 m), which represents the shallowest and northernmost site sampled during SO202-INOPEX (**Fig. 1.2-1**). The site is close to the average winter sea ice edge which extends in the south-eastward direction along the Bering Shelf break (**Fig. 1.3-1**) Sediment coring was successfully completed at the southern flank of the Navarin

Canyon at mid-slope water depth around 1100 m (SO202-17, -18), and at the base of the slope off the Pervenet Canyon at 3100 m (SO202-15, (**Fig. 1.2-7**). At the mid-slope depth cores were recovered at two sites to gather a low-resolution (SO202-17, **Fig. A.6-17**) and a high-resolution record (SO202-18, **Fig. A.6-18**) from this area, which is close to the seaway connecting the Bering Sea and the Arctic Ocean during interglacial sea level high stand. Besides a 18.49 m long piston core, a 7.21 m kasten core (SO202-18-1) was recovered at the high-resolution site to gather large volume samples. At this site, Termination I is marked by thick (>1 m) laminated intervals (**Fig. A.5-5a,b**) that may reach sedimentation rates >200 cm/kyr, considering dating results of Cook et al. (2005). The sediments recovered at the slope are rich in biogenic gas, which leads to sediment core expansion. Related diagenetic processes disturb the geomagnetic signal of the sediment.

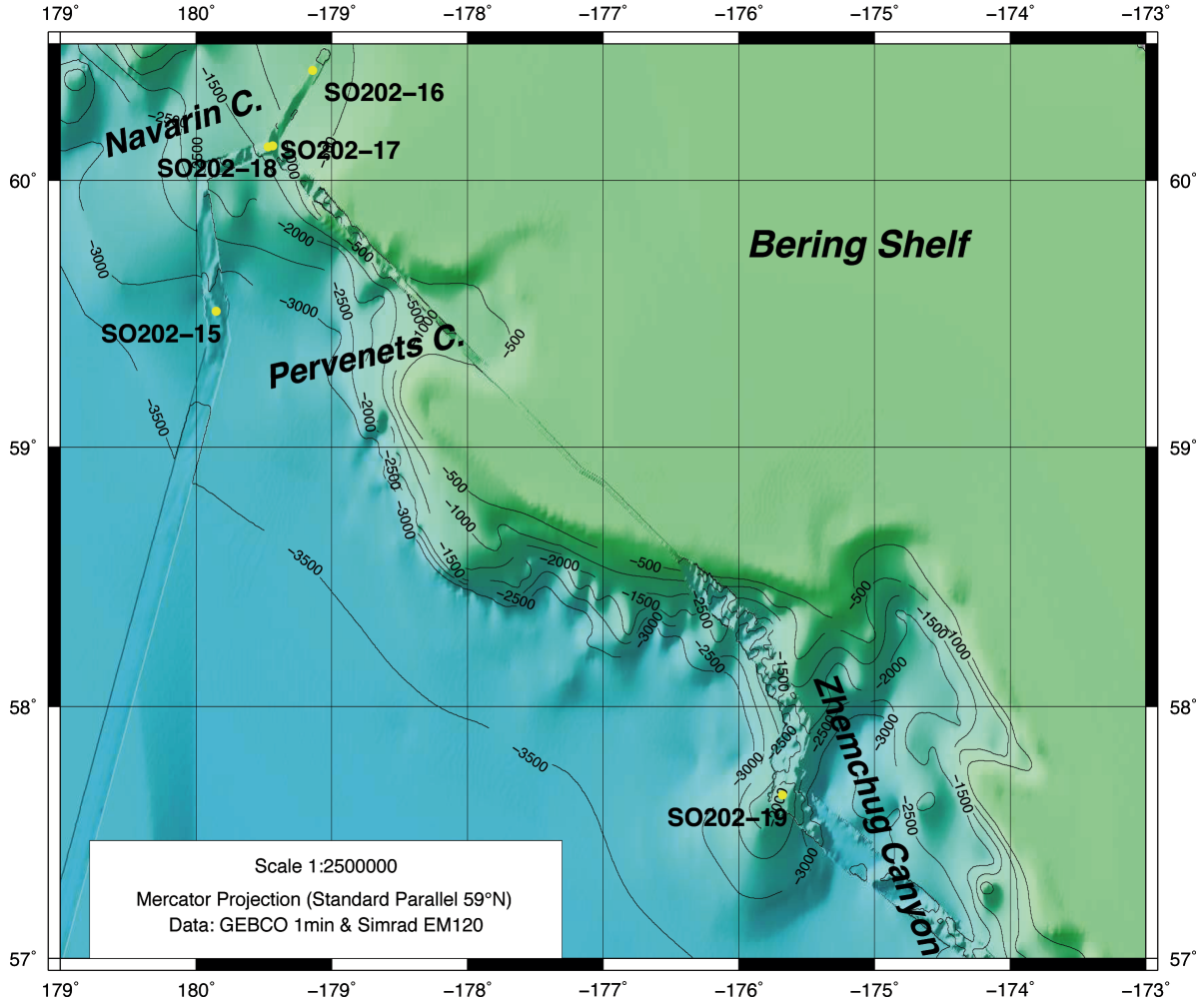

Fig. 1.2-7: *Northern Bering Slope with Navarin, Pervenets and Zhemchug Canyon and location of SO202-INOPEX sites. Bathymetric data include GEBCO 1min and SO202 survey with SIMRAD EM120.*

Survey and sampling on our way along the Bering Slope towards the Unimak Passage (July 25 – 28) was facilitated by perfect weather conditions. Although visibility was generally low due to fog and drizzle, low wind speeds resulted in a very calm sea. Water and sea surface temperatures ranged between 7 and 9°C (**Fig. 1.2-4**). On this way sampling of the water column and the sediment was accomplished at Site SO202-19, located at 1750 m water depth on a small ridge bounding the

Zhemchug Canyon (**Fig. 1.2-7**) to its North. The canyon is reported to represent one of the largest known submarine canyon systems (Normark and Carlson, 2003). This was followed by the sampling of a depth transect in the southeastern Bering Sea between 2980 m (SO202-20) and 1480 m (SO202-22) on the Umnak Plateau. The bathymetric survey in this region results in generally lower water depth compared with the GEBCO (1 min) data set (**Fig. 1.2-8**).

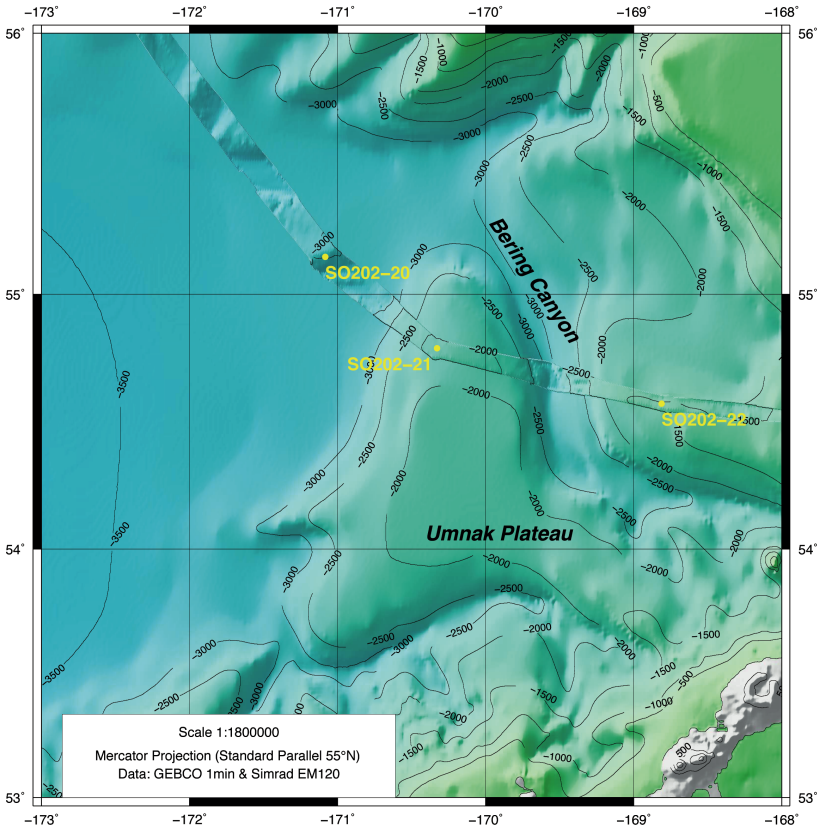

Fig. 1.2-8: *Southern Bering Slope, Umnak Plateau with Bering Canyon and location of SO202-INOPEX sites. Bathymetric data include GEBCO 1min and SO202 survey with SIMRAD EM120.*

At Site SO202-22, located East of the Bering Canyon the third kasten core was deployed in the Bering Sea. This resulted in a 9.69 m long large volume core, which can be combined with a 22.18 m long piston core recovered at the same site where PARASOUND shows a penetration of ca. 125 m (**Fig. A.6-22**). The kasten core SO202-22-4 contains two laminated intervals between 2.40 m and 2.94 m (**Fig. A.5-6a, b**)
R/V *Sonne* reentered the Subarctic Pacific via the Unimak Pass in the night of July 28/29. After crossing the Aleutian Trench, station work was continued on the eastern flank of Sirius Seamount at a water depth of 4600 m (SO202-23, **Fig. 1.2-9**), where PARASOUND indicated well-stratified sediments with prominent reflectors (**Fig. A.6-23**). This was the first site located in the realm of the Alaska Current, which results from a northward diversion of the warm North Pacific Current (**Fig. 1.3-1**). En route to the Patton Seamounts in the northeastern SAP, the sediments deposited south of the Alaska Peninsula have been sampled at two other sites. On August 1, 2009 the Northern topographic high of the Patton Seamounts was reached and a first sample site was occupied at a water depth of 740 m (SO202-26), were surface sediment and a short piston core could be recovered. The gathered sediments are rich in biogenic carbonate and paleoceanographic studies of the recorded planktic and benthic foraminifers may enhance knowledge on North Pacific intermediate water history

back into the last glacial. After some acoustic survey sampling of the Patton Seamounts was continued at two other sites at a water depth of 2900 and 3700 m, respectively. At the first of these sites (SO202-27) another kasten corer was deployed. The rather dense and carbonate rich sediments prevented deep penetration of the corer. Preliminary dating indicates that the base of this 2.91 m long core (**Fig. A.5-7**) is in the last glacial. The piston cores recovered at the Sites SO202-27 and -28 reach a length around 15 m and may document the past 300.000 years. The sites are close to the boundary of the U.S. EEZ, which was left on our further way with southward heading (**Fig. 1.2-2**).

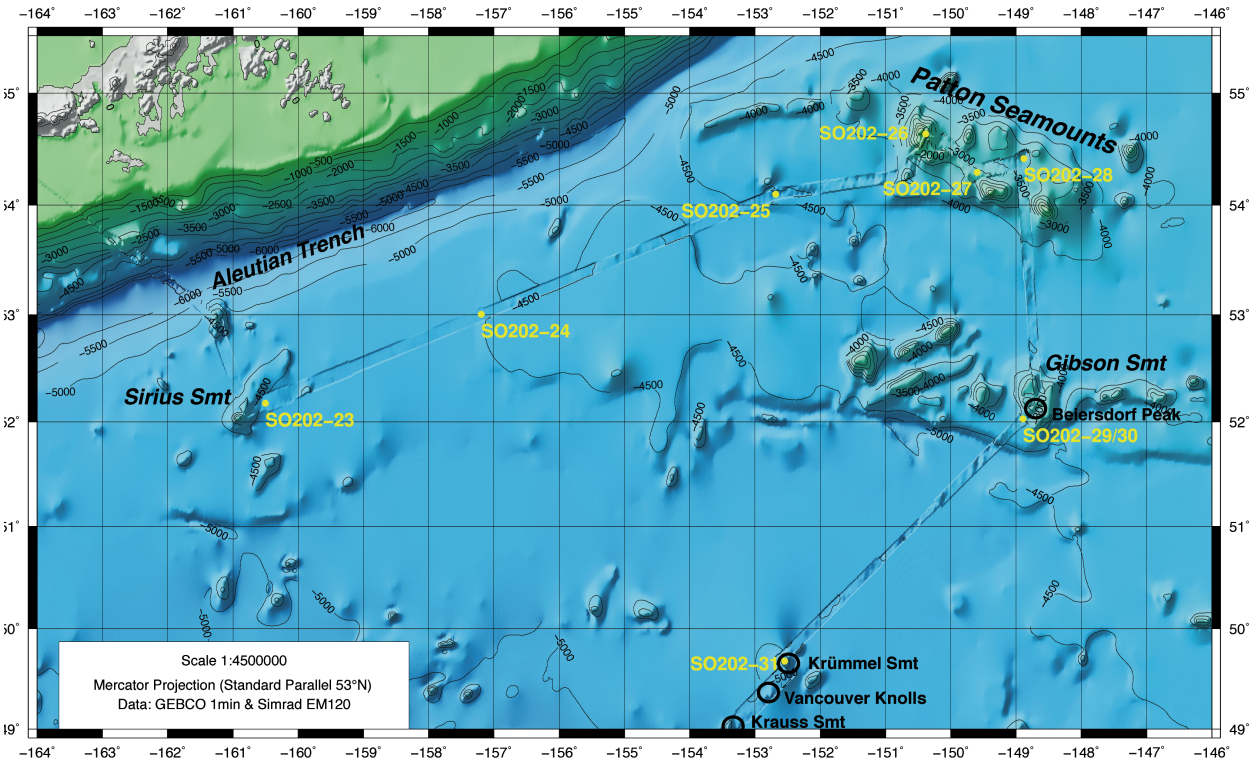

Fig. 1.2-9: *Northeastern Subarctic Pacific Basin with Sirius Seamount, Patton Seamounts, Gibson Seamount and newly named undersea topographic structures (encircled). The name Beiersdorf Peak is yet not approved by GEBCO (see **Table 1.2-1**) . Also indicated locations of SO202-INOPEX sites. Bathymetric data include GEBCO 1min and SO202 survey with SIMRAD EM120.*

August 3 the Gibson Seamount was reached, where the PARASOUND survey revealed a penetration of ca. 70 m and topographic structures with outcropping older sediments (**Figs. A.6-29, -30a,b**). Besides sampling of the water column (upper 1000 m) and the surface sediments (12 multicorer tubes), two piston cores were recovered at Site SO202-29 at a water depth of 3980 m. The nearby Site SO202-30 is located at the upper portion of a submarine outcrop, which allowed sampling of stratigraphically older sediments that may be as old as 900.000 years. It was proposed to name an isolated topographic structure in this area Beiersdorf Peak **(Fig. 1.2-9, Table 1.2-1),** but this has yet not approved been approved by GEBCO.

August 5 another so far unnamed seamount was visited and the opportunity was taken to recover further carbonate-bearing sediment deposited at the flank of this structure at a water depth of 3750 m (**Fig. A.6-31**). Surrounding this structure, the bathymetry of other undersea features was mapped (see 2.1.3) to generate the

baselines to propose new names for the seamounts. The names of three features, Krümmel Seamount, Vancouver Knolls and Krauss Seamount have been accepted by the GEBCO Sub-Committee on Undersea Feature Names **(Fig. 1.2-9, Table 1.2-1).**

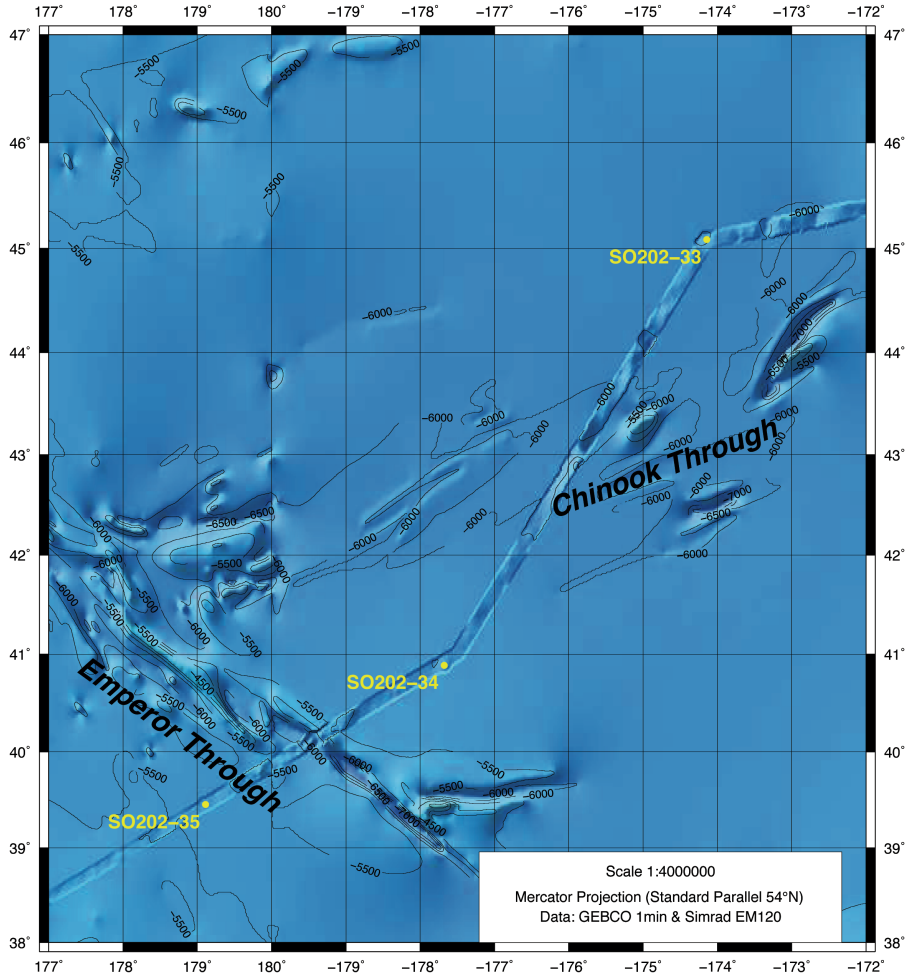

Fig. 1.2-10: *Central Subarctic Pacific Basin with Chinook Trough, Emperor Trough and location of SO202-INOPEX sites. Bathymetric data include GEBCO 1min and SO202 survey with SIMRAD EM120.*

At Site SO202-32 located in the abyssal plain (5300 m) the station work in the eastern Subarctic Pacific was completed and heading was set to the westerly direction. Station work was continued after a longer transit across the abyssal plan and the eastern extension of Chinook Trough where the PARASOUND survey did not indicate the presence of corable sediment. Site SO202-33 located north of Chinook Trough was the deepest (6160 m) sampled during the cruise **(Fig. 1.2-10)**. Sediment-echosounding revealed a penetration of >100 m (**Fig. A.6-33**). Preliminary biostratigraphic dating of the 22.70 m long core recovered at SO202-33 indicates the presence of a continuous section reaching back to >4 Ma (see 8.1). This makes core SO202-33-4 possibly the oldest of all cores recovered during SO202-INOPEX. Together with other low-resolution records recovered on the central SAP (SO202-32-4, SO202-34-5) the core will allow for additional studies of the paleoceanographic changes in the SAP related with the onset of Northern Hemisphere glaciation around 2.7 Ma (Haug et al. 2005).

After crossing Chinook Trough two other deep sites were sampled north and south of Emperor Trough (**Fig. 1.2-10**) before the shallower waters of northern Hess Rise were attained on late April 13. On the southwest-ward transit towards Hess Rise the sea surface and air temperatures started to increase to values >16°C north of Emperor Trough (April 11/12) (**Fig. 1.2-11**), when the Oyashio Current and the Subarctic Front was reached (**Fig. 1.3-1**).

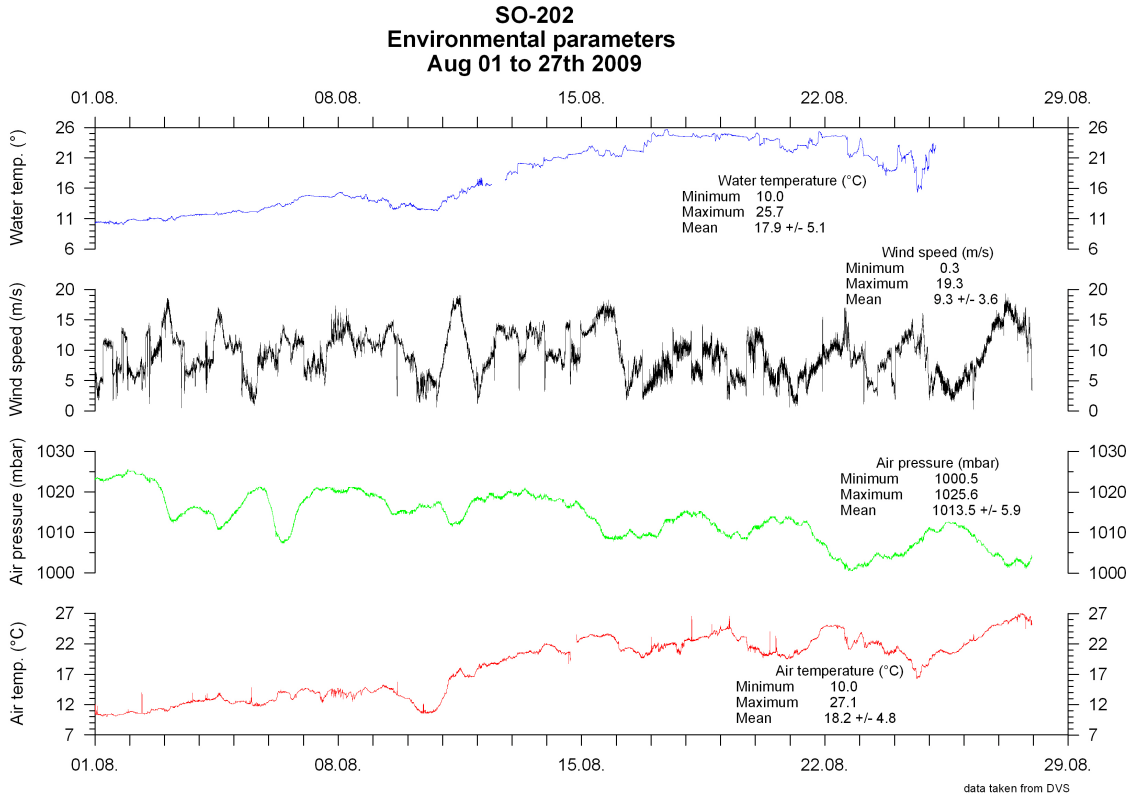

***Fig. 1.2-11**: Surface water temperature, wind speed, air pressure and air temperature as monitored by ships sensors between August 1 and 27, 2009.*

On the northward extension of Hess Rise, a large plateau in the central North Pacific, a deep (4525 m, SO202-36) and a shallower (3568 m, SO202-37) site were occupied to sample the water column and the sediments (**Fig. 1.2-12**). SO202-37 represents the most southerly site (37°46´N) sampled during SO202-INOPEX (**Fig. 1.2-1**) and locates close to the eastward flowing warm North Pacific Current (**Fig. 1.3-1**). Here the longest sediment core (SO202-37-2, 24.35 m) was recovered with a 30 m long piston corer. Preliminary dating indicates that basal age of the core, which contains besides biogenic opal significant amounts of carbonate, is >1 Ma and thus records the transition of the 40 kyr to the 100 kyr-World.

After completion of SO202-37 on August 14, R/V *Sonne* headed westward towards another large topographic structure, the Shatsky Rise. On the way the Ojin Guyot, which belongs to the Emperor Seamount Chain was crossed (**Fig. 1.2-12**). The PARASOUND survey did not reveal corable sediment on this volcanic structure. Before Shatsky Rise was reached sampling was continued at two deep sites with water depth >5000 m. In this area PARASOUND penetration was >100 m (**Figs. A.6-38, -39**). Preliminary dating of the 22.67m and 20.23 m long core obtained at SO202-38 and –39 indicate that the base of the cores is close to the Plio-/Pleistocene boundary. These cores may document the history of bottom water flow from the South.

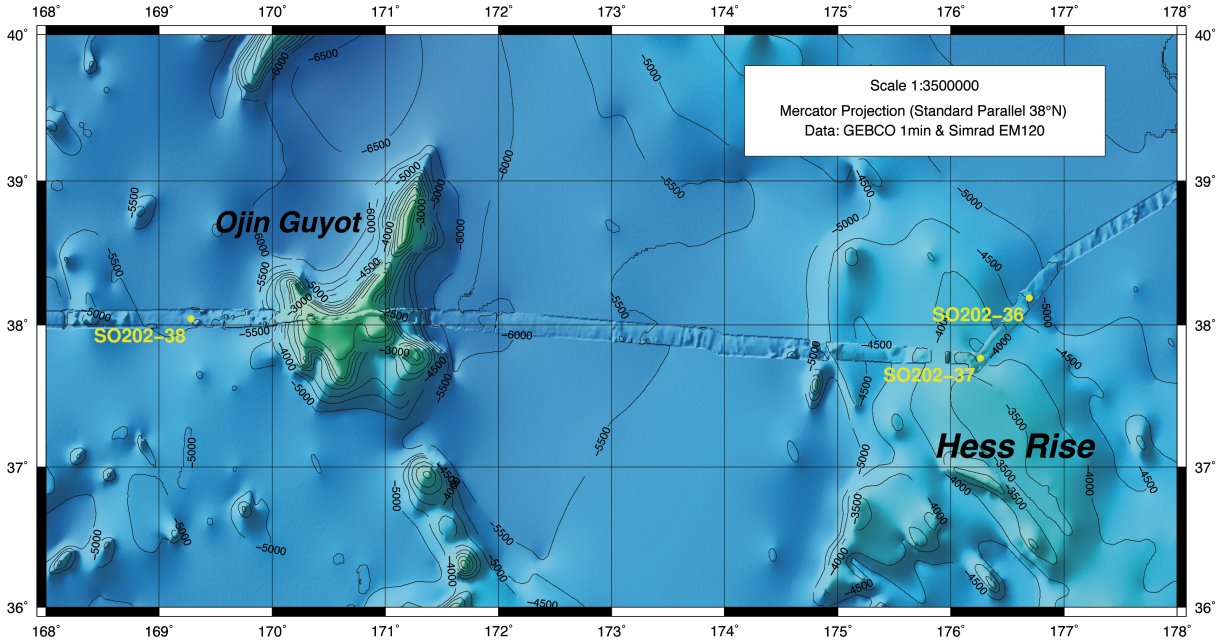

Fig. 1.2-12: *Central North Pacific Basin with northern Hess Rise (SO202-36, -37), Ojin Guyot and location of SO202-INOPEX sites. Bathymetric data include GEBCO 1min and SO202 survey with SIMRAD EM120.*

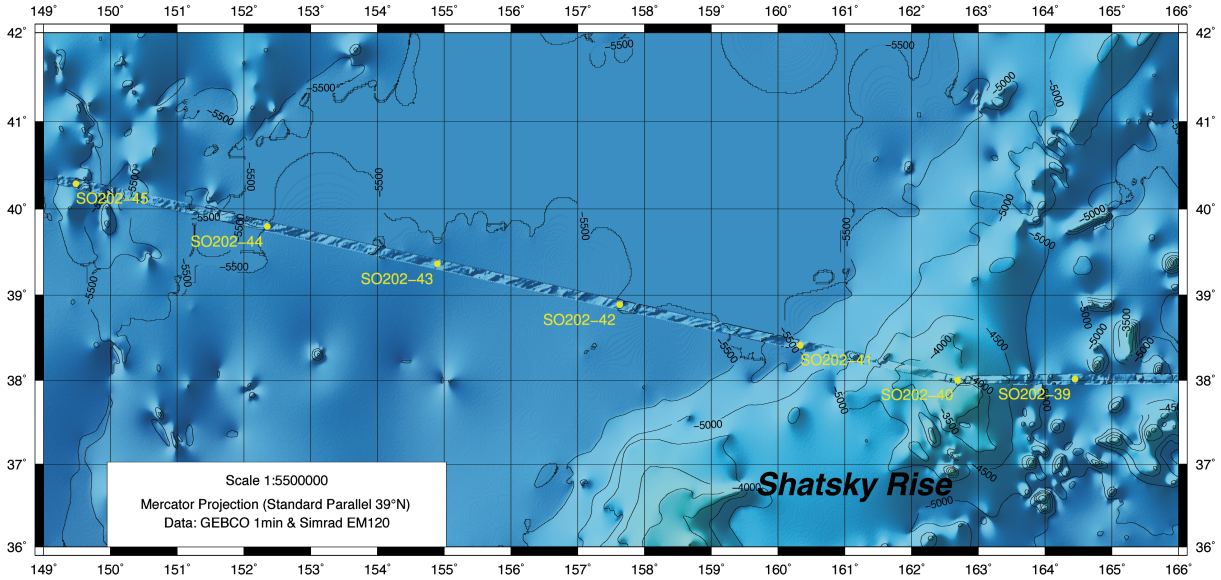

Fig. 1.2-13: *Western North Pacific Basin with northern Shatsky Rise (Shirshov Massif, SO202-40) and location of SO202-INOPEX sites. Bathymetric data include GEBCO 1min and SO202 survey with SIMRAD EM120.*

The volcanic Shirshov Massif, representing the northern extent of Shatsky Rise was reached on August 18 and the sediment was sampled on a sediment drift (**Fig. A.6-40**) at a water depth of 3446 m (SO202-40). The obtained core with a length of 15.38 m presumably documents the paleoceanographic record back into the Early Pleistocene. The last five sites were occupied on the way towards the Tsugaru Strait, which separates the Japanese Hokkaido and the Honshu Islands. These sites are at water depths between 5400 and 5670 m, all located along the Subarctic Front. The last site SO202-45 located in the Oyashio Current completes the NE-SW transect along the Kuril-Kamchatka Trench (**Fig. 1.2-1**). Station work was finished on August

23, at 12:11 h UTC. The Tsugaru Strait was passed late August 24 – early August 25 and the port of Busan (Korea) was reached in the morning of August 28, where SO202-INOPEX ended.

1.3 Summary of SO202-INOPEX Outcome

The surveys and sampling completed during SO202-INOPEX will fully allow for the accomplishment of all scientific studies proposed for the INOPEX project. Favorable weather conditions during all days of the cruise have permitted the bathymetric (SIMRAD EM120) and sediment-echosounding (PARASOUND P70) survey along the cruise track and the sampling of the water column and the sediments at a total of 45 sites.

The acoustic survey along 6677 nm provides new insight in North Pacific and Bering Sea bottom topography at high accuracy and allows for a refinement of the GEBCO maps. For six seamount/guyot structures mapped in more detail new names have been proposed to GEBCO. The names of five structures located in the eastern and western North Pacific have yet been accepted. The PARASOUND survey was fundamental for the understanding of the sediment distribution in the visited working areas and the selection of appropriate sediment sample sites.

Despite the loss of one piston corer device at the first site and a winch that operated at restricted velocity especially at deep-water sites the sediment sampling was unexpectedly successful. Only at one out of the 40 deployments of the multicorer no sediment was recovered, possibly due to strong water velocities in the realm of the Oyashio Current, which prevented the vertical lowering of the instrument. At most sites the maximum of 12 multicorer sediment cores was recovered, which summed up to a total of 444 multicorer-cores (**Table 1.3-1**). This new set of high-quality surface sediment covers a broad range of environmental settings (temperature, salinity, productivity, sea ice, water depths) and will allow for a series of studies including

- the generation/enhancement of paleobiological (diatoms, radiolarians, dinoflagellates) and geochemical (e.g. alkenone, TEX_{86}, C25-HBI) reference data sets for proxy development and paleoenvironmental reconstructions; the documentation/mapping of biogenic and terrestrial component fluxes in the Subarctic Pacific and Bering Sea;
- the documentation of ^{14}C reservoirs;
- the reconstruction of Holocene paleoceanography.

Sediment coring at 44 sites resulted in a total recovery (including trigger cores) of 862.15 m of sediment. Most of the obtained 50 cores, recovered primarily with a piston corer, exceed a length of 15 m. Recovery rates are generally between 80-90% **(Table 1.3-1)**. At five sites (three at locations in the Bering Sea and two on seamounts in the eastern and western Subarctic Pacific) large-volume cores could be gathered with the kasten corer in addition to the piston cores. These large-volume cores provide the appropriate sample material needed for multi-proxy studies at individual sample depths and for combined opal and carbonate isotope studies, as well as for ^{14}C dating.

Site	W. d. (m)	CTD bot	CTD+Fl (1000 m)	MN (1000 m)	PLA (100 m)	MUC	MUC tubes	KOL	KOL l. (m)	TC core (m)	KOL core (m)	Rec. (%)	SL	SL l. (m)	SL core (m)	Rec. (%)	KAL	KL l. (m)	KAL core (m)	Rec. (%)
SO202-1	5277	1				1	11	1	20	0.84	0.00	0.00								
SO202-2	4823		1	1	1	1	10	1	20	0.86	12.15	60.75								
SO202-3	5428		1	1	1	1	12	1	20	0.99	15.56	77.80								
SO202-4	5273				1	1	12	1	15	0.51	11.80	78.67								
SO202-5	3369		1	1	1	1	12	1	15	0.77	10.01	66.73	1	10	1.26	12.60				
SO202-6	3426					1	12	1	15	0.77	13.70	91.33								
SO202-7	2350				3	1	12	1	20	0.64	17.97	89.85					1	11.5	4.77	41.48
SO202-8	3630					1	12	1	25	0.79	22.75	91.00								
SO202-9	5026		1	1	1	1	12	1	25	0.97	23.01	92.04								
SO202-10	1470		1	1	1	1	12	1	25	0.63	22.63	90.52								
SO202-11	2703					1	12	1	25	0.45	22.96	91.84								
SO202-12	2109					1	12	1	25	0.69	23.17	92.68					1	11.5	10.69	92.96
SO202-13	1382		1	1	1	1	12	1	15	0.27	6.58	43.87								
SO202-14	3821		1	1	1	1	12	1	20	0.67	17.97	89.85								
SO202-15	3129		1	1	1	1	12	1	25	0.70	23.43	93.72								
SO202-16	548					1	7													
SO202-17	1066							1	25	0.10	18.15	72.60								
SO202-18	1111		1	1	1	1	11	1	25	0.05	18.49	73.96					1	11.5	7.21	62.70
SO202-19	1752		1	1	1	1	11	1	25	0.35	19.97	79.88								
SO202-20	2984							1	25	0.40	22.58	90.32								
SO202-21	1911					1	11	1	25	0.86	21.80	87.20								
SO202-22	1482		1	1	1	1	11	1	25	0.53	22.18	88.72					1	11.5	9.69	84.26
SO202-23	4615		1	1	1	1	12	1	20	0.00	17.76	88.80								
SO202-24	4573	1				1	12	1	20	0.05	17.27	86.35								
SO202-25	4596					1	11	1	20	0.92	17.75	88.75								
SO202-26	748					1	7	1	15	0.00	1.82	12.13								
SO202-27	2921		1	1	1	1	11	1	20	0.91	15.66	78.30					1	11.5	2.92	25.39
SO202-28	3709					1	12	1	25	1.00	14.59	58.36								
SO202-29	3991		1	1	1	1	12	1	15	0.98	12.97	86.47								
SO202-29	3983							1	20	0.75	16.83	84.15								
SO202-30	4043							1	20	0.58	17.81	89.05								
SO202-31	3746		1	1	1	1	10	1	15	0.20	10.54	70.27								
SO202-32	5300	1	1	1	1	1	12	1	15	0.95	13.94	92.93								
SO202-33	6159		1	1	1	1	12	1	25	0.91	22.70	90.80								
SO202-34	5724		1	1	1	1	12						1	18	15.83	87.94				
SO202-35	5581												1	20	19.29	96.45				
SO202-36	4525	1	1	1	1	1	12	1	25	0.92	23.00	92.00								
SO202-37	3568					1	11	1	30	0.77	24.35	81.17								
SO202-38	5501					1	12	1	25	0.95	22.67	90.68								
SO202-39	5102	1				1	11	1	25	0.95	20.23	80.92								
SO202-40	3446					1	12	1	25	0.96	15.38	61.52								
SO202-41	5395	1				1	12	1	25	0.94	22.71	90.84								
SO202-42	5537	1				1	11	1	25	0.92	22.18	88.72								
SO202-43	5670							1	25	0.92	21.27	85.08								
SO202-44	5497	1	1	1		1	0	1	25	1.00	21.42	85.68								
SO202-45	5476					1	12	1	25	0.76	21.60	86.40								
		8	**20**	**20**	**23**	**40**	**444**	**43**		**29.18**	**761.31**	**79.37**	**3**		**36.38**	**65.66**	**5**		**35.28**	**61.36**

Table 1.3-1: *Summary of SO202-INOPEX work at sites including the number of deployments at each site. CTD bot: CTD+Rosette to bottom; CTD+Fl: CTD+Rosette and fluorometer to 1000 m depth; MN: multinet; PLA: plankton net; MUC: Multicorer; KOL: piston corer; KOL l.: length of corer; TC core: length of trigger core; KOL core: length of piston core; Rec.: recovery (%); SL: gravity corer; KAL: kasten corer.*

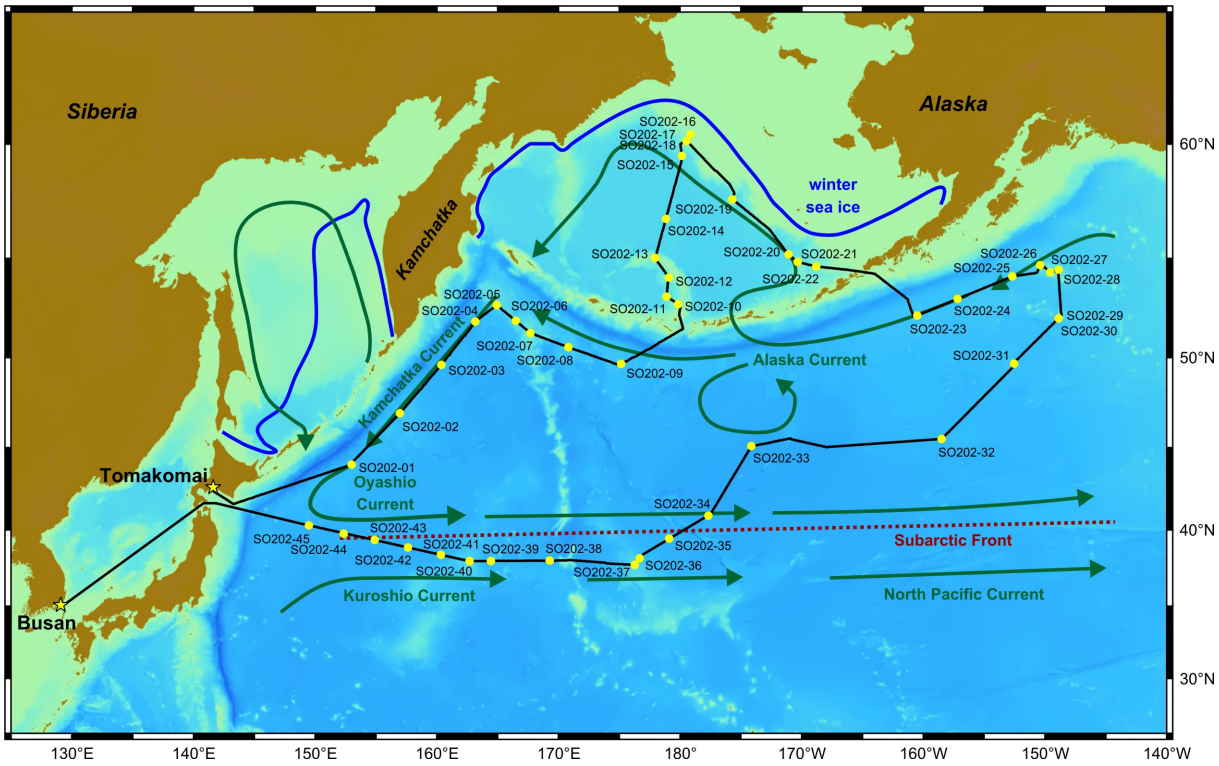

Fig. 1.3-1: *SO202-INOPEX cruise track, sample sites together with schematic representation of major current systems, the Subarctic Front and the winter sea ice edge. Information on currents and sea ice according to Dodimead et al. (1963) and Comiso (2003). Bathymetry according to GEBCO 1min.*

This is of special importance for the studies planned to reveal the nature and significance of the lamination recorded in Bering Sea sediment sections in water depth around 1000 m. The SO202-INOPEX sediments deposited at ultra-high (laminated sediments) to orbital time-resolution will allow for the completion of all scientific goals in all time windows proposed for INOPEX. As an example this will significantly improve the knowledge on the environmental conditions in the polar North Pacific and Bering Sea during the Last Glacial Maximum, which is still rather limited (e.g. Waelbroeck et al. 2009) and it will further elucidate the role of biological and physical processes in the study area on biogeochemical cycles, global climate and changes in atmospheric CO_2. The study of paleoceanographic contrasts between the western and eastern polar North Pacific will provide new insight in the role of Asian dust deposition on biological productivity during glacial periods. The water mass history can be studied on depth transects cored in the Bering Sea (Bowers Ridge, northern Bering Slope, Umnak Plateau), the western Subarctic Pacific (Obruchev Rise-Detroit Seamount-Aleutian Rise), the eastern Subarctic Pacific (Patton Seamounts, with one site as shallow as 740 m) and on northern Hess Rise. Sediments have been recovered in the realm of all North Pacific current systems, along the modern winter sea ice edge in the eastern Bering Sea, close to gateways between the Arctic Ocean and the Bering Sea, the Bering Sea and the North Pacific, and the Sea of Okhotsk and the North Pacific (**Fig. 1.3-1**).

The sites are aligned on a meridional transect across the central Bering Sea and the Subarctic Pacific between 60°N and 38°N, along the Bering Slope, along the Kuril-Kamchatka Trench and on a longitudinal transect east of Japan. Together with the

cores recovered south of Alaska the latter two core transects will improve knowledge on the deposition of ash and the tephrochronology in the polar North Pacific, as well as the deposition of dust originating in Asian deserts (e.g. the Taklamakan Desert).

SO202-INOPEX has successfully combined the geoscientific sampling with hydrological, biological and geochemical analyses of the water column to improve our understanding of present biological production processes and the generation of paleobiological and geochemical signals in the sediment record.

2. ACOUSTIC SURVEY

2.1 Bathymetric Survey with SIMRAD EM120

Tanja Dufek, Cornelia Heinzl, Ann-Kathrin Rohardt
Alfred Wegener Institute, Bremerhaven, Germany

2.1.1 Instrument Description

The multibeam sonar system SIMRAD EM120 (Kongsberg) is permanently installed on R/V *Sonne*. The system transmits 191 beams per ping as narrow as 1° with an operating frequency of 12 kHz. The angular coverage sector can be set up to 150°. Thus a maximum swath width of 5.5 times the water depth can be achieved.

Echo sounders calculate the water depth by runtime measurement of the acoustic signal, which is transmitted and again received by the transducer mounted underneath the vessel. Therefore information about the water sound velocity is very important to obtain bathymetric data in high quality.

2.1.2 Work at Sea

Bathymetric mapping with SIMRAD EM120 was conducted during SO202-INOPEX along 6677 nm. It was monitored during data acquisition to ensure high-resolution measurements. The bathymetric data was used to provide the scientists on board with precise depth information and bathymetric charts of research areas. Furthermore the global bathymetric datasets of GEBCO (The General Bathymetric Chart of the Ocean, version 2.0, 2008, 2009) with bin sizes of 1 arc minutes and 30 arc seconds were used to generate charts with the open-source software GMT (Generic Mapping Tool, Wessel and Smith 1995) of research areas or for visualization with Fledermaus (Version 7.0, IVS) for detailed cruise planning.

The bathymetric data acquisition was started on the 9th of July at 23:00 UTC after leaving the Exclusive Economic Zone (EEZ) of Japan. The system was switched off again on the 28th of August at 13:26 UTC before reentering the Japanese EEZ.

The SIMRAD fan opening angle can be set to automatic mode so that the system adapts the swath width according to the water depth. During SO202-INOPEX the opening angle was monitored 24 hours and adjusted manually to the particular conditions (e.g. water depth, topography, movement of the vessel) from 90° to 140°. Approaching shallower waters a larger swath width was chosen because of smaller errors in the outer beams due to the shorter propagation distance of the signal. The recorded water depths ranged between 57 m (Aleutian Shelf) and 7340 m (Aleutian Trench). Approaching areas of very shallow waters (< 100 m) such as on the Aleutian Shelf and the continental shelf of Alaska, the data quality was poor. In some flat areas of the Bering Sea (4000m) and deeper areas with rough topography like in the fraction zone in the Northern Pacific (6000m) the SIMRAD data showed many errors. In order to minimize these blunders the fan aperture angle and the depth range were narrowed.

During SO202-INOPEX CTD (Conductivity Temperature Depth) measurements down to the seafloor were carried out. This information was used for calculating the sound velocity for the water column and entered into the echosounder system by the System-Manager on board. All together six CTD measurements from SO202-INOPEX and one from the previous R/V *Sonne* cruise SO201-1b were used to obtain water sound velocity information for high quality depth measurements (**Fig. 2.1.2-1**).

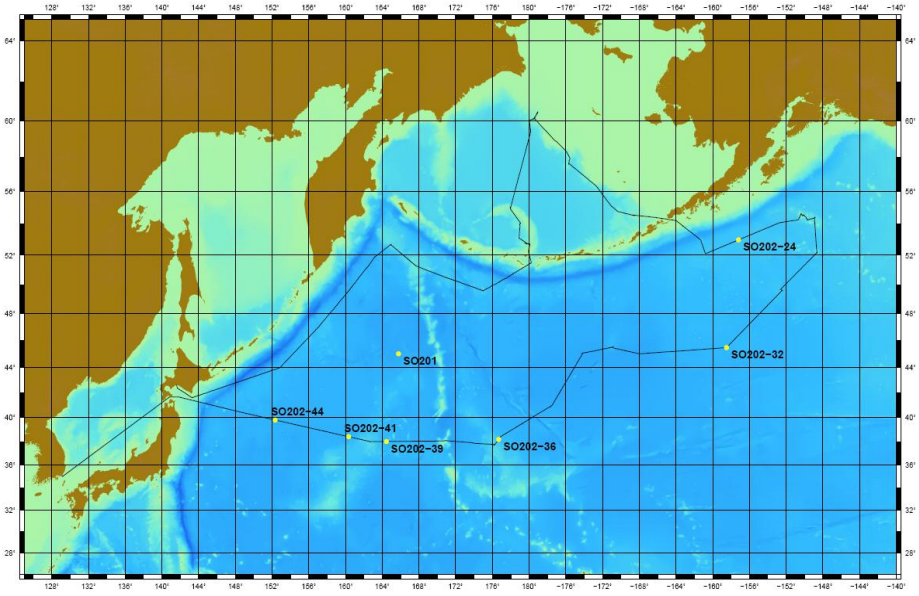

Fig. 2.1.2-1: *Locations of CDT casts used for sound velocity calibration.*

The recorded data were exported once a day in files of one-hour duration. It was checked manually for blunders in navigation and was cleaned from wrong depth measurements with the CARIS HIPS and SIPS 6.1 software. The edited data was exported as ASCII-format and further used for generating bathymetric charts with GMT or visualization in Fledermaus 7.0.

The data showed larger standard deviation in the outer beams as is typical for multibeam echo sounders. Furthermore systematic errors in the middle of the swath were regularly observed.

Rare system crashes occurred mainly due to failures of connected sensors (e.g. GPS, salinity sensor) and could quickly be fixed by restarting the software with the help of the system manager. This way large losses of data were avoided.

2.1.3 Results and Discoveries

During the cruise multibeam data was recorded in the Russian Federation and U.S. EEZ and in international waters. This data was controlled and processed on board. It was used on board for providing the scientists with precise depth information and bathymetric charts of the research areas. Furthermore the collected data will be contributed to the global bathymetric dataset GEBCO for further improvement.

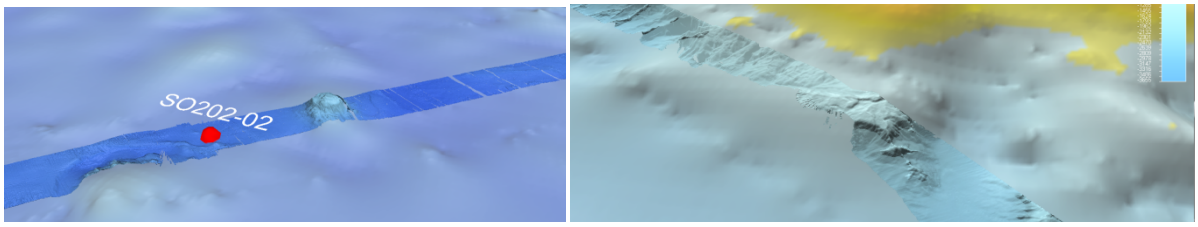

***Fig. 2.1.3-1**: Examples for differences of GEBCO and SIMRAD data*

During data acquisition and processing differences in the seafloor topography between GEBCO and the collected SIMRAD EM120 data became obvious. Some new seamounts were mapped and new names were proposed (**Table 1.2-1**). This includes Svarichevskiy Seamount (**Fig. 2.1.3-2**) and Billings Seamount (**Fig. 2.1.3-3**), both located off the Kurile-Kamchatka Trench (**Fig. 1.2-3**), and Krümmel Seamount (Fig. 2.1.3-4), Vancouver Knolls (**Fig. 2.1.3-5**) and Krauss Seamount (**Fig. 2.1.3-6**), all located in the NE-Pacific basin (**Fig. 1.2-9**). The names of the five undersea features have been accepted by GEBCO in 2010. Approval of the name of one other feature surveyed in the NE-Pacific (Beiersdorf Peak, **Fig. 2.1.3-7**) is still pending. Names of other undersea features (e.g. **Figs. 2.1.4-8, -9**) documented by SO202 bathymetric mapping have yet not been proposed. The bathymetric data are presented as day-by-day maps in Appendix A.7.

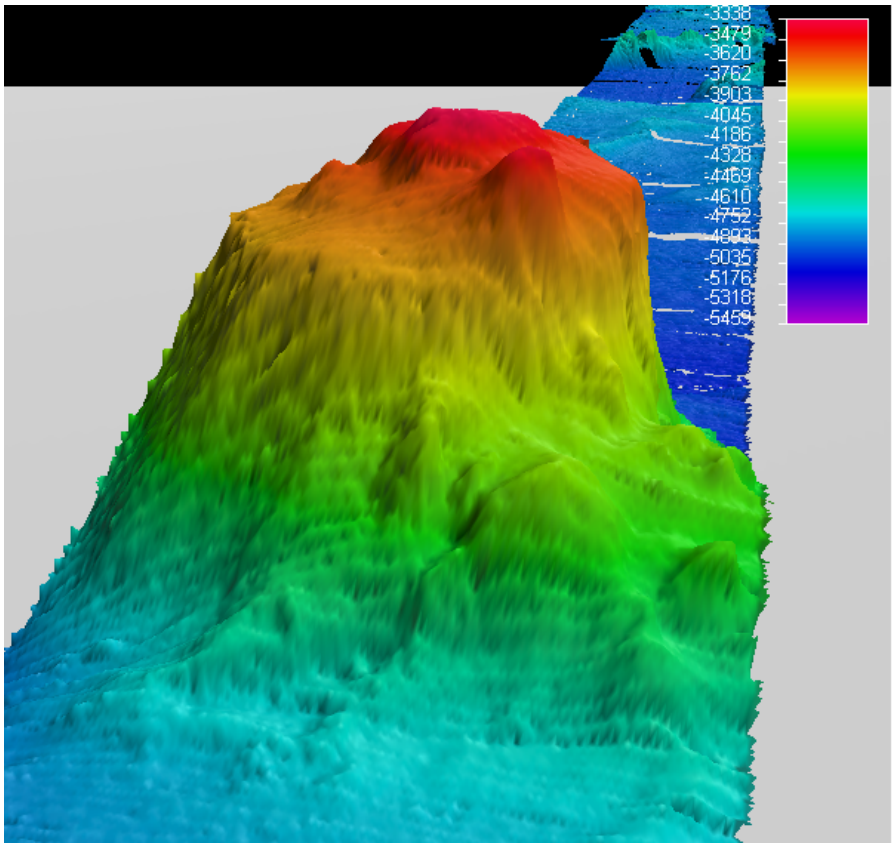

***Fig. 2.1.3-2:** 3-D representation (created with Fledermaus 7.0) of Svarichevskij Seamount off Kurile-Kamchatka trench, for location see **Fig. 1.2-3** and **Table 1.2-1**.*

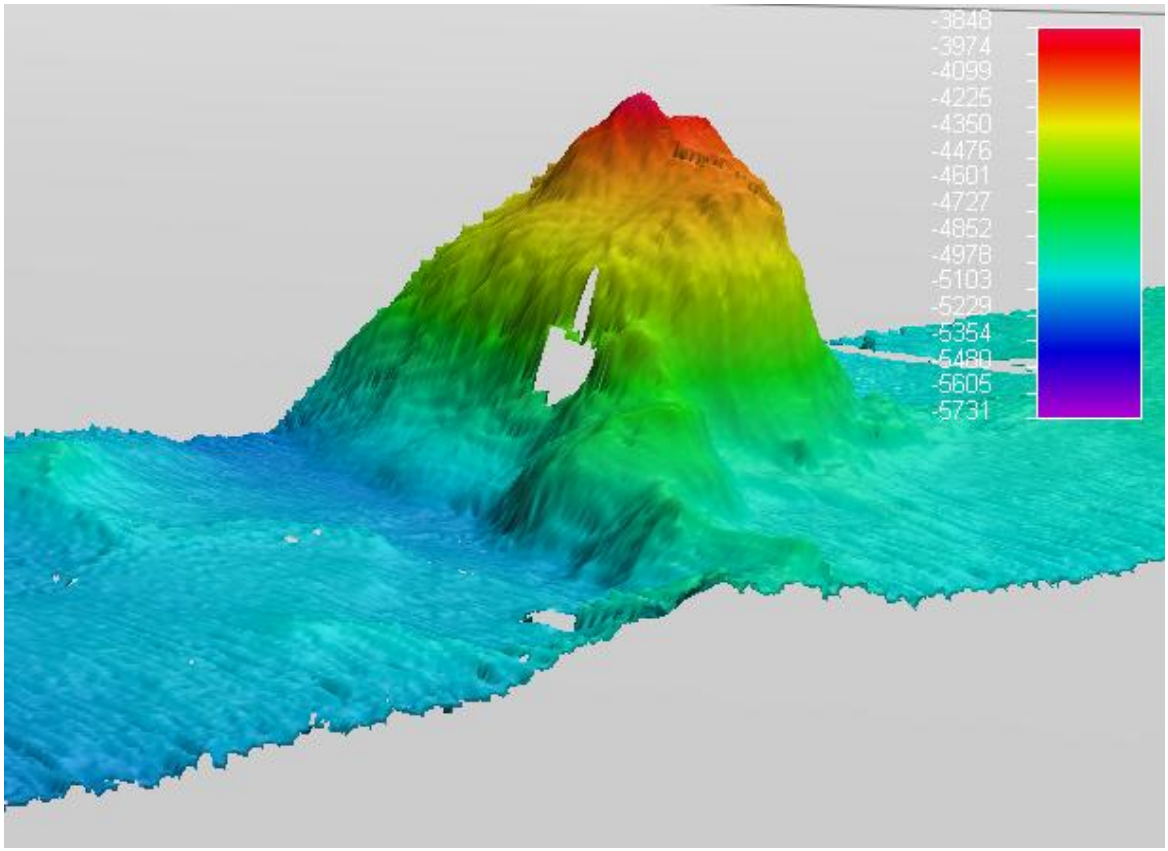

Fig. 2.1.3-3: *3-D representation (created with Fledermaus 7.0) of Billings Seamount off Kurile-Kamchatka trench, for location see* ***Fig. 1.2-3*** *and* ***Table 1.2-1****.*

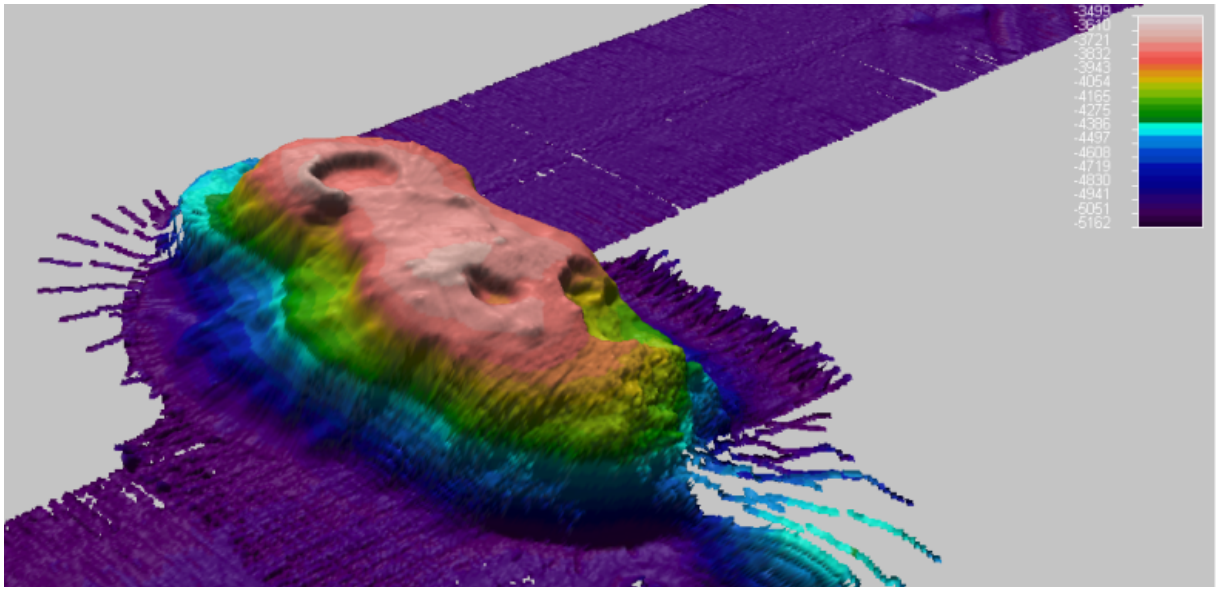

Fig. 2.1.3-4: *3-D representation (created with Fledermaus 7.0) of Krümmel Seamount in the NE Pacific Basin, for location see* ***Fig. 1.2-9*** *and* ***Table 1.2-1****.*

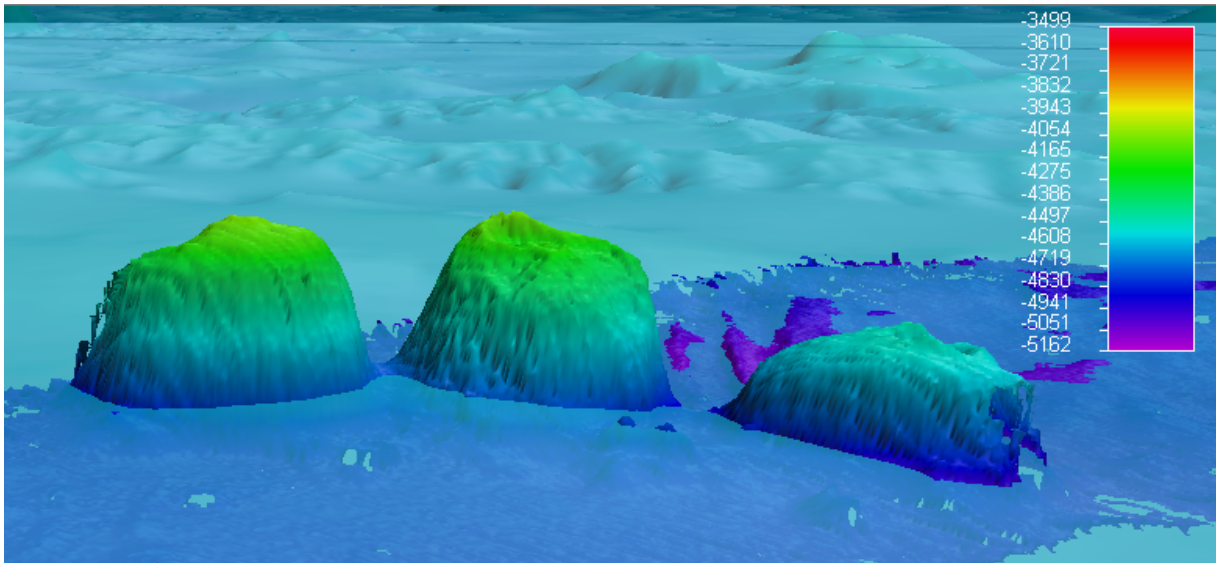

Fig. 2.1.3-5: *3-D representation (created with Fledermaus 7.0) of Vancouver Knolls in the NE Pacific Basin, for location see* ***Fig. 1.2-9*** *and* ***Table 1.2-1****.*

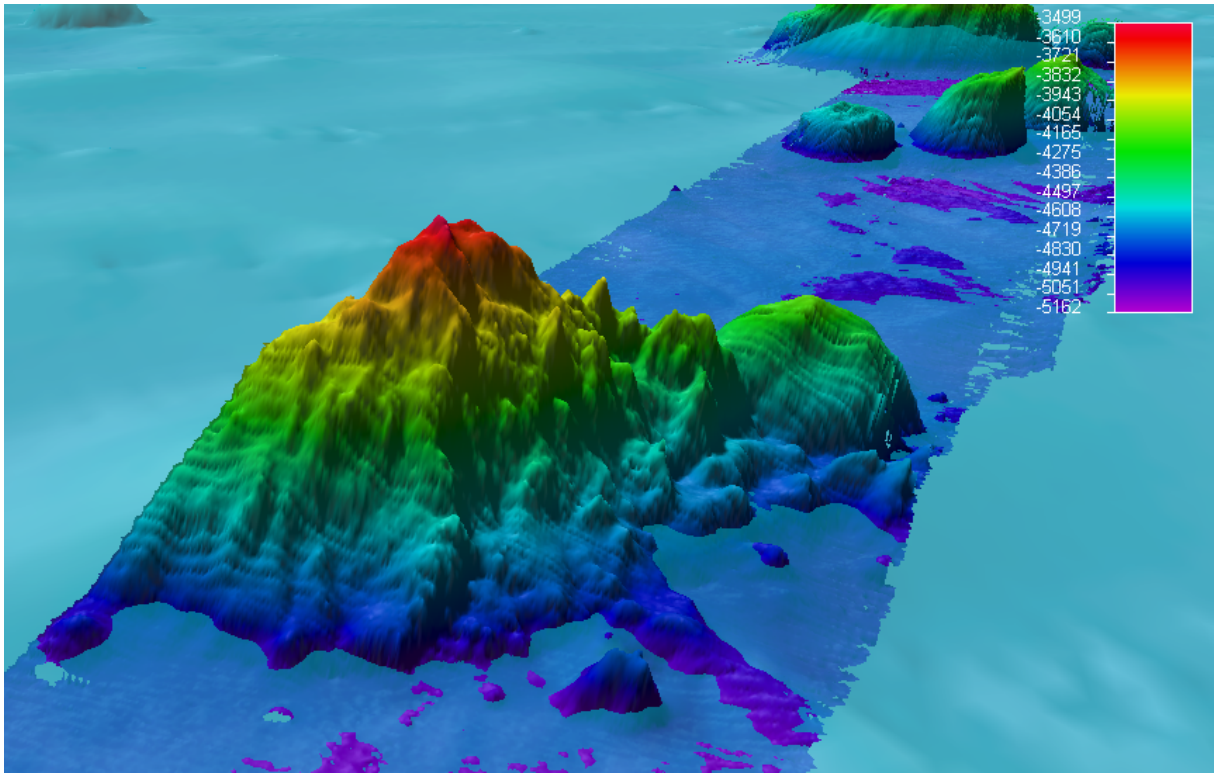

Fig. 2.1.3-6: *3-D representation (created with Fledermaus 7.0) of Krauss Seamount in the NE Pacific Basin, for location see* ***Fig. 1.2-9*** *and* ***Table 1.2-1****.*

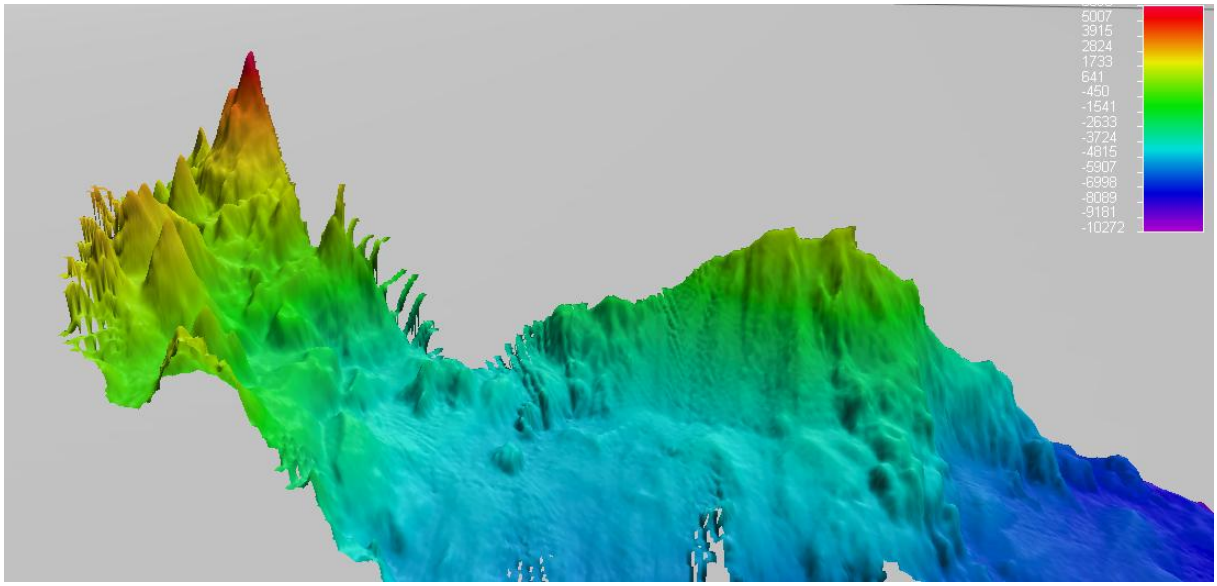

Fig. 2.1.3-7: *3-D representation (created with Fledermaus 7.0) of undersea feature surveyed in the NE Pacific Basin proposed to be named Beiersdorf Peak, for location see* ***Fig. 1.2-9*** *and* ***Table 1.2-1****.*

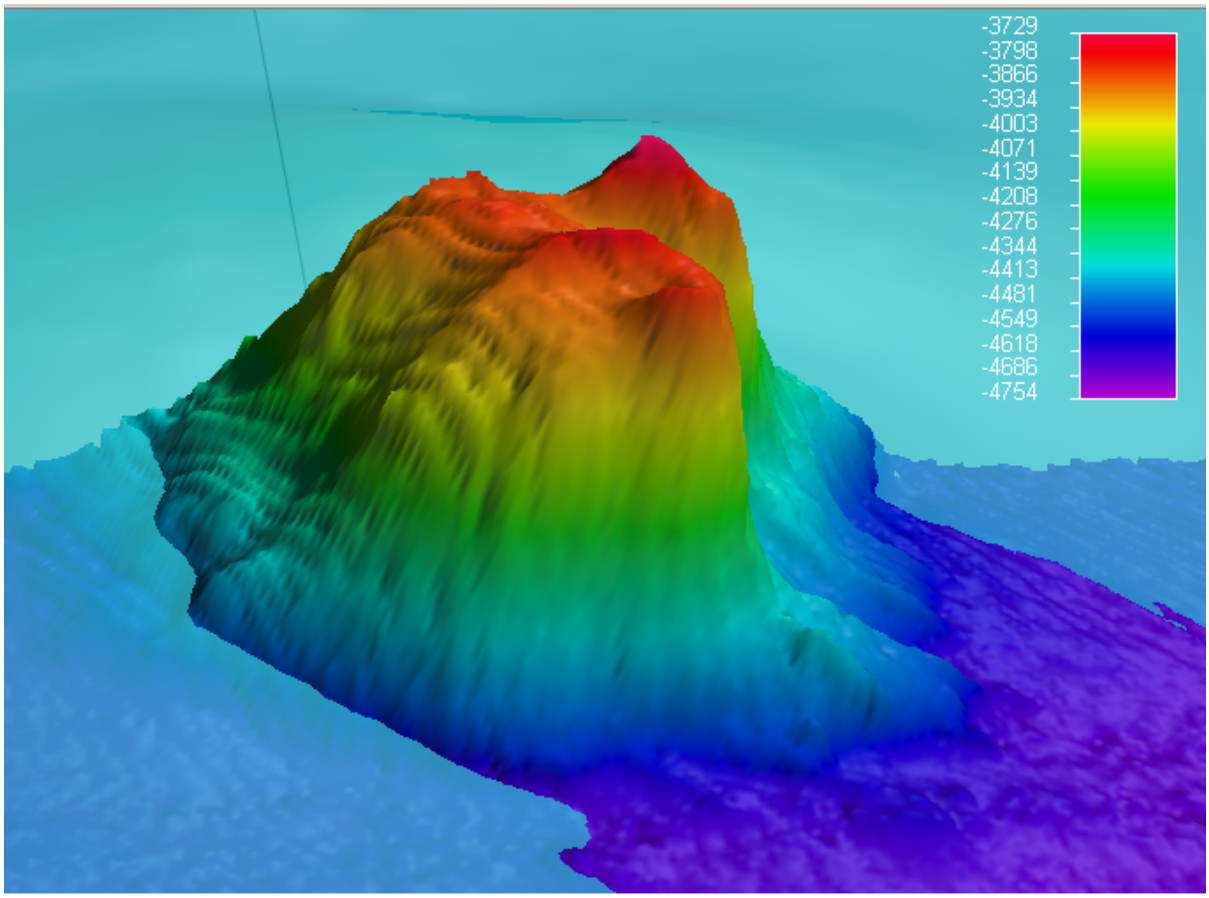

Fig. 2.1.3-8: *3-D representation (created with Fledermaus 7.0) of not fully mapped seamount surveyed on July 30, 2009 close to Sirius Seamount in the eastern Northern Pacific.*

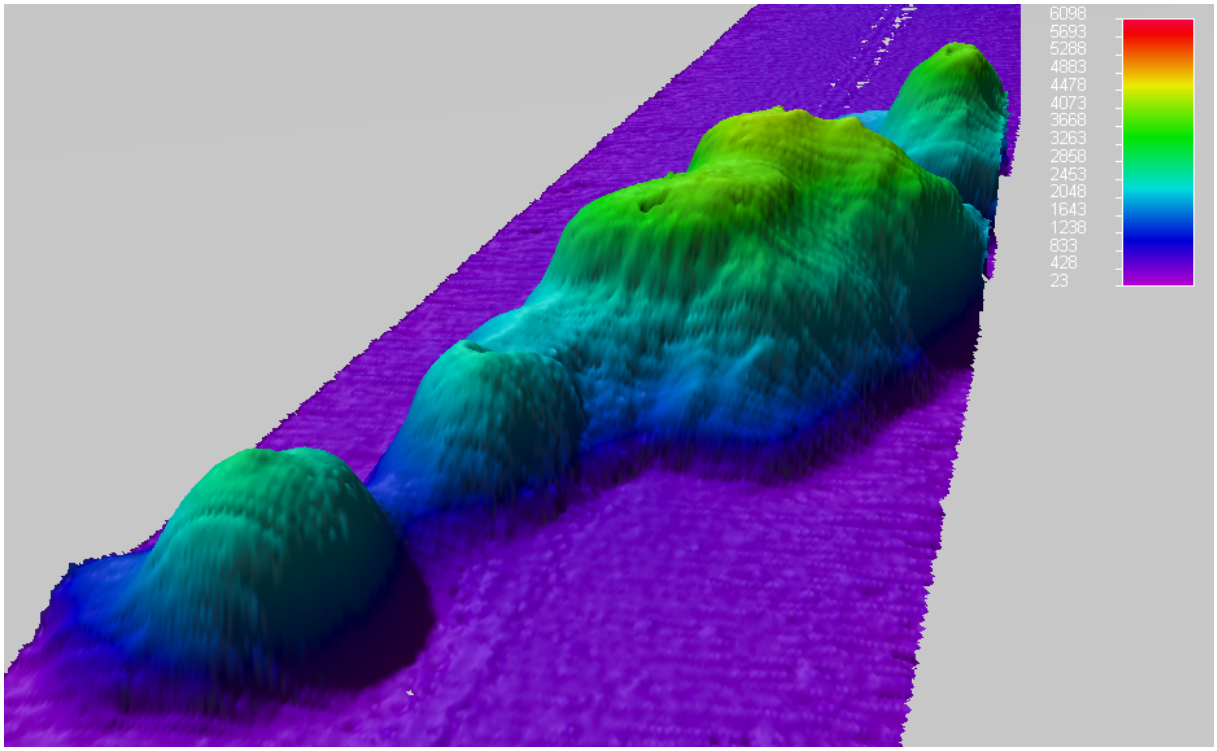

Fig. 2.1.3-9: *3-D representation (created with Fledermaus 7.0) of chain of volcanic structures mapped on August 8, 2009 around 47°18´S, 155°55´W (NE Pacific). These features are shown in the GEBCO map as soft rising (**Fig. A.7-27**)*

2.2 Sediment Echosounding with PARASOUND P70

Victor N. Karnaukh[1], Tanja Dufek[2], Cornelia Heinzl[2], Ann-Kathrin Rohardt[2]
[1]V.I. Il'ichev Pacific Oceanological Institute (POI) FEB RAS, Vladivostok, Russia
[2]Alfred Wegener Institute, Bremerhaven, Germany

2.2.1 Instrument Description

The sediment echo sounder PARASOUND P70 (ATLAS HYDROGRAPHIC, Bremen, Germany) is permanently installed on R/V *Sonne*. It observes sea floor and sub-bottom reflection patterns and thus characterizes the upper sediment layers according to their acoustic behavior.

Signals of lower frequency with longer wavelength possess good penetration but poor spatial resolution. On the other hand a high frequency signal with shorter wavelength results in a good spatial resolution but with shallow penetration. The aim is to utilize a signal, which combines both qualities of deep bottom penetration and high spatial resolution.

Therefore, PARASOUND P70 uses the parametric effect. It produces additional frequencies through non-linear acoustic interactions of finite amplitude waves. By emitting two primary sound waves of similar frequencies (during SO202-INOPEX 18 kHz and 22 kHz) simultaneously a signal of the difference frequency (4 kHz) is generated. This achieves a better bottom penetration than higher frequencies due to its longer wavelength. This new component is travelling within the emissions cone

(4°) of the primary high-frequency waves and reaches the high horizontal resolution of these as well as the deep sediment penetration of a low frequency

The PARASOUND system is operated by a software package, which consists of the control software for the echo sounder (*ATLAS HYDROMAP CONTROL*) and an acquisition and visualizing software for sediment profiles and water columns (*ATLAS PARASTORE*).

2.2.2 Settings and Data Storage

The PARASOUND P70 system combines a high-frequency deep-sea echo sounder for water depth sounding with a low-frequency sediment echo sounder. During SO202 SIMRAD EM120 was used for water depth sounding, and the difference frequency of 4 kHz (SLF – secondary low frequency) of PARASOUND P70 was used for sub-bottom profiling in order to find suitable coring locations. The primary high frequency (PHF) of 18 kHz was employed for seafloor detection for shifting the reception window of 200 m.

The acquired data was stored in the ASD, PS3 and SEG-Y formats. The ASD (Atlas Sounding Data) is a raw data file format and stores the complete sounding profiles including reflections from the water column, the seafloor and the subsurface echoes down to approximately 200 m for SLF and PHF. PS3 and SEG-Y only save data that is seen in the PARASOUND reception window whose range was set to 200 m. The PS3 data and the SEG-Y data were only stored for the SLF signal. Furthermore the auxiliary data storage was activated to save navigation and depth information for the duration of data acquisition. The record interval was set to one minute.

For signal transmission the quasi-equidistant transmission mode with a desired time interval of 500 ms was used. In some cases (e.g. steep slopes, tough ground layer) it was necessary to choose a larger time interval (2000 ms) or to change the transmission mode to single pulse in order to decrease the noise in the water column.

Because the SIMRAD depth was more accurate and stable than the PARASOUND depth the SIMRAD depth served as the system depth source. In cases of erroneous SIMRAD depths (as reported in 2.1.2) the system depth source was set to manual and entered by the operator to avoid PARASTORE crashes.

The reception window can be adjusted automatically or manually. However, automatic mode operation was mostly avoided because it could not recognize important sedimentary features and caused system crashes. Thus the system was manually controlled 24 hours a day by four operators who worked in six-hour shifts. The other cruise participants supported the operators as watch keepers in two-hour shifts.

While at station the system remained in sounding mode. To keep the data volume under control the transmission mode was changed from quasi-equidistant to single pulse and the waiting time from zero to 30 seconds. There was no watch keeping while the ship was at stations aside from half hour checks to ensure that the system was operating appropriately.

The data was post processed on-board by using the open-source software SeNT from the University of Bremen, Germany. PS3-files were used to create echograms of the sediments at each site. Resulting echographs for each site setting can be found in the Attachment A.6.

2.2.3 Problems

The bottom penetration of the SLF signal usually ranged according to sediment properties between 30 and 60 meters. Apart from some minor failures and one major crash the PARASOUND system worked smoothly during the entire cruise. Some PARASTORE crashes occurred and HYDROMAP CONTROL had to be restarted occasionally (e.g. loss of PHF or SLF depth for a longer duration). Loss of data could not be avoided during restarts.

The water depths obtained by the SLF and PHF signal were often unstable and offset from the SIMRAD EM120 depth by about 50 m. Occasionally larger discrepancies up to 200 meters were observed. By reducing the range of the depth finding window for the PARASOUND signals it could be adjusted to the more stable depth obtained by the SIMRAD system.

Losses of the return signal appeared within areas of greater water depths and over slopes steeper than 2°. In the North Pacific fracture zones, increased noise was observed especially in the PHF signal, which led to problems of seafloor detection. Simultaneously precise depth measurement of the SIMRAD EM120 system could be observed (2.1.2). A possible explanation might be the rough topography in combination with large water depth. The noise declined when the data acquisition time interval was increased.

2.2.4 Preliminary results of high-resolution subbottom profiling

The acoustic survey with the subbottom echosounder PARASOUND P70 allowed for continuous documentation of the upper sediment column along the cruise track with a penetration of up to 150 m, depending on the type of sediment, the water depth, the slope angle, the ship´s speed and weather conditions. In total, PARASOUND P70 operated over 6677 nm. This survey was fundamental for general understanding of the deposition pattern and nature of the uppermost sediments in the study area and for the selection of appropriate sediment sampling sites (see Appendix A.6).

The cruise track covered a large range of tectonic and sedimentary settings including the North Pacific abyssal plain, large volcanic plateaus (Hess Rise, Shatsky Rise), volcanic chains (e.g. Emperor Seamount Chain), isolated seamounts and seamount groups (e.g. Sirius Seamount, Vancouver Knolls), the full succession of structures of the island arc type of convergent margins along the Kurile-Kamchatka Trench and the Aleutian Trench, marginal sea basins (Alaskan Basin), continental slopes (Bering Slope) and continental shelf (Bering Shelf). Here we present a selection of PARASOUND-profiles and preliminary interpretations from a series of sites to show the large variety of sedimentary and tectonic settings visited during the SO202 cruise. (**Fig. 2.2.4**).

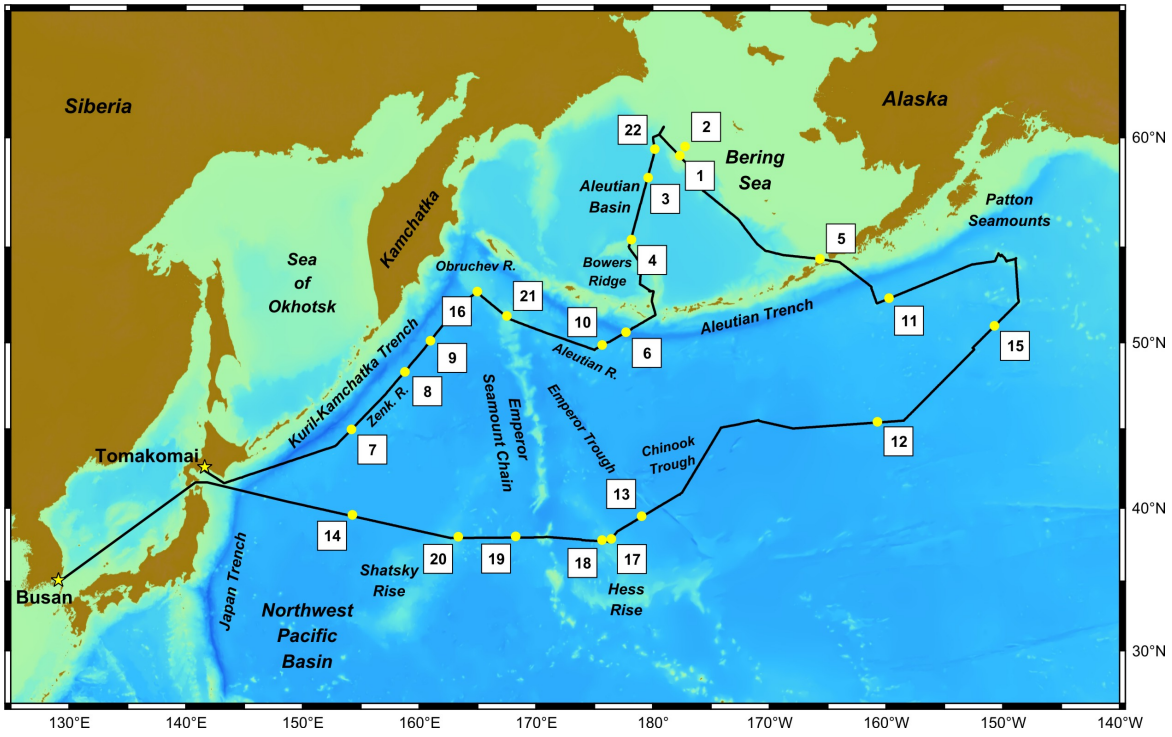

Fig. 2.2.4: *Overview of the PARASOUND profile positions shown in Chapter 2.2.4. The numbers **1** to **22** refer to the figures **2.2.4-1** to **2.2.4-22**.*

Shelf, slopes and basins in the Bering Sea

The uppermost sediment column deposited on the Bering Shelf consists of two acoustic units separated by an unconformity, which is marked by a high amplitude reflector. Probably, the unconformity was formed during the glacial last sea level fall. The upper acoustic unit is characterized by high frequency stratified reflectors with variable amplitudes. The lower unit is acoustically semi-transparent and contains continuous reflectors of variable amplitude (**Fig. 2.2.4-1**).

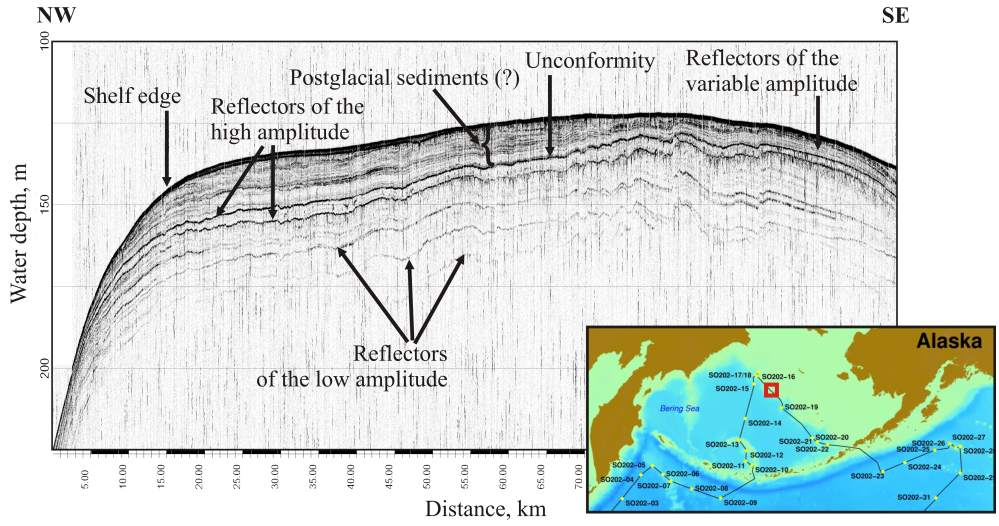

Fig. 2.2.4-1: *Bering Shelf profile close to shelf edge documenting two acoustic units separated by an unconformity.*

The acoustic structure of sediments deposited on the uppermost section of the Bering Sea continental slope is similar to the visited shelf area. The sediments at the

steep upper slope can be disturbed by gullies, sediment mass transport and slided or rotated sediment blocks. Sediment block sliding generates undersea outcrops of older sediment sequences, which can be sampled with coring instruments (**Fig. 2.2.4-2**). The lower portion of the slope is characterized by a series of transparent units, separated by thin units of continuous high or low amplitude reflectors. This setting may reflect the presence of debrite deposits (transparent units) intersecting normal sedimentation (**Fig. 2.2.4-3**).

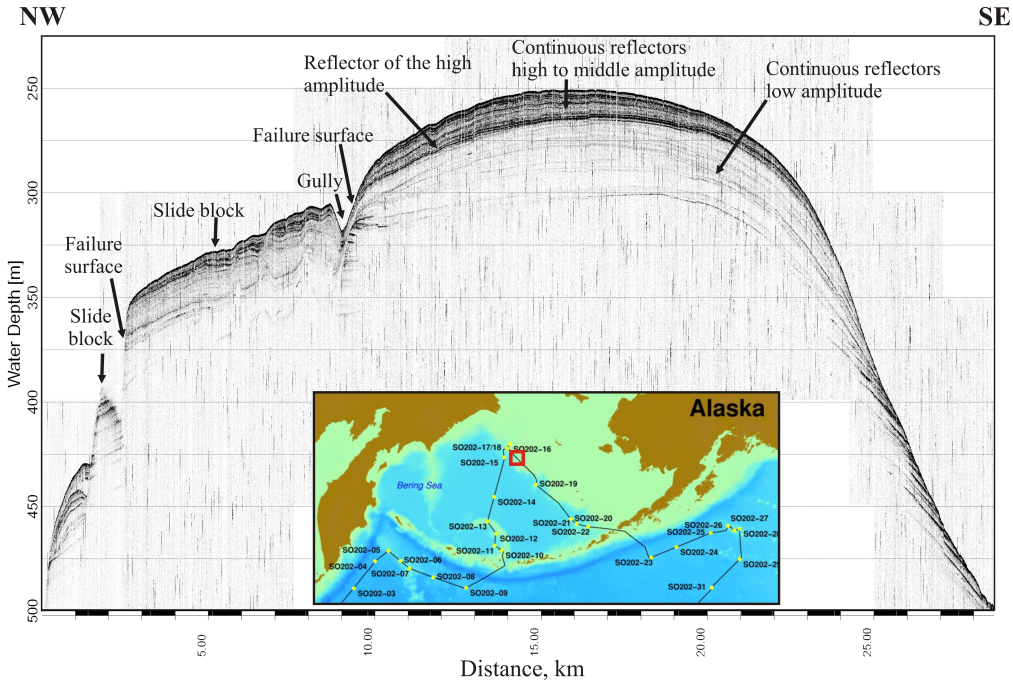

Fig. 2.2.4-2: *Structure of the upper part of the Bering Sea continental slope with sediment block slides.*

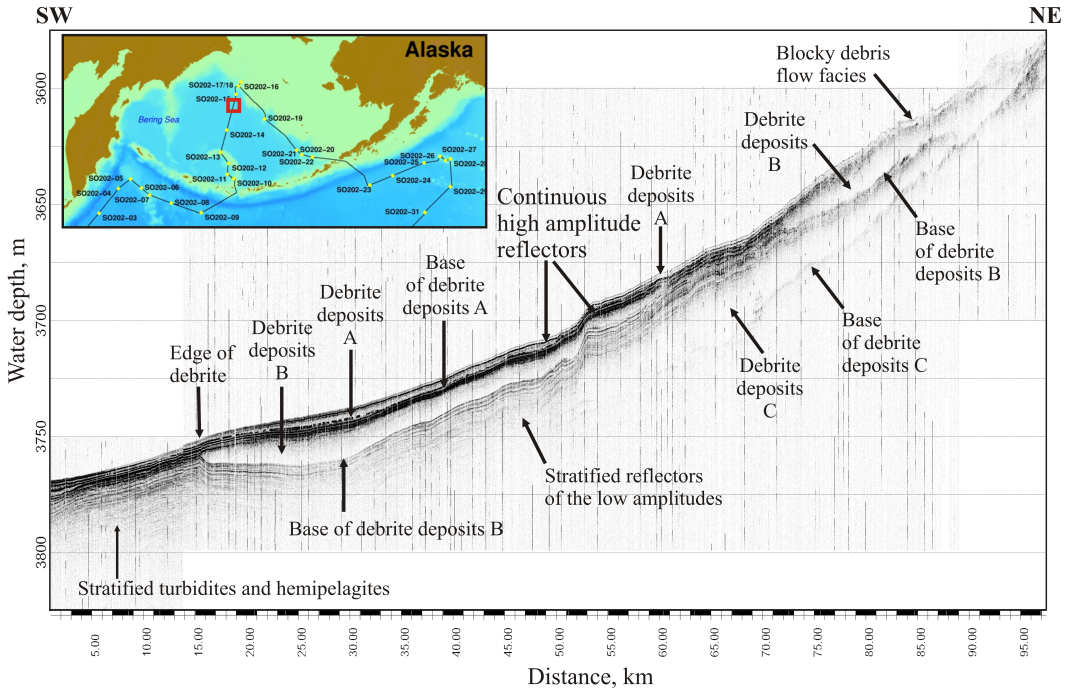

Fig. 2.2.4-3: *Profile across the lower part of the Bering Sea continental slope with a sequence of debrite deposits.*

Multiple debrite deposits are also present at the slope of the Bowers Ridge. The debrite layers are separated by rough boundaries of slumping origin. This pattern may be indicative of repeated periods of tectonic instabilities that cause distinct sediment disturbances at the Bowers Ridge Slope (**Fig. 2.2.4-4)**. In contrast, the acoustic structure of sediments deposited in the Aleutian Basin is characterized by flat sea floor and well-stratified sediments. The succession of reflectors with variable amplitude indicates the presence of turbidites alternating with pelagic and/or hemipelagic deposition. Near the base of the Bowers Ridge Slope a buried moat was recognized. This is indication of past changes in bottom water erosional activity causing the deposition of contourites.

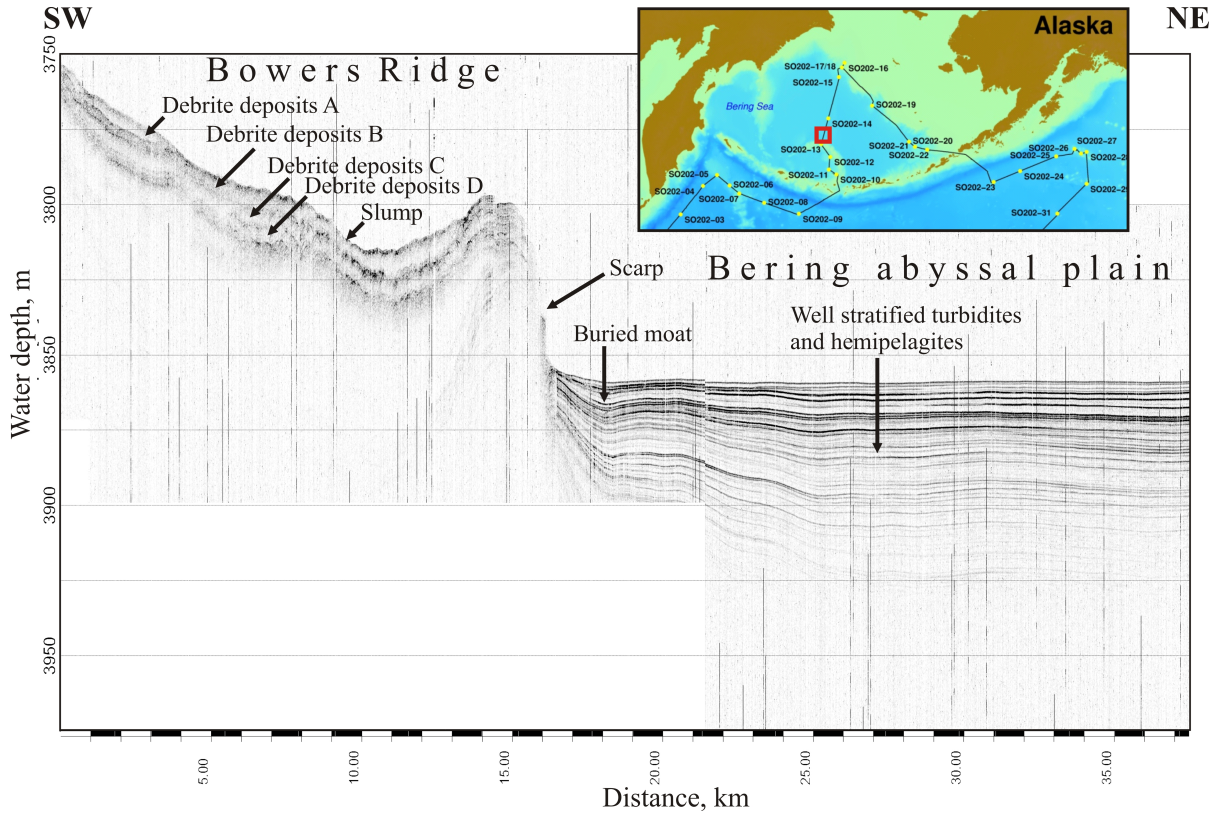

Fig. 2.2.4-4: *Northern Bowers Ridge slope with adjacent Aleutian basin*

Submarine structures and sediment deposits in conjunction with North Pacific island arcs and subduction zones

The submarine relief in the Unimak Passage, which represents the easternmost connection between the Bering Sea and the North Pacific, is characterized by intensive vertical indentation and strong erosion. This relief is formed by tectonic and volcanic activities in the Aleutian Island Arc but possibly also by erosion during the last glacial sea level low stand, which may have formed flattened surfaces on the tops of the topographic highs. Remaining sediments in the incisions show erosional events and disconformities (**Fig. 2.2.4-5**).

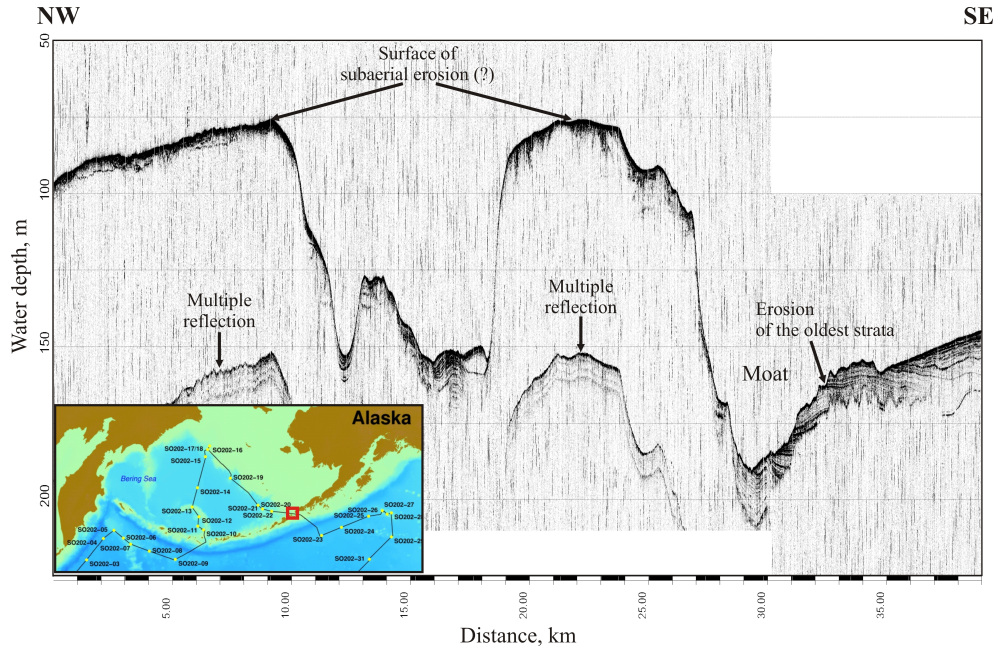

***Fig. 2.2.4-5**: Profile along the Unimak Passage (eastern Aleutian Island Arc) with distinct incisions and erosional structures.*

Sediments deposited in the deep sections of Aleutian Trench are characterized by successions of undeformed well-stratified reflectors separated by acoustically transparent layers with weak reflections. Generally, the thickness of the layers is approximately constant (**Fig. 2.2.4-6**), which points to sedimentation under conditions that are not disturbed by tectonic movements. It can be deduced from drilling results obtained at DSDP Site 186 (Creager et al. 1973) that the acoustically stratified layers are silty sediments with ash and transparent zones represent diatom ooze.

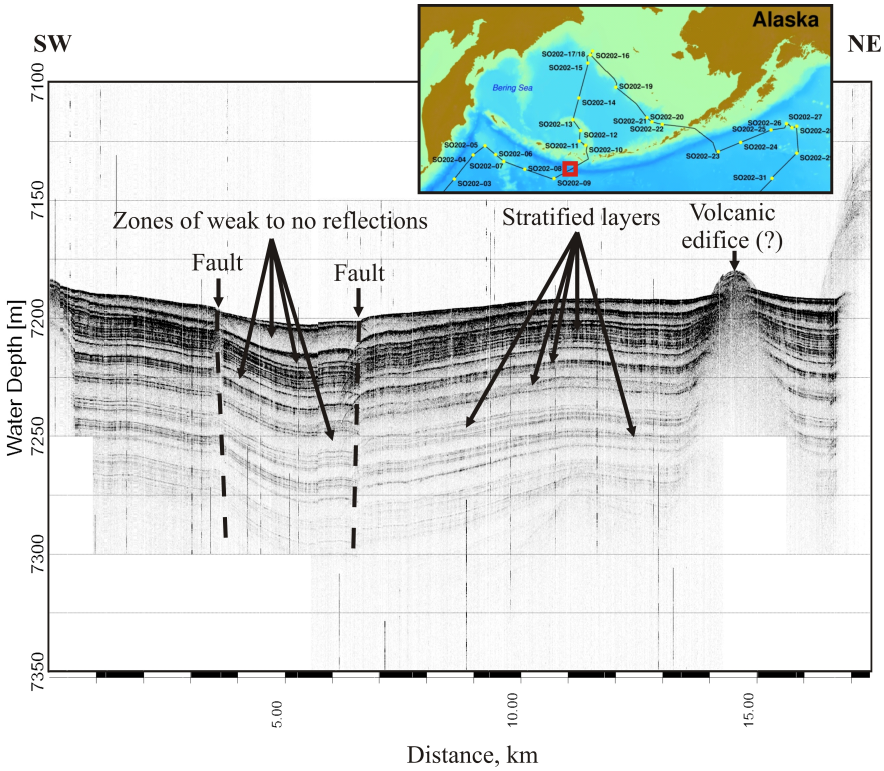

***Fig. 2.2.4-6:** Profile across the Aleutian Trench with mostly undisturbed sediment sequence.*

The border rises on the Pacific oceanic plate (Zenkevich Ridge along Kurile-Kamchatka Trench and Aleutian Rise along Aleutian Trench, **Fig. 2.2.4**) are characterized by different structural features. The southern part of the Zenkevich Ridge is characterized by a sequence of topographic elevations covered by stratified sediments without significant deformation (**Fig. 2.2.4-7**). However, slumps and slides may complicate the sediment structure at the slopes of the topographic highs. These structures can probably be associated with the raising of the ridge resulting from frontal convergence of the Pacific and the Okhotsk Plates. In contrast, the northern section of the Zenkevich Ridge is characterized by existence of an echelon of small ridges, which extend NE and oblique to the ridge strike over distances of up to 350 km (**Fig. 2.2.4-8**). These structures may result from a strike slip mode of convergence of the Pacific and the Okhotsk Plates. The small ridges usually are covered by wavy stratified sediments, deformed sediments with slumps and slides and rarely by undeformed stratified sediments. The existence of slumps and slides on the ridge slopes may be indicative of ongoing enhanced tectonic activity, growth of individual ridges and formation mass-transport deposits (**Fig. 2.2.4-9**). The acoustic and geometric characters and association with downslope slides and slumps on the steeper slopes suggest that the wavy stratified sediments were most probably formed by slow creep movements, as described by (Lee and Chough 2001).

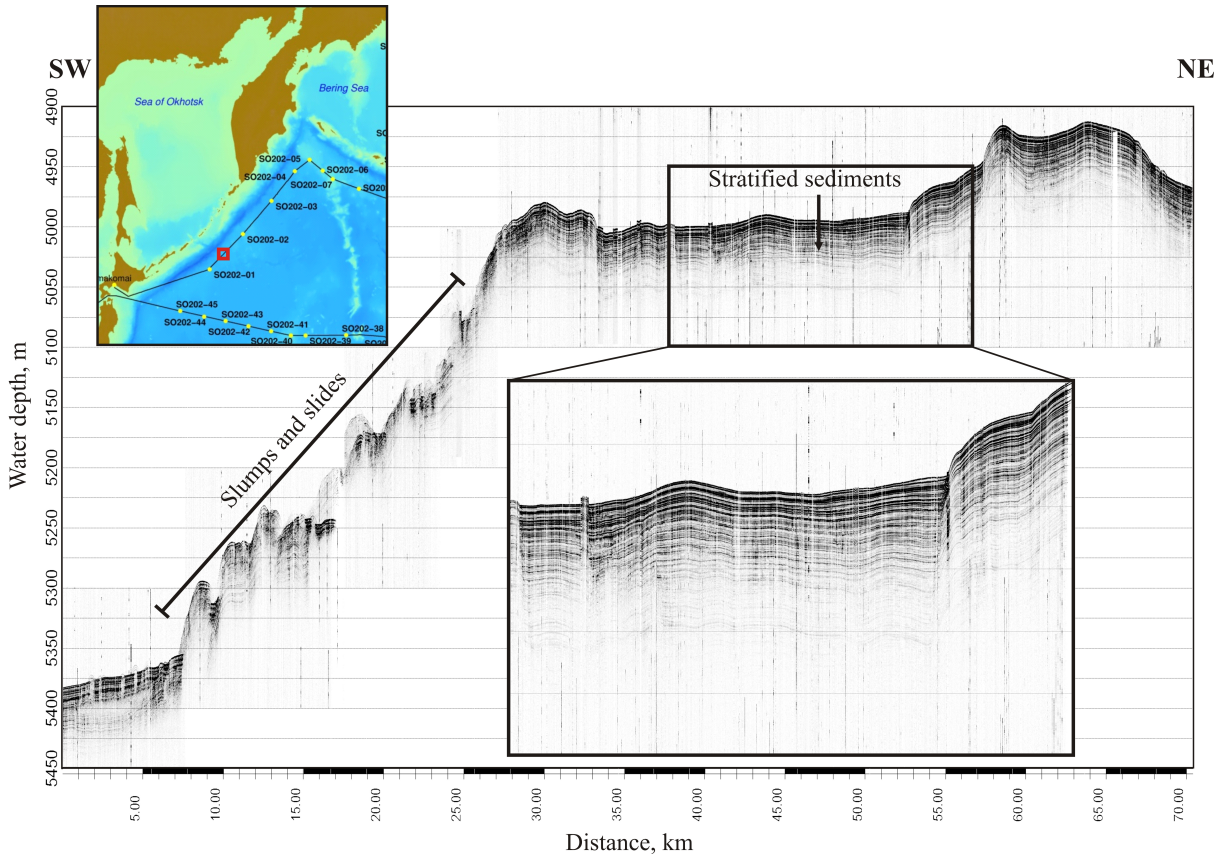

Fig. 2.2.4-7: *Profile along the southern part of the Zenkevich Ridge with continuously well-stratified and undeformed sediments on topographic highs.*

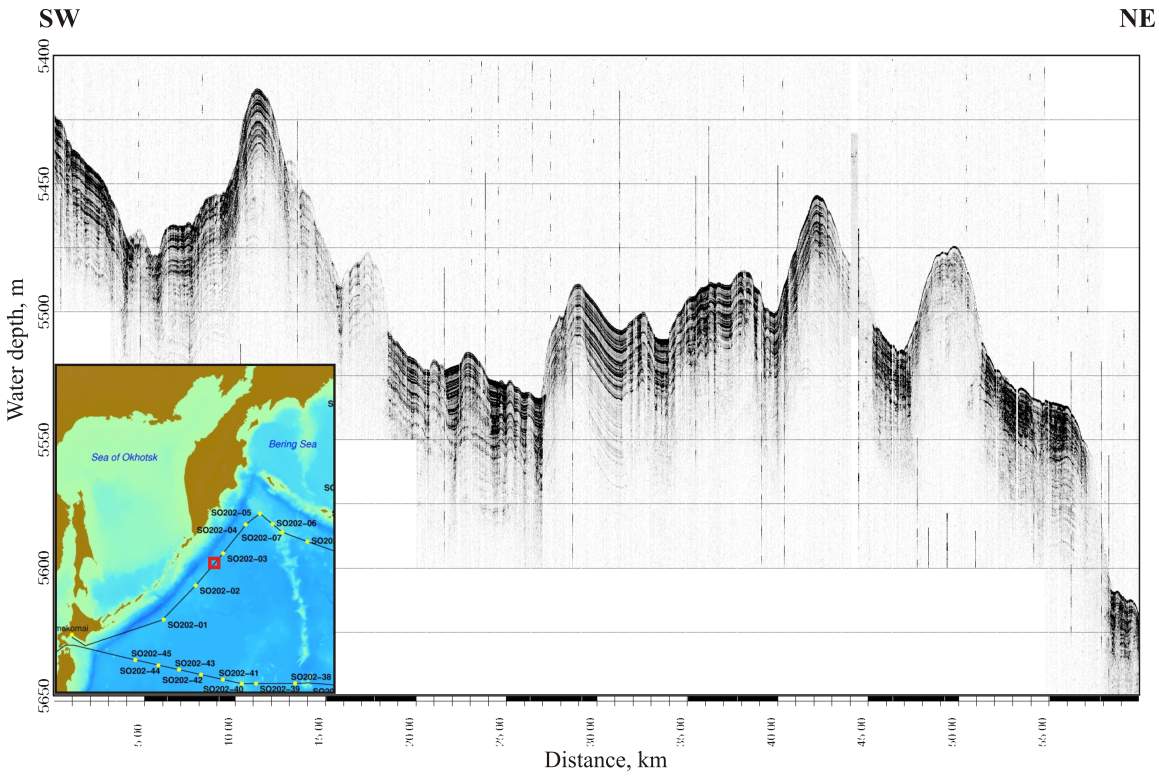

Fig. 2.2.4-8: *Profile along the northern part of the Zenkevich Ridge with echelons of small ridges and indication of ongoing tectonic movements and sediment deformation.*

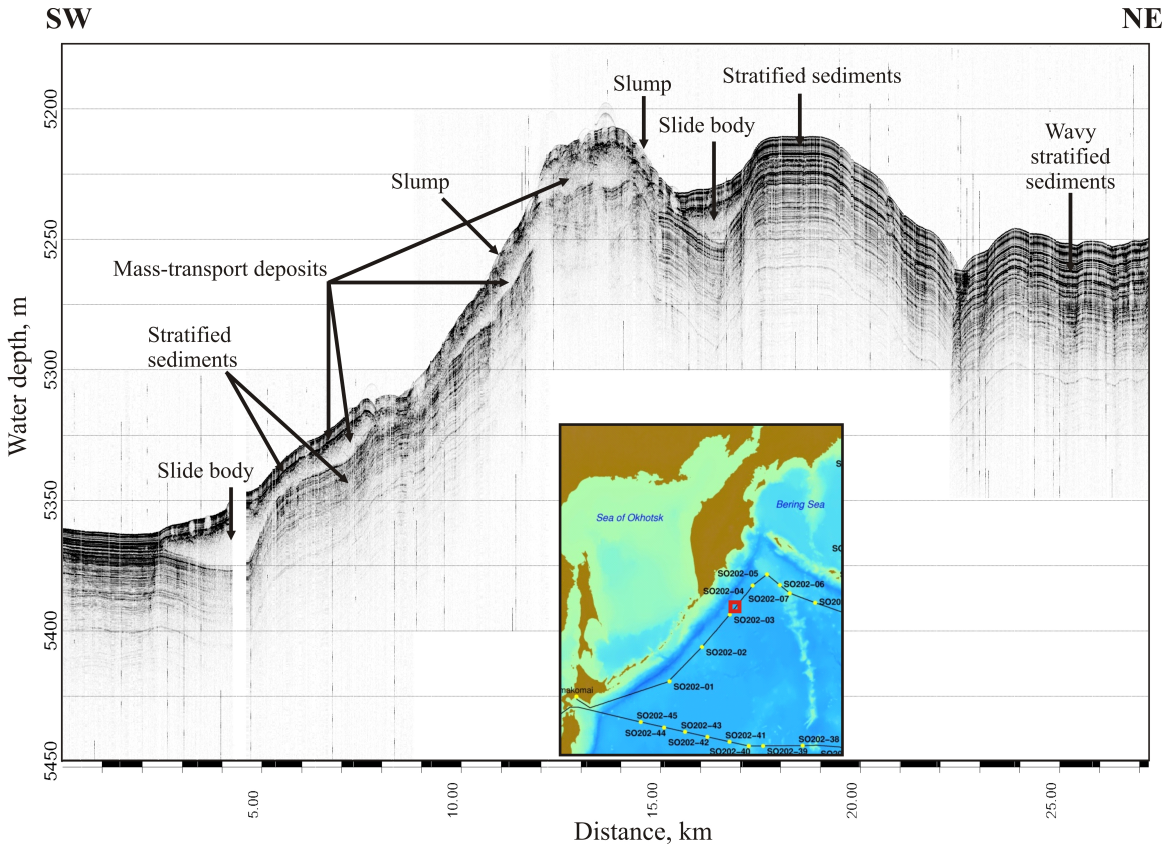

Fig. 2.2.4-9: *Profile along the northern part of the Zenkevich Ridge with indication of active tectonic activities, ridge growing and related sediment mass-transport.*

At the contrast to the complex structures at the Zenkevich Ridge, the Aleutian Rise along Aleutian Trench is characterized by low tectonic activity and absence of active deformation. This is indicated by the presence of continuous and undisturbed layering of the deposited sediments (**Figs. 2.2.4-10,11**).

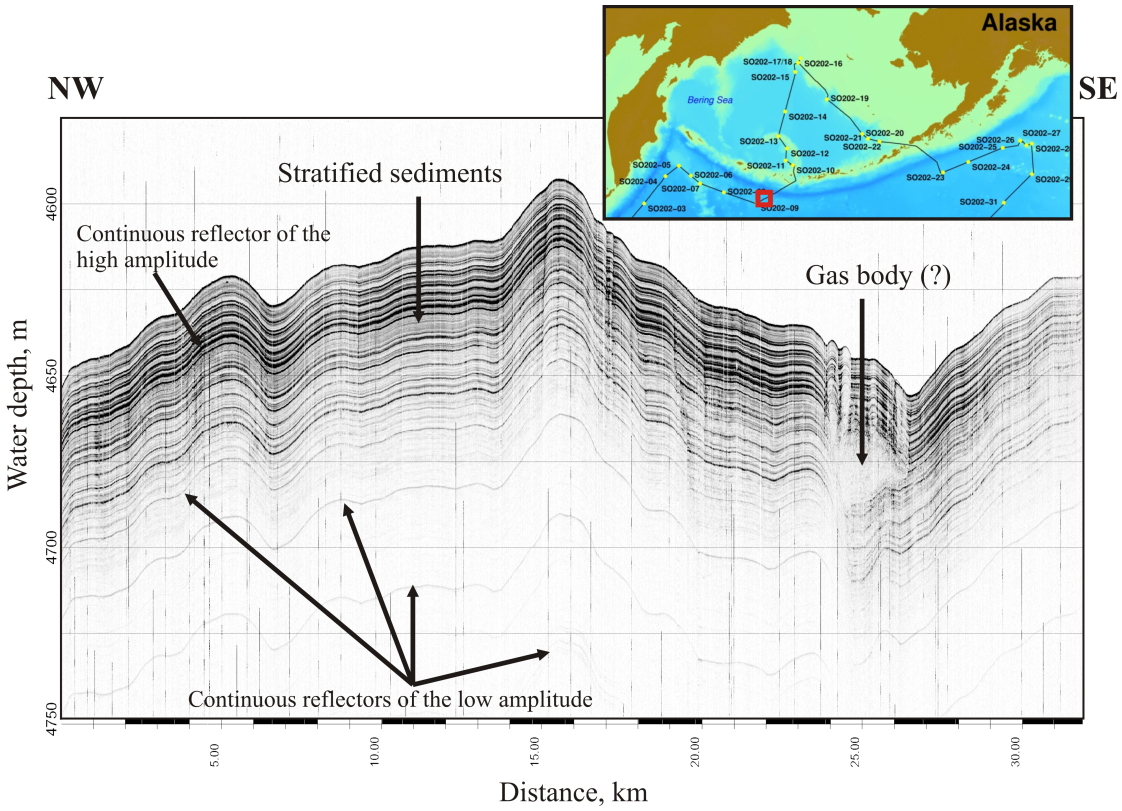

Fig. 2.2.4-10: *Profile from Aleutian Rise closely south of Aleutian Trench indicates largely undisturbed sediment deposition not affected by enhanced tectonic activities.*

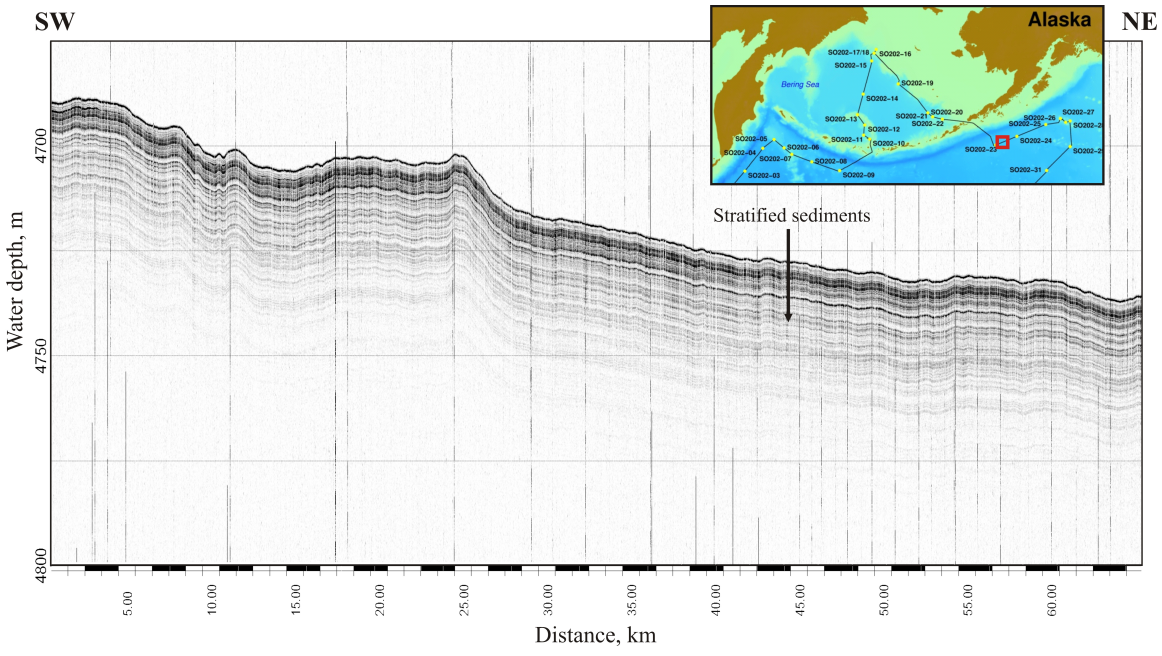

Fig. 2.2.4-11: *Profile from the north-eastern Pacific Ocean closely to the Aleutian Trench shows undisturbed sediment deposition.*

North Pacific Abyssal Plain sediments

The structures of the sedimentary layers within the abyssal plain of the North Pacific Ocean are variable. One important and widespread feature of the sedimentary structure is the occurrence of subparallel reflectors of high amplitude. These reflectors can be traced over the hundreds kilometers on the seismic profiles. The number of discerned reflectors increases towards to the Aleutian and Kurile island arc, Kamchatka and Japan. It is suggested that this feature reflects the existence of ash layers. In some abyssal plain regions we mark intervals of chaotic reflections and deformation of sediment layers indicative of tectonic activity below the well-stratified section upper sediment sequence (**Figs. 2.2.4-12,13,14**).

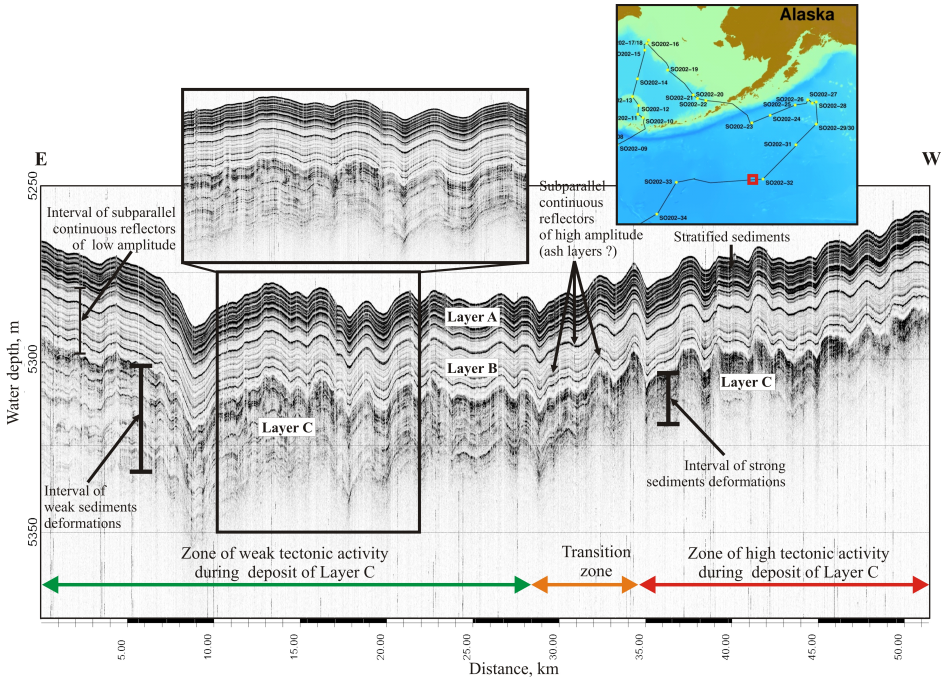

Fig. 2.2.4-12: *Abyssal plain profile within from the north-eastern North Pacific Ocean showing different sequences of well stratified sediments (Layers A and B) above less stratified sediment section (Layer C).*

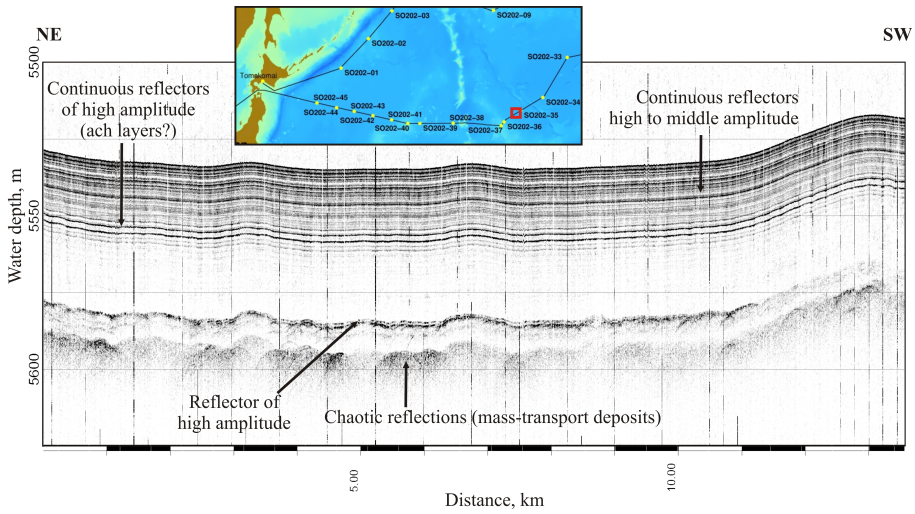

Fig. 2.2.4-13: *Abyssal plain east of Hess Rise showing the well stratified section on top and chaotic reflection at the base.*

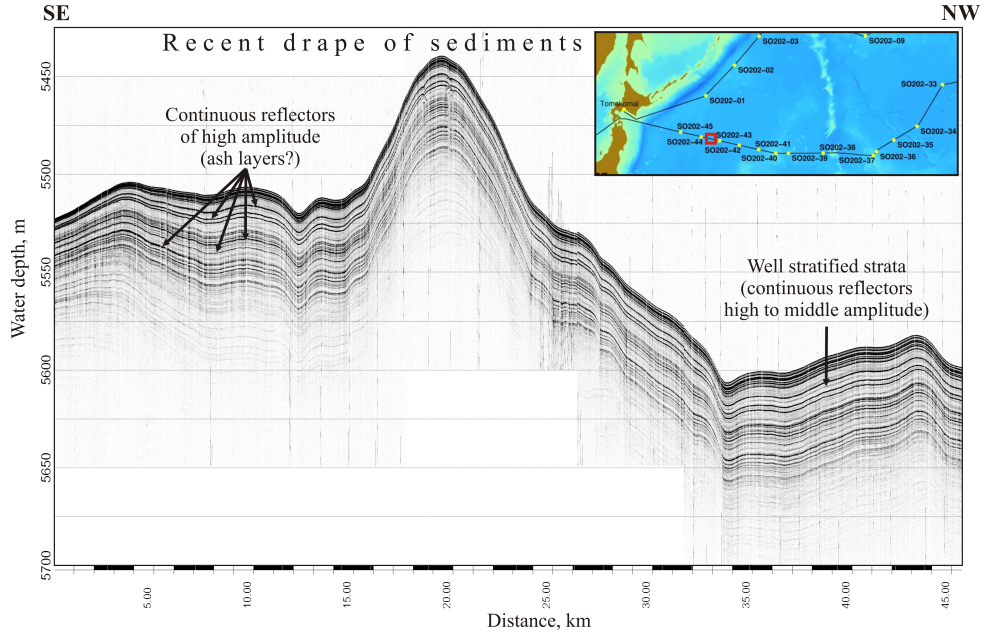

Fig. 2.2.4-14: *Abyssal plain in the west off Shatsky Rise showing well-stratified layering of sediments.*

Different abyssal fault zones were crossed during SO202. Generally, such areas are characterized by a rather complex and indented relief resulting from enhanced tectonic activity. Vertical relief amplitudes are in the range of several hundreds meters and may reach more than 1000 m. The fault zones contain limited quantities of sediment detectable with the PARASOUND echosounder (**Fig. 2.2.4-15**).

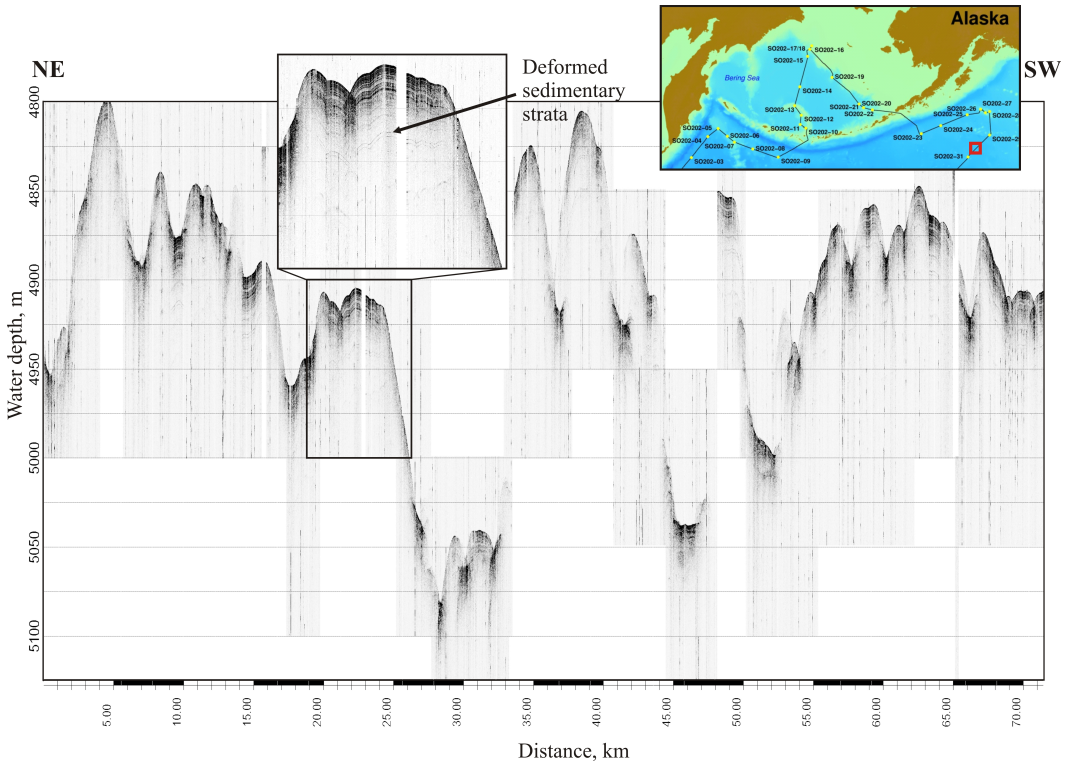

Fig. 2.2.4-15: *Profile along an abyssal fault zone south-west of Patton Seamounts.*

Seamounts, undersea rises and plateaus

Sediment deposition on the crest, the slopes and proximal surroundings of seamounts, undersea rises and plateaus, such as Hess Rise, Shatsky Rise, Obruchev Rise and Detroit Seamount is mainly controlled by two mechanisms. One mechanism includes mass-transport processes – slumps, slides, creeps etc. (**Figs. 2.2.4-16,17**), the other is related to sedimentation affected by bottom water currents water along bathymetric contours generating so-called contourites and sediment drift deposits (**Figs. 2.2.4-18,19,20**).

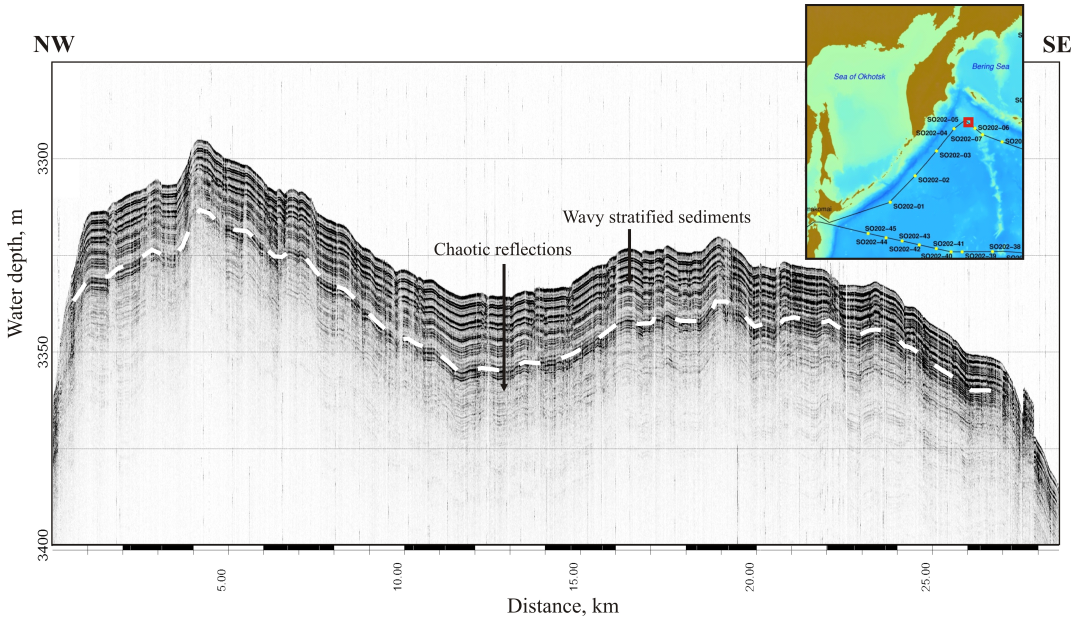

Fig. 2.2.4-16: *Profile across of Obruchev Rise (Meiji Drift) displaying the occurrence of wavy stratified sediments (creep activity) on its top.*

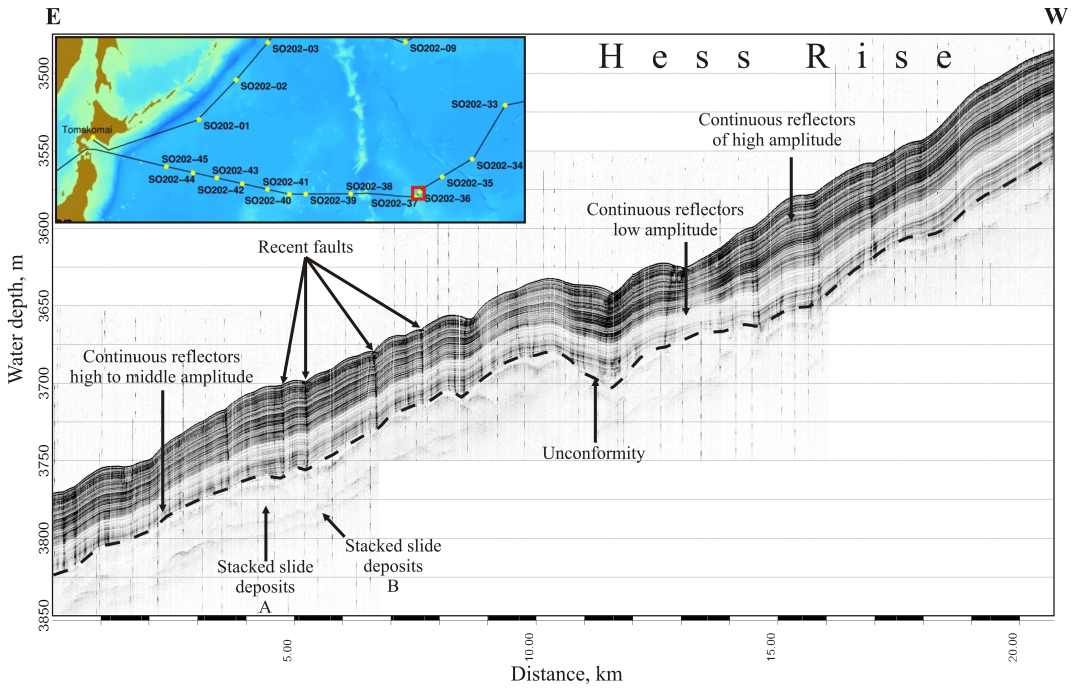

Fig. 2.2.4-17: *Profile across the eastern slope of Hess Rise showing deposition at different sedimentation regimes.*

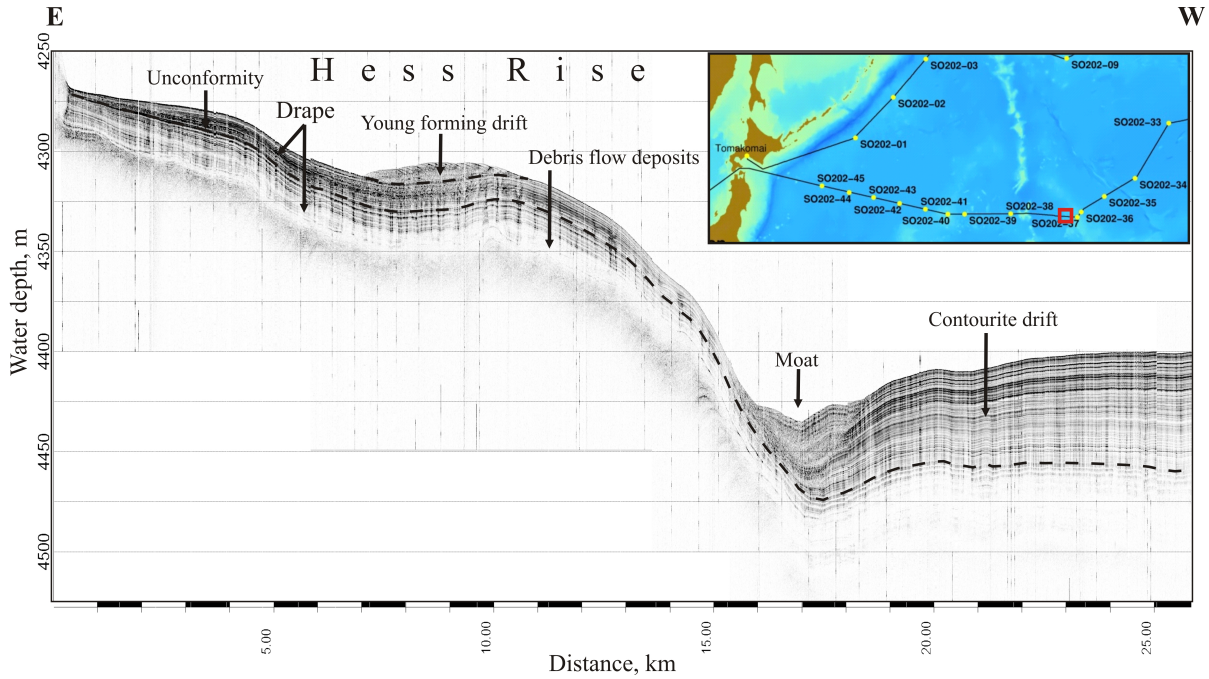

Fig. 2.2.4-18: *Profile across of the western slope of Hess Rise with debris flows and drift deposits.*

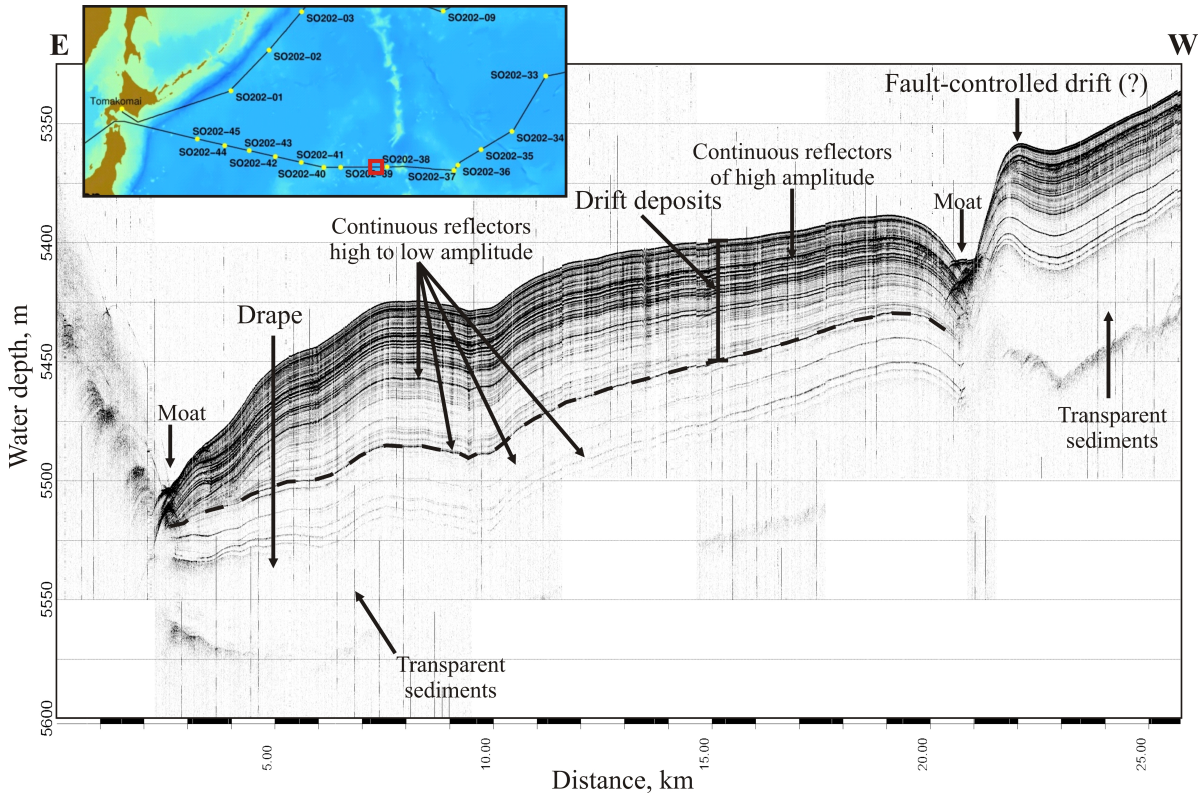

Fig. 2.2.4-19: *Profile east of Shatsky Rise with moats and related drift deposits.*

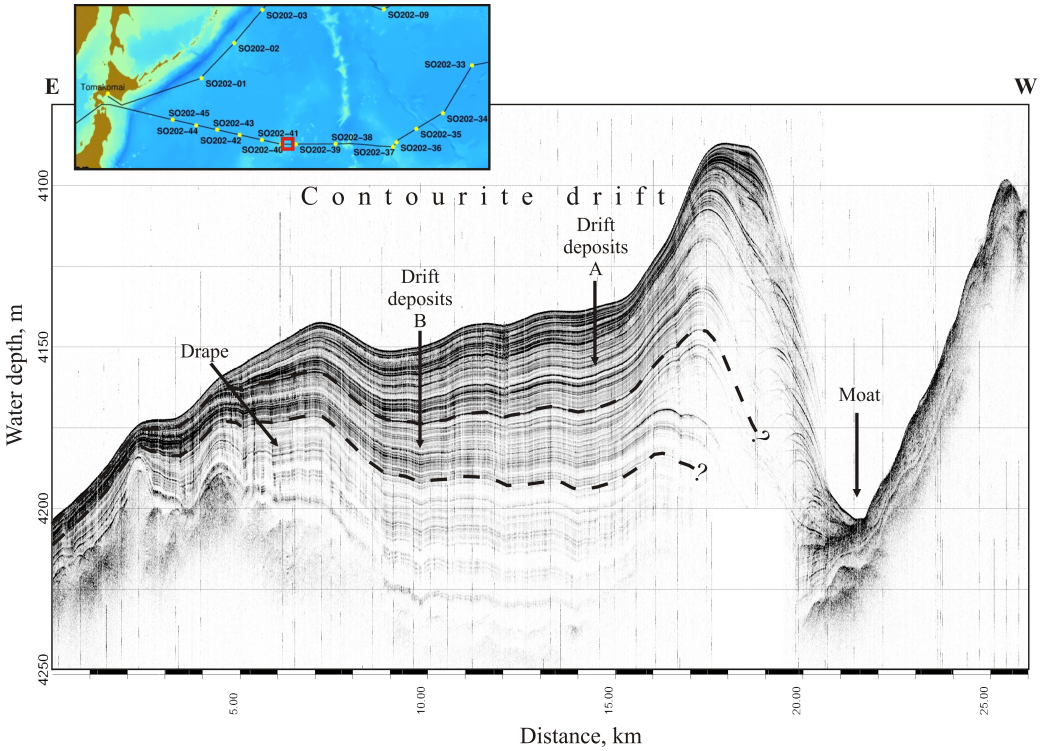

Fig. 2.2.4-20: *Profile across of the eastern slope of Shatsky Rise with contourite drift deposits.*

On Detroit Seamount an elliptic crater-like structure was observed (**Fig. 2.2.4-21**). The structure with a central high has a diameter of – 5-7 km and a depth of approximately 100 m. At the structure rim the reflectors are truncated.

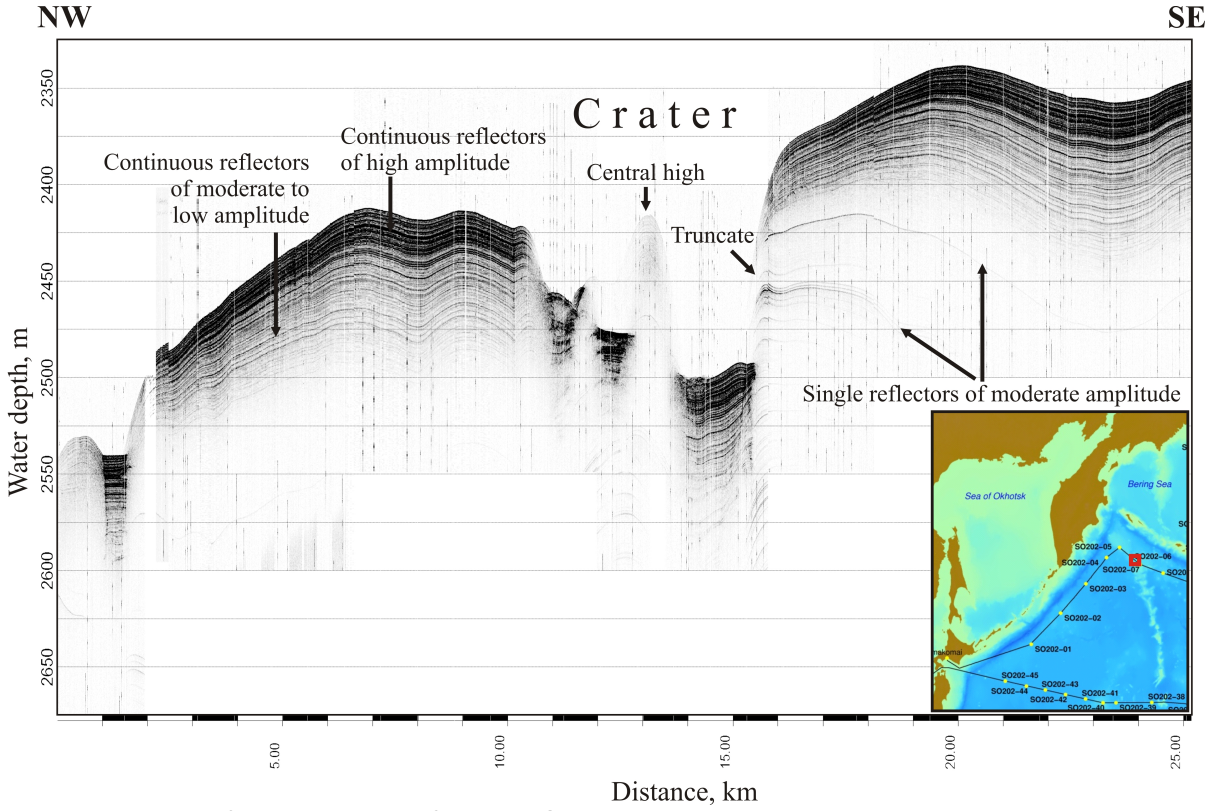

Fig. 2.2.4-21: *Profile across top of Detroit Seamount displaying crater-like structure.*

PARASOUND signals from gassy sediments

In areas with gassy sediments, e.g. at the northern Bering Slope (Navarin Canyon), the PARASOUND signals remain blurred, which results from the present of gas in the sediment (**Fig. 2.2.4-22**).

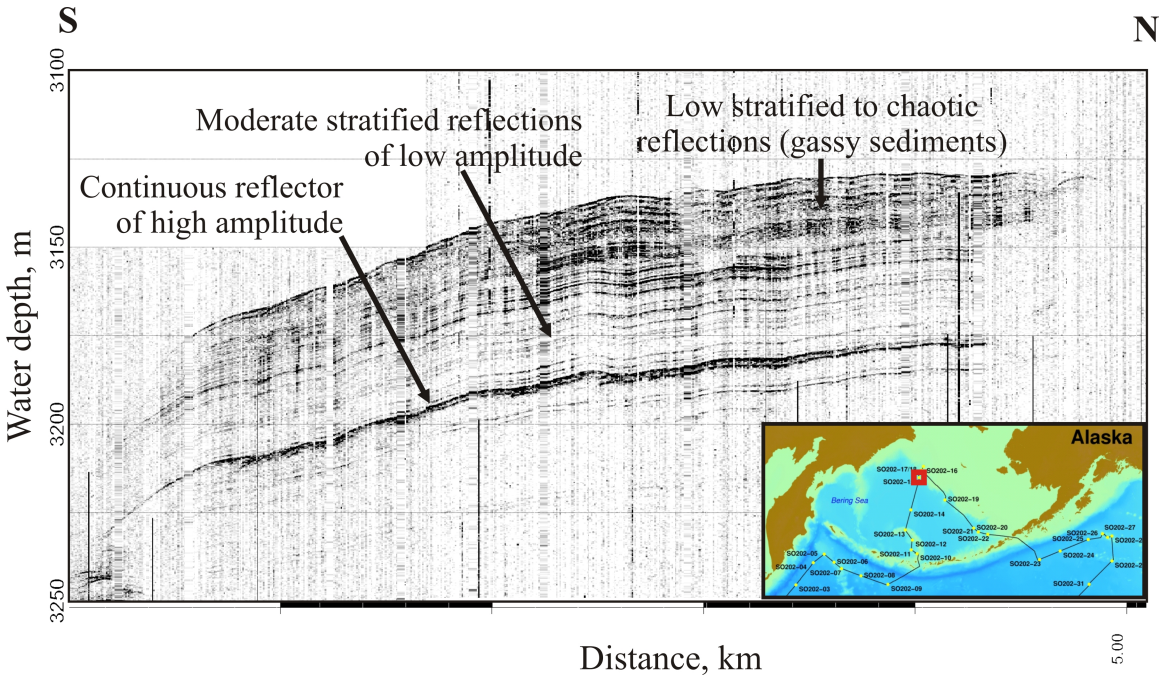

Fig. 2.2.4-22: *Profile from northern Bering Slope with blurred echosounding signals caused by sedimentary gas.*

3. DESCRIPTION OF SAMPLING INSTRUMENTS AND EQUIPMENT HANDLING

3.1. CTD and Rosette

Oliver Esper
Alfred Wegener Institute, Bremerhaven, Germany

The CTD and rosette is a combined device to measure hydrographic variables and to sample the water column simultaneously (**Fig. 3.1-1**). The Seabird 911 CTD device measures water temperature, conductivity and depth of the seawater. Furthermore, the oxygen concentration of the water is measured. The basic CTD device can be used to display variations in the hydrographic variables directly during the deployment, as the CTD data is transferred to an onboard computer device. The measured variables are instantaneously stored on hard disk. The Seabird 911 CTD can be used to analyze the water column from the sea surface to the sea floor down to 6000 meters. On selected sites the basic Seabird 911 CTD, belonging to the RV *Sonne*, was appended with a fluorometer to measure the phytoplankton concentration in the upper 1000 meters of the water column.

In addition to the probe measuring hydrographic variables the device consists of a 24-bottle water collector, the so-called rosette. Each of the 24 10-liter bottles of the rosette can be closed separately via the data wire of the winch cable. Before deployment, all the bottles have to be opened; the closing mechanism of each bottle has to be connected with the release-switches of the central controlling device. When triggered via computer command from the board unit a magnetic switch releases strong rubber bands, which close the selected bottle immediately. When all bottles are closed/filled and the device is back on deck, small vents on top and bottom of each bottle allow for an easy access to the collected water. These vents should be closed during the deployment.

Lowering of the CTD and rosette occurs with 0.5 m/s for the first 100 meters of the water column. Below 100 meters lowering can be done with up to 1.0 m/s. On the last 100 meters of the lowering to the sea floor, speed should be reduced to at most 0.5 m/s. Twenty meters above the expected sea floor depth; speed should be reduced again to 0.3 m/s. The CTD is equipped with a mechanic ground detector, a small rope of 5 meters length with a heavy weight on its lower end. When the weight gets ground contact, an acoustic signal from the board unit occurs, informing that the ground is just 5 meters below the CTD. Lowering has then immediately to be stopped. Release of the bottles occurs when the CTD and rosette is heaved up. Heave speed is 1.0 m/s except for the upper 100 meters of the water column, for which heave speed is 0.5 m/s.

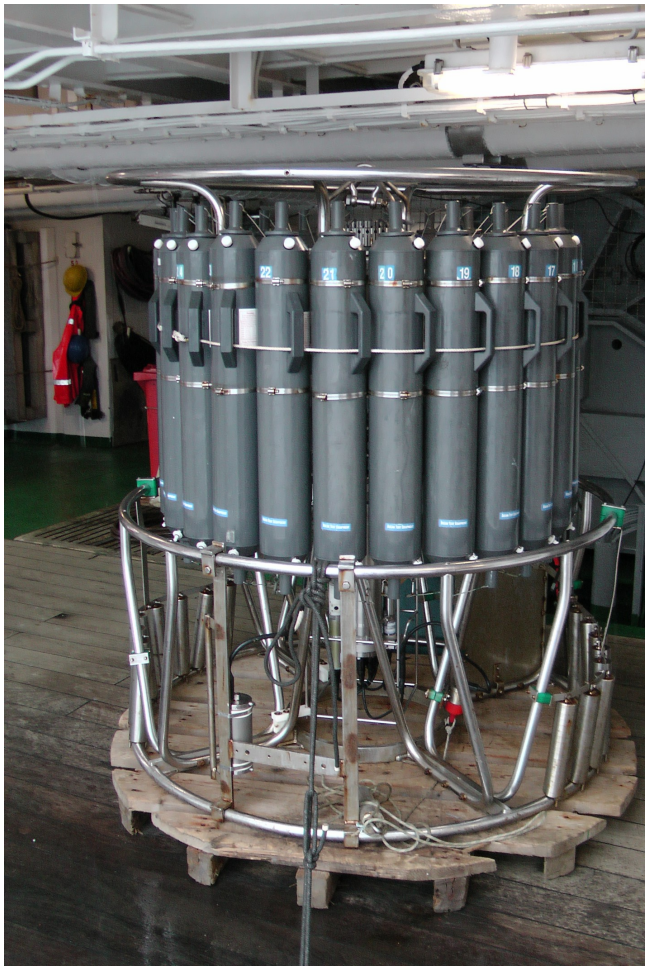

***Fig. 3.1-1**: CTD and rosette.*

3.2. Multinet

Oliver Esper
Alfred Wegener Institute, Bremerhaven, Germany

The Multinet consists of a steel box with 5 net hoses with a mesh size of 55 µm (**Fig. 3.2-1**). On the lower end of the multinet a frame with 5 net beakers is attached. Each net beaker can be equipped either with 41 µm or 10 µm filters, depending on the particle size of the plankton to be collected. The beakers have a maximum volume of 1 liter each. Release of the single nets occurs via the data wire of the winch cable. With a board unit the actual water depth of the multinet, measured with a pressure sensor, can be displayed instantaneously. During deployment, the multinet is lowered with closed nets down to a maximum of 1000 meter water depth with a maximum speed of 0.5 m/s. After reaching the lowest depth, net no. 1 is released via command from the board unit and the device is heaved with 0.3 m/s up to the next selected depth, sampling plankton along the profile. In that way, 5 profiles of distinct length can be sampled on the way up to the sea surface. When the multinet is lifted on board, remaining plankton in the net hoses are washed into the beakers by use of a seawater hose. The full beakers can be removed easily from the frame, containing plankton and remaining sea water is transferred to 1 liter bottles and can be fixed e.g. with formalin solution or ethanol.

Fig. 3.2-1: *The multinet, preparation and handling.*

3.3. Multicorer

Oliver Esper
Alfred Wegener Institute, Bremerhaven, Germany

The multicorer (MUC) used during the SO-202-INOPEX cruise consisted of 12 tubes each 60cm in length and 6cm in diameter **(Fig. 3.3-1a**). Before charging the MUC, the screws and nuts as well as all hinges were checked regularly for their firmness and correct function, respectively.

First of all, the top covers of the tubes were put up and attached to the circular steel trigger in the centre of the device (**Fig. 3.3-1d**) by pushing down the hooks. This is important, because as the MUC hits the ground the trigger will release the upper and lower caps and by that close the sediment-filled tubes when the device is heaved. Afterwards, the plastic tubes were placed in the device with the sharpened end downward to provide a better penetration in the sea floor (**Fig. 3.3-1b**). Further, the arms with the bottom caps have to be pulled up by bowing the hinges and then hooked up (**Fig. 3.3-1c**). Before lowering the MUC to the sea floor, the safety bar has to be removed by all means when the device is lifted about 50 cm off the deck. Otherwise the tubes will not be released to penetrate the ground.

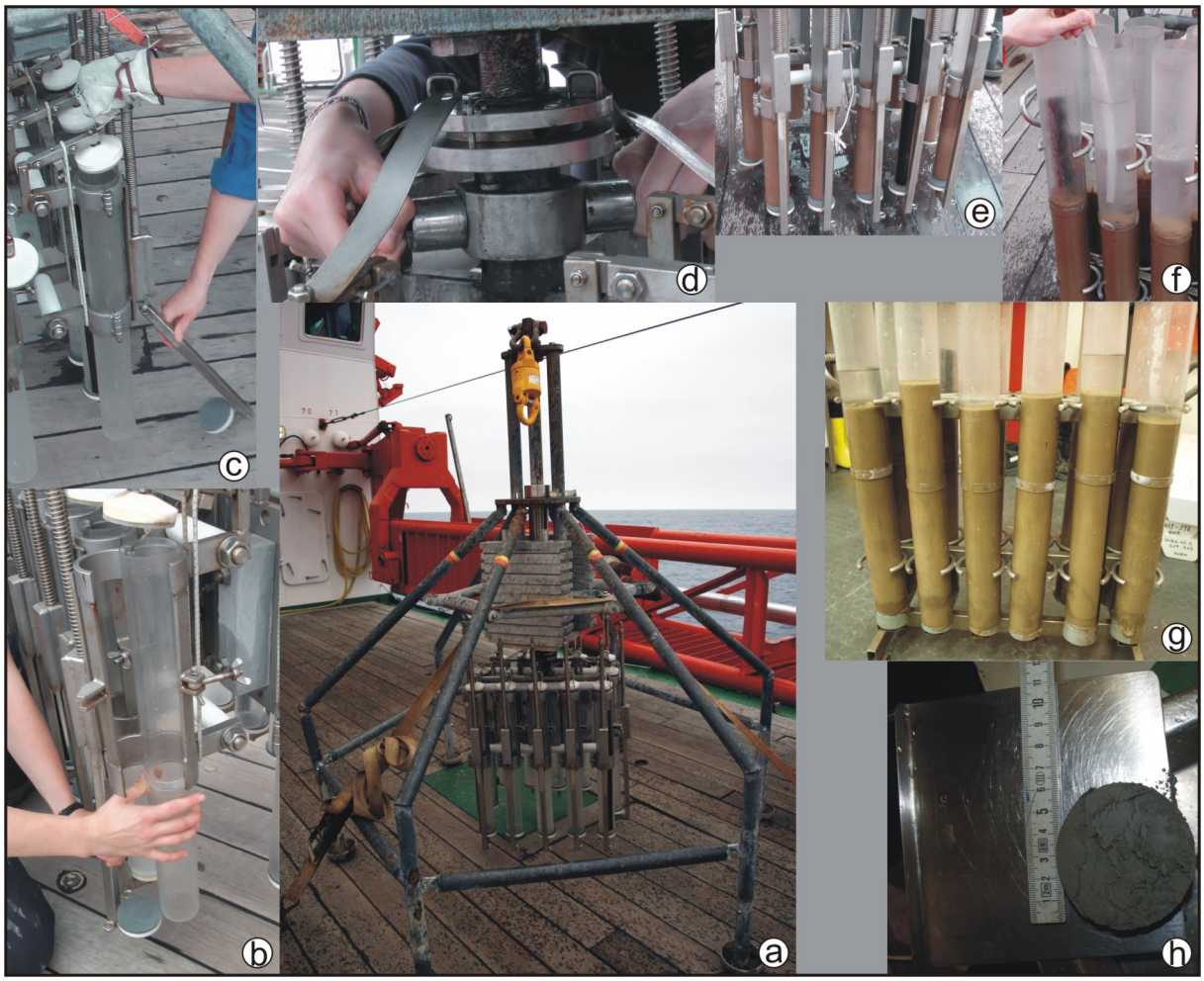

Fig. 3.3-1: *The multicorer, preparation of the device and handling of the samples.*

In the upper 200 m of the water column the MUC was lowered with 0.5 m/s and then continuing with 1.0 m/s until approximately 100 m above sea floor. At regular weather conditions the MUC is lowered to the sea floor with 0.7 m/s.

When the device is heaved up on deck the safety bar has to be put in again before the device is set down on the deck to prevent the destruction of the plastic tubes (**Fig 3.3-1e**). After fixing the MUC properly on deck, the tubes were taken off by putting a plug in the bottom and subsequently opening the screws to place the tubes in the tube-holder (**Fig. 3.3-1g**). Then the supernatant bottom water was extracted with a small hose (**Fig 3.3-1f**).

3.4 Sediment Coring Gears

Bernhard Diekmann[1], Norbert Lensch[2], Friedrich Striewski[2]
[1]Alfred Wegener Institute, Potsdam, Germany
[2]Alfred Wegener Institute, Bremerhaven, Germany

Sediment coring during SO202-INOPEX was accomplished with three coring devices: the gravity corer (Schwerelot – SL), the kasten corer (Kastenlot – KAL), and the piston corer (Kolbenlot – KOL). The selection of a coring device depended on acoustic wave penetration and the intensity of hard reflections, displayed by PARASOUND echograms. In most cases the piston corer was chosen as it is best suited for the coring of diatomaceous oozes and muds that dominate in the study area.

In addition to the brief description of coring and sampling procedures in this cruise report, a comprehensive photo documentation of the various coring operations and sampling techniques is presented in the Appendix section A.8.

The preparation of all coring devices took place in horizontal position in the core frame on the ship's working deck. On station, the frame with the included coring device was put to water by the deck crew. Before lowering of the coring devices, the frame was brought back on deck. Lowering and heaving of the different coring devices in the water column was achieved with the main ship winch. It is equipped with a 18 mm thick steel rope that can be lowered to sea floor at a maximum speed of 1.0 m/sec (**Tab. 3.4-1**). On other ships, the used devices are normally run at higher speeds of up to 1.8 m/sec. Another complication and time loss arose from the low load capacity of the used winch. At stations deeper than 4500 m, the rope load usually passed the critical threshold value of tension around 60.0 kN, such that the maximum speed had to be reduced to less than 0.7 m/sec, and in cases of high weights even to 0.3 m/sec (**Tab. 3.4-1**).

Device	Lowering to 3500 m below sea surface (m/sec)	Lowering deeper than 3500 m below sea surface (m/sec)	Lowering from 50 m above sea floor until ground penetration (m/sec)	Heave after ground penetration out of sediment (m/sec)	Heave after device is out of sediment to 3500 m water depth (m/sec)	Heave from 3500 m to sea surface (m/sec)
MUC	1.0	0.7	0.5 – 0.7	0.2	0.7	1.0
SL	1.0	0.7	0.7 – 1.0	0.2	0.7	1.0
KAL	1.0	-	1.0	0.2	-	0.7
KOL	1.0	0.7	0.3	0.2	0.7	1.0

***Table 3.4-1**. Rope speeds used for the lowering and heaving of coring devices.*

Gravity Corer (Schwerelot – SL)

The gravity corer was mainly used at stations deeper than 5000 m water depth in case of rough sea conditions. Under such circumstances, the use of the complex piston-coring system was too risky. The upper part of the gravity corer comprises a

heavy weight unit made of stacked lead rings with a total weight of 1.5 tons. The coring tubes have a diameter of 140 mm and lengths of either 5 m or 3 m. They are made of steel and connected through steel sleeves, fixed by nails. The nails are inserted trough wholes in the sleeves and fittings on the core tubes. After the core tubes were connected at desired core length, plastic liners were inserted. The liner tubes are 125 mm in diameter and 5 m long, respectively. The liners were marked with arrows in downcore direction and connected with Scotch Tape (10 cm width). Prior to taping, cleaning of the liner rims with acetone and wiping paper was done to remove fat and dirt. In the final step, the core bit was attached to the lowermost core section and fixed by nailing. The core bit includes a core catcher, consisting of a rosette of overlapping steel laminae that dip into the core tube and prevent the loss of recovered sediment. Lowering and heaving of the instrument was at 1.0 m/sec, if possible. Depending on sediment composition, penetration into the sea floor was driven between 0.5 m/sec for soft muds and oozes and 0.7 m/sec for stiff muds with volcanic ash layers (**Tab. 3.4-1**). Information on sediment hardness came from the continuous PARASOUND echosounding survey and surface sediment sampling with the multicorer.

Kasten Corer (Kastenlot - KAL)

As the gravity corer, the kasten corer represents a coring device that penetrates into the marine mud under gravitational forcing of a heavy weight on top. The used weight was 3.5 tons. In contrast to the gravity corer, the kasten corer consists of 5.5 m long rectangular box elements with 30 cm edge length. They are made of steel and are attached below the weight unit. Each box unit consists of two folded plates that are screwed together to form the box unit. The box units are connected with steel sleeves, which also consist of two folded steel plates. A rectangular core bit forms the base of the coring device. It includes two claps as core catcher that close after sediment retrieval. The kasten corer does not include plastic liners for sediment storage. After recovery of the kasten corer, it has to be opened and sampled ship-board. Because of the high sediment volume the kasten corer recovers (each 5.5 m segment filled with sediment represents ca. 1 ton), its use was restricted to sites with water depth less than 3000 m, considering the limited winch capacities. The lowering and penetration speed of the kasten corer was 1.0 m/sec. Heaving took place at 0.7 m/sec (**Tab. 3.4-1**).

Piston Corer (Kolbenlot – KOL)

The most used coring device during cruise SO202 was the piston corer (**Fig. 3.4-1**). This coring technique provided the longest sediment cores of the cruise with maximum sediment recovery at lengths of up to 24.35 m. The main construction of the piston corer is comparable with the gravity corer. The coring string consists of steel tubes, 105 mm in diameter, connected to each other with steel sleeves (**Fig. 3.4-1**). The sleeves are fixed with screws. The core tubes are topped by a weight unit of 1.5 tons. The design of the core bit and core catcher nearly corresponds to that of the gravity corer. As the gravity corer, the piston corer is fed with plastic liners, 90 mm in diameter. The corer was run at 15 m, 20 m, and 25 m lengths. With the exception of the 4 m long upper core element below the weight unit and the 1-m core tube, the piston corer is assembled with 5-m core-tube elements. The lowermost 1-m piece is removed after core retrieval to expose the liners, which then can easily be pulled out of the core string.

***Fig. 3.4-1**. The 25 m long piston corer on the R/V Sonne working deck.*

In addition to this basic design, the piston coring device is driven with a piston inside that causes suction in the core pipe, supporting sediment retrieval in addition to gravitational forcing during sediment penetration. During operation, the piston corer is lowered in conjunction with a trigger core (**Fig. 3.4.1**). Both of them are attached to a trigger arm. During preparation of the device, the piston is inserted into the bottom of the main core pipe above the core bit and connected to the lower end of the piston

cable. The outlooking piston cable at the top of the core is attached to the main lock of the trigger arm, while the cable of the pilot corer is fixed at the outer end of the trigger arm. The cables of both the pilot corer and the piston are five meters longer than the length of the main core. During lowering of the device, the pilot corer touches the sea floor before the main coring device. The effect is that the tension on the trigger arm declines and that the locked main core is released from the trigger arm. The winch has to be stopped immediately to keep the piston fixed in position. In free fall, the main core slides along the fixed piston into the sediment. In case of incomplete penetration the piston separates during slow heaving. The upper piston then moves towards the uppermost core pipe and carries the whole coring device during heave. The lowering and heaving took place at 0.7 – 1.0 m/sec, depending on water depth (**Tab. 3.4-1**).

4. WATER COLUMN SAMPLING

To gain insight into the hydrographic structure of the water column of the North Pacific Ocean and the Bering Sea, in situ measurements of hydrographic variables have been carried out with a CTD probe. The measurements were accompanied by simultaneous water sampling with a water collector (rosette) to measure concentrations of chlorophyll-*a* and dissolved nutrients (nitrate, phosphate) (for instrument description see 3.1).

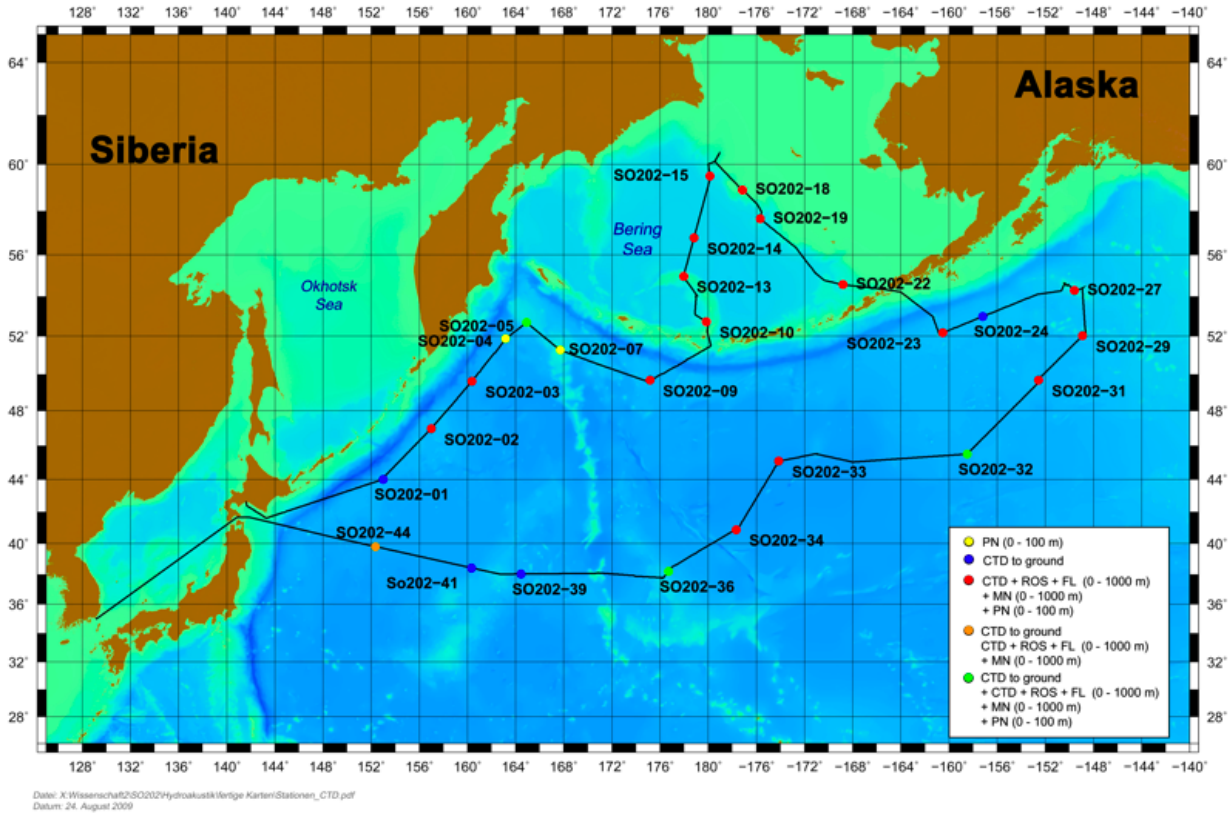

Fig. 4-1: *CTD, multinet (MN) and plankton net (PN) sample sites.*

Based on net samples and water pump samples collected during SO-202 the horizontal and vertical distribution of living diatoms, radiolarians and other prominent plankton will be analyzed. In combination with hydrographic data from the CTD probe and nutrient distribution profiles derived from rosette water samples information on the autecology of these organism groups can be gained. As the hard parts of these microorganisms are preserved in the sediment record the data gained from the water column are important information to solve paleoceanographic questions. Therefore, CTD and rosette, multinet and plankton net were deployed at 25 stations. The different sample locations result in several north to south transects from the Bering Sea across the Aleutian Islands to the North Pacific region around 38°N (**Fig. 4-1**).

Bottle	SO202-05-5	SO202-24-1	SO202-32-6	SO202-36-4	SO202-39-1	SO202-41-2	SO202-44-1
1	3360	4570	5313	4539	5109	5402	5506
2	2500	3500	5280	4506	4500	4500	4500
3	2000	2500	5246	4472	3500	3500	3500
4	1500	2000	5213	4438	2500	2500	2500
5	1000	1500	5180	4406	1500	1500	1500
6	500	1000	5146	4372	1000	1000	1000
7	400	500	5113	4339	500	500	500
8	300	400	4500	3500	400	400	400
9	200	300	3500	2500	300	300	300
10	150	200	2500	2000	200	200	200
11	100	100	1500	1500	100	100	100
12	10	10	1000	1000	10	10	10
13	\	\	500	500	\	\	\
14	\	\	400	400	\	\	\
15	\	\	300	300	\	\	\
16	\	\	200	200	\	\	\
17	\	\	100	100	\	\	\
18	\	\	10	10	\	\	\

Tab. 4.1-1: *CTD/Rosette – Deep Cast Water Samples (depth in meter), 10 L each 0.45 µm filtered directly from Rosette*

4.1 CTD Casts to Bottom

Oliver Esper[1], Christopher Hayes[2]
[1]Alfred Wegener Institute, Bremerhaven, Germany
[2]Lamont-Doherty Earth Observatory, United States

The CTD/Rosette instrument provided full water column profiles of temperature, salinity and oxygen at 8 stations along our cruise track (**Fig. 4.0-1**). See **Table 4.1-1** for a list of the station numbers as well as the water samples taken at these sites. Size of water samples was 10 L and the water was 0.45 µm filtered directly from the rosette bottles.

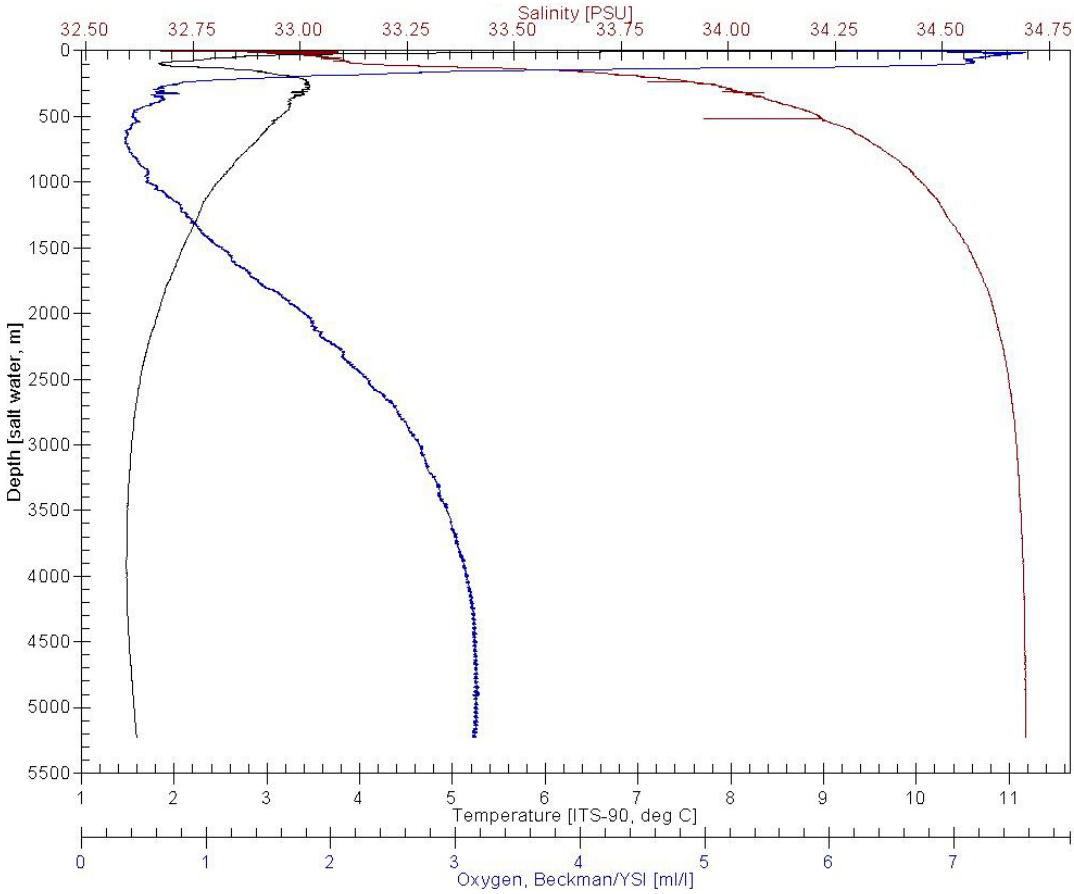

Fig. 4.1-1: *Temperature, salinity and oxygen profile of water column at Site SO202-01*

The temperature, salinity and oxygen data, immediately available on the ship, are of use in interpreting the vertical structure (i.e. density distribution) of the water column, local hydrography, and the relation of the study area to the global ocean circulation. Notably, in the profile seen in **Fig. 4.1-1** (Site SO202-01), a relatively highly oxygenated (3 ml O_2 per liter seawater) bottom water mass (uniform in temperature and salinity) is visible within the bottom 1000 m of the water column. This water mass likely has its origin in the Southern Ocean, where surface water is densified and spreads down the Antarctic slope to travel northwards, ventilating the world's bottom water. Additionally, a sub-surface cold layer is visible around 150 m which is likely the result of deep winter time mixing and out of flow of the surrounding marginal seas

(Sea of Okhotsk and the Bering Sea). This water layer was tracked along the Kuril Trench and into the Bering Sea. It may represent a precursor to North Pacific Intermediate Water which subducts near the sub-Arctic front and ventilates the thermocline at lower latitudes.

The water samples taken during the deep CTD deployment are intended to investigate the nature of three trace metals dissolved in the ocean throughout the water column, namely thorium (Th), protactinium (Pa), and neodymium (Nd). These trace metals and their isotopes are used increasingly in paleoceanography as proxies in sediments for oceanic processes. Yet, their behavior in the modern ocean is poorly documented. This is primarily because they exist in such low concentrations that only recently have methods become available to accurately determine them. For instance: ^{230}Th is widely used as a proxy for constant flux into the sediments and is used to determine mass accumulation rates; the ratio ^{231}Pa / ^{230}Th in sediments has been interpreted as representing, in separate instances, productivity, opal flux and the strength of the North Atlantic Deep Water circulation; and the ratio ^{143}Nd/^{144}Nd appears to conservatively trace waters masses. Questions remain about the assumptions made in the use of these tracers, which can be answered, in part, by better knowledge of their modern dissolved concentration. The sites for full water column sampling were chosen as transects away from the coast. Generally the coasts have higher lithogenic and biogenic particulate fluxes when compared with the open ocean. The natural variability in particle concentration allows one to investigate the effect this has on these elements. Additionally at two open ocean sites, whose surface sediments presumably have a high biogenic/lithogenic ratio, six extra samples were taken within the bottom 200 m to investigate possible regeneration of the dissolved metals upon the degradation of biological particles on the seafloor.

4.2 CTD Cast with Fluorometer to 1000 m

Oliver Esper[1], Christopher Hayes[2]
[1]Alfred Wegener Institute, Bremerhaven, Germany
[2]Lamont-Doherty Earth Observatory, United States

The CTD/Rosette instrument provided water column profiles of temperature, salinity and oxygen from 1000 m water depth up to the sea surface at 20 stations along the cruise track. See **Table 4.2-1** for a list of the station numbers as well as the water samples taken at these sites. For this shallow cast, the CTD was affixed with a fluorometer to measure the fluorescence of green light (λ = 540 nm), the value of which is known to vary with the concentration of chlorophyll-*a*. The fluorometer data immediately provides a qualitative indicator of chlorophyll concentration, producing values between the arbitrary limits of 0 and 10 (0 meaning no chlorophyll, 10 abundant chlorophyll). To measure the nutrient concentration in selected water depth, 50ml samples were taken in 12 different depths, treated with $HgCl_2$ solution and were frozen at -20°C. In addition, 2L water samples were taken from 10 selected depths (sample intervals between 240 m and 10 m) of each CTD + Fluorometer deployment for chlorophyll-*a* measurements. The samples were filtered with 25 µm glass microfibre filters (GF/F); the filters were afterwards packed in aluminum foil and stored at –20°C. Once the filters are analyzed for chlorophyll-*a* concentration, a calibration can be created to convert the fluorescence data into chlorophyll-*a* data throughout the 1000 m interval.

Cast	1	2	3	4	5	6	7	8	9	10	11	12
SO202-02-1	1000	500	240	210	180	150	120	90	70	50	30	10
SO202-03-1	1000	500	240	210	180	150	120	90	70	50	30	10
SO202-05-1	1000	500	240	210	180	150	120	90	70	50	30	10
SO202-09-1	1000	500	240	210	180	150	120	90	70	50	30	10
SO202-10-1	1000	500	240	210	180	150	120	90	70	50	30	10
SO202-13-1	1000	500	240	210	180	150	120	90	70	50	30	10
SO202-14-1	1000	500	240	210	180	150	120	90	70	50	30	10
SO202-15-1	1000	500	240	210	180	150	120	90	70	50	30	10
SO202-18-4	1000	500	240	210	180	150	120	90	70	50	30	10
SO202-19-1	1000	500	240	210	180	150	120	90	70	50	30	10
SO202-22-3	1000	500	240	210	180	150	120	90	70	50	30	10
SO202-23-1	1000	500	240	210	180	150	120	90	70	50	30	10
SO202-27-2	1000	500	240	210	180	150	120	90	70	50	30	10
SO202-29-1	1000	500	240	210	180	150	120	90	70	50	30	10
SO202-31-1	1000	500	240	210	180	150	120	90	70	50	30	10
SO202-32-1	1000	500	240	210	180	150	120	90	70	50	30	10
SO202-33-1	1000	500	240	210	180	150	120	90	60	50	30	10
SO202-34-1	1000	485	240	210	180	150	120	90	70	50	30	10
SO202-36-1	1000	500	240	210	180	150	120	90	70	50	30	10
SO202-44-3	1000	500	240	210	180	150	120	90	70	50	30	10

Table 4.2-1: *CTD/Rosette cast to 1000 m and rosette sample depth (depth in meter)*

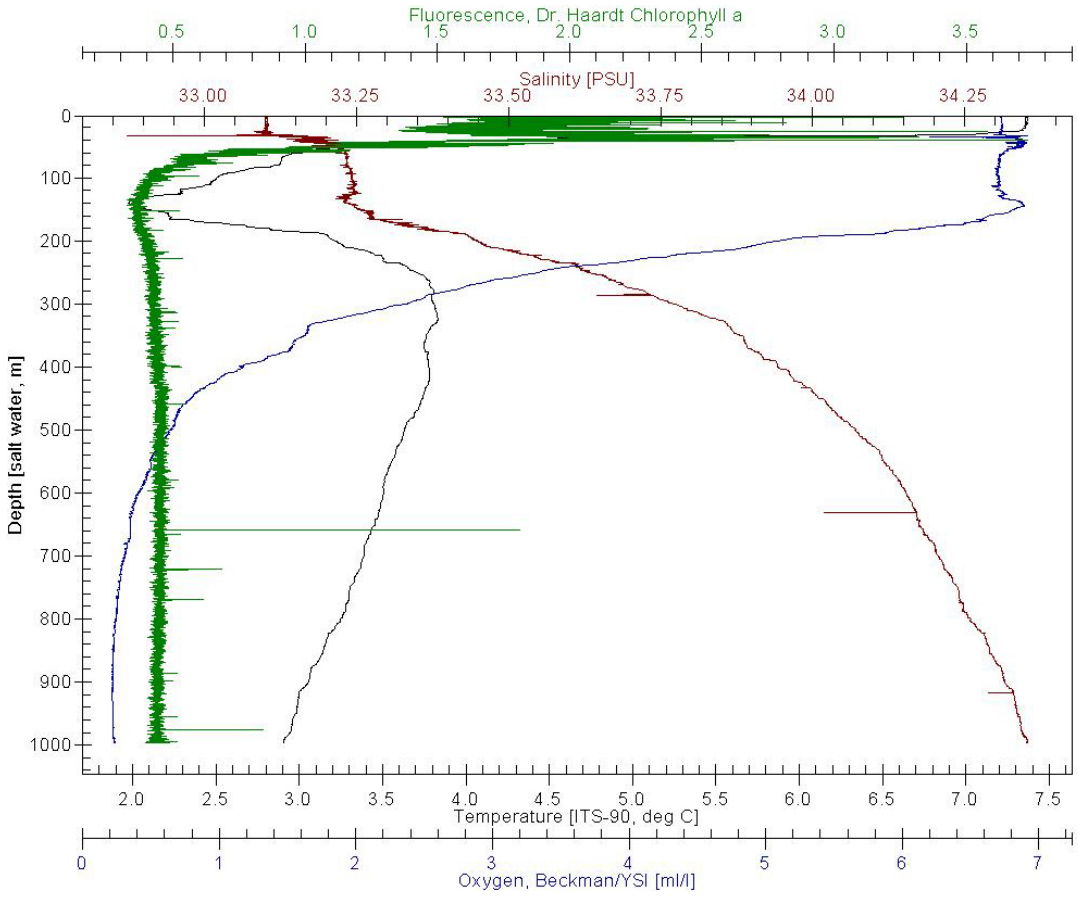

Fig. 4.2-1: *CTD cast with fluorometer to 1000 m at Site SO202-13 (northern Bowers Ridge, Bering Sea) showing distinct subsurface temperature minimum.*

Hydrographic data selected from survey in the Bering Sea and in the central North Pacific provide examples of the suite of data collected on the shallow casts with contrasting stratification and biological productivity. Hydrographic survey in the Bering Sea (Site SO202-13, **Fig. 4.2-1**) records the abovementioned subsurface cold layer, showing that this layer is relatively enriched in oxygen, supporting the view that this layer arises from mixing in contact with the atmosphere. In contrast the hydrographic data obtained at the northern Hess Rise (Site SO202-36) displays (1) a temperature structure more characteristic of the open ocean with a gradual increase to the surface, (2) a single, slightly deeper fluorescence maximum, and (3) more saline surface waters, indicative of the influence of the Kuroshio Extension, the remnants of the western boundary current bringing warm, salty water from low to high latitudes (**Fig. 4.2-2)**.

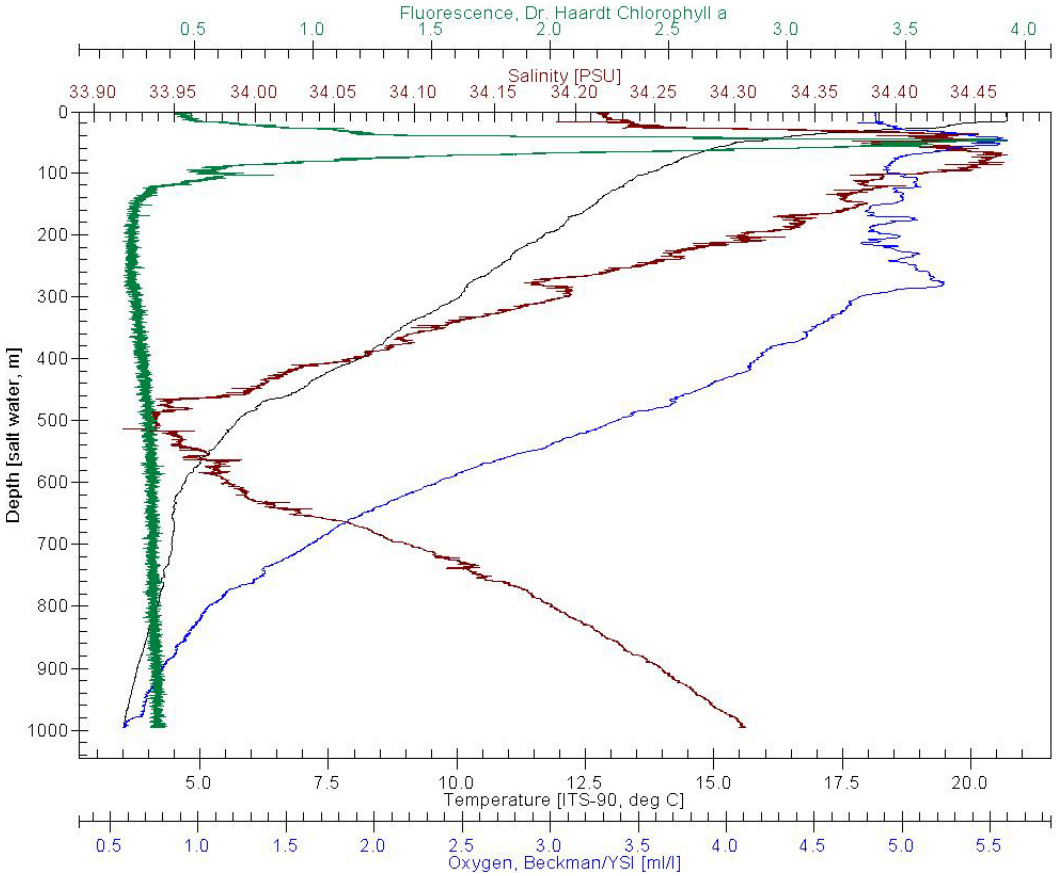

Fig. 4.2-2: *CTD cast with fluorometer to 1000 m at Site SO202-36 (central North Pacific, Hess Rise) as an example of open ocean hydrography.*

4.3 Multinet

Oliver Esper, Jian Ren
Alfred Wegener Institute, Bremerhaven, Germany

The multinet (MN) was deployed at 20 stations to gain plankton samples from 5 different water depth intervals between 1000 m and the sea surface (**Tab. 4.3-1**). The depth intervals have been chosen according to the hydrographic structure at each

site obtained from CTD casts. Mainly to collect larger plankton fractions such as zooplankton (radiolarians, foraminifera, dinoflagellates), the net beakers have been equipped with 41 µm mesh size gaze. The samples were stored in 1000 ml bottles and were fixed with formalin (2% end concentration, by volume). In general, the samples showed quite a similar distribution of larger plankton particles along the sampled geographic transects. Samples from the upper 50 m were characterized by high amounts of phytoplankton aggregates, whereas the low profiles between 500m and 1000 m revealed higher numbers of small arthropods and some cnidarians (medusa). Especially in the western North Pacific and the Bering Sea, the layers between 150 m and 500 m were relatively abandoned of larger sized plankton. At Site SO202-19 (central portion of Bering Slope, **Fig. 4.1**) the net beakers from the upper 300 m of the water column contained plankton particles, which showed strong autoluminescence. This may be related to the presence of dinoflagellates such as of the genus *Noctiluca*.

MN Haul	Depth 1 [m]	Depth 2 [m]	Depth 3 [m]	Depth 4 [m]	Depth 5 [m]
SO202-02-5	1000-500	500-300	300-150	150-50	50-0
SO202-03-5	1000-500	500-300	300-150	150-50	50-0
SO202-05-6	1000-500	500-300	300-150	150-50	50-0
SO202-09-5	1000-500	500-300	300-150	150-50	50-0
SO202-10-4	1000-500	500-300	300-150	150-50	50-0
SO202-13-3	1000-500	500-300	300-150	150-50	50-0
SO202-14-4	1000-500	500-300	300-150	150-50	50-0
SO202-15-3	1000-500	500-300	300-150	150-50	50-0
SO202-18-5	1000-500	500-300	300-150	150-50	50-0
SO202-19-3	1000-500	500-300	300-150	150-50	50-0
SO202-22-6	1000-500	500-300	300-150	150-50	50-0
SO202-23-3	1000-500	500-300	300-150	150-50	50-0
SO202-27-4	1000-500	500-300	300-150	150-50	50-0
SO202-29-3	1000-500	500-300	300-150	150-50	50-0
SO202-31-2	1000-500	500-300	300-150	150-50	50-0
SO202-32-2	1000-500	500-300	300-150	150-50	50-0
SO202-33-2	1000-500	500-300	300-150	150-50	50-0
SO202-34-2	1000-500	500-300	300-150	150-50	50-0
SO202-36-2	1000-500	500-300	300-150	150-50	50-0
SO202-44-4	1000-500	500-300	300-150	150-50	50-0

Table 4.3-1: *Multinet hauls and collected depth intervals at each site.*

4.4 Plankton Net

Maria Obrezkova[1], Oliver Esper[2]
[1]V.I. Il´ichev Pacific Oceanological Institute, Russia
[2]Alfred Wegener Institute, Bremerhaven, Germany

To gain phytoplankton samples from the upper 100 meters of the water column, the plankton net (PLA) was deployed 23 times (**Table 4.4-1**). It collected plankton particles >10 µm on a depth profile from 100 m up to the sea surface. The samples were stored in 500 ml bottles and were fixed with formalin (2% end concentration, by volume).

PLA Haul	Depth [m]
SO202-02-3	100-0
SO202-03-3	100-0
SO202-04-2	100-0
SO202-05-4	100-0
SO202-07-3	100-0
SO202-07-4	100-0
SO202-07-5	100-0
SO202-09-3	100-0
SO202-10-3	100-0
SO202-13-2	100-0
SO202-14-2	100-0
SO202-15-2	100-0
SO202-18-2	100-0
SO202-19-4	100-0
SO202-22-5	100-0
SO202-23-2	100-0
SO202-27-5	100-0
SO202-29-2	100-0
SO202-31-3	100-0
SO202-32-3	100-0
SO202-33-3	100-0
SO202-34-3	100-0
SO202-36-3	100-0

Table 4.4-1: *Plankton net hauls and collected depth interval.*

4.5 Water Pump Samples

Oliver Esper[1], Jian Ren[1], Maria Winterfeld[1], Maria Obrezkova[2]
[1]Alfred Wegener Institute, Bremerhaven, Germany
[2]V.I. Il´ichev Pacific Oceanological Institute, Russia

To obtain plankton samples from the sea surface, a total of 68 water samples were collected with the onboard membrane pump from 5 m water depth. Up to three times a day sea water was filtered with a 10 µm filter (**Tab. 4.5-1).** The filter and remaining sea water were then transferred to 100 ml bottles and preserved with formalin (2% end concentration, by volume). At 17 locations (**Tab. 4.5-2**) membrane pump water was filtered with 142 µm glass microfibre filters (GF/F) to collect particulate matter. The filters were stored at –20°C.

Sample no.	Date 2009	Time start	Latitude start	Longitude start	Time stop	Latitude stop	Longitude stop	flow [ml/min]
01	10.07.	23:30	44°55.45´N	153°55.45´E	00:21	44°50.05´N	154°00.87´E	1860
02	11.07.	03:43	45°13.36´N	154°32.81´E	04:03	45°15.53´N	154°35.74´E	2490
03	11.07.	09:00	45°46.62´N	155°18.68´E	09:12	45°47.82´N	155°20.29´E	2580
04	12.07.	11:43	47°07.94´N	157°11.21´E	12:03	47°10.54´N	157°14.45´E	3480
05	12.07.	22:50	48°32.20´N	158°58.86´E	23:04	48°34.32´N	159°01.90´E	3000
06	13.07.	03:23	49°15.57´N	159°54.59´E	03:42	49°18.35´N	159°58.37´E	2760
07	13.07.	22:50	50°05.51´N	160°57.51´E	23:02	50°07.17´N	160°59.52´E	2430
08	14.07.	03:27	50°41.25´N	161°41.36´E	03:31	50°41.77´N	161°42.04´E	2250
11	14.07.	11:05	51°41.15´N	162°57.21´E	03:14	51°44.68´N	163°00.55´E	2430
12	14.07.	23:09	51°57.41´N	163°20.40´E	23:14	51°57.67´N	163°21.42´E	4260
13	15.07.	03:23	52°23.65´N	164°16.55´E	03:39	52°25.36´N	164°20.00´E	2910
14	15.07.	23:04	52°37.10´N	165°04.47´E	23:10	52°36.47´N	165°04.47´E	2250
15	16.07.	03:39	52°07.28´N	166°03.53´E	03:56	52°05.55´N	166°06.90´E	2040
16	17.07.	09:13	51°11.36´N	168°05.80´E	09:24	51°10.73´N	168°08.30´E	1860
17	18.07.	03:58	50°29.53´N	171°02.68´E	04:05	50°29.12´N	171°04.58´E	2760
18	18.07.	08:56	50°13.17´N	172°15.81´E	09:15	50°12.18´N	172°20.42´E	2010
19	19.07.	09:39	49°41.07´N	175°13.59´E	09:47	49°41.72´N	175°15.43´E	2760
20	19.07.	22:57	50°45.47´N	178°14.52´E	23:10	50°47.06´N	178°14.85´E	2700
21	20.07.	03:13	51°05.90´N	179°11.16´E	03:29	51°07.71´N	179°13.84´E	2550
22	20.07.	08:46	51°43.51´N	179°50.93´W	09:02	51°46.37´N	179°52.25´W	2760
23	21.07.	08:54	53°08.28´N	178°54.35´E	09:03	53°09.87´N	178°54.53´E	3760
24	21.07.	22:52	54°03.79´N	179°04.31´E	23:03	54°05.39´N	179°02.40´E	3480
25	22.07.	03:06	54°35.50´N	178°24.17´E	03:12	54°36.50´N	178°23.46´E	3640
26	23.07.	09:37	56°52.40´N	178°52.36´E	09:47	56°54.08´N	178°53.18´E	2400
27	23.07.	22:57	59°13.69´N	179°55.47´W	23:21	59°17.70´N	179°53.29´W	1890
28	25.07.	09:28	59°59.85´N	179°11.18´W	09:31	59°59.41´N	179°10.33´W	4000
29	25.07.	22:55	58°14.89´N	175°57.78´W	23:00	58°14.11´N	175°50.99´W	4500
30	27.07.	03:20	55°33.36´N	171°38.60´W	03:25	55°32.60´N	171°37.56´W	2970
31	28.07.	23:19	54°15.98´N	164°26.84´W	23:24	54°15.86´N	164°25.35´W	3640
32	29.07.	02:15	54°03.85´N	163°38.33´W	02:26	54°02.59´N	163°35.57´W	1890
33	30.07.	07:22	52°16.87´N	160°04.41´W	07:32	52°17.58´N	160°01.66´W	1650
34	01.08.	19:52	51°34.11´N	150°04.44´W	20:02	54°32.81´N	150°02.30´W	3080
35	03.08.	00:16	53°59.85´N	148°52.50´W	00:18	53°59.56´N	148°52.47´W	4380
36	03.08.	06:02	53°08.15´N	148°46.57´W	06:17	53°06.63´N	148°46.25´W	2430
37	06.08.	00:30	48°34.28´N	154°01.97´W	00:39	48°33.16´N	154°03.66´W	2920
38	06.08.	05:57	47°57.23´N	155°05.98´W	06:08	47°49.76´N	155°08.15´W	2400
39	06.08.	19:50	46°03.30´N	157°42.70´W	20:05	46°01.51´N	157°45.27´W	2040
40	06.08.	23:50	45°33.08´N	158°25.64´W	23:54	45°35.79´N	158°26.05´W	4000
41	07.08.	19:54	45°26.88´N	159°32.43´W	19:58	45°26.84´N	159°33.50´W	3680
42	08.08.	00:16	45°23.55´N	160°40.50´W	00:26	45°23.42´N	160°43.08´W	2160
43	08.08.	06:04	45°19.10´N	162°09.61´W	06:20	45°18.92´N	162°13.59´W	2220
44	09.08.	00:07	45°05.16´N	166°49.44´W	00:24	45°04.96´N	166°52.68´W	2250
45	09.08.	05:57	45°04.68´N	168°18.32´W	06:13	45°05.54´N	168°23.84´W	2220
46	09.08.	19:53	45°25.51´N	171°42.08´W	20:08	45°24.99´N	171°45.83´W	2400
47	10.08.	00:17	45°15.51´N	172°49.54´W	00:27	45°15.20´N	172°52.05´W	2040
48	10.08.	19:57	45°02.78´N	174°10.37´W	20:06	45°01.34´N	174°11.54´W	2640
49	11.08.	00:07	44°23.82´N	174°43.29´W	00:13	44°22.87´N	174°44.07´W	2550
50	11.08.	05:59	43°29.23´N	175°28.90´W	00:19	43°26.18´N	175°31.43´W	2580
51	11.08.	23:55	40°53.06´N	177°40.48´W	23:59	40°53.56´N	177°40.75´W	4000
52	13.08.	00:17	39°51.34´N	179°59.19´E	00:23	39°50.78´N	179°57.64´E	4000
53	13.08.	19:53	38°30.27´N	177°04.39´E	20:06	38°23.06´N	177°01.80´E	3200
54	15.08.	00:09	37°46.18´N	176°03.84´E	00:31	37°46.43´N	175°58.92´E	2920
55	15.08.	06:09	37°46.77´N	174°49.88´E	06:23	37°49.89´N	174°37.65´E	1260

56	15.08.	20:19	38°01.40´N	171°52.35´E	20:31	38°01.56´N	171°50.17´E	2700
57	16.08.	01:12	38°04.97´N	170°52.57´E	01:28	38°04.68´N	170°49.02´E	2640
58	16.08.	06:49	38°02.69´N	169°35.36´E	07:09	38°02.70´N	169°30.73´E	2670
59	17.08.	01:08	38°01.96´N	167°38.56´E	01:18	38°01.97´N	167°36.03´E	2580
60	17.08.	07:21	38°01.44´N	166°13.78´E	07:31	38°01.41´N	166°11.42´E	2130
61	18.08.	06:48	38°00.47´N	163°43.11´E	07:19	38°00.43´N	163°36.01´E	2610
62	19.08.	02:10	38°19.53´N	160°50.24´E	02:23	38°20.01´N	160°47.39´E	3200
63	19.08.	21:50	38°34.77´N	159°23.44´E	22:10	38°35.54´N	159°18.85´E	3000
64	20.08.	21:48	39°05.80´N	156°25.36´E	22:01	39°06.37´N	156°22.23´E	6000
65	21.08.	02:20	39°14.76´N	155°33.69´E	02:37	39°15.46´N	155°29.62´E	3400
66	21.08.	21:48	39°47.16´N	152°26.02´E	22:03	39°47.76´N	152°22.45´E	3780
67	22.08.	21:50	40°05.81´N	150°37.31´E	22:05	40°06.43´N	150°33.71´E	3520
68	23.08.	02:43	40°17.36´N	149°29.84´E	02:53	40°17.85´N	149°28.86´E	3480

Table 4.5-1: *Membrane pump samples – plankton (10 μm mesh; 100 ml bottle)*

Sample no.	Date 2009	Time start	Latitude start	Longitude start	Time stop	Latitude stop	Longitude stop	Volume [liter]
M01	13.07.	01:58	49°02.31´N	159°37.51´E	03:14	49°13.93´N	159°53.30´E	191
M02	14.07.	07:03	51°07.33´N	162°17.50´E	08:04	51°16.05´N	162°27.91´E	147
M03	14.07.	08:13	51°17.29´N	162°29.43´E	08:50	51°22.10´N	162°35.05´E	97
M04	17.07.	10:19	51°07.16´N	168°22.41´E	12:50	50°58.90´N	169°03.20´E	251
M05	18.07.	06:03	50°22.52´N	171°34.29´E	07:22	50°18.43´N	171°52.43´E	165
M06	19.07.	23:33	50°48.62´N	178°18.62´E	00:48	50°53.76´N	178°35.83´E	241
M07	21.07.	00:24	52°53.54´N	179°27.79´E	01:26	52°59.40´N	179°12.75´E	208
M08	24.07.	00:42	59°31.98´N	179°51.48´W	01:25	59°30.79´N	179°50.92´W	186
M09	27.07.	00:31	55°59.08´N	172°13.68´W	02:22	55°46.37´N	171°58.11´W	294
M10	29.07.	03:00	53°58.88´N	163°27.21´W	03:44	53°53.83´N	163°16.35´W	98
M11	02.08.	22:32	54°18.76´N	148°54.72´W	23:11	54°11.56´N	148°53.93´W	113
M12	13.08.	02:05	39°41.05´N	179°36.77´E	03:02	39°35.41´N	179°24.59´E	264
M13	13.08.	20:39	38°25.44´N	176°55.86´E	22:28	38°10.46´N	176°40.25´E	399
M14	17.08.	01:29	38°01.92´N	167°33.45´E	02:25	38°01.88´N	167°21.05´E	271
M15	20.08.	03:40	38°48.79´N	158°02.99´E	04:54	38°51.81´N	157°45.86´E	299
M16	21.08.	20:12	39°43.32´N	152°48.24´E	21:25	39°46.24´N	152°31.42´E	370
M17	22.08.	22:52	40°08.31´N	150°22.70´E	02:24	40°16.61´N	149°34.25´E	698

Table 4.5-2 : *Membrane pump samples – particles (GF/F filter)*

5. SEDIMENT SAMPLING

5.1. Surface Sediment Sampling

Oliver Esper[1], Maria Winterfeld[1], Sophie Bonnet[2]
[1]Alfred Wegener Institute, Bremerhaven, Germany
[2]GEOTOP - Université du Québec à Montréal, Canada

During the SO202 - INOPEX cruise, the multicorer (MUC) was successfully deployed at 39 stations (**Fig. 5.1-1**) to obtain undisturbed surface sediment samples. The MUC consists of 12 tubes, each 60 cm in length and 6 cm in diameter.

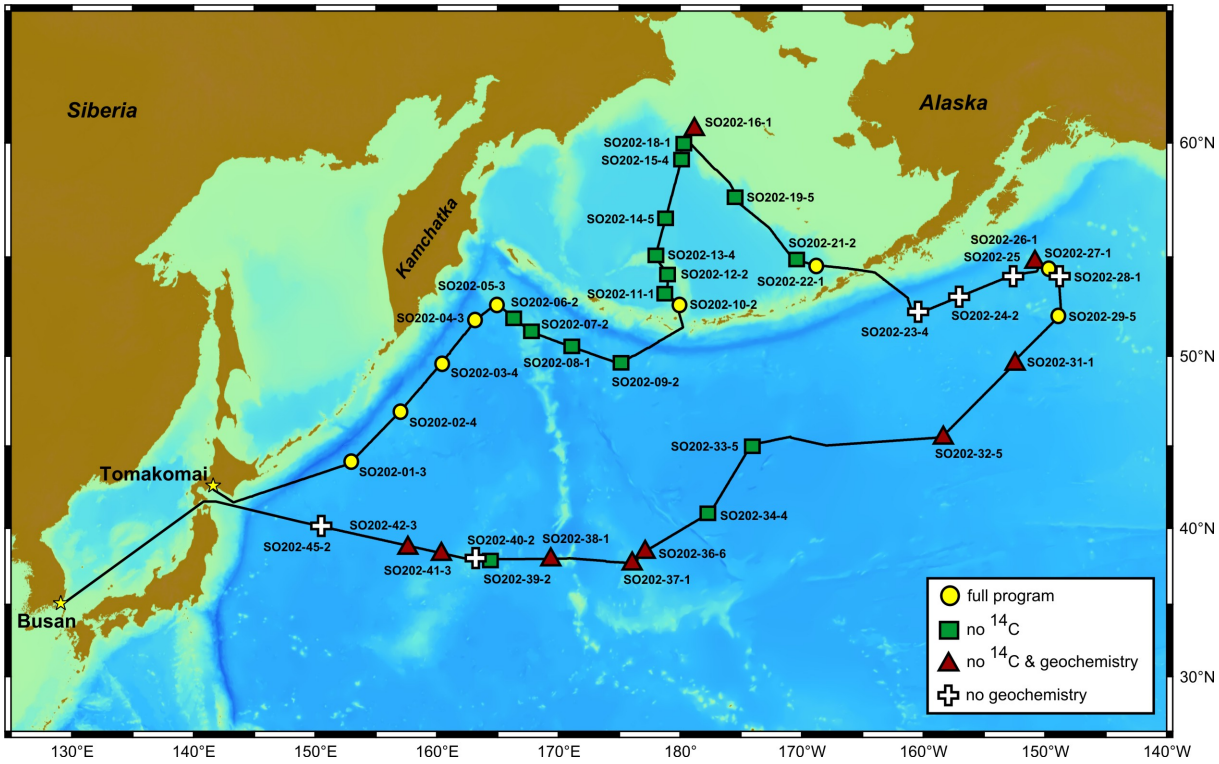

Fig. 5.1-1: *Multicorer sample sites and overview on sampling program at each site.*

The recovered cores were sampled for different sedimentological, geochemical and micropaleontological analyses and were distributed to the respective working groups. This included sediment samples for the analyses of opal isotope composition of diatoms and radiolarians for paleoenvironmental reconstructions (e.g. productivity and sea surface salinity), of ice-rafted debris for iceberg drift reconstruction, of diatoms and radiolarians for paleoceanographic reconstructions, of dinoflagellate cysts for the reconstruction of past sea-surface conditions (e.g. sea surface temperature, salinity, sea ice, productivity), for sediment geochemical and grain size analyses, age determination (^{14}C bulk), for trace metal analysis and proxy validation (e.g. Helium, Protactinium, Thorium), for biomarker analysis (e.g. sea surface temperature, sea ice, productivity), and for biomarker-specific radiocarbon dating (e.g. determining terrigenous input and sediment re-deposition).

Furthermore, at 24 sites (see **Fig. 5.1-1**) pore water was extracted via rhizons from one of the cores for hydrochemical analyses and a second core was further sampled for geochemical sediment analysis of the solid phase. For that purpose, at every MUC deployment three tubes with small holes, which were closed with scotch tape, were placed in the MUC. For biomarker-specific radiocarbon analysis two cores were sampled at 15 selected sites (see **Fig. 5.1-1** for location).

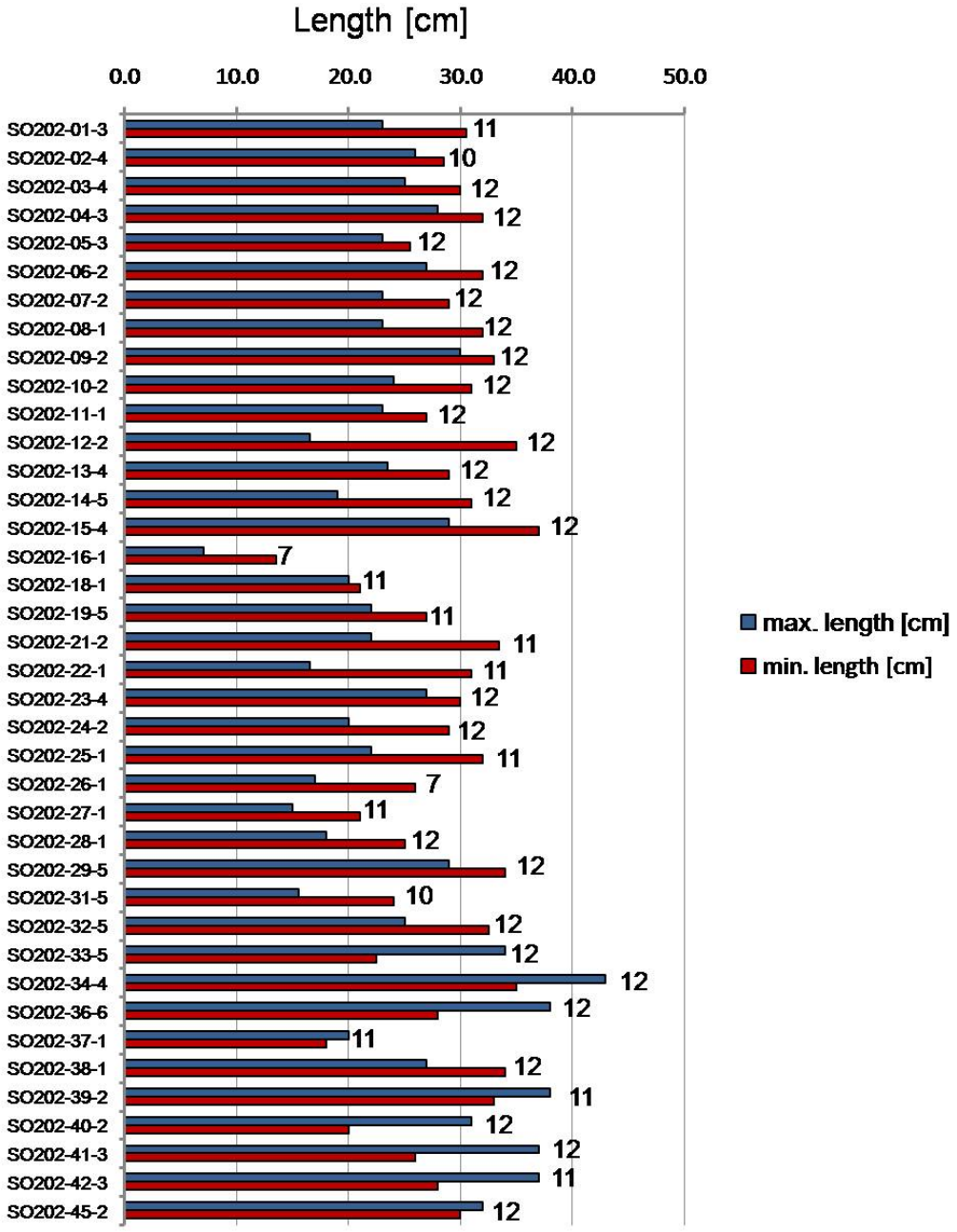

Fig. 5.1-2: *Multicorer recovery. Numbers indicate number of tubes recovered at individual sites.*

In total, 444 sediment-filled tubes were recovered (**Fig. 5.1-2**) and sampled at 1cm interval. The sediment type varied strongly within the different regions and depositional milieus covered by the cruise including clay-bearing and diatomaceous

muds, and foraminiferal sands. At two sites (SO202-16, SO202-26) only 7 filled tubes could be obtained due to the relatively sandy and foraminifera-bearing deposits. Furthermore, because of small sharp-edged gravel in the hinge, the proper closure of two or three tubes was blocked several times. Gravel was also observed within the recovered sediments. At Site SO202-34 (east of Emperor Trough) manganese nodules of varying size (from 0.5 cm to 4 cm in diameter) were found in the clay-rich sediment.

5.2 Sediment Coring, Sampling and Documentation

Bernhard Diekmann[1], Andreas Borchers[1], Katja Hockun[1], Marie Meheust[2], Wenbao Li[3], Anja Studer[4]
[1]Alfred Wegener Institute, Potsdam, Germany
[2]Alfred Wegener Institute, Bremerhaven, Germany
[3]School of Ocean and Earth Science, Tongji University, Shanghai, PR China
[4]ETH Zürich, Switzerland

5.2.1 Sediment Coring

At 43 sites, a total of 50 sediment cores were recovered: 42 with the piston corer, 5 with the kasten corer (KAL), and 3 with the gravity corer (**Tab. 5.2.1-1**, **Fig. 5.2.1-1**). Only a trigger core was recovered at the first site located east of the Kuril-Kamchatka Trench, as a result of a loss of the piston corer, and at Site SO202-16 (Bering Slope). The longest core (24.35 m) was gained with a 30-meter piston corer at Site SO202-37 on northern Hess Rise.

Recovery (m)	All Cores (50)	Piston Corer (42)	Kasten Corer (5)	Gravity Corer (3)
Total	834.00	761.26	36.11	36.39
Mean	16.68	18.13	7.22	12.13
Minimum	1.27	1.82	2.92	1.27
Maximum	24.35	24.35	10.96	19.29

Table 5.2.1-1: *SO202-INOPEX sediment core recovery.*

5.2.2 Opening, Documentation and Sampling of Sediment Cores

Apart from those sediment cores that were opened for geochemistry sampling, all retrieved sediment cores taken with the piston and gravity corer have been logged as whole-core sections with a Multi-Sensor-Core-Logger (MSCL) to determine petrophysical properties of the sediment cores (see Chapter 6). MSCL measurements on opened cores were done on core halves. The sediments recovered with a kasten corer were measured in the boxes used for sampling. In total, five sediment cores taken with the kasten corer, one sediment core from a gravity corer, and three sediment cores recovered with the piston corer were opened, sampled and examined on-board. For sediment core description of all cores opened on-board and shore-based until 2011, see Appendix A.5.

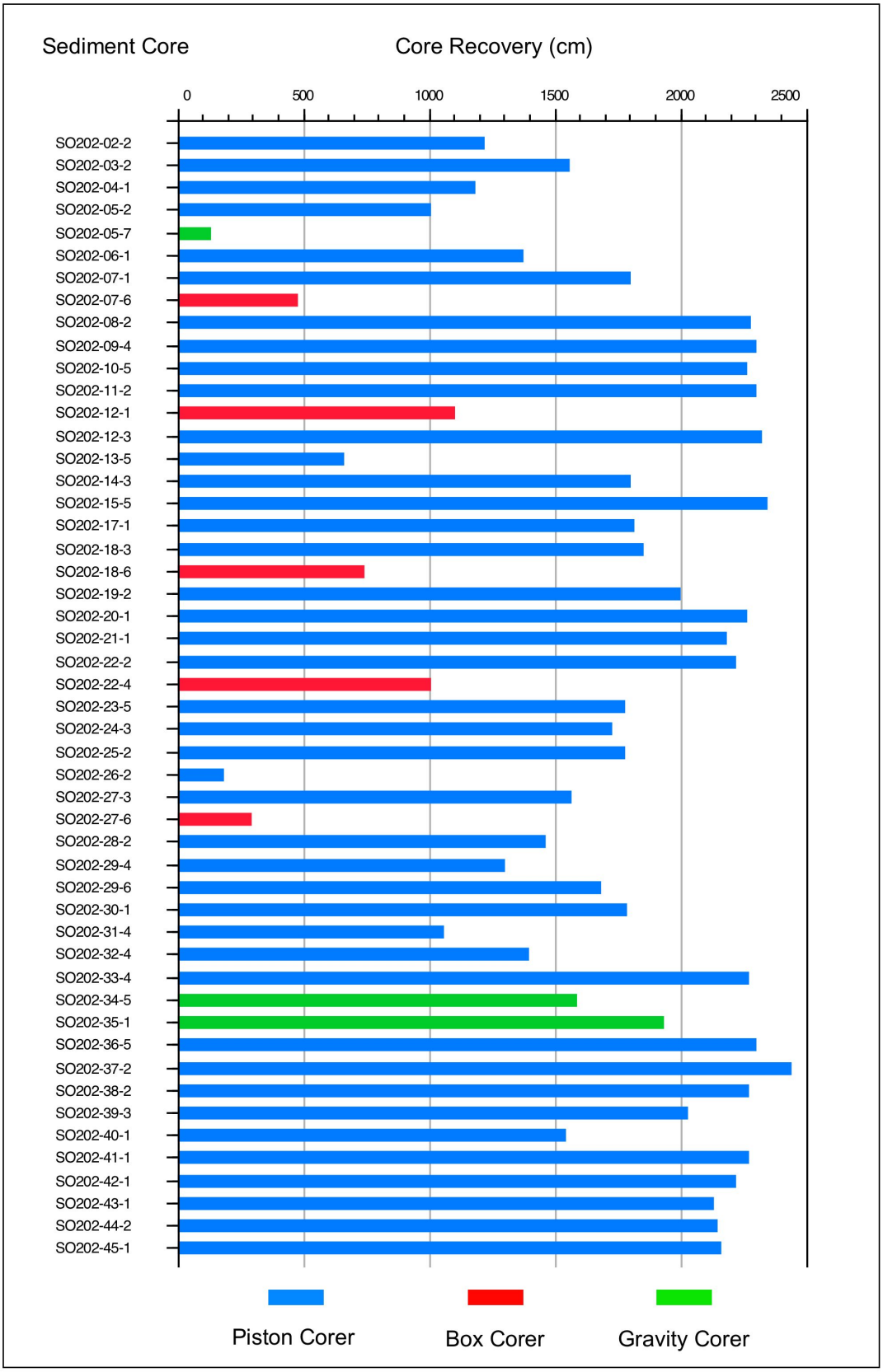

***Fig. 5.2.1-1**: Core recovery of piston corer, kasten (box) corer and gravity corer deployments.*

After opening of SL and KOL sediment cores with a double-bladed vibro-saw, they were split into archive and work halves, respectively. The 1-cm slice between the work and archive halves was put into foil and sealed after vacuation in 25-cm pieces. They later will be used to obtain radiographs, which provide information on downcore variations in clast concentrations, bedding features, and the intensity of bioturbation (Grobe 1987, Diekmann and Kuhn 1997). After photographic documentation, visual core description was conducted and supported by smear-slide analysis (see 5.2.3 and Appendix A.5). Assignments of lithofacies followed standard terminology in marine geology (e.g. Gersonde et al., 1999). Color description is according to the color coding of the Munsell Soil Color Chart. The working half was sampled for pore water (see geochemistry). Sediment samples (10-ccm volume) for the determination of water contents were taken every 10 cm in pre-weight sample glass jars. In addition, plastic cubes were taken every 5 cm for paleomagnetic studies. Three sediment cores were sampled in total for different kind of proxy studies, according to a predefined scheme (**Fig. 5.2.2-1**).

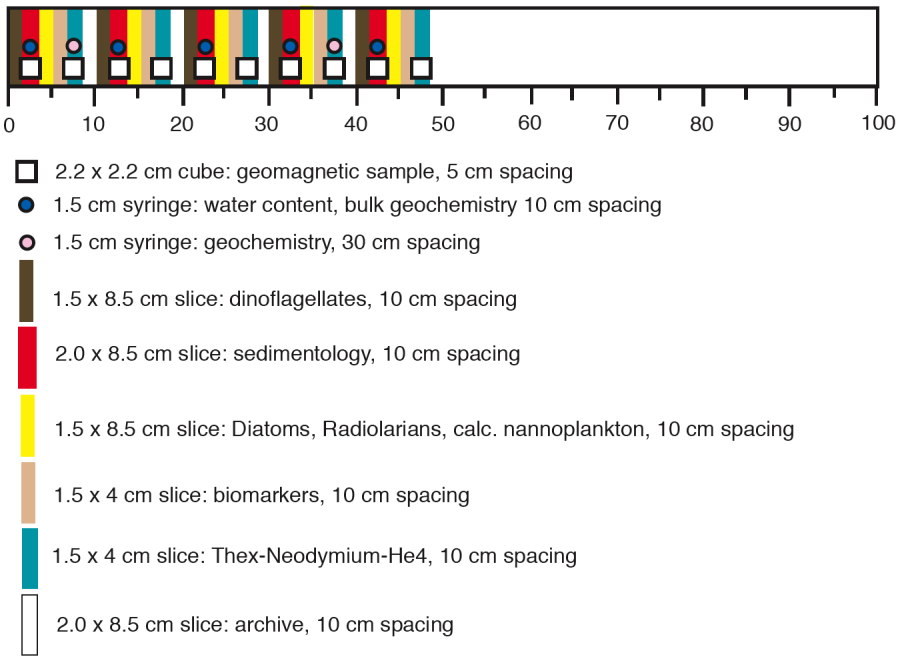

Fig. 5.2.2-1: *Sampling scheme applied for piston core sampling*

All 5.5 m long kasten corer sections were sampled in total on-board. After opening of the box and exposure of the sediment content, the outer 2 cm of the sediment margins were removed by pushing a steel string through the sediment and manual picking of the produced sediment laps. The remaining sediment was sampled in three layers. The first layer was put into two rows of plastic boxes. One row with one meter long plastic boxes, 8 x 15 cm in diameter, the other row with boxes, 8 x 8 cm in diameter. The middle layer, again was sampled with one row of the wide plastic boxes. In addition, U-channels were taken for paleomagnetic studies together with samples for water contents at 10-cm intervals. In some cores, discrete mud samples were taken for radiocarbon dating. Large samples, comprising 5-cm or 2-cm steps, were taken for the later determination of sand and pebble concentrations. One row of the third layer also was put into wide plastic boxes. The remaining part was used for sampling of samples for radiography, as described for the other cores (**Figs. 5.2.2-2, -3**).

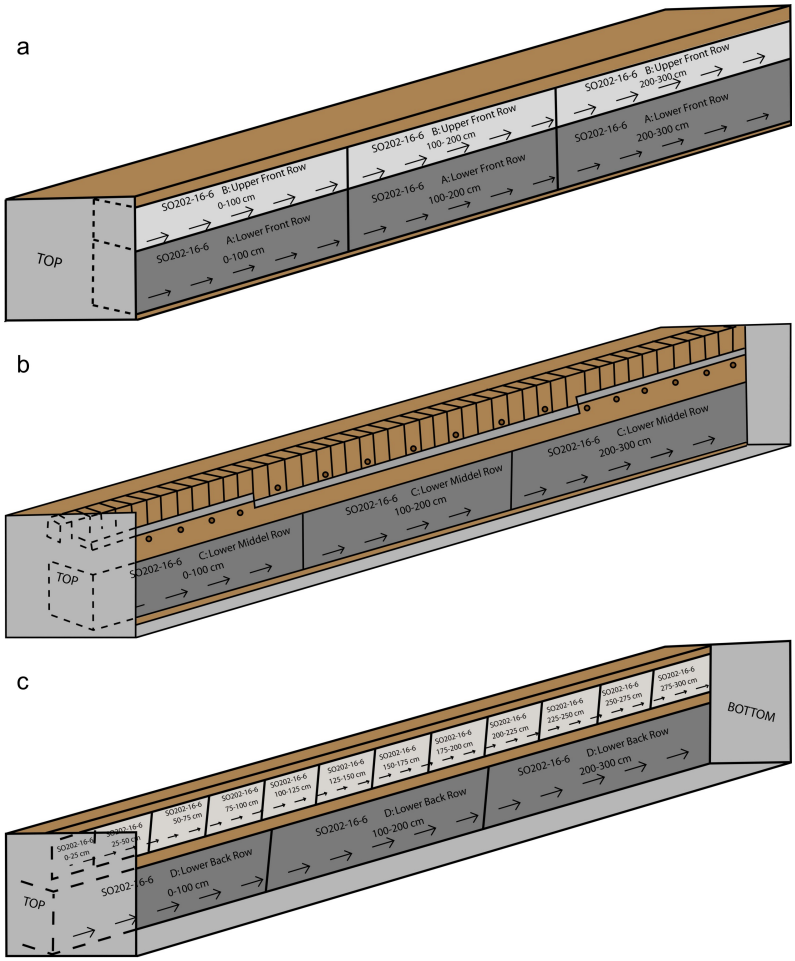

Fig. 5.2.2.-2: *Schematic representation of kasten core sampling strategy. a) front layer sampled with 1 m boxes, b) middle layer sampled with 1 m boxes at base, U-channels, water content samples and samples for sedimentological and radiocarbon analysis, c) lower layer sampled with 1 m boxes and samples for radiography.*

Fig. 5.2.2-3: *Sampling of a kasten core section (SO202-27-6) in the R/V Sonne geolab.*

5.2.3 Description of Sediment Cores

The sediment cores of the study area are dominated by biosiliceous ooze and muds with minor amounts of calcareous biogenic remains (foraminifers and coccoliths) in sediment cores taken from approximately ≤4000 m water depth. At the shallow sites on the Patton Seamounts (SO202-27, -28), the Hess Rise (SO202-37), and the Shatsky Rise (SO202-40), white-colored calcareous nannofossil ooze was encountered in some core intervals. Eight sediment cores were opened and sampled on board (see sediment-core descriptions in the Appendix section A.5).

SO202-02-2 KOL – Zenkevich Rise off Kuril-Kamchatka Trench
Core SO202-02-2 (46°58.1' N, 156°58.8' E) was taken with a piston corer at 4795 water depth east of the Kuril-Kamchatka Trench. This site is devoted to the reconstruction of water-mass exchange between the Sea of Okhotsk and the northwestern Pacific Ocean and the identification of volcanic ashes from Japan.

The recovered section comprises 12.15 m of marine sediments, comprising diatomaceous oozes, diatomaceous and diatom-bearing muds in alternation with terrigenous mud, as well as numerous discrete ash layers, ranging in thickness between 3 and 12 cm (see Section 7). Below 9.0 m lithogenic muds become more abundant. The diatom-rich sediments possibly represent interglacial stages and stadials. The lower terrigenous interval according to preliminary stratigraphic clues possibly belongs to MIS 6 and includes one lonestone of possibly glacial origin at 11.87 m.

SO202-04-1 KOL – off Kuril-Kamchatka Trench
Core SO202-04-1 was taken with a piston corer in a similar setting as Core SO202-02-2. The coring site is located at 5248 m water depth, east of the southern tip of Kamchatka (51°51.8' N, 163°09.6' E). It lies south of the Kamchatka Strait that forms the main surface and deep-water conduit between the Bering Sea and the North Pacific. The main objective is to study late Quaternary paleoceanography under the special focus on water-mass-stratification, sub-Arctic water-mass exchange, and the input of terrigenous sediment, ice-rafted debris, and volcanic ashes from Kamchatka.

Compared to sediment Core SO202-02-2, at this site, the relative amount of diatoms is lower without any appearance of pure diatomaceous oozes. Terrigenous muds dominate below 8.34 m down to the base of the core at 11.8 m and might be correlated with the basal terrigenous muds in Core SO202-02-2. The record includes about twelve ash layers, ranging in thickness between 2 and 38 cm (see Section 7). Ice-rafted debris in the form of lonestones only occurs at 3.87 m core depth.

SO202-07-6 KAL – Detroit Seamount, northwestern North Pacific
Core SO202-07-6 was taken from 2340 m water depth with a box corer from the Detroit Seamount in the northeastern Pacific Ocean (51°16.29' N, 167°41.98'E). According to the downcore record of magnetic susceptibility (see 6.1), the 4.69 m long sediment record comprises the last 95 kyr and can be used for the reconstruction of paleoceanographic changes in surface and intermediate waters.

The lithological composition of the sediments is quite heterogeneous and includes at least trace amounts of biogenic carbonate throughout the record. It can be roughly divided into five units. The lowermost interval below 4.37 consists of diatomaceous

oozes and might represent the younger time of MIS 5. The interval between 4.37-2.29 m includes variable amounts of diatoms and terrigenous mud, possibly documenting the stadials and interstadials between MIS 4 and MIS 2. The interval between 2.29 and 1.98 m includes abundant calcareous remains of foraminifera and coccoliths and might be attributed to a warmer interstadial. The interval between 1.98 and 0.6 m consists of diatomaceous oozes, likely representing MIS 2. The uppermost sediments above 60 cm again include ubiquitous calcareous biogenic remains and likely represents the Holocene. The highest amounts of carbonate appear between 25 and 35 cm. One prominent ash is intercalated between 1.95 and 1.89 m. The presence of ice-rafted debris has not been recognized.

SO202-12-1 KAL - Bowers Ridge, southern Bering Sea

Core SO202-12-1 was recovered from 2115 m water depth on the Bowers Ridge (54°03.0' N, 179°05.2' E). The objective was to gain a late Pleistocene-Holocene sediment record at high temporal resolution. Main scientific questions concern the modes of biological productivity, ocean stratification, and terrigenous sediment supply in the past. The site is expected to include ice-rafted debris from both western and eastern Beringian sources. The sediment core comprises diatomaceous oozes and muds that in some core intervals also include calcareous biogenic remains (**Fig. 5.2.3-1**). Three discrete ash layers were identified. The lower section from 6.78 m to 10.96 m consists of a chaotic contorted succession of diatom oozes with streaks of diatom mud, interpreted as a slump deposit.

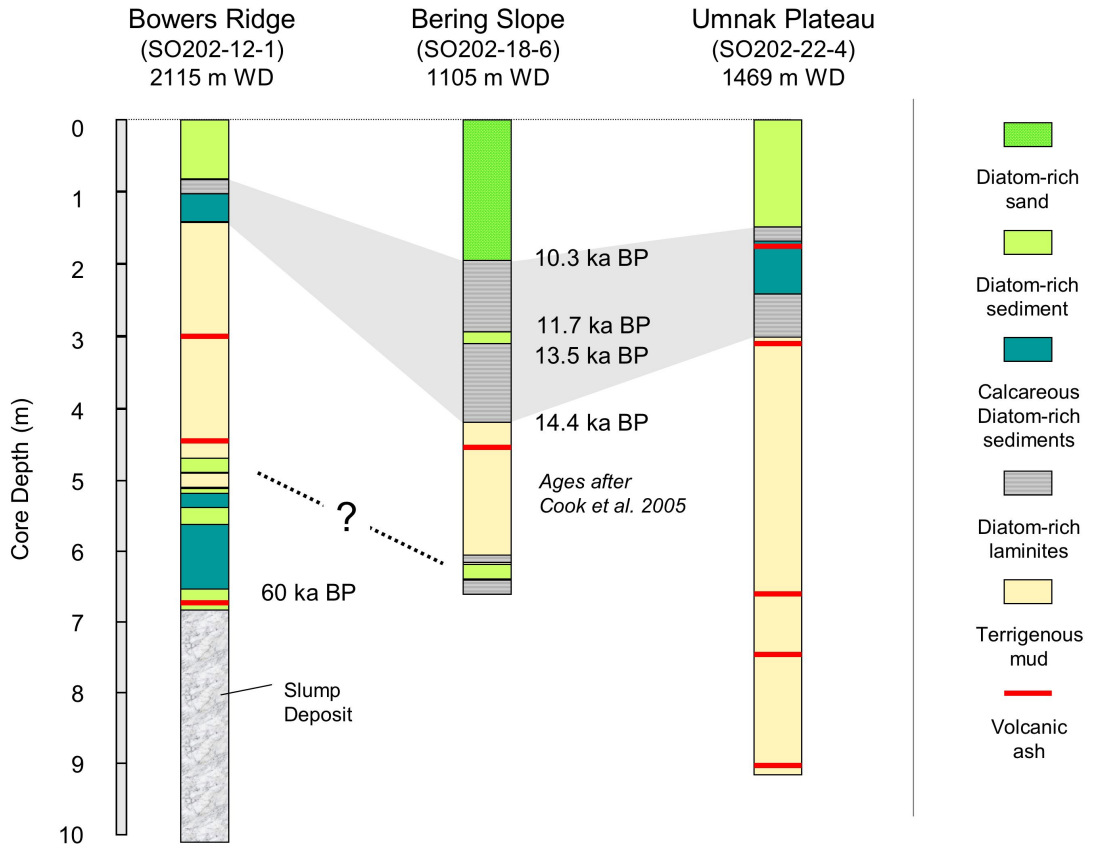

***Fig. 5.2.3-1**: Lithostratigraphic correlation of the kasten corer sediment records from the Bering Sea with simplified presentation of lithofacies. The detailed sediment descriptions are in Appendix A.5.*

According to preliminary age assignments on the basis of lithogenic criteria and the correlation of magnetic susceptibility with other sediment cores of that area (see stratigraphy), the base of the undisturbed section starts in the older part of MIS 3. The intervals between 5.69 and 6.60 cm and between 5.12 and 5.29 cm reveal the presence of planktonic foraminifera and coccoliths that might indicate warmer interstadials of MIS 3 (**Fig. 5.2.3-1)**. The lower of both intervals is strongly bioturbated, pointing to former favorable living conditions for benthic organisms on the sea floor. The section between 1.45 m and 5.12 m reveals a quite uniform lithology of diatom-bearing silty clays with a pure diatom ooze layer between 4.68-4.78 m. The upper diatom-rich sediments above 1.45 m tentatively represent MIS 1. In the older part, between 145 and 80 cm, they include calcareous biogenic remains. An outstanding feature of this latter interval is the presence of laminated sediments that can be correlated with the other sediment cores from the Bering Sea **(Fig. 5.2.3-1**).

SO202-18-6 KAL – Bering Slope, northern Bering Sea

A 7.21 m long sediment record was gained with the kasten corer at 1105 m water depth from the continental slope off the wide Alaskan shelf area in the northern Bering Sea (60°07.6'N, 179°26.1'W). The record is devoted to the reconstruction of paleoceanographic conditions during MIS 3 to MIS 1 at high temporal resolution. Another objective concerns the reconstruction of both glacigenic and fluvial detrital sediment supply from eastern Beringia.

The section is characterized by the presence of laminations and well preserved bivalves. One discrete ash layer appears between 4.54 and 4.48 m. The sediment record basically shows a fourfold pattern of lithological change (**Fig. 5.2.3-1**). The lowermost unit below 6.31 m consists of diatomaceous oozes and muds that are partly laminated. These biosiliceous sediments are overlain by terrigenous muds between 6.31 and 4.8 m. Another diatom-rich unit between 4.8 and 1.9 m consist of laminated sediments interrupted by a non-laminated interval between 2.95 and 3.15 m. The laminae are composed of mm- to sub-mm thick couplets of pure light-colored diatomaceous ooze, alternating with dark diatom-bearing terrigenous clayey silt, frequently including remains and fibers of marine macro algae (**Fig. 5.2.3-2**).

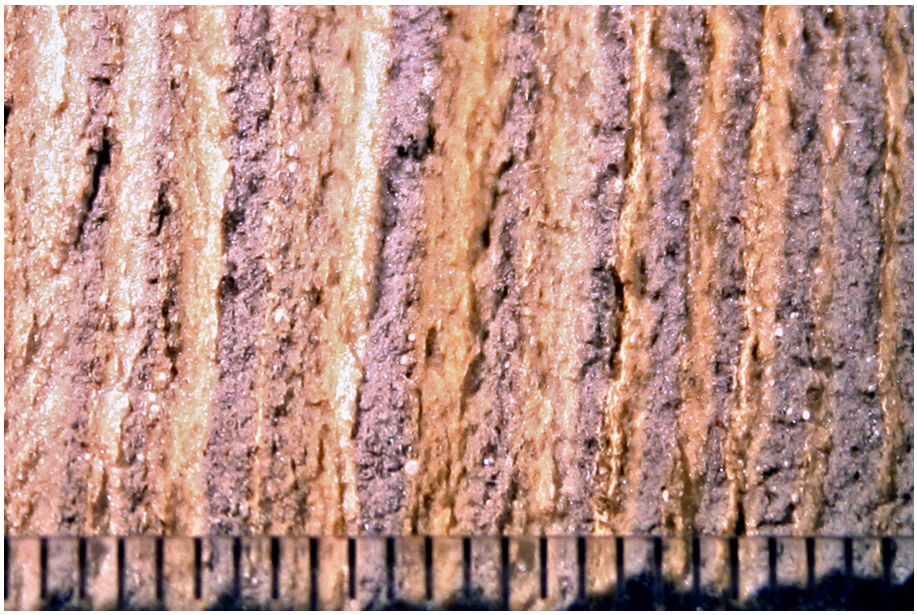

***Fig. 5.2.3-2**: Laminated section of core SO202-18-6 (scale mm).*
Whether these laminae represent annual layers (varves) has to be checked during later microfacies research. The diatom layers might represent algae blooms during the warm and sea-ice-free season, while the dark layers document detrital background sedimentation in the hemipelagic setting of the continental slope. According to Cook et al. (2005), the laminated sediments were deposited during the late glacial stage (Termination I, comprising the Bølling-Allerød interstadial, the Younger Dryas stadial, and the preboreal interstadial) between 14.4 and 10.3 ka BP. The laminated sediments are overlain by Holocene diatom-bearing terrigenous sediments, including a high portion of fine-grained quartz sand and mica.

SO202-22-4 KAL – Umnak Plateau, southeastern Bering Sea
The third kasten corer from the Bering Sea was taken from the Umnak Plateau at 1469 m water depth (54°34.4'N, 168°48.6'W) in a similar setting as Core SO202-18-6. The site is located in the southeastern Bering Sea close to the Alaska shelf and the Aleutian Islands. The scientific objectives are identical with those from Site SO202-18, described in the previous sub-chapter.

The sediment record exhibits a threefold lithological pattern and includes several ash layers and abundant lonestones. An extended interval of strongly bioturbated terrigenous silty clays makes up the lower unit between 9.69 and 3.19 m core depth. The unit between 3.19 and 1.75 m includes two intervals of laminated sediments, interrupted by calcareous diatomaceous oozes between 2.40 and 1.91 m. This unit shows lithological affinities to those late glacial sediments encountered on the Bering Slope (SO202-18) and the Bowers Ridge (SO202-12) (**Fig. 5.2.3-1**). The upper, possibly Holocene unit comprises diatomaceous muds and oozes.

SO202-27-6 KAL – Patton Seamouts, northeastern Pacific Ocean
A 2.91 m long sediment record was recovered with a kasten corer from the Patton Seamounts at a water depth of 2919 m (54°117.8'N, 149°36.0'W). The record possibly represents a sedimentary record of late Pleistocene-Holocene variability in paleoceanographic conditions in the northeastern Pacific realm at glacial-interglacial (Milankovitch) time scales with high amounts of ice-rafted lonestones from the southern coastal areas of Alaska. It comprises biosiliceous oozes with variable amounts of calcareous biogenic remains and terrigenous mud, in places strongly bioturbated.

SO202-29-4 KOL – Gibson Seamount, northeastern Pacific Ocean
The 12.97 m long sediment record of SO202-29-6 was taken with the piston corer south from the Patton Seamounts on the Gibson Seamount at 3983 m water depth (52°01.7'N, 148°53.7'W). The scientific objectives are identical to those of Site SO202-27. The marine sediments include several ash layers and abundant lonestones. They comprise a diverse suite of sediment composition with alternations of diatomaceous oozes and muds and terrigenous muds. A number of nine intervals, ranging in thickness between a few centimeters and 100 cm, include calcareous biogenic remains, possibly reflecting changes in carbonate preservation in response to repeated vertical shifts of the lysocline.

SO202-35-1 SL– Central North Pacific
A 19.29 m long sediment core was retrieved with the gravity corer at 5507 m water depth in the deep pelagic setting of the central North Pacific (39°27.2'N, 179°06.7'W).

The site is dedicated to the reconstruction of long-term paleoceanographic changes during the Plio-Pleistocene and the characterization of dust fluxes from central and eastern Asia. The record comprises a quite monotonous record of light brownish diatom-bearing clay, bioturbated to variable extent. The presence of manganese nodules and streaks gives evidence of very low sedimentation rates.

6. SEDIMENT PHYSICAL PROPERTIES

Thomas Frederichs, Lucia Reichelt
Marine Geophysik, FB Geowissenschaften Universität Bremen, Germany

All sediment series recovered during R/V *Sonne* Cruise SO202-INOPEX by gravity, piston and kasten coring were subject to routine geophysical shipboard measurements. These were usually performed on closed full cores and only partially on split half cores (SO202-04-1, SO202-29-4, SO202-35-1, SO202-39-3). Kasten corer sediments (SO202-07-6, SO202-12-1, SO202-18-6, SO202-22-4, SO202-27-6) were measured as 8 x 8 x 100 cm boxes. Measurements comprised three basic parameters:

- magnetic volume susceptibility κ,
- electric resistivity R_s (as a measure of porosity and density), and,
- spectral light reflectance

These properties are closely related to sediment lithology and provide high-resolution core logs with a standard spacing of 2 cm for electric resistivity and magnetic susceptibility and 0.01 cm for light reflectance. They were measured with a customized GEOTEK Multi-Sensor Core Logger (MSCL) utilizing a stepper motor to convey core segments along a track and through a series of sensors. Positions and lengths are automatically detected. The separate logging measurements are controlled and rapidly collated by the systems computer terminal.

6.1 Magnetic Susceptibility

The magnetic volume susceptibility κ is defined by the equations

$$B = \mu_0 \cdot \mu_r \cdot H = \mu_0 \cdot (1 + \kappa) \cdot H = \mu_0 \cdot H + \mu_0 \cdot \kappa \cdot H = B_0 + M$$

with magnetic induction B, absolute and relative permeabilities μ_0 and μ_r, magnetizing field H, magnetic volume susceptibility κ and volume magnetization M. As can be seen from the third term, κ is a dimensionless physical quantity. It records the degree to which a material is magnetized by an external magnetic field.

For marine sediments the magnetic susceptibility may vary from an absolute minimum value of $-15 \cdot 10^{-6}$ (diamagnetic minerals such as pure carbonate or silicate) to a maximum of some $10.000 \cdot 10^{-6}$ for basaltic debris rich in (titano-) magnetite. In most cases κ is primarily determined by the concentration of ferrimagnetic minerals, while paramagnetic matrix components such as clays are of minor importance. Enhanced susceptibilities indicate higher concentrations of lithogenic or authigenic components. This relation may serve for correlating sedimentary sequences deposited under similar global or regional conditions.

The core logger is mounted with a commercial BARTINGTON M.S.2 susceptibility meter with a 140 mm loop sensor. Due to the sensor's size, its sensitivity extends over a core interval of about 8 cm. Consequently, sharp susceptibility changes in the sediment column will appear smoothed in the κ core log and thin layers such as ashes cannot be appropriately resolved in any case. In order to make an accurate end correction at the base of each segment and to assess the drift of the

susceptibility meter, a spacer cylinder of 29.5 cm length was placed between each segment during the measurement procedure. The measurements taken at the centre of the spacer was used to assess and compensate the instrumental drift. During post-processing all data related to void sections were removed to provide a continuous composite core log. In case of piston and kasten cores, a calibration factor of 14.03 was applied to convert the digital readings of the M.S.2 into volume magnetic susceptibility values in 10E 6 SI units. The factor is in accordance with the equation given in the GEOTEK MSCL manual:

$k_{rel} = 4.8566 (d/D)^2 - 3.0163 (d/D) + 0.6448 = 0.713 \rightarrow 1/k_{rel}\ 10 = 14.03$

with d = core diameter = 90 mm, D = loop diameter = 140 mm

In case of gravity cores with a diameter d = 120 mm, a factor of $1/k_{rel}$ 10 = 6.14 was applied.

During SO202-INOPEX coring stations were located between 36° and 60°N across the Northern Pacific and the Bering Sea. The coring locations comprise sediments from water depths between 723 m (SO202-26-2) and 6133 m (SO202-33-4). Piston core lengths varied between 1.27 m (SO202-05-7) and 24.35 m (SO202-37-2). A total of 50 sediment cores with a cumulative length of 857.69 m were investigated by physical properties methods completed by 115.99 m of line scan data from ten of these cores. The data from Core SO202-29-4 are shown in **Fig. 6.3-1** as example for the results from core logging.

The general characteristics of magnetic susceptibility are compiled in the upper part of **Fig. 6.1-1**. Dots mark mean values for individual cores, vertical error bars denote standard deviations. Each diagram is divided into subsets of cores of similar magnetic susceptibility patterns.

Mean magnetic susceptibilities of all cores with the exception of those from the Bering Sea (SO202-14-3 through SO202-19-2) and those from the southwestern part of the working area (SO202-32-4 through SO202-40-1) are comparably high in relation to other marine deep-sea sediments. This is obviously related to a continual high terrigenous input of volcanic material also in times between volcanic eruptions, maybe by resuspension or ocean currents or bottom currents. The highest value of about 13341·10E 6 SI was found in sediments from Site SO202-24 located between the Sirius and the Patton Seamounts (**Fig. 1.2-9**). High peaks are usually related to tephra layers or in some instances to drop stones. The low mean values in the southwestern cores in the area from Chinook Trough to Emperor Trough, Ojin Guyot and Shatsky Rise may be ascribed to the far distance of the sites to volcanic sources. A trend to lower susceptibilities and reduced variability, indicated by lower standard deviations, for the cores from the continental shelf areas of the Bering Sea probably reflects increasing destruction of the original magnetic signal as a result of diagenetic overprint.

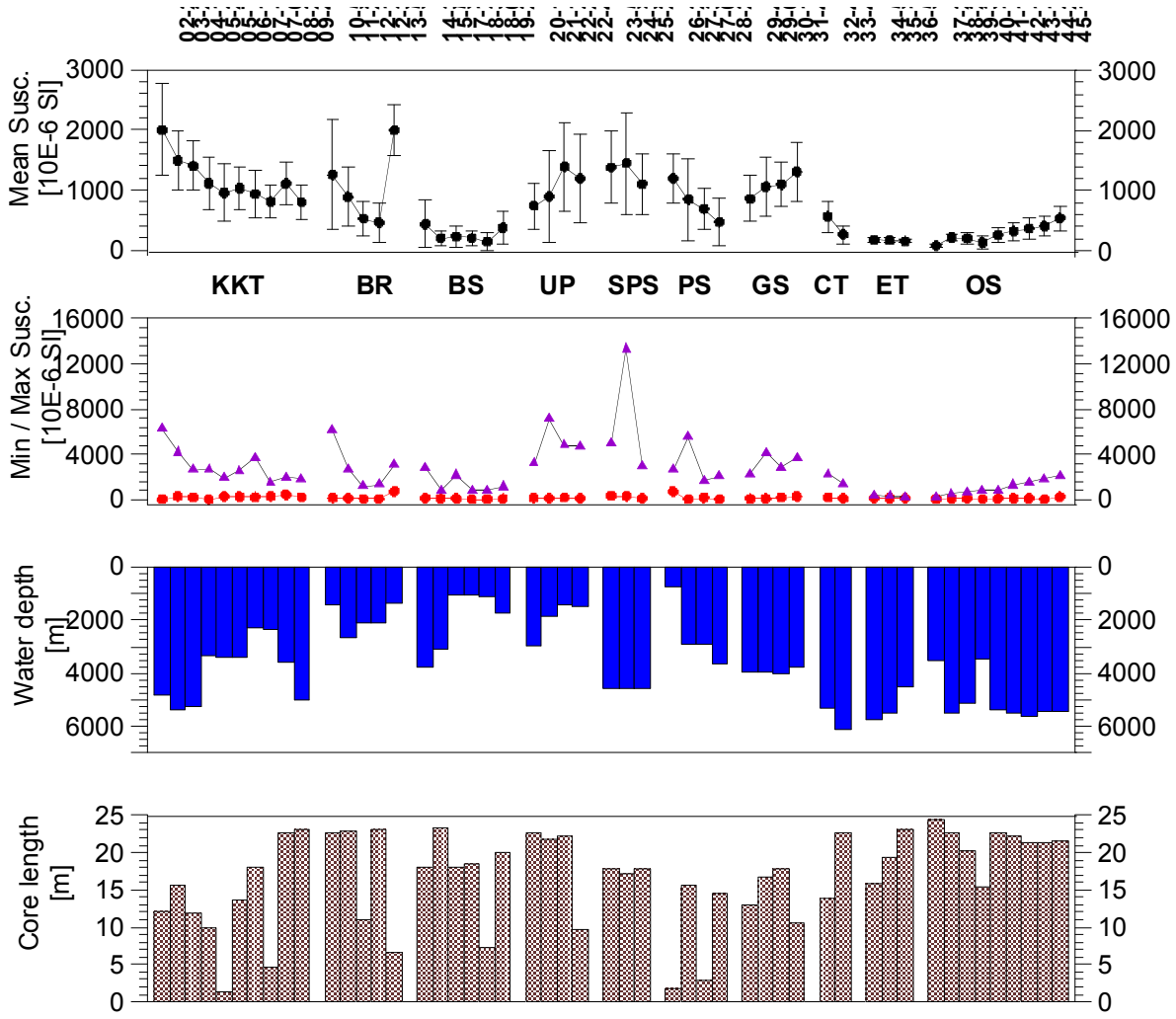

Fig. 6.1-1: *Mean magnetic susceptibilities of cores SO202-02-2 through SO202-45-1 compared to variations in water depth at the sampling sites and core recovery. The vertical error bars denote standard deviations. KKT: Kuril-Kamchatka Trench, BR: Bowers Ridge, BS: Bering Sea, UP: Umnak Plateau, SPS: Sirius / Patton Seamounts, PS: Patton Seamount, GS: Gibson Seamount, CT: Chinook Trough, ET: Emperor Trough, OS: Ojin Guyot - Shatsky Rise.*

As a first assessment of the magnetic susceptibility data we tried to divide the sites into ten subsets according to their signal patterns and regarding their site locations. **Fig. 6.1-2** exhibits representative records of magnetic susceptibility for each of the ten subsets. The map in **Fig. 6.1-3** displays the geographical distribution of the core subsets.

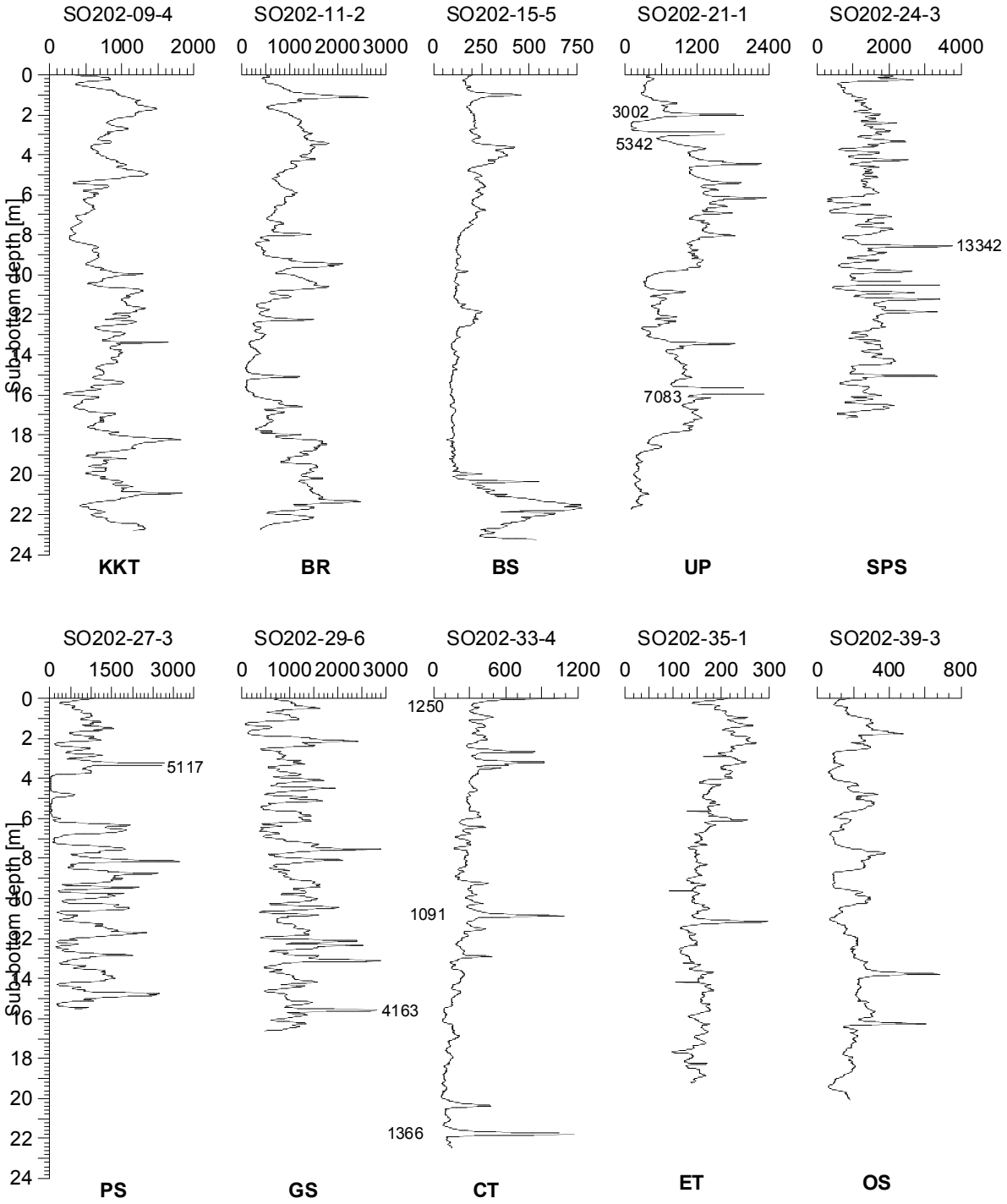

Fig. 6.1-2: *Representative records of magnetic susceptibility for each of the ten core subsets. KKT: Kuril-Kamchatka Trench, BR: Bowers Ridge, BS: Bering Sea, UP: Umnak Plateau, SPS: Sirius / Patton Seamounts, PS: Patton Seamount, GS: Gibson Seamount, CT: Chinook Trough, ET: Emperor Trough, OS: Ojin Guyot - Shatsky Rise.*

A first subset (KKT; cores recovered east of the Kuril-Kamchatka trench) comprises sites SO202-02-2 trough SO202-09-4 from the Kuril to the Aleutian Rise including cores from the Obruchev Rise and the Detroit Seamount (**Figs. 1.2-4/-5**). These cores demonstrate comparable smooth cyclic variations, which might be associated with glacial-interglacial cycles. Mean susceptibilities within this subset vary from about 800 to 2000 10E-SI showing the highest values with also the highest standard

deviations at the western locations. There is a regular decreasing trend in both, mean values and standard deviations, towards the east, possibly indicating that tephra supply diminishes with distance from the volcanic sources in Japan and the Kamchatka Peninsula.

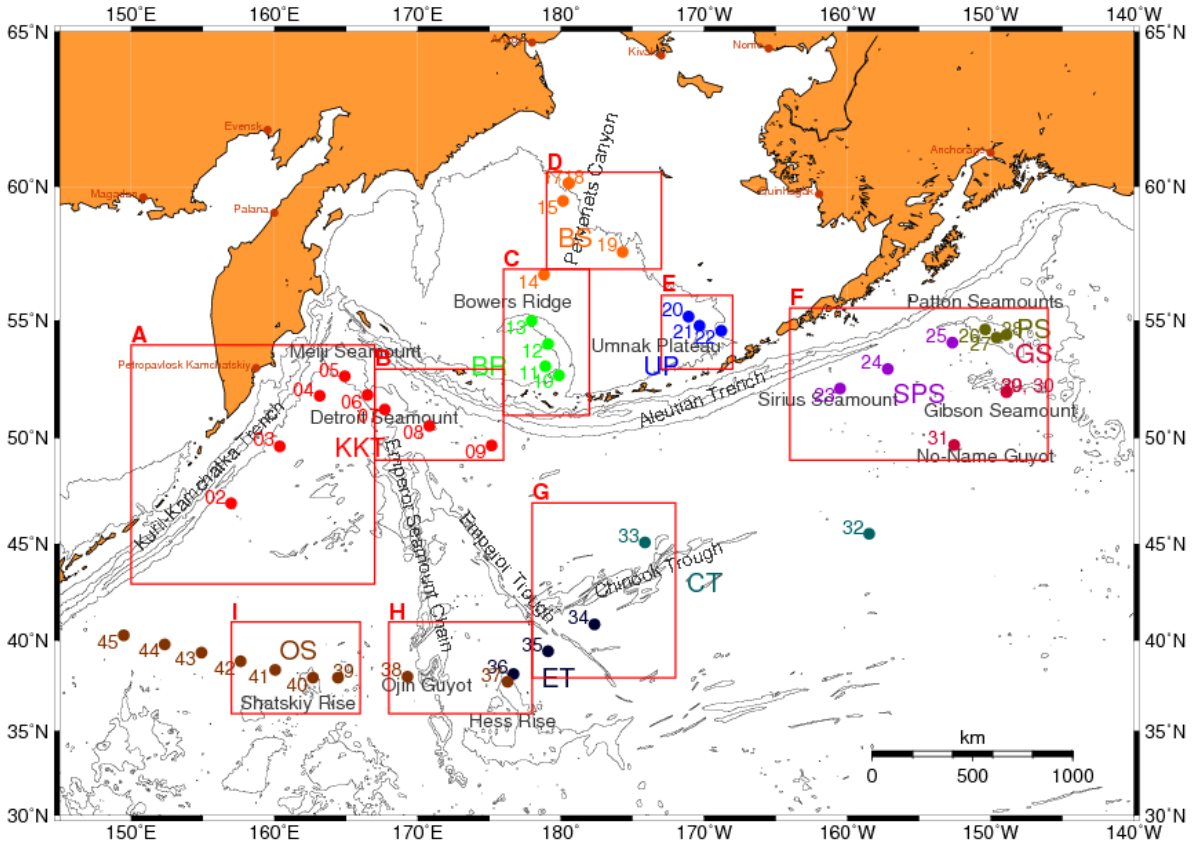

Fig. 6.1-3: *Map with subsets of sediment cores indicated by different colors and abbreviations (see below). Subset classification is made according to the cores' magnetic susceptibility patterns. Working areas A to I are overlain as rectangles. Kuril-Kamchatka Trench, BR: Bowers Ridge, BS: Bering Sea, UP: Umnak Plateau, SPS: Sirius / Patton Seamounts, PS: Patton Seamount, GS: Gibson Seamount, CT: Chinook Trough, ET: Emperor Trough, OS: Ojin Guyot - Shatsky Rise.*

The cores from Sites SO202-10-5, SO202-11-2, SO202-12-1/3 and SO202-13-5 from Bowers Ridge (**Fig. 1.2-6**) were summarized in the third subset (BR; Bowers Ridge). These show similar background variations as found in the signals of the cores from subset KKT of the Kuril-Kamchatka Trench - Aleutian Rise but with higher variabilities expressed by higher standard deviations (288 to 917 10E-6 SI). Additionally we found decreasing mean values from 1253 to 459 10E-6 SI from the southern (SO202-10-5) to the northern part (SO202-12-1/3) of Bowers Ridge.

Somehow special is the high-frequency magnetic susceptibility pattern of Core SO202-13-5 from the northern part of Bowers Ridge. Along with Core SO202-02-2 from the Kuril-Kamchatka trench it exhibits the highest mean value of magnetic susceptibility of 1993 10E-6 with a standard deviation of about 415 10E-6 SI and with a unique prominent linear trend to higher values towards larger core depths.

Regarding only these characteristics, the core would rather fit into subset SPS from the Sirius / Patton seamounts. If this is due to a missing top sequence in the core or due to a distinctly different sedimentation regime is yet an open question.

A third subset (BS) is composed of sites from the northern Bering Sea (SO202-14-3 through SO202-19-2) (**Fig. 1.2-7**). These cores show significantly lower mean susceptibilities, ranging from 138 to 432 10E-6 SI with reduced variability expressed by lower standard deviations. This holds in particular for cores SO202-15-5 through SO202-18-6, where as core SO202-14-3 from the Bering Sea Basin and SO202-19-2 from a more southerly location on the Alaskan Shelf show slightly higher mean values and standard deviations as well. This subset is characterized by high gas contents indicating reductive conditions in the sediment leading to mineral alteration or dissolution of iron oxides and thus to decreased susceptibilities as low as less than 20 10E-6 SI.

The susceptibility patterns of the fourth subset (Cores SO202-20-1, SO202-21-1, SO202-22-2/4) from the Umnak Plateau (UP) located at the southeastern part of the Bering Sea (**Fig. 1.2-8**) are very similar to those from the cores from Bowers Ridge but with higher standard deviations of up to 767 10E-6 SI. Mean susceptibilities increase from 739 to 1385 10E-6 SI from the north (SO202-20-1) to the south (SO202-22-2).

A fifth subset (SPS; Sirius / Patton Seamounts) consisting of cores SO202-23-5, SO202-24-3 and SO202-25-2 was recovered between the Sirius and Patton Seamounts (**Fig. 1.2-9**). They demonstrate relatively high mean susceptibilities (1100 to 1476 10E-6 SI) with relatively high standard deviations (varying from 410 to 844 10E-6 SI). The most prominent characteristic is their high-frequency susceptibility pattern which can be found as well but in a slightly reduced way in the susceptibility logs of the cores of subset PS (Patton Seamount) (SO202-26-2, SO202-27-3/6 and SO202-28-2, mean values 464 to 843 10E-6 SI, standard deviations between 344 to 684 10E-6 SI) which are located a little bit more to the east in the Patton Seamount area. Likewise similar high-frequent susceptibility patterns along with higher mean values (854 to 1301 10E-6 SI, standard deviations from 373 to 484 10E-6 SI) were found in Cores SO202-29-4/6, SO202-30-1 and SO202-31-4 of subset GS originating from an area between the Gibson Seamount and another yet unnamed seamount (**Fig. 1.2-9**).

Again high-frequent variations combined with a slightly lower variability in magnetic susceptibility (standard deviation of 258 10E-6 SI) was found for Core SO202-32-4 with a relatively low mean susceptibility of 558 10E-6 SI. Additionally to this core of subset CT (Chinook Trough), which is to be expected to extent further into the past, a core (SO202-33-4) was recovered north of the Chinook Trough fracture zone (**Fig. 1.2-10**). This core demonstrates a mean magnetic susceptibility of 260 +/- 153 10E-6 SI. Only the gas containing cores of subset BS from the Bering Sea continental slope exhibit lower values. The low mean susceptibility may be related to the large the distance to the sources of volcanic material in Alaska and/or on the Kamchatka Peninsula. A prominent ash layer at the base of the core may provide an opportunity for age determination. Preliminary correlation of Cores SO202-32-4 and 33-4 relates two ash layers in Core SO202-32-4 at a core depth of about 8 to 9 meters to a depth interval of about 2.5 to 3.5 m in Core SO202-33-4, suggesting much lower sedimentation rates at the latter site.

The subset ET (Emperor Trough) comprises Cores SO202-34-5, SO202-35-1 and SO202-36-5 demonstrating significantly low mean susceptibilities between 147 and 169 E-6 SI with the lowest variability (standard deviations below 35 10E-6 SI) of all sites. This may reflect the farthest distance from volcanic sources compared to all other sites (**Fig. 7.1-1**).

Core SO202-37-2 exhibits similar low mean susceptibility and standard deviation as the cores from subset ET. Since its record resembles, at least the topmost 12 m, the susceptibility logs of cores SO202-38-2, 39-3, 40-1, 41-1, 43-1, 44-1 and 45-2 we pooled these cores into subset OS (Ojin Guyot / Shatsky Rise). The seven cores show increasing mean magnetic susceptibilities varying from 129 (SO202-40-1) to 532 10E-6 SI (SO202-45-1) with comparable low standard deviations ranging from 36 to 202 10E-6 SI. The mean values are partly as low as for the diagenetically overprinted cores from the Bering Sea and significantly lower as for the cores located further north, probably reflecting the far distance from volcanic sources. Nevertheless, ash layers were found in these cores as well and may be used for correlation of the cores. At least for the younger sequences of the cores such a correlation seems to be reasonable. Cores SO202-41-1 and 42-1 show almost identical sedimentation rates with respect to their susceptibility logs. Core SO202-41-1 is stratigraphically slightly older. The ash layers are most pronounced in Core SO202-45-1. The magnetic susceptibility signal of Core SO202-40-1 differs a little bit from the other cores of the subset resulting in a less obvious correlation as for the other cores. Furthermore, the correlation seems to indicate that the topmost sediments are missing in Core SO202-40-1.

In summary, no clear trend in magnetic susceptibility depending on the water depth of the core locations is obvious. Thus, the geographical locations of the coring sites seem to be more relevant for the magnetic susceptibility patterns of the cores, in particular their distance from volcanic sources.

The most prominent features in most of the cores are the distinct ash layers which are in most cases, besides the ‘white ashes’ (see Section 7) indicated by high values of magnetic susceptibilities. In some instances ice-transported drop stones cause high susceptibility values as well. Thus, some caution is advisable when correlating sediment cores only by their magnetic susceptibilities.

Further aspects

At five core locations, both, a piston core and a kasten core were recovered. Assuming the kasten core is less deformed than the piston core due to its large cross-section of 30 by 30 cm, it provides the opportunity to check the ’quality’ of the piston core in terms of deformation of the sediment column. As an example, the data of Cores SO202-12-1 (kasten corer) and SO202-12-3 (piston corer) originating from Bowers Ridge are shown in **Fig.6.1-4**.

Comparison of their magnetic susceptibility records reveals an obvious correlation of both cores. We determined 27 tie points resulting in the correlation shown in **Fig. 6.1-4**. It turns out that a core depth of 6.28 m in the kasten core complies with a core depth of 6.94 m in the piston core (**Fig. 6.1-5**), implying that the piston core is extended by less than 10% compared to the kasten core. A core depth of 0.02 m in the kasten core was related to a core depth of 0.22 m in the piston core, suggesting

that the topmost centimeters of the sediment column are represented more accurately in the piston core than in the kasten core. The minimal differences in the depth of respective horizons in both cores give rise for reliable calculations of sedimentation and/or accumulation rates at this site.

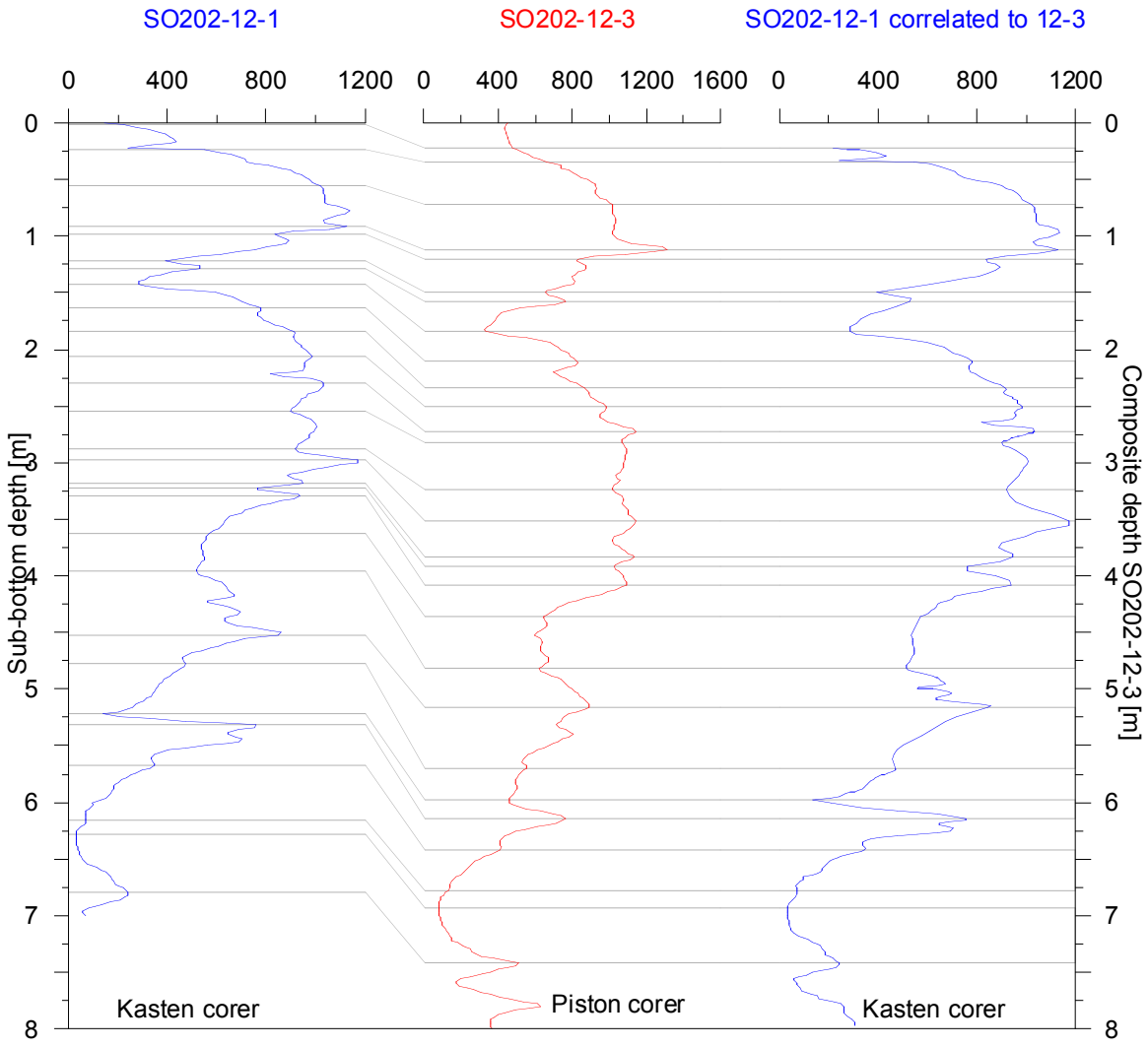

Fig. 6.1-4: *Correlation of the upper undisturbed part of kasten core SO202-12-1 with piston core SO202-12-3 based on their magnetic susceptibility records. Below a core depth of 6.78 m, SO202-12-1 was disturbed. Grey lines indicate 27 correlation tie points.*

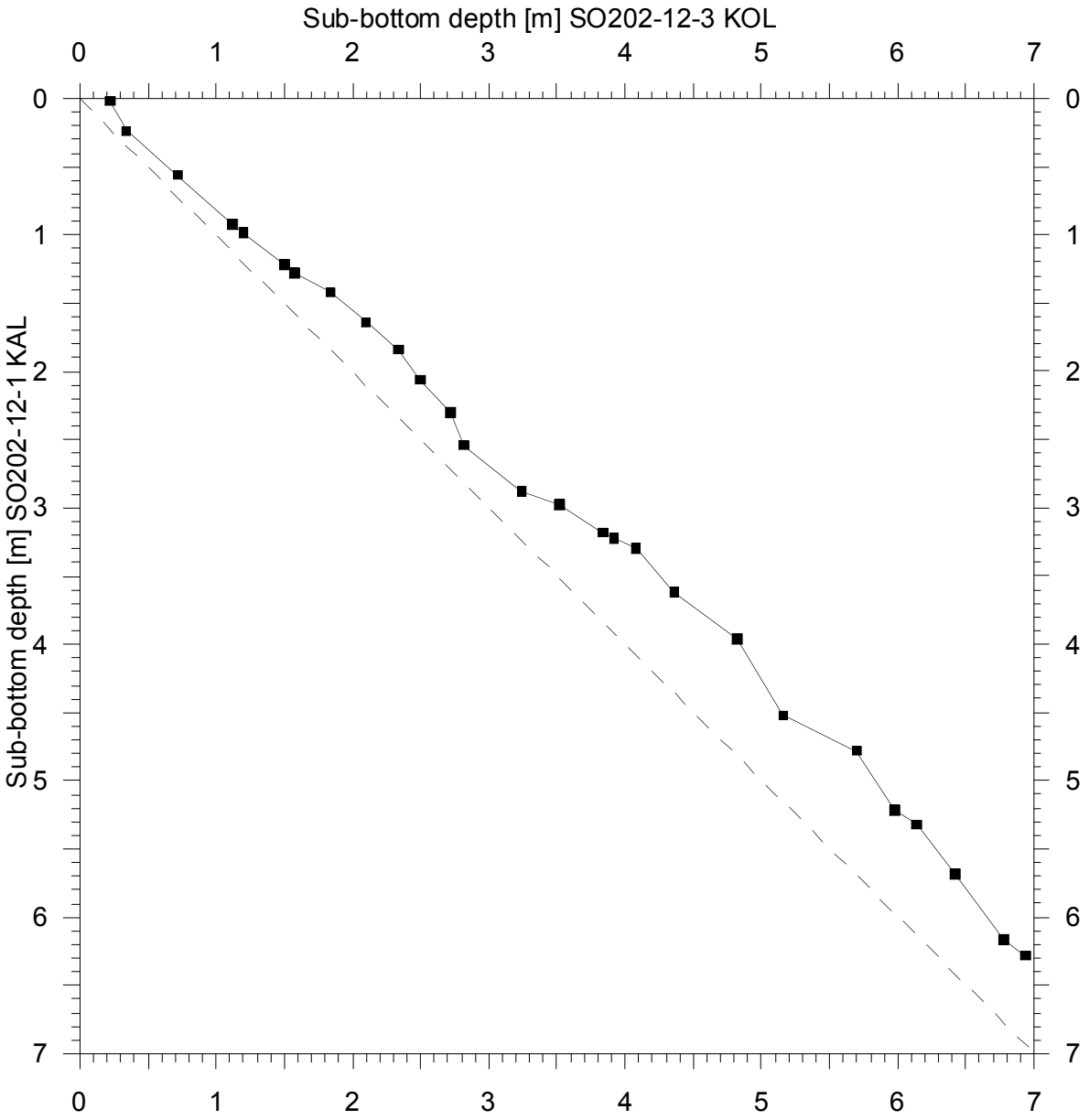

Fig. 6.1-5: *Sub-bottom depth of kasten core SO202-12-1 plotted versus sub-bottom depth of piston core SO202-12-3. The dashed line indicates an identical depth relation.*

In order to tentatively attribute an absolute age to the sediment cores recovered during cruise SO202-INOPEX, the magnetic susceptibility record of core SO202-07-1 was correlated to the dated almost 45 m long N.S. Marion Dufresne core MD01-2416 from Detroit Seamount (Bassinot et al., 2002).

Figure 6.1-6 shows a correlation based on 54 tie points of the magnetic susceptibility records of both cores. A core depth of 17.54 m at the base of core SO202-07-1 was related to a core depth of 21.52 m in core MD01-2416. This implies that the time interval represented by core SO202-07-1 is stretched by about 18% in core MD01-2416. Using the age model of Gebhardt et al. (2008) we assigned an age of 391 ka to the base of core SO202-07-1 resulting in a mean sedimentation rate of about 4.6 cm/kyr (**Fig. 6.1-7**). The boundary of MIS 7/8 with an age of 245 ka is attributed to a core depth of 11.85 m.

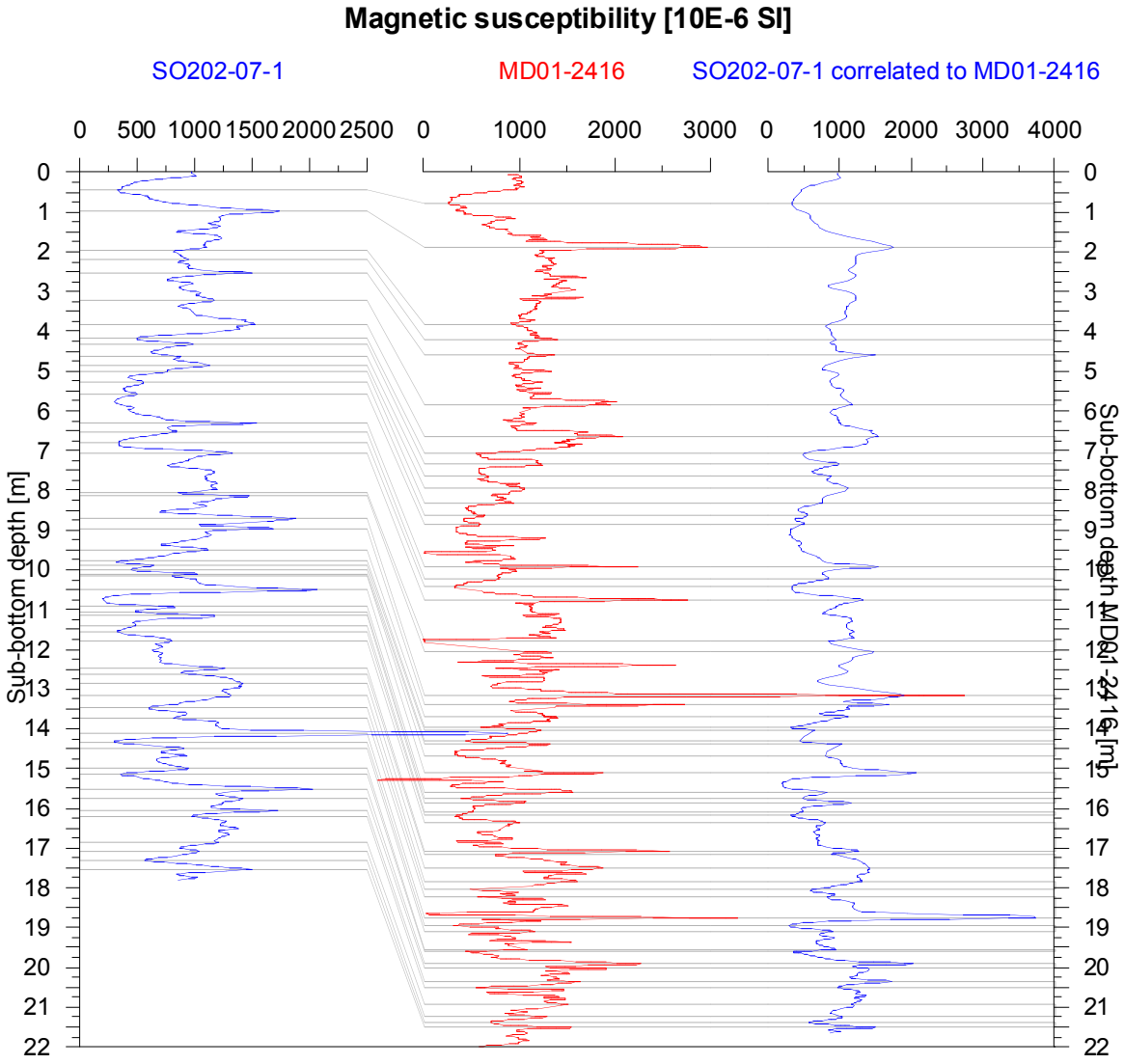

Fig. 6.1-6 *Correlation of piston core SO202-07-1 from Detroit Seamount with piston core MD01-2416 based on their magnetic susceptibility records. Grey lines indicate 54 correlation tie points. Please note the different scales of susceptibility axes for core SO202-07-1 in the left and right plot, respectively.*

An independent correlation of the susceptibility record of Core SO202-07-1 to that of the upper 16 m of ODP core 883D recovered also from the Detroit Seamount based on 51 tie points relates a depth of 12.13 m in Core SO202-07-1 to an age of 243 ka. This was done using the age model of Keigwin (1995), which identifies a composite depth of 14.50 m at Site 883 (assigned to stage boundary MIS 7/8, 243 ka) with core depth of 13.00 m in core 883D correlating to a depth of 12.13 m in Core SO202-7-1.

Okada et al. (2005) determined a sedimentation rate of only about 3 cm/kyr for core ES recovered from almost the same water depth of 2388 m but from an about 100 nm more southerly located site on the Emperor Seamount Chain. This results in an age of about 350 ka at a core depth of only 8.5 m.

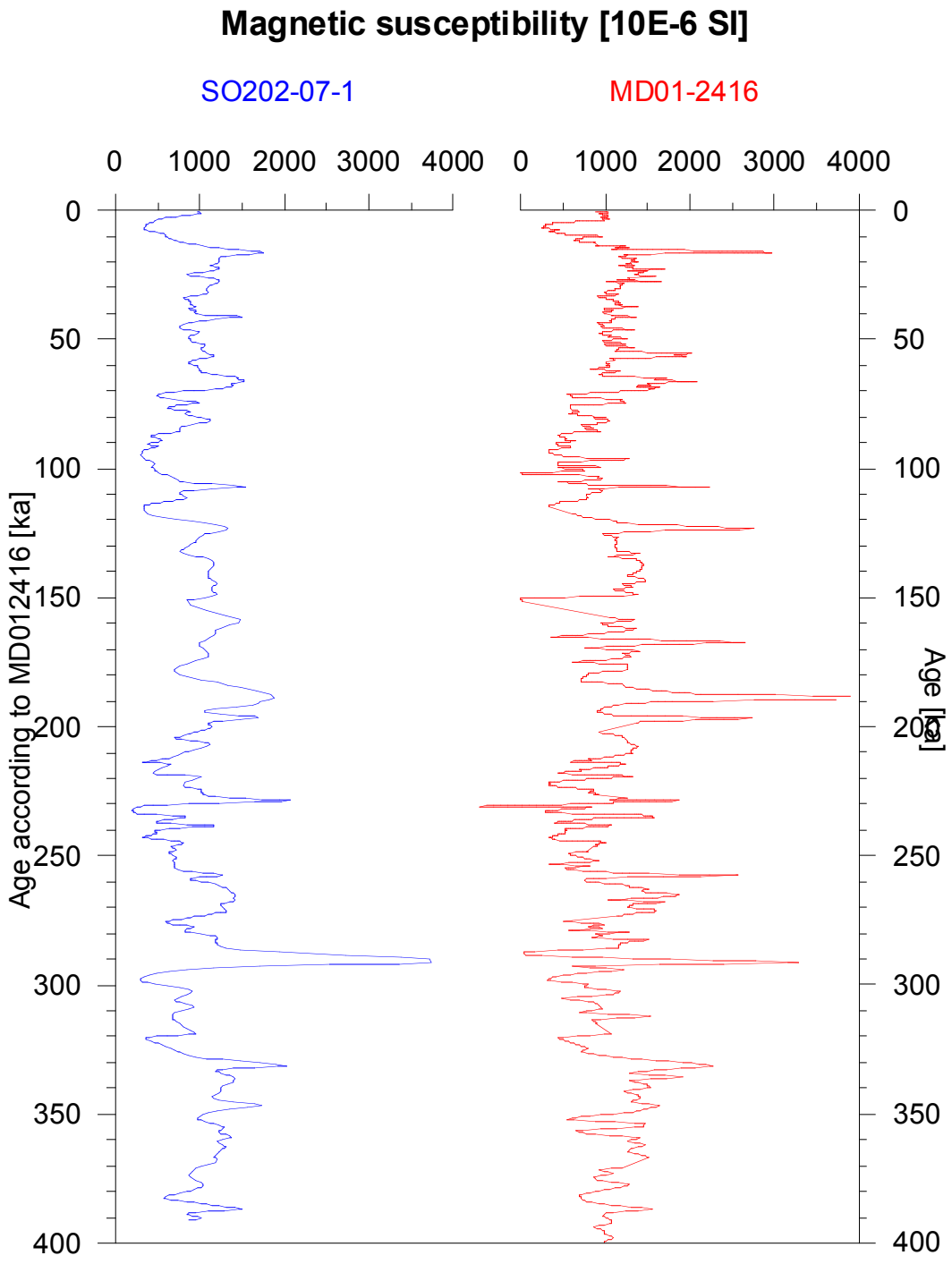

Fig. 6.1-7 *Magnetic susceptibility records of piston cores SO202-07-1 and MD01-2416 from Detroit Seamount plotted versus the age of piston core MD01-2416 using the correlation shown in Fig. 6.1-5 and the age model of Gebhardt et al. (2008). Peak values of magnetic susceptibility in Core MD01-2416 at about 190 ka were clipped for the sake of equal axis scales of both cores.*

On the basis of the magnetic susceptibility records we tentatively correlated cores SO202-02-2 through SO202-9-4 with Core SO202-07-1. According to this correlation, cores SO202-02-2, 03-2, 04-1, 05-2 reach back in time as far as to the boundary of MIS 6/7 according to an age of 190 ka. Core SO202-06-1 reaches an age of 270 ka at its base, which corresponds to the middle MIS 8. Core SO202-07-6 extends back to MIS 5 to about 95 ka. Cores SO202-08-2 and SO202-09-4 cover the time back to

early MIS 7 (about 240 ka). Mean linear sedimentation rates were calculated to values ranging from less than 5 cm/kyr to almost 10 cm/kyr as listed in **Table 6.1-1**.

Based on age models derived from geomagnetic paleointensity measurements and oxygen isotope stratigraphy, Okada et al. (2005) calculated linear sedimentation rates of about 3 cm/kyr to 13 cm/kyr for sediments recovered from Bowers Ridge. The location of Core BOW-08 of their study conforms roughly to that of our Core SO202-13-5, that of Core BOW-09 with SO202-12-3 and that of BOW-12 with SO202-11-2, respectively.

Core SO202-	Water depth [m]	Core length [m]	Base age [ka]	LSR [cm/kyr]
02-2	4795	12.15	190	6.4
03-2	5397	15.56	190	8.2
04-1	5248	11.80	190	6.2
05-2	3336	10.01	190	5.3
06-1	3398	13.70	275	5.0
07-1	2315	17.97	390	4.6
07-6 KAL	2340	4.69	95	4.9
08-2	3596	22.75	240	9.5
09-4	5024	23.01	240	9.6

Table 6.1-1: *Mean linear sedimentation rates and base ages of cores SO202-02-2 through SO202-09-4 according to the correlation of each individual core to Core SO202-07-1. Ages were assigned to each core by transferring the age model of Core SO202-07-1 from* ***Fig. 6.1-5*** *to the respective cores.*

Cores of subset UP from Umnak Plateau maybe tentatively correlated to Core UMK-3A from Okada et al. (2005). The authors assigned an age of about 47 ka to a core depth of 12.23 m. This depth corresponds to a depth of about 11.20 m in Core SO202-21-1 from an almost identical location and water depth of 1878 m. Extrapolating this age to the core base of 21.80 m leads to an age of about 91 ka complying to the middle of MIS 5. Core SO202-22-2 seems to be the stratigraphically oldest core. The respective horizon with an age of about 47 ka maybe found in a core depth of about 7.20 m. Linear extrapolation of this age to the base of the core results in a maximum age of about 145 ka complying to late MIS 6. The correspondent kasten core SO202-22-4 reaches the age of 47 ka in a depth of about 7.80 m. The linearly extrapolated age of the core base computes to about 60 ka corresponding to late MIS 4.

Core SO202-15-5 from the continental slope of the Bering Sea (subset BS) was recovered at a nearby location of Core GAT-3A from the study of Okada et al. (2005). The authors attribute an age of 104 ka to a core depth of 8.92 m corresponding to a linear sedimentation rate of about 8.5 cm/kyr. Applying this value to Core SO202-15-5 results in a maximum age of about 200 ka according to late MIS 7at a core depth of 23.43 m. Contradictory to this interpretation is the fact that the highest susceptibility values were found at the base of Core SO202-15-5 therefore for interglacial MIS 7, although high susceptibility values usually correspond to glacial periods. Unfortunately Okada et al. (2005) presented no susceptibility data for this core. Thus there was no opportunity to correlate both cores in order to validate the

assumption of identical sedimentation rates for both cores. With respect to the susceptibility data, it seems, there is some top sediment missing in this core.

Interesting in terms of the distribution of ashes is the transect of cores starting at the Ojin Guyot towards Japan (SO20-37-2 through 45-1) for which we found increasing mean magnetic susceptibilities towards more the western sites. Correlation of the magnetic susceptibility records of all the cores to that of Core SO202-41-1 results in the depth relations displayed in **Fig. 6.1-8**. We found that Core SO202-40-1 is the oldest one with a change in sedimentation rate at a core depth of about 10 m. According to this correlation, cores SO202-42-1 and 43-1 show a similar sedimentation rate as Core SO202-41-1, which is higher than for the cores from the more easterly locations (SO202-37-2, 38-2, 39-3). Furthermore Core SO202-44-2 demonstrates a shift in sedimentation rates from values lower than Core SO202-41-1 to higher values at depths below about 18 m.

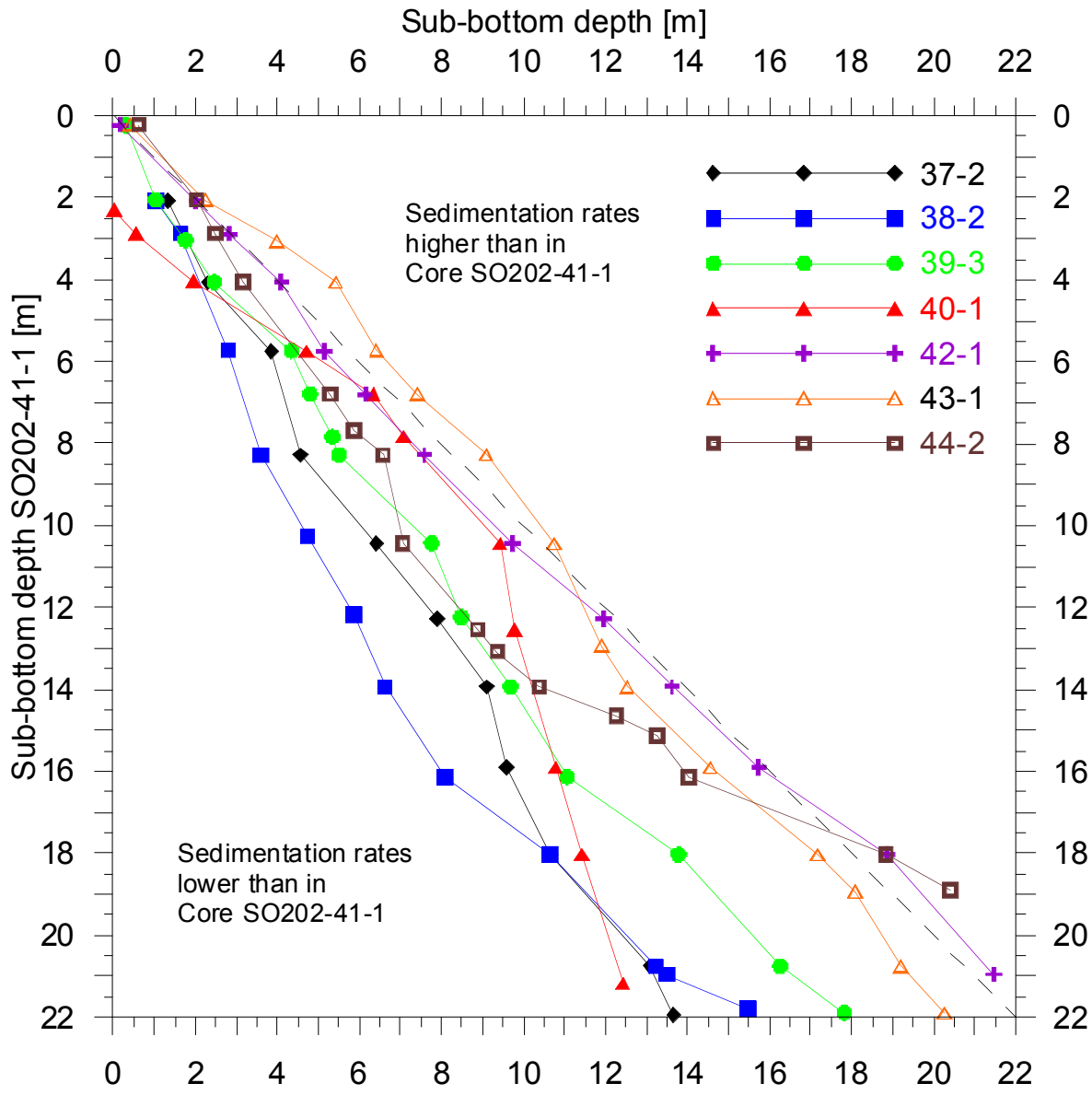

Fig. 6.1-8: *Depth correlation of core sediment cores from subset OS of the transect from Ojin Guyot towards Japan. Each individual core was correlated to Core SO202-41-1. The dashed line indicates an 1:1 depth relation to core SO202-41-1.*

6.2 Electric Resistivity and Porosity

The electric sediment resistivity Rs was determined using an inductive non-contact sensor. The system applies high-frequency magnetic fields by a transmitter coil inducing electrical eddy currents in the sediment, which are proportional to conductivity. Their secondary field is recorded and yields raw and calibrated values for conductivity and resistivity. Porosity was calculated according to the empirical Archie's equation

$$R_s/R_w = k \cdot \phi^{-m}$$

where the ratio of sediment resistivity R_s and pore water resistivity R_w can be approximated by a power function of porosity ϕ. Following a recommendation by Boyce (1968), suitable for sea water saturated clay-rich sediments, values of 1.30 and 1.45 were used for the constants k and m, respectively. The calculated porosity ϕ is subsequently converted to wet bulk density ρ_{wet} using the equation (BOYCE, 1968)

$$\rho_{wet} = \phi \cdot \rho_f + (1 - \phi) \cdot \rho_m$$

with a pore water density ρ_f of 1030 kg/m^3 and a matrix density ρ_m of 2670 kg/m^3. For a uniform treatment of all cores, these empirical coefficients were not adapted to individual sediment lithologies. Yet, relative porosity and density changes should be well documented.

The resistivity sensor averages over approximately 12 cm core length. A platinum thermometer inserted into a segment continuously measures sediment temperature for temperature compensation. Absolute sensor calibrations using a series of saline standards are performed daily. For subsequent drift and segment end correction, 29.5 cm long insulating spacers were placed between segments during logging. Thus, the characteristic decay of the eddy currents nearby the end-caps was separately recorded for each segment and corrected on basis of a model curve. This method provides a continuous composite record, however the first 2-3 data points from each intersection were discarded due to some overshooting.

Ash layer often show reduced porosities (**Fig. 6.3-1**) while diatom ooze layers are often reflected by higher porosities. The opposite relation (increased values in ash layers, reduced values in diatom ooze layers) was found for the magnetic susceptibility records. In case of the physical properties parameters, the signal is smoothed and broadened due to the several cm broad characteristic of the respective sensors (see above).

6.3 Digital Imaging – Color Scanning

Spectral light reflectance is a measure of the relative amount of light reflected by a material under incident white light. It is expressed within an absolute range from 0 (minimum) to 255 (maximum) and specified as average value for the red (600-700 nm), green (500-600 nm) and blue (400-500 nm) color band (RGB system). The reflectance properties of sediments relate to their chemistry and structure and are dominated by pigmented trace constituents, typically Fe and Mn bearing minerals (clays, oxides, sulfides) and organic enrichments. Reflectance logs provide high-

resolution records of terrigenous content (total reflectance) and redox state (red/blue ratio). Scanned at high spatial resolution, reflectance images provide sharp, undistorted, true-color core photographs scarcely affected by undesirable artifacts known from classical core photography (shadows, reflections etc.).

The digital imaging module of the GEOTEK MSCL consists of a camera containing three separate 3*1024 pixel CCD detectors mounted in the focal planes of split light beams ~40 cm above the surface of the sediment and equipped with red, green and blue dichroic filters. This camera captures consecutive, strictly orthogonal line images of the bypassing split core surface. The sediment is illuminated from above by two white fluorescent tubes. Freshly cut archive halves were carefully leveled to prevent shadows from residual surface roughness. All cores were scanned at an axial resolution setting of 100, corresponding to 1 row of pixels for every 100 µm in core depth. The resolution achieved across the core is nearly equivalent. The brightest part of each core was selected to determine the lens aperture value, which allows the entire core to be measured on the same setting without saturating any of the color channels. Each reflectance value is calibrated against the range defined by a white tile (white calibration) and a closed lens cap (black calibration). Color test cards were measured before and after each core to determine and linearly correct drift effects of the CCD sensors.

A special post-processing software was used on board to perform all necessary image corrections and calculations. The processing starts out by cropping end-cap and cavity sections and by removing spurious color stripes caused by a non-uniform response of individual color channels. This task is efficiently solved by normalizing the means within each down-core column of data to the same mean-core value. The individual segment images are then merged into a full core image and numerically compressed in various ways. The median value of each data row was chosen as representative reflectance value in the depth series of red, green and blue reflectance, total reflectance (mean value of R, G and B) and for the red/blue ratio.

Contrast-enhanced color images were produced to improve the identification of layers, gradients, and textures. For this purpose, the RGB images were transformed to the equivalent hue, saturation and value (HSV) color system. By linearly expanding the data range of the value (intensity) parameter, the available contrast is broadened without shifting hue (dominant wavelength) and saturation (degree of purity) of each color, hence, the specific aspects of mineral color. In the standard processing, the 10% and 90% percentiles of V were determined for each core and linearly rescaled to a value range reaching from 25% to 75% total reflectance.

Piston Cores SO202-02-2, SO202-04-1 and SO202-29-4 as well as kasten core SO202-07-6, SO202-12-1, SO202-18-6, SO202-22-4 and SO202-27-6 and gravity core SO202-35-1 were subject to digital imaging. **Fig. 6.3-1** shows exemplarily data of core SO202-29-4.

In the left column, the sediment is displayed in genuine colors, to the right the sediment is shown in contrast enhanced colors (see above). Usually ash layers are related to sharp minima in reflectance due to their dark color, where possibly diatom ooze layers are characterized by an increasing reflectance due to their brighter color. Additionally the red/blue ratio is increased in those sediments suspected to represent diatom ooze.

An example of the results of the physical properties measurements and digital imaging is given in **Fig. 6.3-1**.

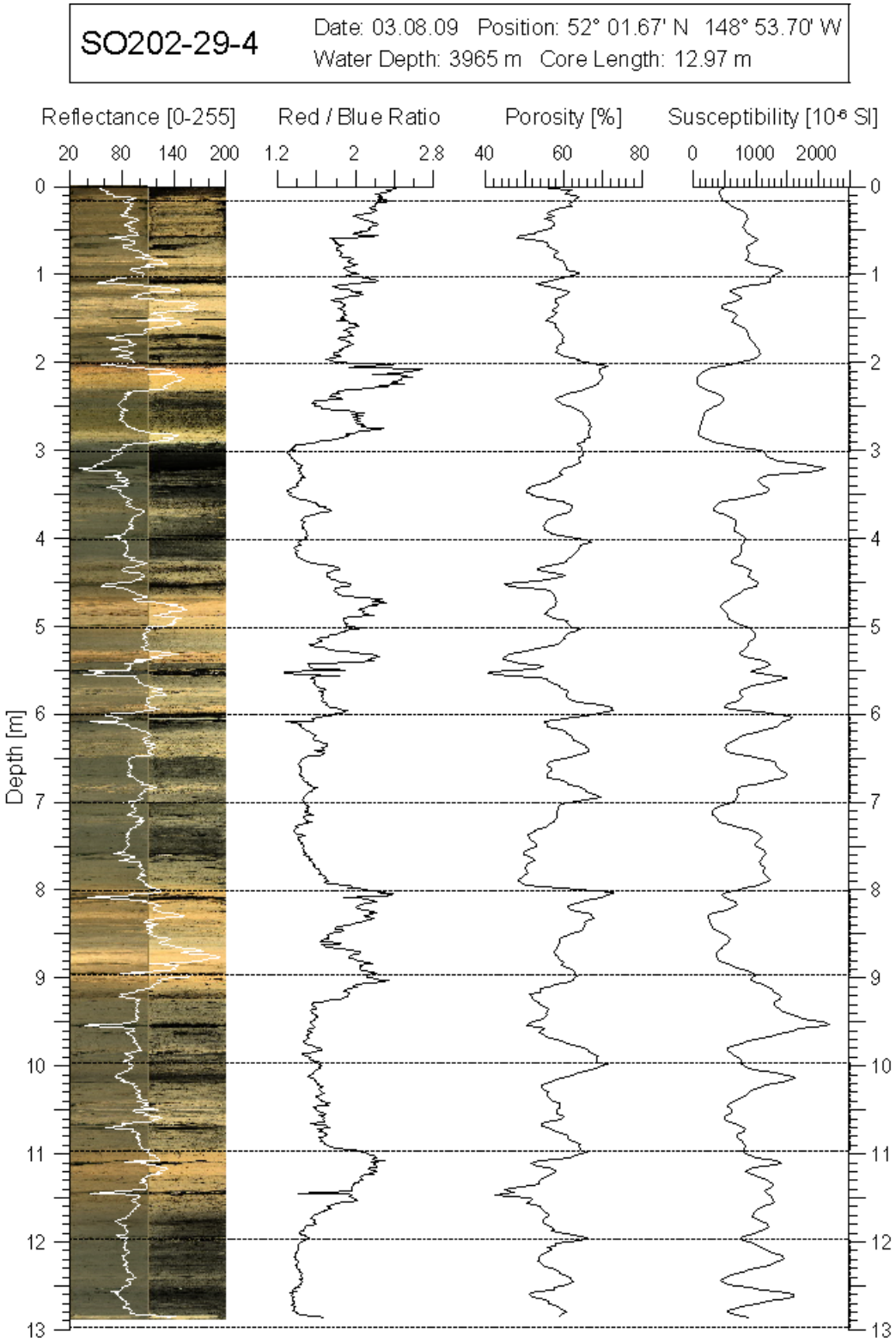

Fig. 6.3-1: *Down-core variations of reflectance, red/blue ratio, magnetic susceptibility and porosity (calculated from electric resistivity) of Core SO202-29-4 from Gibson Seamount. Images are presented in natural (left column) and contrast-enhanced colors (right column), respectively.*

6.4 Sampling for Rock and Paleomagnetic studies

Three piston cores (SO202-02-2, SO202-04-1, SO202-39-3) and one gravity core (SO202-35-1) were sampled at 5 cm intervals with in total 845 oriented cube samples with a volume of about 6 cm^3, while five kasten cores (SO202-07-6, SO202-12-1, SO202-18-6, SO202-22-4, SO202-27-6) were sampled with 35.41 m of U-channels for subsequent shore based rock and paleomagnetic studies.

7. TEPHRA

Kaori Aoki
Rissho University, Japan

7.1 Introduction

The research area of INOPEX covers widely the North Pacific and the Bering Sea along the northern Circum-Pacific Rim to which quite many Quaternary volcanoes belong (**Fig 7.1-1**). Such volcanoes have provided abundant tephras in the North Pacific ("tephra" includes any kind of volcanic material, regardless of size fraction, color, eruptive mechanism or sedimentary process). In the 1960's, the Lamont-Doherty Earth Observatory (LDEO) researched pelagic sediment cores collected from the north Pacific with the R/V *VEMA*. Ninkovich et al. (1966) and Horn et al. (1969) documented the first time the distribution of tephras, e.g. "White Ash" from the western North Pacific and "Brown Ash" from the northeastern North Pacific and off Izu-Bonin Islands, Japan. However, considering the poor geochemical analyses and dating techniques available at that time, "White Ash" and "Brown Ash" reflect only color variations resulting from geochemical composition of source magmas. "White Ash" generally represents vitric tephra from high-SiO_2 magmas (e.g. rhyolite, rhyodacite) originating in volcanic events related to subduction zones (Japanese Islands, Kuril Islands and Kamchatka Peninsula). Because high-SiO_2 magmas have high viscosities they give rise to violent eruptions, when combined with highly dissolved volatiles. This results in the generation of huge amounts of volcanic glass shards during the eruption that are deposited as ash layers with generally white, whitish gray or gray colors. "Brown Ash" generally represents basaltic tephra (low-SiO_2, high-FeO* and low viscosity). Such tephra may also be dark-colored because of a high content of heavy minerals, which was provided from adjacent volcanoes. Research during the past 40 years following strongly improved our understanding of volcanism in the Circum-Pacific Rim and magmatism in the subduction zone.

Tephra constitute valuable stratigraphic markers (Lacasse et al. 1995, Davies et al. 2003, Wastegård 2005) and allow for the inter-correlation of marine, land the ice records; e.g. the Vedde ash originating in Iceland was found in the GRIP ice-core (Grönvold et al. 1995); the Mazama ash (Crater Lake caldera, 6.8 ^{14}C years BP) was identified in sediment cores recovered off the coast of Washington and Oregon (Nelson et al. 1968, Smith and Westgate 1969) but also in the GISP2 ice-core (Zdanowicz et al. 1998); Pearce et al. (2007) showed that the Holocene Aniakchak tephra (3.4 ka) derived from southwest Alaska (source volcano is 48 in **Fig 7.1-1**) can be related to micro glass shards in the GRIP ice-core based on the precise minor-element compositions of individual glass shards determined by LA-ICP-MS and sophisticated data treatment. This underlines that tephra recorded in the north Pacific realm represent a useful stratigraphic tool for correlation of marine an ice core records.

Tephra identified in INOPEX cores are related to two main source regions, the Japan-Kamchatka-Kurile and the Aleutian-Alaska-Bering Shelf realms (**Fig. 7.1-1**). The tephra can be used for intercorrelation of sediment cores close to the source regions. Major goal of the study of INOPEX tephra is the improvement of the tephrostratigraphy in the INOPEX study area and thus to enhance the establishment of the "Circum-Pacific tephrochronology" considering new radiometric dating and astronomical dating results.

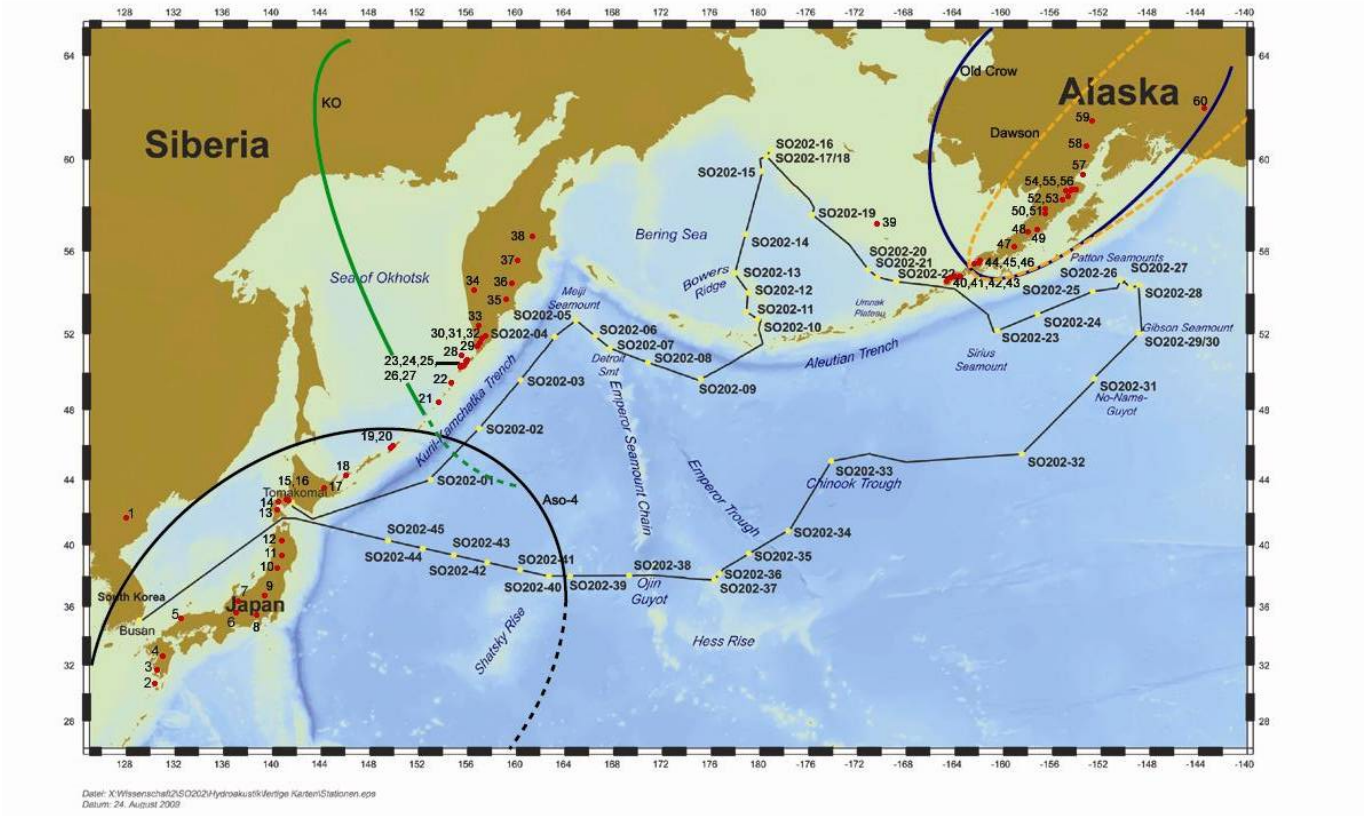

***Fig.7.1-1**: Location map of source volcanoes in the SO202-INOPEX expedition area and the distributions of well-known widespread tephras.*

Site of volcano (C. means caldera); 1:Baitousan, 2:Kikai C., 3:Aira C., 4:Aso C., 5:Sanbe, 6:Ontake, 7:Tateyama, 8:Hakone, 9:Akagi, 10:Naruko C., 11:Iwate, 12:Towada C., 13:Nigorikawa C., 14:Toya C., 15:Shikotsu C., 16:Kuttara C., 17:Kutcharo C., 18:Tjatja, 19:Tresbez, 20:Berga, 21:Tschirimkotan, 22:Tao-Rusyr C., 23:Ebeko, 24:Tschikuratschki, 25:Nebenkegel Tatarinou, 26:Fuss, 27:Karpinski, 28:Oyakoba, 29:Kuril Lake C., 30:Iliinsky, 31:Ksudach C., 32:Khodutkinsky, 33:Opala, 34:Khangar, 35:Avachinsky, 36:Taunshits, 37:Kizimsky, 38:Shiveluch, 39:St.Paul and the Bering Sea basalt province, 40:Westdahl, 41:Fisher, 42:Shishaldin, 43:Isanotski, 44:Dutton, 45:Emmons Lake C., 46:Pavlof, 47:Veniaminof, 48:Aniakchak, 49:Chiginagak, 50:Peulik, 51:Ukinrek, 52:Martin, 53:Mageik, 54:Novarupta, 55:Katmai, 56:Kaguyak, 57:Augustine, 58:Redoubt, 59:Hayes, 60:Wrangell Volcanic Fields.

Source and eruptive age of widespread tephras; Aso-4: Aso C. (site 4), 87+-7ka (Aoki et al. 2008), KO: Kuril Lake C.(site 29), 7600 ^{14}C years B.P.(Ponomareva et al. 2004), Dawson: Emmons Lake C.(site 45; Westgate et al. 2000, Mangan et al., 2003), 25300 ^{14}C years B.P. (Froese et al. 2006), Old Crow: possible source is Emmons Lake C.(site 45; Westgate et al. 1985; personal communication from Prof. J.A. Westgate, University of Toronto), 140 ka (Preece et al. 1999).

7.2. Field setting

Off Kuril Islands and the Kamchatka Peninsula
Sites SO202-2 – SO202-5 are located off the Kuril Islands and the Kamchatka Peninsula, Russia. Of those, Site SO202-2 is relatively close to Hokkaido, northeast Japan, and thus offers the possibility to recognize the stratigraphic relationship between widespread tephras derived from Japan and Russia. Volcanoes in Hokkaido belong to the Chishima (Japanese name of "Kuril") volcanic zone, related to the subduction zone stretching between Japan and Kamchatka Peninsula. In Kamchatka, most of the late Pleistocene Krakatoa-type calderas were established around 30-40 ka, and volcanic activity intensified within the time intervals of 7500-7800 and 1300-1800 ^{14}C years B.P. (Braitseva et al. 1995). Holocene tephrochronology in the northern islands in Kuril and southern Kamchatka are established based on ^{14}C dates and some time-marker tephras. The Kuril Lake caldera (29 in **Fig 7.1-1**) produced the KO tephra (7600 ^{14}C years B.P.), which has been correlated between distal locations and the origin. Considering its Volcanic Explosivity Index (VEI) has been estimated as 7-grade (Ponomareva et al. 2004), it can be assumed that the KO tephra has reach the North Pacific, though report from this area are still lacking. The KO tephra may represent a prominent tephra to correlate the cores from Sites SO202-2 – SO202-5.

Cores recovered at Sites SO202-6, SO202-7, SO202-8 and SO202-9 represent key sections to reveal the stratigraphy of tephra derived from the Kamchatka Peninsula and the eastern Aleutian Islands.

Bering Sea
Though some Quaternary volcanoes belong to the Aleutian Islands, not many tephras have been reported from the central Bering Sea. The recovery of tephra from Sites SO202-10, SO202-11 and SO202-12 (Bowers Ridge) will improve knowledge on the occurrence and distribution of tephra from this area.

Also, St. Paul Island (Site 39 in **Fig.7.1-1**) in the Bering Sea shelf is a small basaltic vent cluster and one of the youngest volcanic islands in the Bering Sea basaltic province (Feeley and Winer 2009). Its youngest eruption occurred 3230 ^{14}C years BP. In 1943, submarine eruptive phenomena were described several kilometers to the southwest of St. Paul. Basaltic tephra, which usually produce lava flow and abundant scoria, do not distribute as widely as vitric tephras by violent eruption caused by high-SiO_2 magmas such as rhyolite. However, potential vents besides St. Paul Island might submerge in the Bering Sea shelf. Such effects may be recorded at sites SO202-14 in the center of the Bering Sea and SO202-15, SO202-17 - SO202-22, located on or close to the Bering Shelf Margin.

Northeast Pacific
There are many Quaternary volcanoes on the Aleutian-Alaska volcanic zone (the area of Aleutian arc front stretching to the Alaska Peninsula; **Fig.7.1-1**). Dawson tephra (25.300 ^{14}C years BP) and Old Crow tephra (140 ka) are significant widespread tephras in this area, and they have already been correlated widely in Alaska and the Yukon. Emmons Lake caldera (site 45 in **Fig.7.1-1**) in the southwestern Alaska Peninsula is recognized as the source of Dawson tephra and possibly of Old Crow tephra. Their isopachs are traced out mostly on the basis of investigation on land, because there is rare information from marine sediments.

Westerly winds could bring them to Sites SO202-25 - SO202-28, which are located on almost the same latitude of the Emmons Lake caldera and other volcanoes on the southwestern Alaska Peninsula. Some widespread tephras originating in the Alaska Peninsula may occur in the cores from Sites SO202-23, SO202-24, SO202-29/30, SO202-31 and SO202-32. Especially, this concerns the Holocene Aniakchak tephra dated 3.400 y BP, which has been identified also in the GRIP ice core (Pearce et al. 2007).

Central and Northwest Pacific

There is rare information on tephra occurrences in the central north Pacific, except from a paper by Ninkovich et al. (1966). Several tephras from volcanoes on the Aleutian arc front might have reached the area of sites SO202-33, SO202-34 and SO202-35.

In northwest Pacific sediments occur many tephras which originate from volcanoes distributed over a wide area, namely from Hokkaido to Kyushu, Japan (**Fig. 7.1-1**). Their geographical distribution, petrography and stratigraphic age assignment was compiled by Machida and Arai (1992, 2003). Aoki and Machida (2006) present a database of major-element compositions of volcanic glass shards in late Quaternary tephra. Aoki (2008) showed that the major-element composition of the glass shards in the Aso-4 tephra is very distinctive and, hence provides an easily recognizable stratigraphic datum and that this ash is present in sediments deposited on the northern Shatsky Rise (**Fig. 7.1-1**; Aoki 2008). Shipboard inspection of the ash layers indicates that Aso-4 is present in Core SO202-39-3 (see 7.3) recovered east of Shatsky Rise. Considering such finding is can be assumed that this tephra is also present in Cores SO202-40 to -45 and possibly even east of Shatsky Rise. This can be tested by the inspection of core recovered at sites SO202-36 and -37 (Hess Rise) and SO202-38.

Considering the results of Furuta et al. (1986), Aoki et al. (2000) and Aoki (2008), Sites SO202-41 to SO202-45 should include many tephras, which were derived from volcanoes located in northeastern Japan. Some of them have been correlated to tephras in the calcareous ooze collected from the continental slope, and their eruptive ages have been estimated based on isotope stratigraphic age models (Aoki and Arai 2000, Aoki and Sakamoto 2003, Aoki et al. 2008).

7.3. Tephra Beds in SO202-INOPEX Cores

Three piston cores (SO202-02-2, SO202-04-1, and SO202-39-3), two gravity cores (SO202-29-4 and SO202-35-1) and five kasten cores (SO202-07-6, SO202-12-1, SO202-18-6, SO202-22-4, and SO202-27-6) were opened and described on board. Except for SO202-29-4 and SO202-35-1 tephra samples have been sampled on-board from all opened cores (**Table 7.3-1)**. Tephra layers, except spotted, inclined or disturbed tephras, are shown in simplified columnar sections of sedimentary cores and have been labeled with ID numbers (**Fig. 7.3-1**).

SO202-02-2

ID9 (284-298 cm), ID10 (373-379 cm), ID30 (892-898 cm) and ID32 (1044.5-1053 cm) are recognized as products by large eruptions, considering their thickness, grain size, and sedimentary condition. Upward grading structure is normally the evidence that ash fall out at once, and was then deposited at the se bed. ID3 (184-194 cm) and ID4 (194-196 cm) are the products of a series of large eruptions. ID4 should be drifted pumices and ID3 is air-fall ash. The eruption, which produced them should have started with the Plinian eruption of pumices (ID4). Then huge pyroclastic flow might have occurred to provide abundant fine ash (ID3), namely co-ignimbrite ash. ID17 (564-571 cm) is a very fine ash layer, which mainly constitutes of volcanic glass shards. It may have been affected by the transport of sea ice, because rounded pebbles were included in it. This may indicated that the eruption occurred during the winter season.

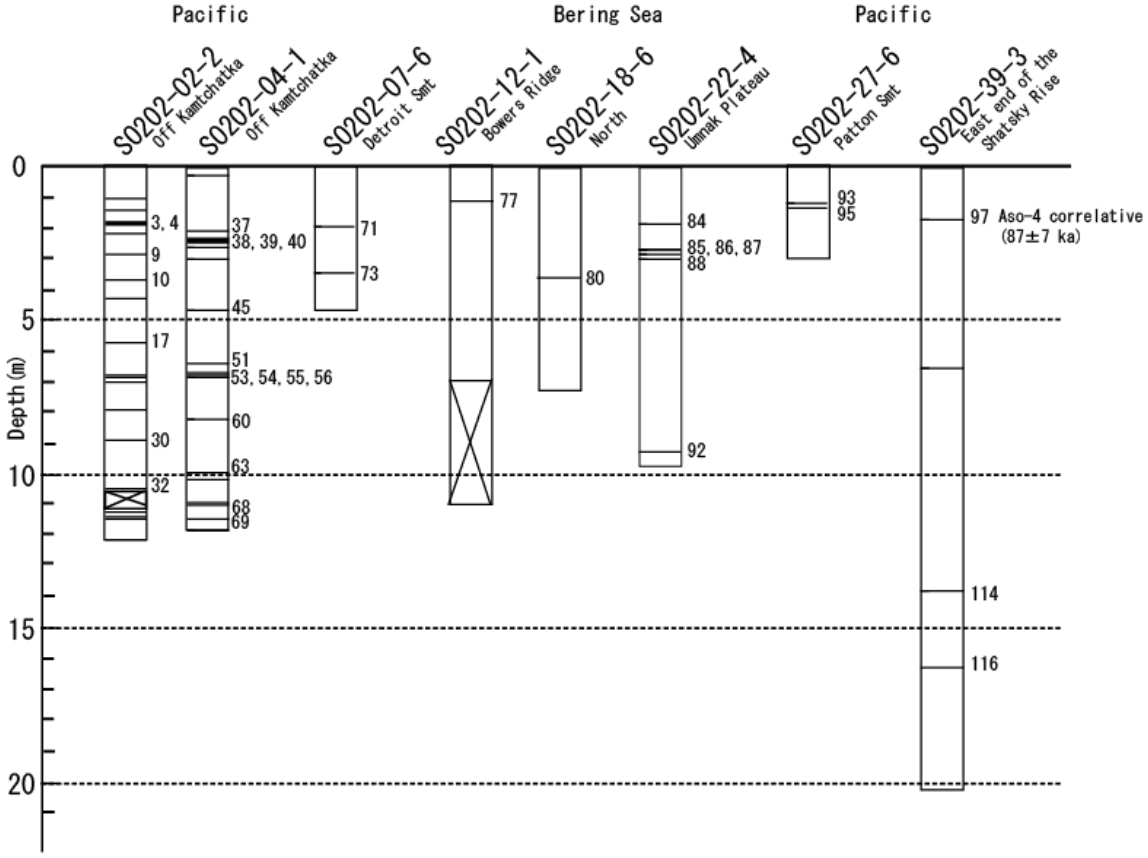

Fig. 7.3-1: *Tephra layers, except spotted, inclined or disturbed tephras, are shown in simplified columnar sections of sediment cores.*

SO202-04-1

ID37 (211.5-215 cm), ID45 (469-478 cm), ID51 (644-648 cm), ID60 (821.5-833.5 cm), ID63 (992.5-998.5 cm), ID68 (1100.5-1104 cm) and ID69 (1141.5-1147.5 cm) are recognized as products by large eruptions, considering their thickness, grain size, and sedimentary condition. ID38 (236-242 cm; black), ID39 (242-246 cm; beige) and ID40 (246-248 cm; gray) looks like gradual settling without gaps. However, the colors of ID38 and ID39 are clearly different. Grains of ID40 grade upward obviously, but ID39 does not. It may be necessary to consider that the ash layers represent a series of eruptions with fluctuation of the explosive momentum, variations of geochemical

composition of magma and effects caused by multiple magma chambers and so on. ID53 (668.5-672.5 cm), ID54 (674-678 cm), ID55 (682.5-685 cm) and ID56 (685-687 cm) lie in an interval of 20 cm. Furthermore, including ID51 (644-648 cm), five ash layers are recognized in an interval of 43 cm. The color of ID53 varies from gray to whitish gray upward. ID54, ID55 and ID56 resemble each other in color (reddish gray). In addition, ID56, which grains grades upward, includes abundant dark-colored minerals. It is possible that ID55 and ID56 represent different ash, because very thin sediment layers (~5 mm thickness, diatomaceous ooze) separate them.

SO202-07-6
SO202-07-6 contains two ash layers. One is in the interval of 193-194 cm (ID71 and ID72) and consists of very fine bubble-wall type glass shards; the other is in the interval of 346-348cm (ID73, ID74, and ID75) and mainly represents well-foamed pumice type glass shards.

SO202-12-1
ID77 (112-113 cm) is a thin gray ash layer in SO202-12-1.This core includes some sand spots besides collected samples (ID79; 532 cm). It is necessary to examine these sandy inclusions carefully by radiography and microscopic inspection whether they represent primary fallout volcanic sand or ice-rafted sand.

SO202-18-6
A prominent ash layer in SO202-18-6 is in the interval of 362-365 cm (ID80 and ID81). This layer exists just below strong laminations, in which some mollusks have been found.

SO202-22-4
There are three prominent ash layers. Both of ID84 (187-189 cm) and ID88 (300-312 cm) are typical basaltic tephras constituting of fine black scoria. Their sources should be the Bering Sea basaltic province, including St. Paul Island (site39 in **Fig.7.1**). ID92 (929-931 cm) is whitish gray coarse pumice layer, of which the average diameter of pumice is approximately 3 mm, and includes abundant heavy minerals. It is speculated that one of the volcanoes in the Aleutian-Alaska volcanic zone produced it by a huge Plinian eruption of pumices.

ID85 (272.8-273 cm), ID86 (274-274.5 cm) and ID87 (283.5-284 cm) are very thin ash layers. They were found in a laminated sediment section. In particular, ID86 and ID87 might represent one of the widespread tephras derived from Aleutian-Alaska volcanic zone, because their colors are gray and whitish gray. This indicates that they are not coming from the Bering Sea basaltic province.

SO202-27-6
Two tephra layers were encountered in SO202-27-6. One is between 119-122 cm (ID93 and ID94). Another one is in the interval 1135-138 cm (ID95). It is suggested that both tephra layers originate from volcanoes of the Aleutian-Alaska volcanic zone.

See text	ID	Core	Corer type	Subbottom depth of Tephra	Color	Remarks
	1	SO202-02-2	Piston	104 - 105.5	Gray	Layer of normal grading ash (sand) which include abundant heavy minerals.
	2	SO202-02-2	Piston	146 - 148	Brown	Layer of normal grading ash (sandy silt) which include abundant heavy minerals. Top and bottom are wavy contact.
*	3	SO202-02-2	Piston	184 - 194	Whitish gray	Layer of normal grading fine ash (sandy silt). Vitric.
*	4	SO202-02-2	Piston	194 - 196	Whitish gray	Pumiceous layer. Diameter of pumice is up to 1.5 cm. This and above ash layer (184-194 cm) are a series of eruptive event.
	5	SO202-02-2	Piston	216 - 218	Brown	Layer of normal grading ash (sandy silt).
	6	SO202-02-2	Piston	247 - 248	-	Possible to find dispersed fine volcanic glass shards.
	7	SO202-02-2	Piston	271 - 272	-	Possible to find dispersed fine volcanic glass shards.
	8	SO202-02-2	Piston	274 - 275	Whitish gray	Spot of very fine ash.
*	9	SO202-02-2	Piston	284 - 298	Whitish gray	Layer of normal grading ash (sand). Bottom is sharp contact. Vitric (pm>>bw).
*	10	SO202-02-2	Piston	373 - 379	Brownish gray	Layer of normal grading ash (sandy silt).
	11	SO202-02-2	Piston	432 - 434.5	Whitish gray	Layer of ash (sandy silt) incline and contacts are slightly wavy.
	12	SO202-02-2	Piston	471	Beige	Spot of ash
	13	SO202-02-2	Piston	483.5	Black	Spot of very fine scoria.
	14	SO202-02-2	Piston	487 - 488.5	-	Possible to find dispersed fine volcanic glass shards.
	15	SO202-02-2	Piston	489	-	Possible to find dispersed fine volcanic glass shards.
	16	SO202-02-2	Piston	509	-	Scattering spots of ash
*	17	SO202-02-2	Piston	569 - 571	White	Layer of fine ash. Vitric. Rounded pebbles are included in bottom, and mixed with ash.
	18	SO202-02-2	Piston	577	Beige	Scattering spots of ash.
	19	SO202-02-2	Piston	577 - 579	Beige	Scattering spots of ash.
	20	SO202-02-2	Piston	598 - 599	-	Possible to find dispersed fine volcanic glass shards.
	21	SO202-02-2	Piston	678 - 682	Whitish gray	Inclined ash spot.
	22	SO202-02-2	Piston	682 687	Whitish gray	Ash spot in one-sided surface of core.
	23	SO202-02-2	Piston	699 - 701	Whitish gray	Inclined fine ash layer.
	24	SO202-02-2	Piston	705 - 710	Whitish gray	Spots of ash.
	25	SO202-02-2	Piston	755.5 - 756.5	Gray	Spot of ash
	26	SO202-02-2	Piston	763.5 - 765.5	Gray	Spot of ash
	27	SO202-02-2	Piston	788 - 791	Brown	Layer of normal grading ash (sandy silt). Bottom is sharp contact.
	28	SO202-02-2	Piston	849 - 850.5	Gray	Spot of ash
	29	SO202-02-2	Piston	869	Whitish gray	Spot of ash
*	30	SO202-02-2	Piston	892 - 898	Reddish brown	Layer of normal grading ash (sandy silt). Bottom is sharp contact.
	31	SO202-02-2	Piston	920.5 - 922	Black	Spots of fine ash.
*	32	SO202-02-2	Piston	1044.5 - 1053	Gray	Layer of normal grading ash (sandy silt). Blank (1053-1109.5 cm) just below ash layer was filled by water.
	33	SO202-02-2	Piston	1120.5 - 1122	Gray	Spots of ash.
	34	SO202-02-2	Piston	1140 - 1141	Black	Scoriacous sand, including pumice grains (dia.2 mm)
	35	SO202-02-2	Piston	1145 - 1147.5	Gray	Scattering spots of volcanic sand.
	36	SO202-04-1	Piston	32 - 33.5	Brown	Layer of normal grading ash (sandy silt).
*	37	SO202-04-1	Piston	211 - 215	Yellowish brown	Layer of normal grading ash (sandy silt). Bottom is sharp contact.
*	38	SO202-04-1	Piston	236 - 242	Black	Layer of fine ash.
*	39	SO202-04-1	Piston	242 - 246	Beige	Layer of normal grading ash (sandy silt).
*	40	SO202-04-1	Piston	246 - 248	Gray	Layer of normal grading ash (sandy silt). Bottom is sharp contact.
	41	SO202-04-1	Piston	261.5 - 264	Dark brown	Layer of normal grading ash (sand). Bottom is sharp contact.
	42	SO202-04-1	Piston	302.5 - 307	Whitish gray	Inclined fine ash layer.
	43	SO202-04-1	Piston	330 - 332	-	Possible to find dispersed fine volcanic glass shards.
	44	SO202-04-1	Piston	382 - 384.5	Black	Scattering fine ash.
*	45	SO202-04-1	Piston	469 - 478	Whitish gray	Layer of normal grading ash (sandy silt). Bottom is sharp contact.
	46	SO202-04-1	Piston	490 - 491	Beige	Spot of ash.
	47	SO202-04-1	Piston	560 - 561.5	Black	Spot of ash.
	48	SO202-04-1	Piston	568 - 570.5	Whitish gray	Spot of ash.
	49	SO202-04-1	Piston	570.5 - 572.5	Whitish gray	Spot of ash.
	50	SO202-04-1	Piston	595.5 - 599	-	Possible to find dispersed fine volcanic glass shards.
*	51	SO202-04-1	Piston	644 - 648	Reddish brown-gray	Layer of normal grading ash (sand). Bottom is sharp contact.
	52	SO202-04-1	Piston	651.5 - 653	Black	Spot of ash.
*	53	SO202-04-1	Piston	668 - 672.5	Whitish gray	Layer of ash (silt). Top and bottom are wavy contact.
*	54	SO202-04-1	Piston	674.5 - 678	Reddish gray	Layer of ash (silt). Bottom is slightly depressed.
*	55	SO202-04-1	Piston	682.5 - 685	Reddish gray	Layer of ash (silt). Bottom is slightly depressed.
*	56	SO202-04-1	Piston	685 - 687.5	Reddish gray	Layer of normal grading ash (sand) which include abundant heavy minerals. Bottom is sharp contact.
	57	SO202-04-1	Piston	682.5 685	Reddish gray	Same as ID55. Picked up from surface.
	58	SO202-04-1	Piston	685 687.5	Reddish gray	Same as ID56. Picked up from surface.
	59	SO202-04-1	Piston	750 - 751.5	-	Possible to find dispersed fine volcanic glass shards.
*	60	SO202-04-1	Piston	821.5 - 833.5	Olive gray	Layer of normal grading ash (sand). Bottom is sharp contact.
	61	SO202-04-1	Piston	869 - 870	-	Possible to find dispersed fine volcanic glass shards.
	62	SO202-04-1	Piston	898.5 - 901.5	Light brown	Possible to find dispersed fine volcanic glass shards.
*	63	SO202-04-1	Piston	992 - 998.5	Brown	Layer of normal grading ash (sand) which include abundant heavy minerals. Bottom is sharp contact.
	64	SO202-04-1	Piston	1016 - 1018.5	Black	Layer of scoriaceous ash (silt).
	65	SO202-04-1	Piston	1037 - 1038	Black	Spot of scoriaceous ash.
	66	SO202-04-1	Piston	1065.5 - 1067.5	Black	Scattering fine ash.
	67	SO202-04-1	Piston	1094 - 1095	Black	Layer of ash (silt).
*	68	SO202-04-1	Piston	1100.5 - 1104	White	Layer of normal grading ash (sand) which include abundant heavy minerals. Bottom is sharp contact.
*	69	SO202-04-1	Piston	1141.5 - 1147.5	Reddish gray	Layer of normal grading ash (sandy silt). Vitric. Bottom is sharp contact.
	70	SO202-04-1	Trigger	16 - 17.5	Whitish gray	Spot of ash.

See text	ID	Core	Corer type	Subbottom depth of Tephra	Color	Remarks
*	71	SO202-07-6	Giant box	193 - 194	Gray	Layer of fine ash. Same as ID72.
*	72	SO202-07-6	Giant box	193 - 194	Gray	Layer of fine ash. Same as ID71.
*	73	SO202-07-6	Giant box	345 - 354	Whitish gray	Layer of ash (sandy silt). Bottom is wavy contact by bioditurbations. Same as ID74,75.
*	74	SO202-07-6	Giant box	346 - 348	Whitish gray	Layer of ash (sandy silt). Bottom is almost sharp contact, however partly biodisturbed. Same as ID73,75.
*	75	SO202-07-6	Giant box	350	Whitish gray	A part of biodisturbed area of 346-348 ash layer. White and clear volcanic glass shards (pm, fb>>bw). Same as ID73,74.
	76	SO202-07-6	Giant box	380	White	a drift pumice
*	77	SO202-12-1	Giant box	112 - 113	Gray	Layer of ash (sandy silt)
	78	SO202-12-1	Giant box	141 - 142	Light brown	Possible to find dispersed fine volcanic glass shards.
	79	SO202-12-1	Giant box	532	Gray	Spot of ash (silt) including heavy minerals.
*	80	SO202-18-6	Giant box	362 - 365	Blackish gray	Layer of ash (sandy silt). Top and bottom are sharp contact. Same as ID81.
*	81	SO202-18-6	Giant box	362 - 365	Blackish gray	Layer of ash (sandy silt). Top and bottom are sharp contact. Same as ID80.
	82	SO202-18-6	Giant box	447 - 454	Gray	Possible to find dispersed fine volcanic glass shards.
	83	SO202-18-6	Giant box	449 - 455	Gray	Possible to find dispersed fine volcanic glass shards. Very hard mud crust.
*	84	SO202-22-4	Giant box	187 - 189	Black	Layer of scoriaceous sand between laminations.
*	85	SO202-22-4	Giant box	272.8 - 273	Black	Layer of scoriaceous sand between laminations.
*	86	SO202-22-4	Giant box	274 - 274.5	Whitish gray	Layer of fine ash between laminations.
*	87	SO202-22-4	Giant box	283.5 - 284	Gray	Layer of fine ash between laminations.
*	88	SO202-22-4	Giant box	300 - 312	Black	Layer of scoriaceous sand between laminations.
	89	SO202-22-4	Giant box	481 - 483	Black	Spots of scoriaceous ash.
	90	SO202-22-4	Giant box	660 - 663	Gray	Possible to find dispersed fine volcanic glass shards.
	91	SO202-22-4	Giant box	758 - 762	Black	Spots of scoriaceous ash.
*	92	SO202-22-4	Giant box	929 - 931	Whitish gray	Layer of normal grading pumices. Top and bottom are sharp contact. Maximum diameter of pumice is 1 cm, and medium diameter is almost 3 mm. Abundant of heavy minerals.
*	93	SO202-27-6	Giant box	119 - 122	Whitish gray	Layer of normal grading ash (sandy silt). Bottom is sharp contact. Same as ID94.
*	94	SO202-27-6	Giant box	119 - 122	Whitish gray	Layer of normal grading ash (sandy silt). Bottom is sharp contact. Same as ID93.
*	95	SO202-27-6	Giant box	135 - 138	Olive gray	Layer of fine ash.
	96	SO202-27-6	Giant box	161 - 167	Light gray	Possible to find dispersed fine volcanic glass shards.
*	97	SO202-39-3	Piston	176 - 178.5	Gray	Layer of normal grading ash (sandy silt). 4cm blank below ash layer.
	98	SO202-39-3	Piston	374 - 376	Greenish gray	Possible to find fine volcanic glass shards.
	99	SO202-39-3	Piston	413 - 414	Gray	Slightly hard layer. Just below blackish band (412-414cm). Possible to find fine volcanic glass shards.
	100	SO202-39-3	Piston	419 - 420	Gray	Slightly hard layer. Possible to find fine volcanic glass shards.
	101	SO202-39-3	Piston	427 - 427.5	Greenish gray	Slightly hard layer. Possible to find fine volcanic glass shards.
	102	SO202-39-3	Piston	497 - 498	Light brown-gray	Possible to find fine volcanic glass shards.
	103	SO202-39-3	Piston	509 - 510	Blackish gray	Possible to find fine volcanic glass shards.
	104	SO202-39-3	Piston	535 - 536	Greenish gray	Possible to find fine volcanic glass shards.
	105	SO202-39-3	Piston	551.5 - 553	Greenish gray	Slightly hard layer. Possible to find fine volcanic glass shards.
	106	SO202-39-3	Piston	605 - 606	Greenish gray	Slightly hard layer. Possible to find fine volcanic glass shards.
	107	SO202-39-3	Piston	655 - 656	Greenish gray	Fine ash layer (2-3 mm thickness) in slightly inclined greenish strata.
	108	SO202-39-3	Piston	673 - 674	Greenish gray	Slightly hard layer. Possible to find fine volcanic glass shards.
	109	SO202-39-3	Piston	713 - 714	Light gray	Possible to find fine volcanic glass shards.
	110	SO202-39-3	Piston	751 - 752	Greenish gray	Slightly hard layer. Possible to find fine volcanic glass shards.
	111	SO202-39-3	Piston	764 - 769	Greenish gray	Greenish strata in hard mud crust. Possible to find fine volcanic glass shards.
	112	SO202-39-3	Piston	854.5 - 855.5	Greenish gray	Slightly hard layer. Possible to find fine volcanic glass shards.
	113	SO202-39-3	Piston	868 - 868.5	Greenish gray	Slightly hard layer. Possible to find fine volcanic glass shards.
*	114	SO202-39-3	Piston	1382 - 1387	Gray	Layer of normal grading ash (sandy silt).
	115	SO202-39-3	Piston	1594.5 - 1595.5	Greenish gray	Slightly hard layer. Possible to find fine volcanic glass shards.
*	116	SO202-39-3	Piston	1630 - 1637	Gray	Layer of normal grading ash (sandy silt). Color of 1cm from bottom is backish, and color of 2-3cm from bottom is green.
	117	SO202-39-3	Piston	1754 - 1755	Greenish gray	Hard layer. Possible to find fine volcanic glass shards.
	118	SO202-39-3	Piston	1859 - 1860	Blackish gray	Hard layer. Possible to find fine volcanic glass shards.
	119	SO202-39-3	Piston	1886.5 - 1887	Greenish gray	Slightly hard layer. Possible to find fine volcanic glass shards.
	120	SO202-39-3	Piston	1900 - 1901.5	Blackish gray	Hard layer. Possible to find fine volcanic glass shards.
	121	SO202-39-3	Piston	1917 - 1918.5	Greenish gray	Slightly hard layer. Possible to find fine volcanic glass shards.
	122	SO202-39-3	Piston	1930 - 1931	Greenish gray	Possible to find fine volcanic glass shards.
	123	SO202-39-3	Piston	1967 - 1967.5	Blackish gray	Slightly hard layer. Possible to find fine volcanic glass shards.

Table 7.3-1: *List of tephras encountered in the sediment cores*

SO202-39-3

Prominent tephras are ID97 (176-178.5 cm), ID114 (1382-1387 cm), and ID116 (1630-1637 cm). Their colors, thickness and stratigraphic positions suggests that ID97 can be assigned to Aso-4 (Aoki, 2008), and both ID114 and ID116 can be related to tephras Harada et al. (2000) and Fukuma and Harada (2001) have reported from the northern part of Shatsky Rise. Microscopic inspection reveals that ID97 consists of relatively thin bubble-wall type glass shards. These properties support that the tephra can be related to the Aso-4 tephra. Considering the ash layer occurrence the Brunhes/Matuyama boundary should occur between ID114 and ID116, and ID116 should fall in the Jaramillo Subchron (Fukuma and Harada, 2001).

Additional Notes

The following notes refer to tephras not included in **Table 7.1**.

- Multicorer SO202-23-4 includes a dark-brown normal grading tephra, whose subbottom depth is 13 to 17 cm. Bottom is sharp contact.
- Sediment in the core catcher of SO202-28-2 includes vitric fine ash, which consists of bubble-wall type glass shards.
- Sediment in the core catcher of SO202-37-2 includes tephra, whose color is greenish gray.

8. PRELIMINARY BIOSTRATIGRAPHIC DATING

Rainer Gersonde[1], Jian Ren[1], Maria Obrezkova[2]
[1]Alfred Wegener Institute, Bremerhaven, Germany
[2]V.I. Il´ichev Pacific Oceanological Institute, Russia

Microfossils are valuable as a primary tool for the establishment of age models of sediments. During SO202-INOPEX on-board biostratigraphy was based on the occurrence of diatoms. The siliceous microfossils are most significant for Cenozoic stratigraphy, especially in the North Pacific, where calcareous microfossils are generally rare in post-Eocene sediments (Gladenkov 2006). The North Pacific diatom zonation has been studied and established by several researchers (e.g. Koizumi 1973, Akiba 1986). During SO202-INOPEX we have used the zonation established by Gladenkov (2006) as a reference (**Fig. 8-1**).

Age	Diatom zone	Boundary diatoms	Ma
Quaternary	*Neodenticula seminae*		
		→ LO *Proboscia curvirostris*	0. 3
	Proboscia curvirostris		
		→ LCO *Actinocyclus oculatus*	1. 0
	Actinocyclus oculatus		
		→ LO *Neodenticula koizumii*	2. 0
Pliocene	*Neodenticula koizumii*		
		→ LCO *Neodenticula kamtschatica*	2. 7
	Neodenticula koizumii - Neodenticula kamtschatica		
		→ FO *Neodenticula koizumii*	4. 0
Upper Miocene	*Neodenticula kamtschatica*	→ LCO *Neodenticula kamtschatica*	7. 4

Fig. 8-1: *Late Neogene and Quaternary diatom zonation for the middle-to-high latitudes of the North Pacific according to Gladenkov (2006). LO = last occurrence, LCO = last common occurrence, FO = first occurrence.*

In sediments attributed to the *Neodenticula seminae* Zone abundance fluctuations of *N. seminae,* were used as a stratigraphic tool. *Neodenticula seminae* has been recorded to mirror the marine isotope record from Marine Isotope Stage (MIS) 1 through MIS 12, with high relative abundance during interglacials (Sancetta and Silvestri 1984).

8.1 Methods

Nine piston cores (SO202-02-2, SO202-27-3, SO202-32-4, SO202-33-4, SO202-37-2, SO202-38-2, SO202-39-3, SO202-40-1, SO202-43-1) and one gravity core (SO202-34-5) located at the North Pacific were investigated on board (**Fig. 8.1-1**).

Smear slides for biostratigraphy study were prepared from core top to bottom at 30-40 cm intervals for Cores SO202-02-2 and SO202-27-3 and from tops of every liner

as well as core catchers for the other cores. Leica and Zeiss microscopes with phase-contrast were employed for diatom identification at a magnification of ×630 and ×1000, respectively. The abundances of each species are marked as follows: A=Abundance (>50%); C=Common (>25%); F=Few (>10%); R=Rare (>3%); T=Trace (1%); B=Barren.

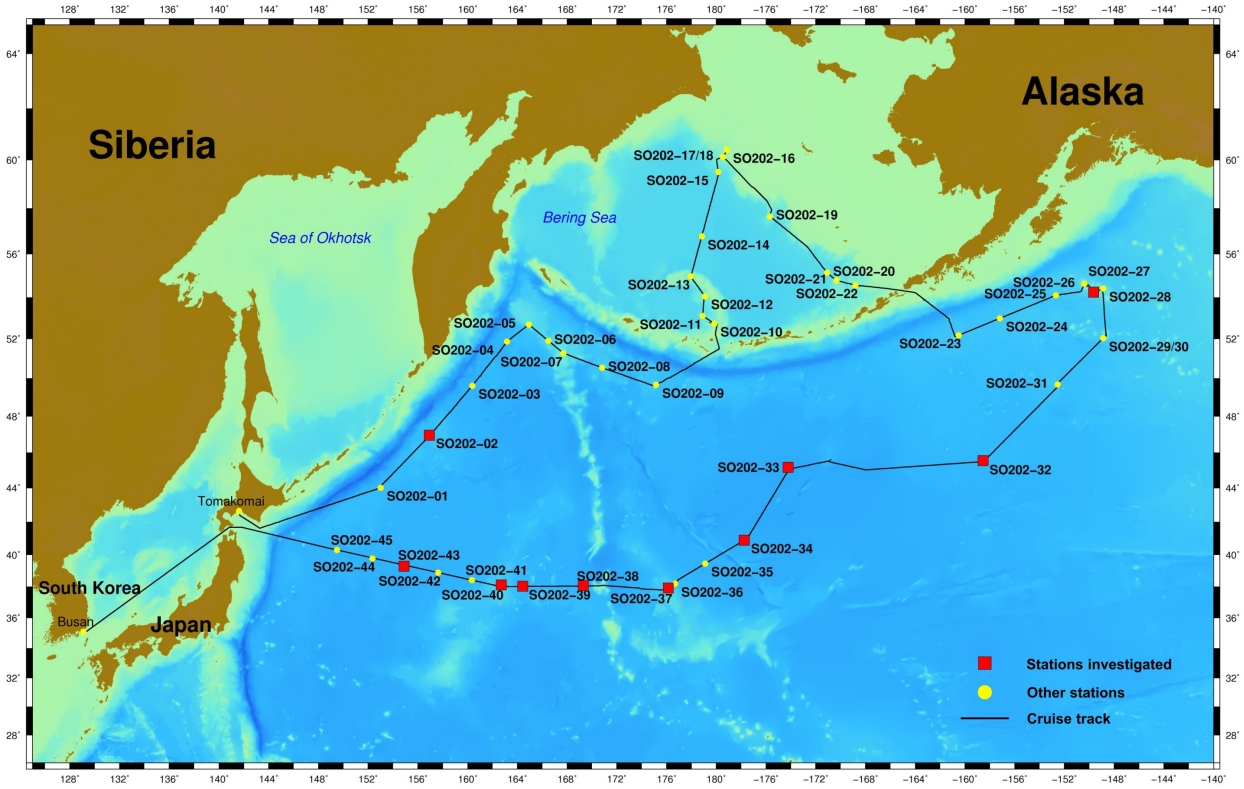

Fig. 8.1-1: *Sites selected for diatom biostratigraphic age determination.*

8.2 Results

SO202-02-2

Piston core SO202-02-2 (46°58.08' N, 156°58.8' E; water depth 4823 m), which has a total length of 12.15 m was recovered east of the Kuril-Kamchatka Trench. Diatoms are frequent to abundant from top to 2.60 m and from 4.50 to 11.20 cm.

The absence of *Proboscia curvirostris* in SO202-02-2 suggests that the sediments are younger than 280 kyrs, its Last Occurrence Datum (LOD) in the North Pacific (Akiba 1986, Sancetta and Silvestri 1984). The abundance of *N. seminae* ranges between few to abundant possibly indicating a Holocene age. Between 2.20 m and 4.50 m a strong decrease is marked, which suggests a glacial age (?MIS 2) of this interval. Strong fluctuations occur between 4.50 m and 9.50 m, while the sea ice related diatom species (*Thalassiosira gravida*, T. *antarctica* var. *borealis)* are common, indicating cold and unstable environments that may be attributed to MIS 3 and 4. It is likely that an abundance peak of *N. seminae* around 9.90 m marks the warm MIS 5.5. This is supported by the occurrence of *Coscinodiscus marginatus,* another indicator of interglacial conditions (Sancetta and Silvestri 1984). Considering this pattern, it is suggested that the base of SO202-02 is in MIS 6.

SO202-27-3
The base of the 15.5 m long core is marked by the Last Occurrence (LO) of *Rhizosolenia barboi*. This suggests an age around 0.3 Ma.

SO202-32-4
In SO202-32-4 a distinct change of diatom assemblages has been found around 12.5 m where dominant occurrences of *C. marginatus* together with occurrences of *Neodenticula kamtschatica* and *N. koizumii* are replaced by dominant occurrences of *N. seminae.* A similar shift in diatom assemblage has been found in Core SO202-33-4 around 14.70 m were it was interpreted to mark a paleoceanographic event at 2.7 Ma (Haug et al. 2005).

SO-202-33-4
In the 22.7 m long piston core SO202-33 (45°05.97' N, 174°08.39 W; water depth 6159 m) diatoms are generally common and abundant below 5.69 m, while in the upper section of the core diatom abundance decreases.

Generally the diatom assemblages are characterized by subarctic taxa and contain significant numbers of *Thalassiotrix longissima*. In some levels the occurrence of *Thalassiosira oestrupii* indicates intrusions of warmer waters associated with the Subarctic Polar Front. Occurrences of subtropical taxa (*Hemidiscus cuneiformis* and *H. simplissimus*) are sparse.

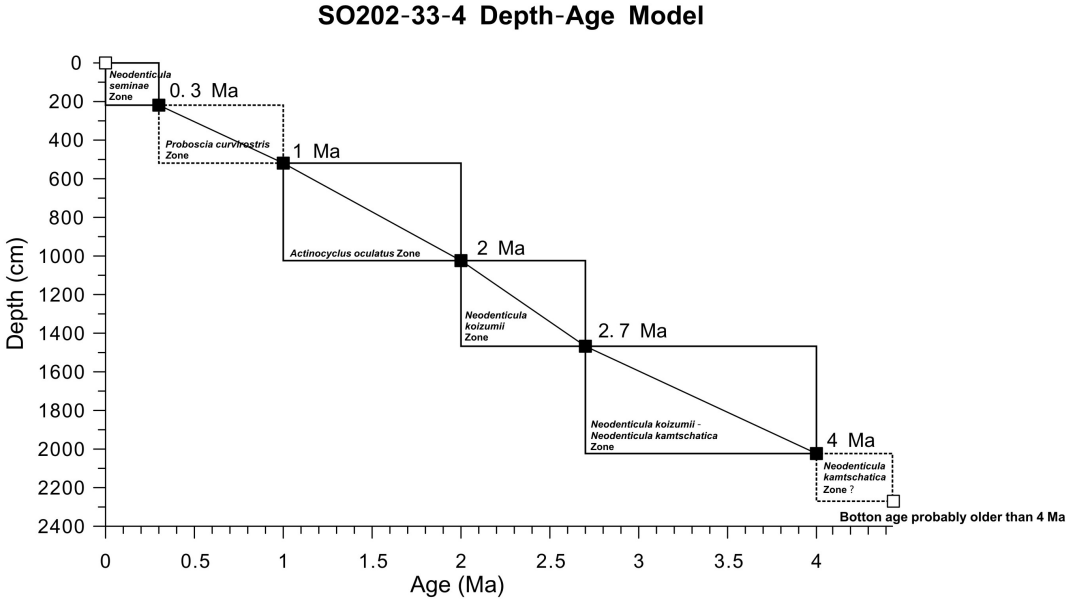

Fig 8.2-1: *Diatom biostratigraphic dating of SO202-33-4. Proboscia curvirostris is rare in the corresponding zone, which makes the upper boundary uncertain. The possible occurrence of the Neodenticula kamtschatica zone at the base of the core places the lowermost portion of the core at an age older than 4 Ma.*

Five diatom zones extending from the lower Pliocene into the Quaternary were identified in SO202-33-4, suggesting a continuous sediment record deposited at low sedimentations rates since >4 Ma (**Fig. 8.2-1**). Sediments of the lowermost core section (22.70-20.25 m) may be placed in the lower Pliocene *Neodenticula kamchatica* Zone. Around 20.25 m is the boundary between the *Neodenticula*

kamchatica Zone and the *Neodenticula koizumii – N. kamchatica* Zone (3.9-2.7 Ma). Diatom assemblages in both zones are strongly dominated by *Coscinodiscus marginatus*, typical for the early Pliocene assemblages of the subarctic North Pacific (Gladenkov and Barron 1996). The following zonal boundary marked by the First Occurrence (FO) of *N. seminae* and the LO of *Neodenticula kamchatica* is at 14.70 m and corresponds to an age of 2.7 Ma. Sediments between 14.70-10.20 m can be attributed to the *Neodenticula koizumii* Zone (2.7 – 2 Ma), followed by the *Actinocyclus oculatus* Zone (2-1 Ma) until 5.19 m core depth. The sediments recorded up to 2.18 m belong to the *Proboscia curvirostris* Zone (1-0.3 Ma).

SO-202-34-5
In gravity core SO202-34 (40°53.26' N, 177°40.52’ W; water depth 5724 m, length 15.8 m) three diatom zones in the Pliocene and Quaternary were identified. In the lower section of the core (15.83-10.99 m) the diatom assemblages are dominated by *Coscinodiscus marginatus* in the presence of warm water species such as *Thalassiosira oestrupii* and *Hemidiscus cuneiformis*. The top of this interval corresponds to the Last Occurrence of *N. kamchatica* and indicates a Pliocene age of this section. The occurrence of *Rhizosolenia curvirostris* above this section suggests the presence of a hiatus between 10.99 and 9.99 m considering that the FO of this taxon is at 1.6 Ma. The section between 9.99 and 2.99 m has been deposited between 1.6 and 1 Ma, indicated by the LO of *Actinocyclus oculatus*.

SO202-37-2
In Core SO202-37-2 two biostratigraphic datums could be encountered. At around 14 m is the LO of *Fragilariopsis fossilis* and *F. reinholdii* which occur at 0.7 and 0.6 Ma, respectively. At 6 m core depth is the LO of *Proboscia curvirostris*, which occurs at 0.3 Ma. This suggests an average sedimentation rate of 2 cm/kyr. In case this sedimentation rates would be constant throughout the entire core the base of the core at 24.34 m may be as old as 1.2 Ma.

SO202-38-2
The base of SO202-38-2 is not older than 1.6 Ma considering the occurrence of *Proboscia curvirostris*. Around 15 m occurs the LO of *F. fossilis* (0.7 Ma) and at 11 m the LO *F. reinholdii* (0.6 Ma) was encountered.

SO202-40-1
In SO202-40-1 the LO of *F. reinholdii* (LO at 0.6 Ma) is around 9 m and the LO of *P. curvirostris* (0.3 Ma) has been encountered at 1 m core depth.

SO202-43-1
The LO of *F. reinholdii* at the bottom of the core (at 21 m), places the core base at 0.6 Ma.

9. GEOCHEMISTRY

Ludmila Baumann, Jan Hansen, Olaf Kreft
Alfred Wegener Institute, Bremerhaven

The working group *Marine Geochemistry* of the AWI investigates and quantifies early diagenetic processes in surface sediments and more deeply buried marine deposits. One major focus of this cruise was to examine how and to which extent primary sediment components (e.g. various mineral phases, organic compounds, rock magnetic signatures, etc.) are altered geochemically in dependence on productivity regimes, geochemical environment, intensity of biogeochemical turn-over processes and depositional conditions. The aim of these studies is to improve the quality of reconstructions of paleoclimatological and paleoceanographic conditions from sediment proxies.

9.1 Pore water and sediment sampling

All sediment samples (multicorer, piston and kasten cores) were immediately processed after recovery. Pore water was extracted by means of rhizon samplers with a pore size 0.1 µm. At most of the sampling sites two Multicorer (MUC) cores were taken for pore water extraction and solid-phase sampling. Before sampling the remaining bottom water was carefully removed from the MUC cores by means of a siphon to avoid destruction of the sediment surface. During subsequent cutting of one of the parallel cores into slices for solid-phase sampling, pH and Eh measurements were performed with a minimum depth resolution of 1 cm.

Piston cores were cut into 1 m long segments on deck and sealed with plastic caps upon recovery. The 1-meter long core segments were then cut lengthwise into halves with a vibro saw and the following samples/measurements were taken/performed at 20 to 30 cm depth resolution: (1) determination of pH and Eh by means of punch-in electrodes, (2) about 10 ml of wet sediment were taken by with cut syringes and stored under argon for subsequent solid-phase analyses (→ anoxic solid-phase samples), and (3) pore water was retrieved by means of rhizon samplers.

9.2 Pore Water Analyses

Pore water analyses of the following parameters were carried out during this cruise: Eh, pH, alkalinity and iron (Fe^{2+}).

Alkalinity was calculated from a volumetric analysis by titration of 1 ml of pore water with 0.01M HCl, respectively. For the analyses of dissolved iron (Fe^{2+}) sub-samples of 1 ml were taken directly from pore water extracted by rhizons, immediately complexed with 50 µl of “Ferrospectral“ and determined photometrically at 565 nm.

For further analyses at the Alfred Wegener Institute for Polar and Marine Research (AWI) in Bremerhaven, aliquots of the remaining pore water samples were diluted 1:10 and acidified with $HNO_{3\ (suprapure)}$ for determination of cations (Ca, Mg, Sr, K, Ba, S, Mn, Si, B, Li) by ICP-AES. Additionally, 1.5 ml subsamples of the pore water were added to a ZnAc solution (600 µl) to fix all hydrogen sulfide present as ZnS for later

analysis. Subsamples for sulfate and chloride determinations were diluted 1:50 and stored frozen for ion chromatography (HPLC) analyses at the AWI in Bremerhaven.

9.3 Preliminary Results and Discussion

During this cruise, 24 multicorer cores, 3 piston cores, 1 gravity core and 5 kasten cores were processed and sampled for pore water and solid phase (**Table 9.3-1**).

Station	Area	Water depth [m]	Device	Rhizon Sampling	Alk.	Fe	HS^- * (fixation)	pH	Eh	Wet Sed.* (frozen)	Area
SO202-01-3	KU 1, 44*01,546'N;152*55,229'E	5282	MUC 1	X	X	X	X			X	off Kurile isl.
SO202-02-4	KU 2, 46*58,057'N;156*58,820'E	4822	MUC 2	X	X	X	x	X	X	X	off Kurile isl.
SO202-03-4	KU 3, 49*36,852'N;160*22,728'E	5429	MUC 3	x	x	x	x	x	x	x	off Kurile isl.
SO202-04-1	Md 1, 51*51,808'N;163*09,59'E	5273	Piston corer 1	x	x	x	x	x	x	x	off Kamchatka
SO202-04-3	Md 1, 51*51,808'N;163*09,59'E	5273	MUC 4	x	x	x	x	x	x	x	off Kamchatka
SO202-05-3	Md 2, 52*41,79'N;164*55,17'E	3362	MUC 5	x	x	x	x	x	x	x	NW-Meiji Drift
SO202-06-2	DS, 51*54,09'N;166*29,44'E	3422	MUC 6	x	x	x	x	x	x	x	NW-Meiji Drift
SO202-07-2	DS, 51*16,39'N;167*41,97'E	2349	MUC 7	x	x	x		x	x	x	Detroit Seamount
SO202-07-6	DS, 51*16,39'N;167*41,97'E	2345	Box corer 1	x	x	x	x	x	x	x	Detroit Seamount
SO202-08-1	NEM, 50*32,537'N;170*49,288'E	3633	MUC 8	x	x	x	x	x	x	x	NE-Meiji drift
SO202-09-2	SCA, 49*39,755'N;175*09,754'E	2346	MUC 9	x	x	x		x	x	x	S of central Aleutian Trench
SO202-10-2	SHBR, 52*44,570'N;179*50,879'E	1488	MUC 10	x	x	x	x	x	x	x	soueth.Bowers Ridge
SO202-11-1	SHBR, 53*6,671'N;178*54,017'E	2704	MUC 11	x	x	x	x	x	x	x	soueth.Bowers Ridge
SO202-12-1	CBR , 54*03,047'N;179*05,250'E	2109	Box corer 2	x	x	x	x	x	x	x	cent.Bowers Ridge
SO202-12-2	CBR , 54*03,047'N;179*05,250'E	2108	MUC 12	x	x	x	x	x	x	x	cent.Bowers Ridge
SO202-13-4	NBR, 54*58,73'N;177*57,43'E	1383	MUC 13	x	x	x	x	x	x	x	North..Bowers Ridge
SO202-14-5	CAB, 56*47,19'N;178*49,45'E	3822	MUC 14	x	x	x	x	x	x	x	cent. Aleutian Basin
SO202-15-4	NBS, 59*30,76'N;179*54,02'W	3137	MUC 15	x	x	x	x	x	x	x	Navarin Canyon
SO202-18-1	NBS, 60*07,59'N;179*26,64'W	1108	MUC 16	x	x	x		x	x	x	Navarin Canyon
SO202-18-6	NBS, 60*07,59'N;179*26,64'W	1107	Box corer 3	x	x	x	x	x	x	x	Navarin Canyon
SO202-19-5	BS, 57*39,06'N;175*40,70'W	1751	MUC 17	x	x	x	x	x	x	x	Bering Slope
SO202-21-2	BS, 54*47,33'N;170*19,67'W	1911	MUC 18	x	x	x	x	x	x	x	North.Umnak Plateau
SO202-22-1	BS 11, 54*34,41'N;168*48,62'W	1478	MUC 19	x	x	x	x	x	x	x	North.Umnak Plateau
SO202-22-4	BS 11, 54*34,41'N;168*48,62'W	1476	Box corer 4	x	x	x	x	x	x	x	North.Umnak Plateau
SO202-27-1	PS , 54*17,77'N;149*35,83'W	2916	MUC 20	x	x	x		x	x	x	Patton Smts
SO202-27-6	PS , 54*17,77'N;149*36,01'W	2919	Box corer 5	x	x	x	x	x	x	x	Patton Smts
SO202-29-5	GS , 52*01,68'N;148*53,68'W	3984	MUC 21	x	x	x		x	x	x	Patton Smts
SO202-29-6	GS , 52*01,68'N;148*53,68'W	3983	Piston corer 2	x	x	x	x	x	x	x	Gibson Smt
SO202-33-5	40*53.25'N:177*40.56'W	5713	MUC 22	x	x	x	x	x	x	x	North Chinook Trough
SO202-34-4	45*05.03'N:174*08.44'W	6159	MUC 23	x	x	x		x	x	x	East of south.Emperor Trough
SO202-35-1	39*27.15'N:179*06.69'E	5581	Gravity corer 1	x	x	x	x	x	x	x	West of south.Emperor Trough
SO202-39-2	38*00,69'N;164*26,80'E	5096	MUC 24	x	x	x		x	x	x	Shatsky Rise
SO202-39-3	38*00,70'N;164*26,78'E	5102	Piston corer 3	x	x	x	x	x	x	x	Shatsky Rise

Table 9.3-1: *Sites investigated geochemically during this cruise, including parameters analyzed on board and aliquots of samples taken and stored for further analyses in the home labs at AWI.*

Pore water concentration profiles for piston core SO202-04-1 are shown in **Fig. 9.3-1**. The core was retrieved off Kamchatka from a water depth of about 5200 m and is characterized by numerous ash layers. All parameters shown in **Fig. 9.3-1** display significant variation over depth which are rather unusual for “normal” deep-sea

pelagic sediments. In particular, the pore water profile of Fe^{2+} is characterized by several pronounced peaks, which might be produced from ongoing iron reduction within the ash layers. Further, more detailed investigations of both the pore water and the sedimentary solid phase will aim at identifying the processes producing the observed distribution patterns of dissolved iron and other pore water constituents.

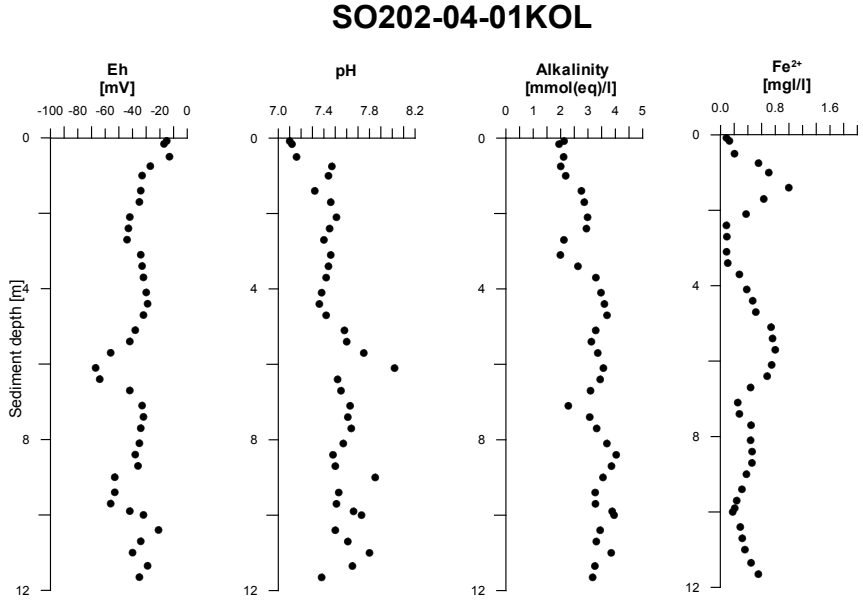

Fig. 9.3-1*: Pore water concentration profiles for piston core SO202-04-1.*

The pore water geochemistry of surface sediments at site SO202-12-2 (central Bowers Ridge) is displayed in **Fig. 9.3-2**. The dissolved iron profile (Fe^{2+}) indicates that the current iron redox boundary is located at a sediment depth of about 3 cm. This relatively shallow depth position of the Fe redox boundary points to a high input of organic matter to this site which is likely to have led to the development of anoxic conditions close to the sediment surface.

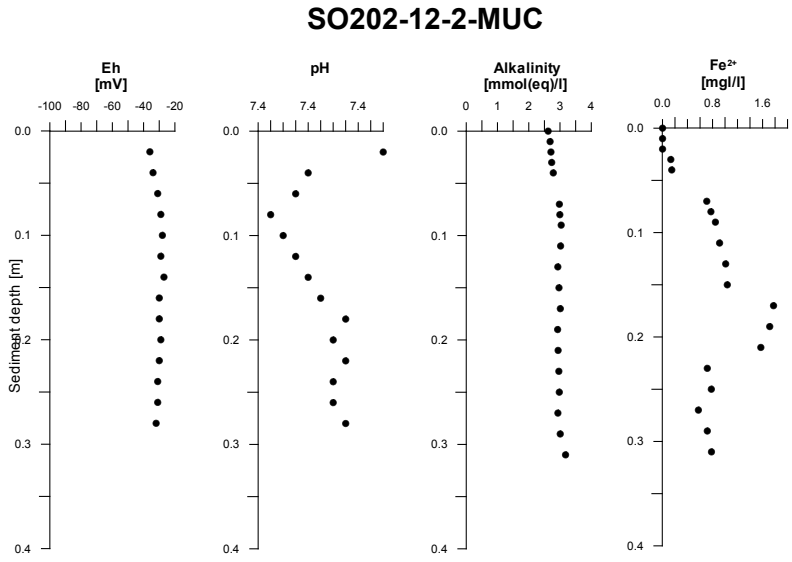

Fig. 9.3-2*: Pore water concentration profiles for multicorer core SO202-12-2.*

10. REFERENCES

Abelmann, A., Gersonde, R. Abelmann, A., Gersonde, R., Cortese, G., Kuhn, G., Smetacek, V., 2006. Extensive phytoplankton blooms in the Atlantic Sector of the glacial Southern Ocean, Paleoceanography 21, doi:10.1029/2005PA001199.

Akiba, 1986. Middle Miocene to Quaternary diatom biostratigraphy in the Nankai Trough and Japan Trench, and modified lower Miocene through Quaternary diatom zones for middle-to-high latitudes of the North Pacific. DSDP report, 87, 393-481.

Anderson, R.F., Fleisher, M.Q., Lao, Y., 2006. Glacial-interglacial variability in the delivery of dust to the central equatorial Pacific Ocean. Earth and Planetary Science Letters 242, 406-414.

Aoki, K., 2008. Revised age and distribution of ca. 87 ka Aso-4 tephra based on new evidence from the northwest Pacific Ocean. Quaternary International, 178, 100-118.

Aoki, K., Arai, F., 2000. Late Quaternary tephrostratigraphy of marine core KH94-3, LM-8 off Sanriku, Japan. The Quaternary Research (Japan Association for Quaternary Research) 39, 107-120. (In Japanese with English abstract)

Aoki, K., Sakamoto, T., 2003. Late Quaternary tephrostratigraphy of marine sediments from the Japan Trench forearc, Holes 1150A and 1151C. In: Suyehiro, K., Sacks, I. S., Acton, G. D., and Oda, M. (Ed.) Proceedings of the Ocean Drilling Program, Scientific Results 186.

Aoki, K., Machida, H., 2006. Major element composition of volcanic glass shards of the late Quaternary widespread tephras in Japan - Distinction of tephras using K_2O-TiO_2 diagrams, Bulletine of the Geological Survey of Japan, 57(7/8), 239-258. (in Japanese with English summary)

Aoki, K., Yamamoto, H., Yamauchi, M., 2000. Late Quaternary tephrostratigraphy of marine cores collected during “Mirai” MR98-03 and MR99-K04 cruises. Report of Japan Marine Science Technology Center 41, 49-56. (In Japanese with English abstract)

Aoki, K., Irino, T., Oba, T., 2008. Middle-late Pleistocene tephrostratigraphy of the sediment core MD01-2421 collected off the Kashima coast, Japan. The Quaternary Research (Japan Association for Quaternary Research) 47, 391-407. (In Japanese with English abstract)

Bassinot, F., Baltzer, A., Chen, M.-T., DeDeckker, P., Khuhnt, W., Levitan, M., Nurnberg, D., Oba, T., Prentice, M., Sarnthein, M., Situmorang, M., Tiedemann, R., Holbourn, A., Kiefer, T., Pflaumann, U., and Rothe, S. (2002). "Scientific Report of the WEPAMA Cruise, MD122/IMAGES VII." Institut Francais pour la Recherche et la Technologie Polaires, France.

Bianchi, G.G. and McCave, I.N., 1999. Holocene periodicity in North Atlantic climate and deep-ocean flow south of Iceland. Nature 397: 515-517.

Belt, S.T., Massé, G., Rowland, S.J., Poulin, M., Michel, C., LeBlanc, B., 2007. A novel chemical fossil of palaeo sea ice: IP25. Organic Geochemistry 38, 16-27.

Bleil, U., von Dobeneck, T. 1999. Geomagnetic events and relative paleointensity records – clues to high-resolution paleomagnetic chronostratigraphies of Late Quaternary marine sediments? In: Fischer, G., Wefer, G. (eds.) Use of proxies in paleoceanography: Examples from the South Atlantic. Springer-Verlag, Berlin, Heidelberg, pp 635 – 654.

Bleil, U., Dillon, M., 2008. Holocene Earth's magnetic field variations recorded in marine sediments of NW African continental margin. Stud. Geophys. Geod. 52, 133−155.

Boyce, R.E., 1968. Electrical resistivity of modern marine sediments from the Bering Sea. J. Geophys. Res. 73, 4759-4766.

Bradtmiller, L.I., Anderson, R.F., Fleisher, M.Q., Burckle, L.H., 2007. Opal burial in the equatorial Atlantic Ocean over the last 30 ka: Implications for glacial-interglacial changes in the ocean silicon cycle. Paleoceanography 22, PA4216, doi:1029/2007PA001443.

Braitseva, O.A., Malekestev, I.V., Ponomareva, V.V., Sulerzhitsky, L.D., 1995. Ages of calderas, large explosive craters and active volcanoes in the Kuril-Kamchatka, Russia. Bulletin of Volcanology 57, 383-402.

Brunelle, B.G., Sigman, D.M., Cook, M.S., Keigwin, L.D., Haug, G.H., Plessen, B., Schettler, G., Jaccard, S.L., 2007. Evidence from diatom-bound nitrogen isotopes for subarctic Pacific stratification during the last ice age and a link to North Pacific denitrification changes. Paleoceanogr. 22, PA1215, doi:10.1029/2005PA001205.

Creager J.S., Scholl D.W. et al., 1973. Initial Reports of the Deep Sea Drilling Project, Volume 19, Washington (U.S. Covernment Printing Office) 913 pp.

Comiso, J.C., 2003. Large-scale characteristics and variability of the global sea-ice cover. In: Thomas, D.N., Diekmann, G.S. (Eds.) Sea ice an Introduction to its Physics, Chemistry, Biology and Geology, Balckwell, Oxford, pp. 112-142.

Cook, M.S., Keigwin, L.D., Sancetta, C.A., 2005. The deglacial history of surface and intermediate water of the Bering Sea. Deep-Sea Research II 52, 2163-2173.

Davies, S. M., Wåstegard, S. and Wohlfarth, B., 2003. Extending the limits the Borrobol Tephra to Scandinavia and detection of new early Holocene tephras. Quaternary Resarch 59, 345-352.

De La Rocha, C. L., Brzezinski, M.A., DeNiro, M.J., Shemesh, A., 1998. Silicon-isotope composition of diatoms as an indicator of past oceanic change. Nature 395, 680-683.

de Vernal, A., Eynaud., F., Henry, M., Hillaire-Marcel, C., Londeix, L., Mangin, S., Matthiessen, J., Marret, F., Radi, T., Rochon, A., Solignac, S., Turon, J.-L., 2005. Reconstruction of sea-surface conditions at middle to high latitudes of the Northern Hemisphere during the Last Glacial Maximum (LGM) based on dinoflagellate cyst assemblages. Quaternary Science Review 24, 897-924.

de Vernal, A., Rosell-Melé, A., Kucera, M., Hillaire-Marcel, C., Eynaud, F., Weinelt, M., Dokken, T., Kageyama, M., 2006. Comparing proxies for the reconstruction of LGM sea-surface conditions in the northern North Atlantic. Quaternary Science Review 25, 2820-2834.

Diekmann, B, Kuhn, G., 1997. Terrigene Partikeltransporte als Abbild spätquartärer Tiefen- und Bodenwasserzirkulation im Südatlantik und angrenzendem Südpolarmeer. Zeitschrift der Deutschen Geologischen Gesellschaft 148: 405-429.

Dodimead, A.J., Favorite, F., Hirano, T., 1963. Salmon of the North Pacific Ocean, Part II: Review of oceanography of the Subarctic Pacific Ocean. Int. North Pacific Fisheries Community Bulletin 13, 1-195.

Duncan, R.A., Keller, R.A., 2004. Radiometric ages for basement rocks from the Emperor Seamounts, ODP Leg 197. Geochem., Geophys., Geosyst. 5, Q08L03.

Feeley, T.C., Winer,G.S., 2009.Volcanic hazards and potential risks on St. Paul Island, Pribilof Islands, Bering Sea, Alaska. Journal of Volcanology and Geothermal Research 182, 57-66.

Francois, R., Frank, M., Rutgers van der Loeff, M.M., Bacon, M., 2004. ^{230}Th normalization: an essential tool for interpreting sedimentary fluxes during the late Quaternary. Paleoceanogr. 19, PA1018, doi:10.1029/2003PA000939.

Franke, C., Hofmann, D., von Dobeneck, T., 2004. Does lithology influence paleointensity records? A statistical analysis on South Atlantic pelagic sediments. Physics of the Earth and Planetary Interiors 147, 285-296

Froese, D.G., Zazula, G.D., Reyes, A.V., 2006. Seasonality of the late Pleistocene Dawson tephra and exceptional preservation of a buried riparian surface in central Yukon Territory, Canada. Quaternary Science Reviews 25, 1542–1551.

Fukuma, K., Harada, N., 2001. Paleointensity stratigraphy of north Pacific sediments. Report of Japan Marine Science and Technology Center (Ocean Research), 43, 83-91. (in English with Japanese summary)

Furuta, T., Fujioka, K., Arai, F., 1986. Widespread submarine tephras around Japan─petrographic and chemical properties. Marine Geology 72, 125-142.

Gebhardt, H., Sarnthein, M., Grootes, P.M., Kiefer, T., Kuehn, H., Schmieder, F., Röhl, U., 2008. Paleonutrient and productivity records from the subarctic North Pacific for Pleistocene glacial terminations I to V. Paleoceanography 23, PA4212, doi:10.1029/2007PA001513.

Gersonde, R., Hodell, D.A., Blum, P. et al., 1999. Proceedings ODP, Initial Reports, 177 [CD-ROM]. Available from: Ocean Drilling Program, Texas A&M University, College Station, TX 77845-9547, USA.

Gersonde, R., Crosta, X., Abelmann, A., Armand, L., 2005. Sea-surface temperature and sea ice distribution of the Southern Ocean at the EPILOG Last Glacial Maximum a circum-Antarctic view based on siliceous microfossil records. Quaternary Science Reviews 24, 869-896, doi:10.1016/j.quascirev.2004.07.015.

Gladenkov, 2006. The Cenozoic Diatom Zonation and Its Significance for Stratigraphic Correlations in the North Pacific. Paleontological Journal, 40, Suppl. 5, S571–S583.

Gladenkov A.Yu., Barron J.A. 1996. Main results of the North Pacific diatom biostratigraphy and paleoceanography based on ODP Leg 145 materials. In: Proceedings of sixth international congress on Pacific Neogene stratigraphy and IGCP-355: Neogene evolution of Pacific: biotic, oceanographic and tectonic development. pp. 2-7.

Grobe, H., 1987. A simple method for the determination of ice-rafted debris in sediment cores. Polarforschung 57: 123-126.

Grönvold, K., Óskarsson, K., Johnsen, S.J., Clausen, H.B., Hammer, C.U., Bond, G., Bard, E., 1995. Ash layers from Iceland in the Greenland GRIP ice core correlated with oceanic and land sediments. Earth and Planetary Science Letters 135, 149–155.

Harada, N., Fukuma, K., Iwai, M., Murayama, M. , Sugawara, T., Matsuhashi, M., Sato, M., Aoki, K. and Kondo, T., 2000. General features of cored sediments collected in the northwestern area of the North Pacific during the MR98-05 (R/V MIRAI) cruise, Report of Japan Marine Science and Technology Center (Ocean Research), 40, 113-124. (in English with Japanese summary)

Hatte, C., Hodgins, G., Jull, A.J.T., Bishop, B., Tesson, B., 2008. Marine chronology based on C-14 dating on diatoms proteins. Marine Chemistry, 109 (1-2), 143-151.

Haug, G. H. et al., 2005. North Pacific seasonality and the glaciation of North America 2.7 million years ago. Nature 433, 821-825.

Heusser, L.E., Morley, J.J., 1985. Pollen and Radiolarian records from deep-sea core RC14-103: Climatic reconstructions of Northeast Japan and Northwest Pacific for the last 90,000 years. Quaternary Research 24, 60-72.

Hofmann, D. I., Fabian, K., 2007. Rock magnetic properties and relative paleointensity stack for the last 300 ka based on a stratigraphic network from the subtropical and subantarctic South Atlantic. Earth and Planetary Science Letters 260 (1-2), 297-312.

Horn, D.R., Delach, M.N., Horn, B.M., 1969. Distribution of volcanic ash layers and turbidites in the north Pacific. Geological Society of America Bulletin 80, 1715-1724.

Ingalls, A.E., Anderson, R.F. Pearson, A., 2004. Radiocarbon dating of diatom-bound organic compounds. Marine Chemistry 92,91-105.

Jansen, J.H.F., van der Gaast, S.J., Kloster, B., Vaars, A.J., 1998. CORTEX, a shipboard XRF scanner for element analyses in split sediment cores. Marine Geology 151, 143-153.

Keigwin, L., D., 1987. North Pacific Deep Water formation during the latest glaciation. Nature 330, 651-655.

Keigwin, L.D., 1995. Stable isotope stratigraphy and chronology of the upper Quaternary section at Site 883, Detroit Seamount. In: Rea, D.K., Basov, I.A., Scholl, D.W., and Allan, J.F. (Eds.), 1995, Proceedings ODP, Scientific Results 145, 257-264.

Keigwin, L.D., Jones, G.A., Froelich, P.N., 1992. A 15,000 year paleoenvironmental record from Meiji Seamount, far northwestern Pacific. Earth and Planetary Science Letters 111 (2-4), 425-440.

Kim, J.-H., Schouten, S., Hopmans, E.C., Donner, B., Sinnighe Damsté, J.S., 2008. Global sediment coretop calibration of the TEX_{86} paleothermometer in the ocean. Geochimica Cosmochimica Acta 72, 1154-1173.

Koizumi, 1973. The Late Cenozoic Diatoms of Sites 183–193, Leg 19, Deep Sea Drilling Project. DSDP report, 19, 805–855.

Kröger, N., Deutzmann, R., Bergsdorf, C., Sumper M., 2000. Species-specific polyamines from diatoms control silica morphology. PNAS 97, 14133-14138.

Lacasse, C., Sigurdsson, H., Johannesson, H., Paterne, M., Carey, S., 1995. Source of Ash Zone 1 in the North Atlantic. Bulletin of Volcanology 57, 18-32.

Lee, S.H., Chough, S.K., 2001. High-resolution (2-7 kHz) acoustic and geometric characters of submarine creep deposits in the South Korea Plateau, East Sea. Sedimentology 48, 629-644.

Lisiecki, L.E., Raymo, M.E., 2005. A Pliocene-Pleistocene stack of 57 globally distributed benthic $\delta^{18}O$ records. Paleoceanogr. 20, PA1003, doi:10.1029/2004PA001071.

Machida, H. and Arai, F., 1992. Atlas of tephra in and around Japan. 276p, Tokyo University Press. (In Japanese)

Machida, H. and Arai, F., 2003. Atlas of tephra in and around Japan. 336p, Tokyo University Press. (In Japanese)

Mangan, M.T., Waythomas, C.F., Miller, T.P., Trusdell, F.A., 2003. Emmons Lake Volcanic Center, Alaska Peninsula: source of the Late Wisconsin Dawson tephra, Yukon Territory, Canada. Canadian Journal of Earth Sciences 40, 925–936.

Martínez-Garcia, A., Rosell-Melé, A., Geibert, W., Gersonde, R., Masqué, P., Gaspari, V., Barbante, C. (2009): Links between iron supply, marine

productivity, sea surface temperature, and CO_2 over the last 1.1 Ma. Paleoceanography, 24, PA1207, doi:10.1029/2008PA001657.

Massé, G., Rowland, S.J., Sicre, M.-A., Jacob, J., Jansen, E., Belt, S.T., 2008. Abrupt climate changes for Iceland during the last millenium: evidence from high resolution sea ice reconstructions. Earth and Planetary Science Letters 269 (3-4), 565-569.

McGee, D., Marcantonio, F, Lynch-Stieglitz, J., 2007. Deglacial changes in dust flux in the eastern equatorial Pacific. Earth and Planetary Science Letters, 257: 215-230.

Nelson, C.H., Kulm, L.D., Carlson, P.R., 1968. Mazama ash in the Northeast Pacific. Science 161, 47-49.

Ninkovich, D., Opdyke, N., Heezen, B. C., Foster, J. H., 1966. Paleomagnetic stratigraphy, rates of deposition and tephrochronology in north pacific deep-sea sediments. Earth and Planetary Science Letters 1, 476-492.

Normark, W. R., Carlson, P. R., 2003. Giant submarine canyons: is size any clue to their importance in the rock record? In: Chan, M. A. and Archer, A. W. (eds.) Extreme depositional environments: Mega end members in geological time. Geol. Soc. Am. Spec. Paper 370, 15 p.

Okada, M., Takagi, M., Narita, H., Takahashi, K., 2005. Chronostratigraphy of sediment cores from the Bering Sea and the subarctic Pacific based on paleomegnetic and oxygen isotope analyses. Deep-Sea Research II 52, 2092-2109.

Otosaka, S., Honda, M.C., Noriki, S., 2004. La/Yb and Th/Sc in settling particles: vertical and horizontal transport of lithogenic material in the western North Pacific. Geochemistry Journal 38, 515–525.

Pearce, N.J.G., Westgate, J.A., Preece, S.J., Eastwood, W.J., Perkins, W.T., Hart, J.S., 2007. Reinterpretation of Greenland ice-core data recognises the presence of the late Holocene Aniakchak tephra (Alaska), not the Minoan tephra (Santorini), at 1645 BC. Proceedings of the SCIEM 2000-2nd Euro Conference, Vienna, 28th of May- 1st of June, 2003, 139-147.

Piotrowski, A.M., Goldstein, S.L., Hemming, S.R., Fairbanks, R.G., 2004. Intensification and variability of ocean thermohaline circulation through the last deglaciation. Earth and Planetary Science Letters 225, 205-220.

Ponomareva, V.V., Kyle, P.R., Melekestsev, I.V., Rinkleff, P.G., Dirksen, O.V., Sulerzhitsky, L.D., Zaretskaia, N.E., Rourke, R., 2004. The 7600 (^{14}C) year BP Kuril Lake caldera-forming eruption, Kamchatka, Russia: Stratigraphy and field relationships. Journal of Volcanology and Geothermal Research 136, 199-222.

Preece, S.J., Westgate, J.A., Stemper, B.A., Péwé, T.L., 1999. Tephrochronology of late Cenozoic loess at Fairbanks, central Alaska. Geological Society of America Bulletin 111, 71–90.

Radi, T., Pospelova, V., de Vernal, A., Barrie, J.V., 2007. Dinoflagellate cysts as indicators of water quality and productivity in British Columbia estuarine environments. Marine Micropaleontology 62, 269-297.

Rea, D. K., Basov, I. A., Janecek, T. R., Palmer-Julson, A. et al., 1993. Proceedings of the Ocean Drilling Program: Initial Reports. 145. Ocean Drilling Program, College Station, Tex.

Ren H, Sigman DM, Meckler AN, Plessen B, Robinson R.S, Rosenthal Y, and Haug GH (2009). Foraminiferal Isotope Evidence of Reduced Nitrogen Fixation in the Ice Age Atlantic Ocean. Science, 323(5911), 244-248.

Robinson RS, and Sigman DM (2008). Nitrogen isotopic evidence for a poleward decrease in surface nitrate within the ice age Antarctic. Quaternary Science Reviews, 27(9-10), 1076-1090.

Röhl, U., Abrams, L.J., 2000. High-resolution, downhole and non-destrctive core measurements from Sites 999 and 1001 in the Caribbean Sea: applications to the Late Paleocene Thermal Maximum. Proceedings ODP, Scientific Results 165, 191-203.

Sancetta, C., Silvestri, S., 1984. Diatom stratigraphy of the late Pleistocene (Brunhes) subarctic Pacific. Marine Micropaleontology 9, 263-274.

Shemesh, A., Hodell, D., Crosta, X., Kanfoush, S., Charles, C., Guilderson, T., 2002. Sequence of events during the Last deglaciation in Southern Ocean Sediments and Antarctic ice cores. Paleoceanography 17, 599-605.

Shigemitsu, M., Narita, H., Watanabe, Y.W., Harada, N., Tsunogai, S., 2007. Ba, Si, U, Al, Sc, La, Th, C and $^{13}C/^{12}C$ in a sediment core in the western subarctic Pacific as proxies of past biological production. Marine Chemistry 106, 442-455.

Smith, D.G. and Westgate, J.A., 1969. Electron probe technique for characterizing pyroclastic deposits. Earth and Planetary Science Letters 5, 313-319.

Taylor, S., Brownlee, D.E., 1991. Cosmic spherules in the geologic record. Meteorites 26, 203-211.

Valet, J.-P., Meynadier, L., Guyodo, Y., 2005. Geomagentic dipole strength and reversal rate over the past two million years. Nature 435, 802-805.

von Dobeneck, T., Schmieder. F., 1999. Using rock magnetic proxy records for orbital tuning and extended time series analyses into the super- and sub-Milankovitch bands. In: Wefer, G., Fischer, G. (Eds.), Use of Proxies in Paleoceanography: Examples from the South Atlantic, Springer, Berlin, pp. 601-633.

Waelbroeck, C., Paul, A., Kucera, M., Rosell-Mele, A., Weinelt, M., Schneider, R., Mix, A.C., Abelmann, A., Armand, L., Barker, S., Barrows, T.T., Benway, H., Cacho, I., Chen, M.-T., Cortijo, E., Crosta, X., de Vernal, A., Dokken, T., Duprat, J., Elderfield, H., Eynaud, F., Gersonde, R., Hayes, A., Henry, M., Hillaire-Marcel, C., Huang, C.-C., Jansen, E., Juggins, S., Kallel, N., Kiefer, T., Kienast, M., Labeyrie, L., Leclaire, H., Londeix, L., Mangin, S., Matthiessen, J., Marret, F., Meland, M., Morey, A. E., Mulitza, S., Pflaumann, U., Pisias, N. G., Radi, T., Rochon, A., Rohling, E. J., Sbaffi, L., Schäfer-Neth, C., Solignac, S., Spero, H., Tachikawa, K., Turon, J.-L., 2009. Constraints on the magnitude and pattern of ocean cooling at the Last Glacial Maximum. Nature Geoscience, doi 10.1038/NGEO411.

Warren, B. A., 1983. Why is no deep water formed in the North Pacific? J. Mar. Res. 41, 327-347.

Wastegård, S., 2005. Late Quaternary tephrochronology of Sweden: a review. Quaternary International 130, 49-62.

Weijers, J.W.H., Schouten, S., Spaargaren, O.C., Sinnighe Damsté, J.S., 2006. Occurrence and distribution of tetraether membrane lipids in soils: Implications for the use of the TEX_{86} proxy and the BIT index. Organic Geochemistry 37, 1680-1693.

Wessel, P., Smith, W.H.F., 1995. New Version of the Generic Mapping Tools Released. EOS Trans. AGU 76, 329.

Westgate, J.A., Walter, R.C., Pearce, G.W., Gorton, M.P., 1985. Distribution, stratigraphy, petrochemistry and palaeomagnetism of the late Pleistocene Old Crow tephra in Alaska and the Yukon. Canadian Journal of Earth Sciences 22, 893–906.

Westgate, J.A., Preece, S.J., Kotler, E., Hall, S., 2000. Dawson tephra: a prominent stratigraphic marker of late Wisconsin age in west-central Yukon. Canadian Journal of Earth Sciences 37, 621–627.

Winckler, G., Anderson, R.F., Fleisher, M.Q., McGee, D., Mahowald, N.M., 2008. Covariant glacial-interglacial dust fluxes in the Equatorial Pacific and Antarctica. Science 320, 93-96.

Zahn, R., Rushdi, A., Pisias, N.G., Bornhold, B.D., Blaise, B., Karlin, R., 1991. Carbonate deposition and benthic $\delta^{13}C$ in the subarctic Pacific: implications for changes of the oceanic carbonate system during the past 750,000 years. Earth and Planetary Science Letters 103, 116-132.

Zdanowicz, C.M., Zielinski, G. A., Germani, M.S. 1999. Mount Mazama eruption: Calendrical age verified and atmospheric impact assessed, Geology 27, 621-624.

A.1 SO202-INOPEX TEILNEHMENDE INSTITUTE / PARTICIPATING INSTITUTIONS

	Address
AWI	Stiftung Alfred-Wegener-Institut für Polar- und Meeresforschung in der Helmholtz-Gemeinschaft Postfach 120161 27515 Bremerhaven GERMANY
AWI (P)	Stiftung Alfred-Wegener-Institut für Polar- und Meeresforschung in der Helmholtz-Gemeinschaft Forschungsstelle Potsdam Telegrafenberg A43 14473 Potsdam GERMANY
ETH	Eidgenössische Technische Hochschule Zürich Geologisches Institut Sonneggstrasse 5 8092 Zürich SWITZERLAND
GEOB	Marine Geophysik Fachbereich Geowissenschaften Universität Bremen Postfach 330440 28344 Bremen GERMANY
GEOTOP	GEOTOP Université du Québec à Montréal C.P. 8888, succursale "centre ville" Montréal, Qc CANADA H3C 3P8
LDEO	Lamont-Doherty Earth Observatory 231 Comer Building P.O. Box 1000 Palisades, NY 10964 USA
POI	V.I. Il´ichev Pacific Oceanological Institute Far Eastern Branch of the Russian Academy of Science Baltijskaya Str. 43 690041 Vladivostok RUSSIA

	Address
RU	Cosmo-Geochemistry Laboratory Faculty of Geo-Environmental Science Rissho University 1700 Magechi, Kumagaya, Saitama pref. JAPAN 360-0194
TU	School of Ocean and Earth Science Tongji University 1239 Siping Road, Shanghai, 20092 PR CHINA

A.2 SO202-INOPEX FAHRTTEILNEHMER / CRUISE PARTICIPANTS

Fahrleiter/ Chief scientist: Rainer Gersonde

Name/ Last name	Vorname/ First name	Institut/ Institute	Beruf/ Profession
Aoki	Kaori	RU	Scientist, geology
Baumann	Ludmila	AWI	Technician, geochemistry
Bonnet	Sophie	GEOTOP	PhD-student, geology
Borchers	Andreas	AWI (P)	PhD-student, geology
Diekmann	Bernhard	AWI (P)	Scientist, geology
Dufek	Tanja	AWI	Student, bathym./echos.
Esper	Oliver	AWI	Scientist, geology
Frederichs	Thomas	GEOB	Scientist, geophysics
Gersonde	Rainer	AWI	Scientist, geology
Hayes	Christopher	LDEO	PhD-student, geology
Heinzl	Cornelia	AWI	Student, bathym./echos.
Hockun	Katja	AWI (P)	Student, geology
Karnaukh	Victor	POI	Scientist, geophysics
Kreft	Olaf	AWI	Student, geochemistry
Lensch	Norbert	AWI	Technician, geology
Li	Wenbao	TU	PhD-student, geology
Meheust	Marie	AWI	PhD-student, geology
Obrezkova	Maria	POI	PhD-student, geology
Reichelt	Lucia	GEOB	PhD-student, geophysics
Ren	Jian	AWI	PhD-student, geology
Rohardt	Ann-Kathrin	AWI	Student, bathym./echos.
Striewski	Friedrich	AWI	Student, geology
Studer	Anja	ETH	PhD-student, geology
Winterfeld	Maria	AWI	PhD-student, geology

A.3 SO202-INOPEX SCHIFFSBESATZUNG / SHIP'S CREW

No.	Name	Rank
1.	Mallon, Lutz	Master
2.	Korte, Detlef	1. Offc.
3.	Rex, Andreas	Ch. Eng.
4.	Schmitz, Olaf	2. Offc.
5.	Büchele, Ulrich	2. Offc.
6.	Walther, Anke	Doctor
7.	Thomsen, Sascha	2. Eng.
8.	Czipull, Michael	2. Eng.
9.	Angermann, Rudolf	Elec. Eng.
10.	Ehmer, Andreas	Syst. Manager
11.	Zebrowski, Dariusz	Electrician
12.	Rosemeyer, Rainer	Locksmith
13.	Schrapel, Andreas	Boatswain
14.	Kraft, Jürgen	A.B.
15.	Dolief, Joachim	A.B.
16.	Bierstedt, Thorsten	A.B.
17.	Stängl, Günther	A.B.
18.	Brusch, Malte	A.B.
19.	Fricke, Ingo	A.B.
20.	Krawczak, Richard	Mot-man
21.	Henning, Tim	Mot-man
22.	Wieden, Wilhelm	1. Cook
23.	Ganagaraj, Antony	2. Cook
24.	Steep, Maik	Steward
25.	Royo, Luis	Steward

A.4 SO202-INOPEX STATION LIST

Station No.	Gear No.	Date (UTC)	Start (UTC)	At seafl./ at depth (UTC)	End (UTC)	Latitude (deg/min)	Longitude (deg/min)	Latitude (decimal)	Longitude (decimal)	Area	Water depth EM120 (m)	Rope length (m)	Gear	Depth interval (m)	Core recovery (m)	Remarks
SO202-01	-1	10/07/2009	05:00	06:37	08:31	44°01.543'N	152°55.238'E	44.0257	152.9206	off Kurile-Kamtchatka Trench	5279	5274	CTD+ROS		-	ROS failure, no samples
	-2	10/07/2009	09:13	10:51	13:22	44°01.549'N	152°55.217'E	44.0258	152.9203		5277	5244	KOL(20 m)+TC			**TC 0.84 m**; KOL lost during recovery
	-3	10/07/2009	13:47	15:29	17:36	44°01.555'N	152°55.194'E	44.0259	152.9199		5282	5278	MUC		11x(0.23-0.32)	
SO202-02	-1	11/07/2009	21:30	21:53	22:18	46°58.035'N	156°58.784'E	46.9673	156.9797	off Kurile-Kamtchatka Trench	4824		CTD+ROS+FL	0-1000		
	-2	11-12/7/09	22:56	00:25	03:04	46°58.081'N	156°58.800'E	46.9680	156.9800		4823	4795	KOL(20 m)+TC		**12.15**	12 water samples **TC 0.86 m**; KOL bent at 0.84-4.59 m
	-3	12/07/2009	03:36		03:53	46°58.052'N	156°58.856'E	46.9675	156.9809		4823		PLA	0-100		
	-4	12/07/2009	04:08	05:42	07:45	46°58.134'N	156°58.925'E	46.9689	156.9821		4822	4824	MUC		10x(0.26-0.29)	
	-5	12/07/2009	08:39	09:15	10:18	46°58.083'N	156°58.825'E	46.9681	156.9804		4824		MN	0-1000		1000-500, 500-300, 300-150, 150-50, 50-0 m
SO202-03	-1	13/07/2009	06:22	06:52	07:19	49°36.836'N	160°22.745'E	49.6139	160.3791	off Kurile-Kamtchatka Trench	5425		CTD+ROS+FL	0-1000		
	-2	13/07/2009	07:49	09:35	12:34	49°36.852'N	160°22.721'E	49.6142	160.3787		5428	5397	KOL(20 m)+TC		**15.56**	**TC 0.99 m**; KOL bent (2.34-5.60 m)
	-3	13/07/2009	13:43		14:02	49°36.825'N	160°22.786'E	49.6138	160.3798		5428		PLA	0-100		
	-4	13/07/2009	14:07	15:40	17:25	49°36.845'N	160°22.739'E	49.6141	160.3790		5429	5426	MUC		12x(0.25-0.31)	
	-5	13/07/2009	17:36	18:17	19:21	49°36.86'N	160°22.78'E	49.6143	160.3797		5428		MN	0-1000		1000-500, 500-300, 300-150, 150-50, 50-0m
SO202-04	-1	14/07/2009	13:49	15:30	18:15	51°51.80'N	163°09.58'E	51.8633	163.1597	off Kurile-Kamtchatka Trench	5273	5248	KOL(15m)+TC		**11.8**	
	-2	14/07/2009	18:22		18:35	51°51.773'N	163°09.520'E	51.8629	163.1587		5273		PLA	0-100		**TC 0.51 m**
	-3	14/07/2009	18:51	20:22	22:06	51°51.799'N	163°09.624'E	51.8633	163.1604		5273	5273	MUC		12x(0.28-0.32)	
SO202-05	-1	15/07/2009	07:14	07:39	08:05	52°41.805'N	164°55.139'E	52.6968	164.9190	Obruchev Rise	3369		CTD+ROS+FL	0-1000		
	-2	15/07/2009	08:33	09:31	11:05	52°41.79'N	164°55.18'E	52.6965	164.9197		3369	3336	KOL(15m)+TC		**10.01**	**TC 0.77 m**; KOL bent (1.41-5.76 m), 2.91-3.29 m still in steel tube
	-3	15/07/2009	12:01	13:03	14:21	52°41.764'N	164°55.157'E	52.6961	164.9193		3362	3364	MUC		12x(0.23-0.26)	
	-4	15/07/2009	14:27		14:45	52°41.767'N	164°55.126'E	52.6961	164.9188		3364		PLA	0-100		
	-5	15/07/2009	14:54	16:03	17:18	52°41.782'N	164°55.165'E	52.6964	164.9194		3364	3360	CTD+ROS			
	-6	15/07/2009	17:27	18:07	19:10	52°41.777'N	164°55.164'E	52.6963	164.9194		3664		MN	0-1000		1000-500, 500-300, 300-150, 150-50, 50-0 m
	-7	15/07/2009	19:28	20:23	21:44	52°41.79'N	164°55.08'E	52.6965	164.9180		3362	3373	SL(10m)		**1.27**	
SO202-06	-1	16/07/2009	07:34	08:58	10:31	51°54.08'N	166°29.44'E	51.9013	166.4907	Obruchev Rise	3426	3398	KOL(15m)+TC		**13.7**	
	-2	16/07/2009	10:39	11:40	13:05	51°54.121'N	166°29.410'E	51.9020	166.4902		3422	3427	MUC		12x(0.27-0.32)	**TC 0.77 m**; KOL liner imploded (8.74-12.90 m), no loss, liner taped
SO202-07	-1	16/07/2009	20:24	21:07	22:22	51°16.30'N	167°41.98'E	51.2717	167.6997	Detroit Smt.	2350	2315	KOL(20 m)+TC		**17.97**	
	-2	16-17/7/09	22:30	23:13	00:14	51°16.296'N	167°41.958'E	51.2716	167.6993		2349	2346	MUC		12x(0.23-0.29)	TC 0.64 m
	-3	17/07/2009	00:17		00:30	51°16.293'N	167°42.003'E	51.2716	167.7001		2348		PLA	0-100		
	-4	17/07/2009	00:36		00:47	51°16.293'N	167°42.003'E	51.2716	167.7001		2348		PLA	0-100		
	-5	17/07/2009	00:50		01:05	51°16.293'N	167°42.003'E	51.2716	167.7001		2348		PLA	0-100		
	-6	17/07/2009	03:11	04:01	05:23	51°16.287'N	167°41.982'E	51.2715	167.6997		2345	2340	KAL(12m)		**4.77**	core top slanted, resulting in core length between 4.69-4.77 m
SO202-08	-1	17/07/2009	20:45	21:46	23:10	50°32.53'N	170°49.28'E	50.5422	170.8213	Aleutian Rise	3630	3636	MUC		12x(0.23-0.32)	
	-2	17-18/7/09	23:45	00:51	02:42	50°32.52'N	170°49.25'E	50.5420	170.8208		3630	3596	KOL(25m)+TC		**22.75**	**TC 0.79 m**
SO202-09	-1	18/07/2009	21:52	22:19	22:49	49°39.937'N	175°09.937'E	49.6634	175.1656	Aleutian Rise	5025		CTD+ROS+FL	0-1000		
	-2	18-19/7/09	23:00	00:32	02:24	49°39.81'N	175°09.69'E	49.6635	175.1615		5028	5024	MUC		12x(0.30-0.33)	
	-3	19/07/2009	02:28		02:43	49°39.81'N	175°09.975'E	49.6635	175.1663		5031		PLA	0-100		
	-4	19/07/2009	03:16	04:54	07:25	49°39.76'N	175°09.75'E	49.6627	175.1625		5024	4985	KOL(25m)+TC		**23.01**	**TC 0.97 m**; KOL 0-0.03 m in sample bag
	-5	19/07/2009	07:38	08:14	09:15	49°39.745'N	175°09.758'E	49.6624	175.1626		5026		MN	0-1000		1000-500, 500-300, 300-150, 150-50, 50-0 m

Station No.	Gear No.	Date (UTC)	Start (UTC)	At seafl./ at depth (UTC)	End (UTC)	Latitude (deg/min)	Longitude (deg/min)	Latitude (decimal)	Longitude (decimal)	Area	Water depth EM120 (m)	Rope length (m)	Gear	Depth interval (m)	Core recovery (m)	Remarks
SO202-10	-1	20/07/2009	16:45	17:13	17:43	52°44.575'N	179°50.980'E	52.7429	179.8497	southern Bowers Ridge	1470		CTD+ROS+FL	0-1000		
	-2	20/07/2009	17:55	18:21	18:55	52°44.56'N	179°50.87'E	52.7427	179.8478		1488	1476	MUC		12x(0.24-0.31)	
	-3	20/07/2009	19:01		19:13	52°44.570'N	179°50.878'E	52.7428	179.8480		1476		PLA	0-100		
	-4	20/07/2009	19:18	19:53	20:54	52°44.577'N	179°50.922'E	52.7430	179.8487		1490		MN	0-1000		1000-500, 500-300, 300-150, 150-50, 50-0 m
	-5	20/07/2009	21:22	21:49	22:48	52°44.57'N	179°50.87'E	52.7428	179.8478		1470	1441	KOL(25m)+TC		**22.63**	**TC 0.63 m**; KOL liner imploded (1.76-5.78 m), liner deformed between 4.74-5.78 m, Foam plugs added between 2.55-5.78 m
SO202-11	-1	21/07/2009	02:50	03:43	04:40	53°06.675'N	178°53.994'E	53.1113	178.8999	southern Bowers Ridge	2704	2706	MUC		12x(0.23-0.27)	
	-2	21/07/2009	05:17	06:07	07:32	53°06.67'N	178°53.99'E	53.1112	178.8998		2703	2670	KOL(25m)+TC		**22.96**	**TC 0.45 m**
SO202-12	-1	21/07/2009	15:32	16:14	18:15	54°03.04'N	179°05.24'E	54.0507	179.0873	central Bowers Ridge	2109	2115	KAL(12m)		**10.69**	core top slanted
	-2	21/07/2009	18:57	19:34	20:19	54°03.04'N	179°05.26'E	54.0507	179.0877		2108	2108	MUC		12x(0.17-0.35)	
	-3	21/07/2009	20:54	21:29	22:37	54°03.04'N	179°05.24'E	54.0507	179.0873		2109	2076	KOL(25m)+TC		**23.17**	**TC 0.69 m**
SO202-13	-1	22/07/2009	06:24	06:48	07:15	54°58.732'N	177°57.447'E	54.9789	177.9575	northern Bowers Ridge	1381		CTD+ROS+FL	0-1000		
	-2	22/07/2009	07:21		07:35	54°58.721'N	177°57.428'E	54.9787	177.9571		1382		PLA	0-100		
	-3	22/07/2009	07:41	08:16	09:17	54°58.718'N	177°57.437'E	54.9786	177.9573		1382		MN	0-1000		1000-500, 500-300, 300-150, 150-50, 50-0 m
	-4	22/07/2009	09:27	09:50	10:21	54°58.73'N	177°57.43'E	54.9788	177.9572		1383	1386	MUC		12x(0.24-0.29)	
	-5	22/07/2009	10:50	11:16	12:12	54°58.72'N	177°57.42'E	54.9787	177.9570		1382	1360	KOL(15m)+TC		**6.58**	**TC 0.27 m**
SO202-14	-1	22/07/2009	23:03	23:26	23:54	56°47.197'N	178°49.497'E	56.7866	178.8250	central Aleutian Basin	3824		CTD+ROS+FL	0-1000		
	-2	22-23/7/09	23:57		00:15	56°47.193'N	178°49.368'E	56.7866	178.8228		3821		PLA	0-100		
	-3	22/07/2009	00:38	01:51	03:51	56°47.19'N	178°49.45'E	56.7865	178.8242		3821	3794	KOL(20m)+TC		**17.97**	**TC 0.67 m;** KOL: slight expansion at caps due to gas content
	-4	22/07/2009	04:04	04:40	05:44	56°47.216'N	178°49.453'E	56.7869	178.8242		3826		MN	0-1000		1000-500, 500-300, 300-150, 150-50, 50-0 m
	-5	22/07/2009	06:26	07:32	08:46	56°47.18'N	178°49.43'E	56.7863	178.8238		3822	3824	MUC		12x(0.19-0.31)	
SO202-15	-1	24/07/2009	01:26	01:49	02:17	59°30.767'N	179°51.012'W	59.5128	-179.8502	N-Bering Slope Pervenets/ Navarin Canyons	3134		CTD+ROS+FL	0-1000		
	-2	24/07/2009	02:24		02:39	59°30.744'N	179°51.003'W	59.5124	-179.8501		3134		PLA	0-100		
	-3	24/07/2009	02:44	03:19	04:23	59°30.748N	179°51.025'W	59.5125	-179.8504		3132		MN	0-1000		1000-500, 500-300, 300-150, 150-50, 50-0 m
	-4	24/07/2009	04:32	05:27	06:32	59°30.741'N	179°50.952'W	59.5124	-179.8492		3137	3134	MUC		12x(0.29-0.37)	
	-5	24/07/2009	07:01	07:57	09:24	59°30.76'N	179°51.00'W	59.5127	-179.8500		3129	3097	KOL(25m)+TC		**23.43**	**TC 0.70 m**; KOL: strong gas expansion, liner pieces added
SO202-16	-1	24/07/2009	17:41	17:51	18:05	60°24.18'N	179°06.60'W	60.4030	-179.1100	N-Bering Slope Pervenets/Navarin Canyons	548	551	MUC		7x(0.07-0.14)	
SO202-17	-1	24/07/2009	20:45	21:05	22:00	60°07.39'N	179°27.95'W	60.1232	-179.4658	N-Bering Slope Pervenets/Navarin Canyons	1066	1035	KOL(25m)		**18.13**	**TC sample bag (0,1 m)**; KOL: strong gas expansion, adding of liner pieces, deformed (0-0.12 m)

Station No.	Gear No.	Date (UTC)	Start (UTC)	At seafl./ at depth (UTC)	End (UTC)	Latitude (deg/min)	Longitude (deg/min)	Latitude (decimal)	Longitude (decimal)	Area	Water depth EM120 (m)	Rope length (m)	Gear	Depth interval (m)	Core recovery (m)	Remarks
SO202-18	-1	24/07/2009	22:37	22:58	23:26	60°07.58'N	179°26.60'W	60.1263	-179.4433	N-Bering Slope	1108	1115	MUC		11x(0.20-0.21)	
	-2	24/07/2009	23:34		23:50	60°07.597'N	179°26.639'W	60.1266	-179.4440	Pervenets/	1110		PLA	0-100		
	-3	25/07/2009	00:27	00:49	01:53	60°07.60'N	179°26.67'W	60.1267	-179.4445	Navarin Canyons	1111	1074	KOL(25 m)		**18.49**	**TC sample bag (0,05 m)**; KOL: strong gas expansion, liner pieces added, liner deformed (5.08-5.86 m)
	-4	25/07/2009	02:01	02:23	02:52	60°07.526'N	179°26.692'W	60.1254	-179.4449		1111		CTD+ROS+FL	0-1000		
	-5	25/07/2009	03:04	03:39	04:45	60°07.594'N	179°26.642'W	60.1266	-179.4440		1111		MN	0-1000		1000-500, 500-300, 300-150, 150-50, 50-0 m
	-6	25/07/2009	05:53	06:24	07:02	60°07.60'N	179°26.61'W	60.1267	-179.4435		1107	1105	KAL(12m)		**7.21**	core top slanted, core catcher sample up to 7.42 m
SO202-19	-1	26/07/2009	03:14	03:37	04:05	57°39.041'N	175°40.746'W	57.6507	-175.6791	Bering Slope	1752		CTD+ROS+FL	0-1000		
	-2	26/07/2009	04:33	05:06	06:11	57°39.05'N	175°40.69'W	57.6508	-175.6782		1752	1718	KOL(25m)+TC		**19.97**	**TC 0.35 m**; KOL: slight gas expansion, caps curved, liner deformed (4.93-5.93 m)
	-3	26/07/2009	06:20	06:55	07:53	57°39.060'N	175°40.717'W	57.6510	-175.6786		1752		MN	0-1000		1000-500, 500-300, 300-150, 150-50, 50-0 m
	-4	26/07/2009	07:56		08:10	57°39.061'N	175°40.706'W	57.6510	-175.6784		1753		PLA	0-100		
	-5	26/07/2009	08:26	08:57	09:37	57°39.07'N	175°40.70'W	57.6512	-175.6783		1751	1755	MUC		11x(0.22-0.27)	
SO202-20	-1	27/07/2009	07:23	08:16	09:42	55°08.68'N	171°04.95'W	55.1447	-171.0825	SE Aleutian Basin	2984	2948	KOL(25m)+TC		**22.58**	**TC 0.40 m**; KOL: caps slightly curved (gas, 11.52-22,58 m), no liner pieces added
SO202-21	-1	27/07/2009	14:01	14:36	15:47	54°47.35'N	170°19.68'W	54.7892	-170.3280	Unmak Plateau	1911	1878	KOL(25m)+TC		**21.80**	**TC 0.86 m;** KOL: caps slightly curved (gas, 12.80-21.80 m)
	-2	27/07/2009	15:57	16:33	17:16	54°47.33'N	170°19.67'W	54.7888	-170.3278		1911	1912	MUC		11x(0.22-0.34)	
SO202-22	-1	27/07/2009	22:51	23:18	23:56	54°34.42'N	168°48.74'W	54.5737	-168.8123	Unmak Plateau	1478	1478	MUC		11x(0.17-0.31)	
	-2	28/07/2009	00:28	00:55	01:58	54°34.45'N	168°48.66'W	54.5742	-168.8110		1482	1444	KOL(25 m)		**22.18**	**TC 0.53 m**; KOL: caps slightly curved (gas, 11.81-22.18 m), small liner pieces added
	-3	28/07/2009	02:15	02:38	03:06	54°34.454'N	168°48.670'W	54.5742	-168.8112		1478		CTD+ROS+FL	0-1000		
	-4	28/07/2009	04:35	05:15	06:12	54°34.41'N	168°48.62'W	54.5735	-168.8103		1476	1469	KAL(12m)		**9.69**	core top slanted, resulting in length between (9.67-9.69 m), core catcher samples up to 10.06 m
	-5	28/07/2009	06:14		06:28	54°34.423'N	168°48.652'W	54.5737	-168.8109		1478		PLA	0-100		
	-6	28/07/2009	07:21	07:56	09:00	54°34.354'N	168°48.658'W	54.5726	-168.8110		1474		MN	0-1000		1000-500, 500-300, 300-150, 150-50, 50-0 m
SO202-23	-1	29/07/2009	19:27	19:49	20:14	52°10.368'N	160°30.186'W	52.1728	-160.5031	NE SAP	4615		CTD+ROS+FL	0-1000		
	-2	29/07/2009	20:18		20:33	52°10.396'N	160°30.219'W	52.1733	-160.5037	Basin	4614		PLA	0-100		
	-3	29/07/2009	20:40	21:15	22:11	52°10.408'N	160°30.163'W	52.1735	-160.5027	East of Sirius Smt	4613		MN	0-1000		1000-500, 500-300, 300-150, 150-50, 50-0 m
	-4	29-30/7/09	22:19	23:41	01:20	52°10.36'N	160°30.26'W	52.1727	-160.5043		4613	4620	MUC		12x(0.23-0.30)	
	-5	30/07/2009	01:51	03:18	05:33	52°10.40'N	160°30.20'W	52.1733	-160.5033		4615	4586	KOL(20m)+TC		**17.76**	**TC empty**
SO202-24	-1	30/07/2009	18:01	19:22	20:56	53°00.133'N	157°11.578'W	53.0022	-157.1930	NE SAP	4567	4570	CTD+ROS			
	-2	30-31/7/09	21:06	22:43	00:29	53°00.15'N	157°11.58'W	53.0025	-157.1930	Basin	4565	4573	MUC		12x(0.20-0.29)	
	-3	31/07/2009	00:53	02:20	04:37	53°00.13'N	157°11.58'W	53.0022	-157.1930		4562	4539	KOL(20 m)+TC		**17.27**	**TC sample bag**
SO202-25	-1	31/7-1/8/09	21:35	23:00	00:41	54°05.91'N	152°41.14'W	54.0985	-152.6857		4588	4595	MUC		11x(0.22-0,32)	
	-2	01/08/2009	01:21	02:49	05:22	54°05.93'N	152°41.13'W	54.0988	-152.6855		4588	4564	KOL(20m)+TC		**17.75**	**TC 0.92 m**
SO202-26	-1	01/08/2009	15:56	16:10	16:33	54°38.27'N	150°23.01'W	54.6378	-150.3835	Patton Smts	742	748	MUC		7x(0.17-0.27)	
	-2	01/08/2009	16:54	17:13	17:57	54°38.26'N	150°22.98'W	54.6377	-150.3830		743	723	KOL(15m)+TC		**1.82**	**TC empty;** KOL bent (0-1.82), upper 0.20 m possibly disturbed

Station No.	Gear No.	Date (UTC)	Start (UTC)	At seafl./ at depth (UTC)	End (UTC)	Latitude (deg/min)	Longitude (deg/min)	Latitude (decimal)	Longitude (decimal)	Area	Water depth EM120 (m)	Rope length (m)	Gear	Depth interval (m)	Core recovery (m)	Remarks
SO202-27	-1	1-2/8/09	22:56	23:49	00:52	54°17.77'N	149°35.83'W	54.2962	-149.5972	Patton Smts	2916	2921	MUC		11x(0.15-0.21)	
	-2	02/08/2009	01:02	01:25	01:55	54°17.783'N	149°35.83'W	54.2964	-149.5972		2915		CTD+ROS+FL	0-1000		
	-3	02/08/2009	02:27	03:18	04:52	54°17.74'N	149°35.84'W	54.2957	-149.5973		2919	2891	KOL(20 m)		**15.66**	**TC 0.91 m**
	-4	02/08/2009	05:01	05:36	06:41	54°17.811'N	149°35.790'W	54.2969	-149.5965		2920		MN	0-1000		1000-500, 500-300, 300-150, 150-50, 50-0 m
	-5	02/08/2009	06:43		06:57	54°17.771'N	149°35.776'W	54.2962	-149.5963		2922		PLA	0-100		
	-6	02/08/2009	07:36	08:30	09:52	54°17.77'N	149°36.01'W	54.2962	-149.6002		2919	2919	KAL(12m)		**2.92**	core top slanted, resulting in length between 2.88-2.92 m, KAL tube damaged above sediment, core catcher sample up to 3.13 m
SO202-28	-1	02/08/2009	14:45	15:49	17:11	54°25.11'N	148°53.06'W	54.4185	-148.8843	Patton Smts	3710	3709	MUC		12x(0.18-0.25)	
	-2	02/08/2009	17:38	18:42	20:51	54°25.10'N	148°53.06'W	54.4183	-148.8843		3704	3671	KOL(25m)+TC		**14.59**	**TC 1.00 m; KOL bent (0-1.64 m)**
SO202-29	-1	03/08/2009	14:22	14:47	15:18	52°01.721'N	148°53.669'W	52.0287	-148.8945	Gibson Smt	3981		CTD+ROS+FL	0-1000		
	-2	03/08/2009	15:22		15:37	52°01.686'N	148°53.657'W	52.0281	-148.8943		3983		PLA	0-100		
	-3	03/08/2009	15:44	16:24	17:25	52°01.673'N	148°53.691'W	52.0279	-148.8949		3983		MN	0-1000		1000-500, 500-300, 300-150, 150-50, 50-0 m
	-4	03/08/2009	17:49	19:01	21:10	52°01.65'N	148°53.70'W	52.0275	-148.8950		3983	3965	KOL(15 m)+TC		**12.97**	**TC 0.98 m** (TC 0-0.04 m missing), no core catcher sample
	-5	3-4/8/2009	21:22	22:34	00:07	52°01.68'N	148°53.68'W	52.0280	-148.8947		3984	3991	MUC		12x(0.29-0.34)	
	-6	04/08/2009	00:43	01:56	03:48	52°01.66'N	148°53.69'W	52.0277	-148.8948		3983	3960	KOL(20m)+TC		**16.83**	**TC 0.75 m**
SO202-30	-1	04/08/2009	06:02	07:35	09:40	52°01.41'N	148°54.68'W	52.0235	-148.9113	Gibson Smt	4043	4015	KOL(20m)+TC		**17.81**	**TC 0.58 m**
SO202-31	-1	05/08/2009	06:59	07:21	07:48	49°40.683'N	152°32.797'W	49.6781	-152.5466	Seamount East SAP	3746		CTD+ROS+FL	0-1000		
	-2	05/08/2009	07:57	08:32	09:39	49°40.636'N	152°32.813'W	49.6773	-152.5469		3746		MN	0-1000		1000-500, 500-300, 300-150, 150-50, 50-0 m
	-3	05/08/2009	09:39		09:57	49°40.618'N	152°32.907'W	49.6770	-152.5485		3746		PLA	0-100		
	-4	05/08/2009	10:17	11:26	13:12	49°40.63'N	152°32.75'W	49.6772	-152.5458		3746	3730	KOL(15m)+TC		**10.54**	**TC 0.20 m;** KOL liner broken at 5.58 m, Liner added
	-5	05/08/2009	13:22	14:28	15:47	49°40.65'N	152°32.85'W	49.6775	-152.5475		3744	3752	MUC		10x(0.16-0.24)	
SO202-32	-1	07/08/2009	00:30	00:51	01:20	45°30.129'N	158°29.918'W	45.5022	-158.4986	Eastern SAP Abyssal Plain	5302		CTD+ROS+FL	0-1000		
	-2	07/08/2009	01:34	02:10	03:13	45°30.023'N	158°29.952'W	45.5004	-158.4992		5302		MN	0-1000		1000-500, 500-300, 300-150, 150-50, 50-0 m
	-3	07/08/2009	03:20		03:33	45°30.006'N	158°29.969'W	45.5001	-158.4995		5304		PLA	0-100		
	-4	07/08/2009	03:53	05:37	08:08	45°30.00'N	158°29.99'W	45.5000	-158.4998		5300	5284	KOL(15m)+TC		**13.94**	**TC 0.95 m**
	-5	07/08/2009	08:14	09:53	11:51	45°30.02'N	158°29.99'W	45.5003	-158.4998		5302	5317	MUC		12x(0.25-0.33)	
	-6	07/08/2009	12:06	13:45	15:39	45°30.009'N	158°29.980'W	45.5002	-158.4997		5301	5313	CTD+ROS			
SO202-33	-1	10/08/2009	06:13	06:36	07:03	45°05.009'N	174°08.427'W	45.0835	-174.1405	North of Chinook Trough	6159		CTD+ROS+FL	0-1000		
	-2	10/08/2009	07:11	07:47	08:52	45°05.042'N	174°08.435'W	45.0840	-174.1406		6157		MN	0-1000		1000-500, 500-300, 300-150, 150-50, 50-0 m
	-3	10/08/2009	08:56		09:12	45°05.014'N	174°08.368'W	45.0836	-174.1395		6158		PLA	0-100		
	-4	10/08/2009	09:31	11:39	14:55	45°04.97'N	174°08.39'W	45.0828	-174.1398		6159	6133	KOL(25m)+TC		**22.70**	**TC 0.91 m;** KOL full penetration of weight unit, upper 0.6 m of sediment possibly lost (TC: upper 0.2 m), implosion at 2.68 m, slight deformation
	-5	10/08/2009	15:04	16:59	19:33	45°05.03'N	174°08.44'W	45.0838	-174.1407		6159	6167	MUC		12x(0.23-0.34)	
SO202-34	-1	12/08/2009	00:37	00:59	01:28	40°53.497'N	177°40.648'W	40.8916	-177.6775	East of southern Emperor Trough	5726		CTD+ROS+FL	0-1000		
	-2	12/08/2009	01:43	02:17	03:19	40°53.386'N	177°40.599'W	40.8898	-177.6767		5728		MN	0-1000		1000-500, 500-300, 300-150, 150-50, 50-0 m
	-3	12/08/2009	03:26		03:43	40°53.330'N	177°40.541'W	40.8888	-177.6757		5718		PLA	0-100		
	-4	12/08/2009	03:50	05:33	07:45	40°53.25'N	177°40.56'W	40.8875	-177.6760		5713	5731	MUC		12x(0.35-0.43)	
	-5	12/08/2009	07:55	09:51	12:34	40°53.258'N	177°40.521'W	40.8876	-177.6754		5724	5754	SL(18m)		**15.83**	
SO202-35	-1	13/08/2009	05:07	06:54	09:32	39°27.15'N	179°06.69'E	39.4525	179.1115	West of southern Emperor Trough	5581	5607	SL(20m)		**19.29**	

Station No.	Gear No.	Date (UTC)	Start (UTC)	At seafl./ at depth (UTC)	End (UTC)	Latitude (deg/min)	Longitude (deg/min)	Latitude (decimal)	Longitude (decimal)	Area	Water depth EM120 (m)	Rope length (m)	Gear	Depth interval (m)	Core recovery (m)	Remarks
SO202-36	-1	13-14/8/09	23:02	23:24	00:08	38°11.59'N	176°41.88'E	38.1932	176.6980	NE Hess Rise	4525		CTD+ROS+FL	0-1000		
	-2	14/08/2009	00:17	00:52	01:54	38°11.486'N	176°41.839'E	38.1914	176.6973		4524		MN	0-1000		1000-500, 500-300, 300-150, 150-50, 50-0 m
	-3	14/08/2009	01:57		02:14	38°11.466'N	176°41.850'E	38.1911	176.6975		4524		PLA	0-100		
	-4	14/08/2009	02:18	03:43	05:17	38°11.405'N	176°41.749'E	38.1901	176.6958		4524	4539	CTD+ROS			
	-5	14/08/2009	05:38	07:02	09:18	38°11.40'N	176°41.74'E	38.1900	176.6957		4525	4502	KOL(25m)+TC		**23.00**	**TC 0.92 m**
	-6	14/08/2009	09:29	10:52	12:37	38°11.39'N	176°41.793'E	38.1898	176.6966		4522	4538	MUC		12x(0.28-0.38)	
SO202-37	-1	14/08/2009	16:49	17:54	19:15	37°46.05'N	176°16.10'E	37.7675	176.2683	N Hess Rise	3573	3583	MUC		11x(0.18-0.20)	
	-2	14/08/2009	19:44	20:51	22:41	37°46.07'N	176°16.13'E	37.7678	176.2688		3568	3544	KOL(30m)+TC		**24.35**	**TC 0.77 m**
SO202-38	-1	16/08/2009	08:36	10:15	12:21	38°02.61'N	169°16.87'E	38.0435	169.2812	west of Ojin Smt.	5503	5516	MUC		12x(0.27-0.34)	
	-2	16/08/2009	12:44	14:36	17:22	38°02.60'N	169°16.85'E	38.0433	169.2808		5501	5473	KOL(25m)+TC		**22.67**	**TC 0.95 m**
SO202-39	-1	17/08/2009	15:40	17:17	19:01	38°00.681'N	164°26.713'E	38.0114	164.4452	east of N Shatsky Rise	5098	5109	CTD+ROS			
	-2	17/08/2009	19:11	20:39	22:34	38°00.69'N	164°26.80'E	38.0115	164.4467		5096	5110	MUC		11x(0.33-0.38)	
	-3	17-18/8/09	22:58	00:42	03:20	38°00.70'N	164°26.78'E	38.0117	164.4463		5102	5072	KOL(25 m)+TC		**20.23**	**TC 0.95 m**
SO202-40	-1	18/08/2009	12:27	13:28	15:15	38°00.06'N	162°41.09'E	38.0010	162.6848	N Shatsky Rise	3446	3418	KOL(25m)+TC		**15.38**	**TC 0.96 m**
	-2	18/08/2009	15:25	16:27	17:42	38°00.08'N	162°41.09'E	38.0013	162.6848		3462	3453	MUC		12x(0.20-0.31)	
SO202-41	-1	19/08/2009	05:21	07:10	09:49	38°24.79'N	160°20.05'E	38.4132	160.3342	west of N Shatsky Rise	5395	5366	KOL(25 m)+TC		**22.71**	**TC 0.94 m**, upper 0.1 m lost
	-2	19/08/2009	09:57	11:37	13:21	38°24.785'N	160°20.105'E	38.4131	160.3351		5396	5402	CTD+ROS			
	-3	19/08/2009	13:30	15:10	17:32	38°24.79'N	160°20.05'E	38.4132	160.3342		5408	5405	MUC		12x(0.26-0.37)	
SO202-42	-1	20/08/2009	06:24	08:10	11:02	38°53.24'N	157°37.55'E	38.8873	157.6258	W SAP Abyssal Plain	5537	5501	KOL(25 m)+TC		**22.18**	**TC 0.92 m,** KOL 4.90-5.40 m slightly deformed
	-2	20/08/2009	11:07		12:36	38°53.47'N	157°37.05'E	38.8912	157.6175				CTD+ROS			Winch failure at 5 m depth, no data, no samples
	-3	20/08/2009	12:45	14:24	16:22	38°53.504'N	157°37.692'E	38.8917	157.6282		5535	5543	MUC		11x(0.29-0.37)	
SO202-43	-1	21/08/2009	05:59	07:50	10:48	39°21.86'N	154°53.70'E	39.3643	154.8950	W SAP Abyssal Plain	5670	5638	KOL(25m)+TC		**21.27**	**TC 0.92 m,** KOL 1..26-3.27 m imploded
SO202-44	-1	21-22/8/2009	22:42	00:25	02:30	39°47.93'N	152°20.85'E	39.7988	152.3475	W SAP Abyssal Plain	5494	5485	MUC		-	tubes empty
	-2	22/08/2009	02:57	04:51	07:37	39°47.91'N	152°20.82'E	39.7985	152.3470		5497	5461	KOL(25m)+TC		**21.42**	**TC 1.00 m**
	-3	22/08/2009	07:45	08:07	08:36	39°47.979'N	152°20.924'E	39.7997	152.3487		5498		CTD+ROS+FL	0-1000		
	-4	22/08/2009	08:43	09:18	10:21	39°47.99'N	152°20.92'E	39.7998	152.3487		5493		MN	0-1000		1000-500, 500-300, 300-150, 150-50, 50-0 m
	-5	22/08/2009	10:36	12:19	14:06	39°48.073'N	152°21.050'E	39.8012	152.3508		5505	5506	CTD+ROS			
SO202-45	-1	23/08/2009	03:34	05:23	08:13	40°17.50'N	149°29.09'E	40.2917	149.4848	W SAP Abyssal Plain	5476	5438	KOL(25m)+TC		**21.60**	**TC 0.76 m**
	-2	23/08/2009	08:20	09:56	12:11	40°17.50'N	149°29.10'E	40.2917	149.4850		5476	5486	MUC		12x(0.30-0.32)	